Development of SNAP-tag based fusion proteins as novel auristatin F-containing immunoconjugates and photoimmunotheranostics in the detection and treatment of triple-negative breast cancer

by **Neelakshi MUNGRA**

Submitted in fulfilment of the requirements for the degree of

Doctor of Philosophy

Supervisor

Professor Dr. Dr. Stefan Barth

Medical Biotechnology and Immunotherapy Research Unit
Division of Chemical and Systems Biology
Department of Integrative Biomedical Sciences
SARChI Chair in Cancer Biotechnology
Faculty of Health Sciences

University of Cape Town

November 2021

Plagiarism Declaration

I, **Neelakshi Mungra**, hereby declare that the work contained in this thesis is my own original unaided work. It is being submitted for the degree of Doctor of Philosophy at the University of Cape Town, South Africa. Neither has any part nor this whole thesis been submitted in the past, is being submitted, or will be submitted at any other university.

I have used the numbered Oncotarget referencing style as the convention for citation and referencing. Each significant contribution to, and quotation in, this thesis from the work or works of other authors and collaborators has been attributed, cited and referenced. I give the university the authority to reproduce the content, either partly or in whole for research purposes.

Signature:

Date: 9th November 2021

Acknowledgements

I would like to express my sincere thanks and gratitude to the following people and funders, without whom this thesis would not have been possible:

To the National Research Foundation (NRF), the Medical Research Council (MRC) of South Africa, the South African Research Chair Initiative (SARChI) in Cancer Biotechnology and the University of Cape Town (UCT) for the financial assistance and for making this project a reality.

To my supervisor, Professor Dr. Dr. Stefan Barth, for his continuous support, unmatched leadership and encouragement. Thank you for providing me with the opportunity to learn, grow and develop into the scientist that I am today. I really appreciate your inspiring words and optimism.

To my mentor, Dr. Shivan Chetty, thank you for your unflinching patience, guidance and help throughout this PhD journey. Your exceptional insight and knowledge have shaped my life in unimaginable ways. I will remain forever grateful.

To Dr. Krupa Naran, Dr. Sandra Jordaan, Dr. Dharanidharan Ramamurthy and Dr. Fleury Nsole Biteghe, for being great teachers and for always encouraging me to think beyond my horizons. This learning experience would not have been the same without you!

To all my colleagues and peers from the MB&I Research Unit, thank you for all the love, support and guidance. To Akiko, Marc, Suresh, Trishana and Maryam, thank you for being such great friends and for the daily dose of insanity. This kept me going through the hard times.

To Professor Roger Hunter, Olaolu Fadeyi and Allan Huysamen from the Chemistry Department at UCT, for synthesizing and providing the BG-Auristatin F used in this research project. Thank you, Allan, for all your hard work, tremendous input and support throughout this journey.

To Dr. Rubina Bunjun from the Division of Medical Virology at UCT, you have been an exemplary and visionary mentor. I am so grateful that you took me under your wings when I first started my flow cytometry experiments. You have really helped me grow into my potential and I would not be where I am today without you.

To Dr. Shameem Zaer Jaumdally, I admire you for your humility, your diligence and your unwavering purpose. Thank you so much for your mentorship throughout my academic journey. I hope to inspire others as you have inspired me.

To Mr Tim Reid, Mrs Susan Cooper and Professor Dirk Lang, for their endless guidance and assistance with flow cytometry and confocal microscopy. I appreciate and treasure everything you have taught me.

To the Blackburn and Sturrock lab, thank you for all the assistance provided to MB&I, in the form of infrastructure and technical support.

To all my friends, thank you for your unconditional love and words of encouragement. Thank you for being the shoulder I can always depend on.

Finally, I owe my deepest gratitude to my family; my parents Mukesh and Kavita, and my brother Durshil, who have always been there to listen and support me throughout my studies. Mum and dad, I have missed you tremendously during these 10 years away from home. This thesis is dedicated to you both.

List of Publications

- Akinrinmade, O., Jordaan, S., Hristodorov, D., Mladenov, R., **Mungra, N.**, Chetty, S. and Barth, S. (2017). Human MAP Tau Based Targeted Cytolytic Fusion Proteins. *Biomedicines*, 5(3), p36.
- Jordaan, S., Chetty, S., **Mungra, N.**, Koopmans, I., van Bommel, P., Helfrich, W. and Barth, S. (2017). CSPG4: A Target for Selective Delivery of Human Cytolytic Fusion Proteins and TRAIL. *Biomedicines*, 5(3), p37.
- Hlongwane, P., **Mungra, N.**, Madheswaran, S., Akinrinmade, O., Chetty, S. and Barth, S. (2018). Human Granzyme B Based Targeted Cytolytic Fusion Proteins. *Biomedicines*, 6(2), p72.
- **Mungra, N.**, Jordaan, S., Hlongwane, P., Naran, K., Chetty, S., and Barth, S. (2019). Targeted Human Cytolytic Fusion Proteins at the Cutting Edge: Harnessing the Apoptosis-Inducing Properties of Human Enzymes for the Selective Killing of Tumor Cells. *Oncotarget*, 10(8), p897-915.
- Madheswaran, S., **Mungra, N.**, Nsole Biteghe, F.A., DelaCroix Ndong, J., Naran, K., Ramamurthy, D., Khumalo, P. and Barth, S. (2020). Antibody based targeted interventions for the diagnosis and treatment of skin cancers. *Anti-cancer agents in medicinal chemistry*, 21(2), p162-186.
- **Mungra, N.***, Nsole Biteghe, F.A.*, Toung Chalomie, N.E., De La Croix Ndong, J., Engohang-Ndong, J., Vignaux, G., Padayachee, E., Naran, K. and Barth, S. (2020). Advances in epidermal growth factor receptor specific immunotherapy – lessons to be learned from armed antibodies. *Oncotarget*, 11(38), p3531-3557.
- Nsole Biteghe F.A.*, Nyangone Ekome Toung, C.*, **Mungra N.**, Vignaux, G., Gao, N., Vergeade, A., Okem, A., Naran, K., Ndong, J. and Barth, S. (2020). Antibody-based immunotherapy: Alternative approaches for the treatment of metastatic melanoma. *Biomedicines*, 8(9), p327.
- Ramamurthy, D., Nundalall, T., Cingo, S., **Mungra, N.**, Karaan, M., Naran, K. and Barth, S. (2020). Recent advances in immunotherapies against infectious diseases. *Advances in Immunotherapy*, 1(1), p1-16.

- **Mungra, N.**, Nsole Biteghe, F.A., Jordaan, S., Huysamen, A., Naran, K., Chetty, S., Padayachee, E., Cooper, S., Lang, D., Bunjun, R., Govender, D., Richter, W., Hunter, R.* and Barth, S.* (2022). CSPG4 as a target for specific killing of triple-negative breast cancer cells by a SNAP tag-based antibody fusion protein conjugated to auristatin F. *International Journal of Cancer*, in preparation.
- **Mungra, N.**, Hardcastle, N., Nsole Biteghe, F.A., Ramamurthy, D., Huysamen, A., Naran, K., Cooper, S., Lang, D., Bunjun, R., Govender, D., Richter, W., Hunter, R.* and Barth, S.* (2022). AURIF-based, anti-CD44 scFv-SNAP for triple-negative breast cancer after confirmation of marker expression on breast cancer tissue sections. *Cancer Letters*, in preparation.
- **Mungra, N.**, Nsole Biteghe, F.A., Ramamurthy, D., Fadeyi, O., Naran, K.*, Hunter, R.* and Barth, S.* (2022). Theranostic effect of anti-CD44(scFv)-IR700 on triple-negative breast cancer cells. *International Journal of Cancer*, in preparation.

Table of Contents

List of Figures

List of Tables

List of Abbreviations

ABC	ATP-binding cassette
AC	Adjuvant chemotherapy
ADC	Antibody-drug conjugate
ADCC	Antibody-dependent cellular cytotoxicity
AGT	Alkylguanine-DNA alkyltransferase
AN2	Aniridia type II
APCs	Antigen-presenting cells
ASPH	Aspartate (aspartyl/asparaginyl) β-hydroxylase
AURIF	Monomethyl auristatin F
BG	Benzylguanine
BiTEs	Bispecific T-cell engagers
BL1	Basal-like 1
BL2	Basal-like 2
BSA	Bovine serum albumin
CAP	Catabolite activator protein
CAR-T	Chimeric antigen receptor T-cell
CD44	Cluster of differentiation 44
CDK	Cyclin-dependent kinase
CDRs	Complementarity determining regions
CEA	Carcinoembryonic antigen
CGH	Comparative genomic hybridization
Chk1	Checkpoint kinase 1
CMV	Cytomegalovirus
CSC	Cancer stem cell
CSPG4	Chondroitin sulfate proteoglycan 4
CT	Computerized tomography
CTLA-4	Cytotoxic T-lymphocyte-associated protein 4
DAR	Drug-to-antibody ratio
DMEM	Dulbecco’s Modified Eagle Medium
DMSO	Dimethyl sulfoxide

DTT	Dithiothreitol
EGFR	Epidermal growth factor receptor
EKS	Enterokinase cleavage site
EpCAM	Epithelial cell adhesion molecule
ER	Estrogen receptor
FDA	Food and drug administration
FGFR	Fibroblast growth receptor
FITC	Fluorescein isothiocyanate
FR	Framework regions
FSC-A	Forward scatter area
FSC-H	Forward scatter height
GAGs	Glycosaminoglycans
GFP	Green fluorescent protein
GTP	Guanosine triphosphate
HA	Hyaluronic acid
HAMA	Human anti-mouse antibody
hCFP	Human cytolytic fusion protein
HDAC	Histone deacetylase
HER2	Human epidermal growth factor receptor 2
HMW-MAA	High molecular weight melanoma-associated antigen
Hsp90	Heat shock protein 90
IC_{50}	Half maximal inhibitory concentration
IgG	Immunoglobulin G
IHC	Immunohistochemistry
IM	Immunomodulatory
IMAC	Immobilized metal affinity chromatography
IRES	Internal ribosome entry site
IT	Immunotoxin
LAR	Luminal androgen receptor
LB	Luria broth
M	Mesenchymal

mAb	Monoclonal antibody
MAPK	Mitogen-activated protein kinase
MCSP	Melanoma-associated chondroitin sulfate proteoglycan
MFI	Median fluorescence intensity
MHC	Major histocompatibility complex
MMAE	Monomethyl auristatin E
MMAF	Monomethyl auristatin F
MSL	Mesenchymal stem-like
MTD	Maximum tolerated dose
NAC	Neoadjuvant chemotherapy
NG2	Neural/glial antigen 2
NHS	*N*-hydroxysuccinimide
NIR	Near-infrared
ORF	Open reading frame
PARP1	Poly (ADP-ribose) polymerase 1
PBS	Phosphate buffered saline
PD-1	Programmed cell death protein 1
PD-L1	Programmed death-ligand 1
PDT	Photodynamic therapy
PET	Positron emission tomography
PFA	Paraformaldehyde
PI3K	Phosphoinositide 3-kinase
PIT	Photoimmunotherapy
PR	Progesterone receptor
PS	Photosensitizer
ROS	Reactive oxygen species
scFv	Single-chain variable fragment
SD	Standard deviation
SDS-PAGE	Sodium dodecyl sulfate-polyacrylamide gel electrophoresis
SI	Staining index
SOC	Super optimal broth with catabolite repression

SSC-A	Side scatter area
STR	Short tandem repeat
SUPR	Super enhanced permeability and retention
TCR	T-cell receptor
TNBC	Triple-negative breast cancer
V_H	Variable heavy chain
V_L	Variable light chain

Abstract

Breast cancer represents one of the most common forms of female malignancy of the 21st century. Among the various breast cancer subtypes, triple-negative breast cancer (TNBC) is phenotypic of breast tumors lacking expression of the estrogen receptor (ER), the progesterone receptor (PR) and the human epidermal growth factor receptor 2 (HER2). As an idiosyncratic disease, TNBC displays a conspicuously aggressive and invasive clinical course, with an unexplained partiality towards women of African ancestry. Its acute heterogeneity and complexity behave as mutually reinforcing negative factors, which further complicate prognosis, thereby increasing the burden of breast cancer-related mortality. With the absence of well-defined molecular targets in TNBC, there is a heightened reliance on tri-modality therapy (surgery, radiotherapy and chemotherapy), albeit with an increasing incidence of adverse effects and disease relapse. To this end, there is an urgent need to develop an arsenal of targeted diagnostics and therapeutics, which can be synergized to cover the vast majority of triple-negative breast tumors, paving the way towards the development of personalized regimens suitable for the particular needs and disease of each patient. As such, achieving selective cytotoxicity, with minimal or no collateral damage to healthy tissues, embodies the holy grail of targeted anti-cancer therapies. For instance, the high affinity and specificity of monoclonal antibodies (mAbs) and derivatives thereof, have cemented their application as revolutionary tools in the selective delivery of drugs to malignant cells. These therapeutic proteins, also known as antibody-drug conjugates (ADCs), might exhibit several advantages compared to their small-molecule counterparts, but their widespread clinical use is hampered by various developmental considerations. Traditional conjugation strategies employed to arm mAbs with cytotoxic warheads, usually give rise to heterogeneous mixtures of ADC species, bearing non-uniform drug-to-antibody ratios (DARs), pharmacologic characteristics and safety profiles.

Fortunately, the implementation of self-labeling tags (such as SNAP-tag, CLIP-tag and Halo-tag) are providing renewed impetus to homogeneous recombinant immunotherapeutics development. More precisely, SNAP-tag is an engineered mutant of the human O(6)-alkylguanine-DNA alkyltransferase, endowed with the ability to specifically and irreversibly react with benzylguanine (BG) derivatives, forming a stable product. Based on the above premises, this research aims to use SNAP-tag technology as a cutting-edge site-specific conjugation method to: (1) develop a

comprehensive antibody platform, consisting of single-chain antibody fragments (scFvs) genetically fused to SNAP-tag, to specifically screen and evaluate their predictive potential for chondroitin sulfate proteoglycan 4 (CSPG4), CD44 and aspartate (aspartyl/asparaginyl) β-hydroxylase (ASPH)-positive TNBC cells, (2) generate functional recombinant ADC formulations as robust delivery systems carrying the antimitotic drug monomethyl auristatin F (MMAF/AURIF), concurrently overcoming production constraints to yield therapeutically viable and homogeneous combination products, and (3) provide a fail-safe system that overcomes the lack of specificity of photodynamic therapy (PDT), by coupling scFv-SNAP-tag to the potent near-infrared (NIR) photosensitizer (PS) IRDye700DX (IR700) and to demonstrate its selective dose-dependent cytotoxic activities *in vitro*.

Following *in silico* design of the open reading frames (ORFs) coding for each construct, standardized molecular cloning techniques were implemented to generate recombinant mammalian expression plasmids, encompassing Ig-*Kappa* leader as an efficient protein secretory system. After confirmation of the DNA integrity, protein expression was achieved through transient transfection into HEK293T cells. Thereafter, the resulting histidine-tagged fusion proteins (αCSPG4(scFv)-SNAP, αCD44(scFv)-SNAPf and αASPH(scFv)-SNAP) were harvested from the cell culture supernatant and subjected to immobilized metal affinity chromatography (IMAC). In order to evaluate the outcome of this protein expression and purification step, sodium dodecyl sulfate-polyacrylamide gel electrophoresis (SDS-PAGE) and western blot analysis were used to confirm the presence of full-length recombinant SNAP-tag based fusion proteins based on their molecular weights. Integration of the fluorescent dye Alexa Fluor 488 into the fusion proteins was carried out to investigate the self-labeling activity of the SNAP-tag moiety, as well as to provide qualitative and quantitative insights into the binding potential of the antibody fragments towards their cognate antigens. Subsequently, the AURIF and IR700-based immunoconjugates were generated by conjugating scFv-SNAP with their respective BG-modified substrates, in a defined 1:1 stoichiometric reaction. The specific and dose-dependent biological activities of the resulting bifunctional therapeutic proteins were then assessed on TNBC cells.

In this study, pCB-αCD44(scFv)-SNAPf was successfully cloned and all 3 fusion proteins were effectively expressed, although with low yields and purity, yet adequate for downstream *in vitro* characterization. After showcasing the self-labeling potential of the SNAP-tag component, surface binding of the fluorescently labeled product was demonstrated on antigen-positive TNBC cell lines through confocal microscopy and flow cytometry. The cell killing ability of the novel AURIF-based recombinant ADCs and IR700 photoimmunoconjugates, was illustrated by the induction of a 50% reduction in cell viability (IC_{50} value) at nanomolar to micromolar concentrations on target cell lines. This observable selective cytotoxicity revealed that conjugation of BG derivatives to SNAP-tag, did not affect the binding potential of the antibody fragment, nor abrogated the cytocidal activity of the payload.

As a proof of concept, this research builds on existing work that promulgates the use of SNAP-tag as a state-of-the-art conjugation strategy that can circumvent the challenges associated with the use of antibodies as effective delivery systems for therapeutic molecules. By harnessing the applicability of SNAP-tag in the unambiguous generation of homogeneous and pharmaceutically acceptable immunoconjugates, the results herein presented, also highlight the prospects of such agents in disease-specific tumor suppression. While various architectural modifications could further improve cytotoxic activities of future combination products, this research underscores the duality of SNAP-tag in the development of immunodiagnostics and therapeutics, that could potentially be instrumental in instilling a shift towards a personalized medicine stratagem. In conclusion, the combination of such immunoconjugates with a robust companion diagnostic panel provided by SNAP-tag, represents a first step towards the effective management of TNBC, with potential impact on the economic, social and clinical settings.

Chapter 1: Literature Review

INTRODUCTION

1.1 Breast cancer prevalence and its molecular subtypes

Breast cancer is a global public health crisis. Being first recognized in 1500 BC in ancient Egypt [1], breast cancer is a disease characterized by the perpetual growth of malignant cells in the tissues of the breast. According to statistics, breast cancer alone is expected to account for the majority (30%) of all new cancer diagnoses in American women in 2020 [2]. On the African continent, more than 50% of women diagnosed with breast cancer usually die of the disease [3]. Similarly, breast cancer incidence is on the rise in South Africa, with the National Cancer Registry (2014) estimates pointing towards a 1 in 27 lifetime-risk of developing the disease, making it a leading cancer in South African women. At present, breast cancer is known as the second-leading cause of death in women (American Cancer Society, 2020) and, on that account, it constitutes an alarming threat to global socioeconomic well-being.

While breast cancer is a complex and heterogeneous disease [4], understanding breast cancer requires a fundamental knowledge about the general structure of the normal female breast (Figure 1). A woman's breast consists of milk secreting sacs called lobules and ducts that drain milk to the nipples [5]. The most common histological types of breast cancers originate in the cells lining these ducts and lobules, thereby resulting in ductal and lobular carcinomas respectively [6].

One important question about breast cancer concerns its emergence in the human body. Throughout history, cancer research has attempted to establish the relationship between the root causes of cancer and its biological characteristics [7]. Eventually, it was found that cancer arises as a result of multiple genetic modifications over time [8]. In most cases, such mutations allow cells to proliferate indefinitely, ultimately facilitating tumor formation. More recently, several lines of evidence suggest the growing recognition of certain hallmarks that promote tumorigenesis in humans. These important hallmarks are: self-sufficiency in growth signals, evasion of apoptosis, sustained angiogenesis, insensitivity to growth-inhibitory signals, limitless replicative potential, and tissue invasion and metastasis [9].

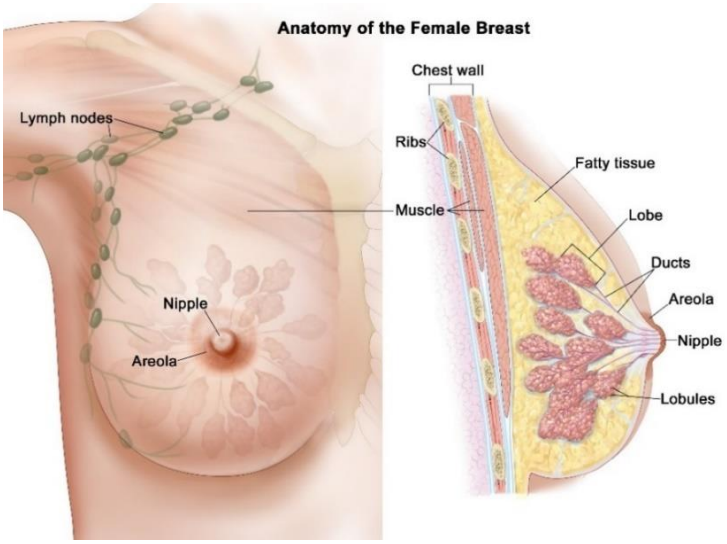

Figure 1: Anatomy of the female breast. The normal female breast is made up of fatty tissue, ducts, lobules, lymph and blood vessels. While cancerous growth can start in the cells of any breast tissue, the most common types occur in the lining of the ducts and lobules (Source: National Cancer Institute, 2011).

However, over the years, epidemiologists have attempted to document the risk factors that may play a profound role in increasing the incidence of this daunting disease. Although knowledge about these risk factors cannot be used to explain an individual's diseased state, it undeniably provides the necessary platform for the implementation of preventive measures. For instance, it has been reported that cancer arises from two different classes of carcinogens: those that can damage genes involved in the control of cell proliferation, and those that can enhance tumor cell growth [8]. In this case, limiting one's exposure to such chemicals, might be a necessary course of action to consider. Similarly, additional risk factors have been identified. These include: age, obesity, late menopause, oral contraceptive use, early abortion, diet and family history [8,10–12]. Nonetheless, the exact mechanism through which some of these risk factors encourage the formation of cancerous cells, is not yet fully understood.

As discussed above, breast cancer is a multifactorial disease, involving the cumulative effect of genetic and environmental influences. Interestingly, one of the most important factors responsible for increased breast cancer susceptibility, is a family history of the disease [13]. Indeed, about 5-10% of all breast cancer cases are the result of inherited gene mutations [14]. Several gene defects can be implicated in the occurrence of hereditary breast cancer. However, little is known about the precise interplay between these genes and the environment and how they tip the balance in favor

of breast carcinogenesis. Among these genes, BRCA1 and BRCA2, appear to exercise a monopoly over the heightened incidence of this disease in the United States and European populations [15]. In addition, the BRCA1 and BRCA2 genes were found to be localized on chromosome 17 and chromosome 13q12-13 respectively [13]. Strikingly, while their expression is not solely restricted to breast tissues, mutations in these genes are most commonly associated with breast and ovarian cancers [16]. In order to explain this strange phenomenon, it was postulated that the inactivation of BRCA1 and BRCA2, promotes estrogen-induced DNA damage in these two specific tissues [17]. As a matter of fact, BRCA1 and BRCA2 are known to be tumor suppressor genes [18]. This means that under normal circumstances, they actively work to regulate the growth of cells. This is made possible through their ability to trigger DNA damage response pathways [13]. As an example for this statement, it was found that mouse embryonic stem cells deficient in BRCA1, are more sensitive to DNA damage and less capable of transcription-coupled repair [19]. Here, BRCA1 is significant since individuals carrying mutations in this gene, are more prone to developing triple-negative breast cancer (TNBC) [20] – the main focus of this PhD dissertation.

Over the years, researchers have realized that the key to effective management of breast cancer, resides in early and accurate diagnosis [21]. The earlier the diagnosis, the higher the long-term survival rate [22]. Being able to detect early signs of breast cancer, implies that the disease is more treatable and less debilitating to patients. Unfortunately, breast cancer is a highly heterogeneous disease [23], and the acute disparity in biological and morphological features of breast tumor cells, directly hinders their clinical classification. This means that patients with the same stage of disease can react differently to the same treatment. Consequently, there is a huge demand for patient-tailored therapeutic strategies that would allow accurate prognostication and a more conducive treatment plan. At present, breast cancer screening is typically done through a physical examination and affordable imaging techniques including x-ray mammography, magnetic resonance imaging and breast ultrasound. With the ongoing outbursts in technological advancement, these imaging tools have witnessed varied opinions from the scientific community. A vast amount of work points towards the inefficiency of such imaging devices. Their lack of sensitivity and specificity [24] does not ensure complete detection of every single carcinoma of the breast. As one of the mainstays of breast cancer detection, x-ray mammography is known to

be responsible for an appreciable reduction in breast cancer mortality for women falling within the 50-69 age group [25]. Nonetheless, many researchers hold the view that the phenomenon of false-negatives in mammography cannot be dismissed [26–28]. Scientists began to understand that gaining further insight into the nature and biochemical diversity between normal and tumor cells, would considerably promote the creation of drugs and therapies targeted towards specific tumor types. Therefore, the primary challenge to breast cancer control involved being able to classify cancerous cells in a simple, yet accurate and effective manner.

To this end, several important aspects are considered for the classification and proper monitoring of breast cancer disease. For instance, in the clinical setting, the traditional TNM staging system (Tumor size, presence of Nodal metastasis, and presence of distant Metastasis) is in popular use [29]. Moreover, if preliminary breast screening examinations reveal a possible predisposition to cancer, a biopsy may be conducted. Such procedure allows pathologists to examine breast tissue samples under the microscope and to assign a histological grading to the tumor type based on the morphological characteristics of the cell [30]. Newer methods for classification rely on DNA microarray platforms, which have enabled researchers to unravel the molecular complexity of the disease. In addition, this approach generates gene expression profiles which can be used to predict the clinical outcome of breast cancers [31]. By determining the expression status of cellular components that play a defining role in signaling pathways, 4 intrinsic breast cancer subtypes were identified [32]. These subtypes are marked by the presence or absence of the estrogen (ER) and progesterone (PR) receptors, as well as the human epidermal growth factor receptor 2 (HER2) [33,34]. They are as follows:

1. Luminal A subtype:

Being the most common subtype, luminal A tumors are characterized by the expression of the ER, PR and cytokeratin CK8/18 [32]. These tumors usually have a well-founded prognostication, along with a lower relapse rate in comparison to other subtypes [35].

2. Luminal B subtype:

While both subtype A and B express ER, subtype B is marked by an overabundance of proliferation genes, besides exhibiting the worse clinical outlook [32].

3. HER2-positive subtype:

The overexpression of HER2 occurs in 20-30% of all breast cancers [36]. They tend to grow more quickly and are generally known for their aggressive behavior [37]. Fortunately, treatment is available; Trastuzumab has demonstrated effectiveness in patients with HER2-positive metastatic breast cancer [38].

4. Basal-like subtype:

One of the most distinctive hallmark of this subtype is the absence of 3 key receptors involved in breast cancer: ER, PR and HER2 [32]. Hence, they are also referred as the 'triple-negative' subtype. Basal-like cancers are known for their aggressive nature and are highly unlikely to benefit from currently available targeted therapies [39].

Therefore, it can be concluded that high-throughput molecular technologies have indeed contributed to significant breakthroughs in cancer research. However, the difficulty lies in implementing this approach into the clinical arena [32]. Perhaps, a tentative solution would be the development of novel serum-based laboratory tests that could facilitate routine breast cancer screening and monitoring.

1.2 Triple-negative breast cancer

Of the estimated 1 million cases of breast cancer diagnosed annually worldwide, approximately over 170,000 will encompass the triple-negative phenotype [40]. Triple-negative breast cancer (TNBC) accounts for 10-15% of all breast cancers and is characterized by the lack of expression of ER, PR and HER2 [41,42]. It seems to occur more predominantly in women of African ancestry than any other ethnic origins, particularly in premenopausal women [43,44]. Although this racial preference has been reported by various studies, an accurate explanation for this observation remains unfounded [44,45]. Whether this association is related to germline genetic factors, environmental factors, or a combination of both, is still poorly understood [46]. Nonetheless, according to the 2008 Carolina breast cancer study, several factors increase the predisposition to TNBC; these include increased parity, younger age at first-term pregnancy and shorter duration of breast-feeding [47]. Therefore, as stated by Brewster *et al*. (2014), it can be concluded that there

is an urgent need for collaborative multinational research focused on the causes, prevention and treatment of TNBC in women of African origin [41].

Among all the breast cancer subtypes, TNBC has the worst prognosis, with a generally aggressive clinical course, and is associated with a large proportion of breast cancer-related mortality [42,48,49]. Indeed, its inherent heterogeneity, along with the lack of tangible molecular targets, represent challenging obstacles to effective TNBC treatment [50,51]. Statistics indicate that despite tri-modality therapy (surgery, radiotherapy, adjuvant/neoadjuvant chemotherapy), as many as 50% of patients with resectable TNBC (stage I-III), experience disease relapse and 37% die in the first 5 years post-surgery [52,53]. Based on these trends, researchers started to recognize the necessity to understand the complexity of this daunting disease. Through extensive genomic and biological analysis across 21 breast cancer data sets, Lehmann and colleagues (2011) were able to identify 6 TNBC subtypes with unique gene expressions and ontologies [54]. These are:

1. Basal-like 1 (BL1) and basal-like 2 (BL2) subtypes:

Although frequently used interchangeably, the terms ‘triple-negative’ and ‘basal-like’ are not completely synonymous, as shown by an estimated 20-30% discordance across several studies [55–58]. More explicitly, TNBC refers to the immunohistochemical classification of breast tumors while ‘basal-like’ is determined via gene expression microarray analysis [42]. As such, the majority of TNBCs are of the basal-like molecular subtype, which are marked by elevated levels of basal cytokeratin expression (cytokeratins 5/6 and 17), higher histological grade, increased mitotic activity, marked cellular pleomorphism, a high Ki67 index, poor differentiation, early relapse and decreased survival [48,56,59,60].

Interestingly, the BL1 subtype is characterized by increased proliferation and cell cycle checkpoint loss (due to increased expression of DNA damage response genes), while BL2 is abundant in genes involved in growth factor signaling, glycolysis and gluconeogenesis [54]. The highly proliferative nature of these subtypes thus warrants the use of antimitotic drugs (such as taxanes) in the treatment of basal-like TNBCs [61,62].

2. Immunomodulatory (IM) subtype:

The IM subtype displays enrichment for genes involved in immune cell processes such as those involved in immune cell signaling, cytokine signaling and antigen presentation (T helper type 1/2 pathway, natural killer cell pathway, B-cell receptor signaling pathway, T-cell receptor signaling, dendritic cell pathway, cytokine signaling pathway, IL-12 and IL-7 pathways) [54].

3. Mesenchymal (M) and mesenchymal stem-like (MSL) subtypes:

The M subtype exhibits an overexpression of genes involved in cell motility, extracellular matrix-receptor interaction and cell differentiation pathways. While the MSL subtype shares a similar gene expression pattern as the M subtype, it is uniquely enriched in genes involved in growth factor signaling, including calcium signaling, inositol phosphate metabolism, epidermal growth factor receptor (EGFR) and ATP-binding cassette (ABC) transporter [54].

4. Luminal androgen receptor (LAR) subtype:

While this subtype is ER negative, its ontologies point to the heightened expression of genes involved in hormone regulation pathways, including steroid synthesis, porphyrin and androgen metabolism [54].

Unfortunately, the detection of TNBC using routine screening methods such as mammography or ultrasound, is not adequate; in 2007, Dent *et al*. reported that detection of triple-negative breast tumors was more plausible via clinical examination than through the application of imaging devices [63]. In agreement with the above statement, it has been shown that TNBCs usually present as ‘interval cancers’ between regular mammograms, most possibly arising from the rapid growth rate or differences in breast tissue density [40,64]. Due to the relative lack of therapeutic target for TNBCs (as compared to endocrine-sensitive and HER2-positive breast cancers) and the absence of specific treatment guidelines, this aggressive disease entity is managed with standard chemotherapeutic treatment [46]. For instance, cytotoxic chemotherapy (using taxanes, anthracyclines, capecitabine and ixabepilone amongst others) remains the treatment of choice for patients presenting with metastatic TNBC [65]. An interesting paradox is the finding that TNBCs are often more responsive to initial chemotherapy treatment than any other breast cancer subtype [51,52]. However, the activities of these agents were usually short-lived, as illustrated by a

retrospective analysis of 111 cases treated with monotherapy or combinations [66]. Moreover, relapse is a common occurrence, arising primarily in visceral organs and in the central nervous system [52,67,68].

Taking these challenges into account, recent advances in drug developmental therapeutics have been centered around the discovery of molecular targets among triple-negative breast tumors. Indeed, the armamentarium of 'targeted' therapeutics for TNBCs is evolving, as exemplified by strategies to inhibit angiogenesis, poly (ADP-ribose) polymerase 1 (PARP1), p53 and its downstream effectors (phosphoinositide 3-kinase (PI3K)/Akt/mTOR, checkpoint kinase 1 (Chk1), heat shock protein 90 (Hsp90), histone deacetylase (HDAC), cyclin-dependent kinase (CDK) and Nutlins), EGFR and the fibroblast growth receptor (FGFR) [40,55,69,70]. Strikingly, despite these Herculean efforts, there are, to this date, no efficacious targeted therapies for TNBCs [70]. However, with rapid evolution in personalized medicine, the identification of transmembrane receptors that drive the biology of TNBCs, becomes more feasible, thereby guiding the development of targeted therapeutics and companion diagnostics with predictive value for TNBC patients [71,72].

1.3 Non-targeted therapy in breast cancer treatment

1.3.1 Chemotherapy

Chemotherapy – the oral or intravenous administration of cancer-killing drugs – remains the cornerstone of treatment for preventing recurrence in women with stage I-III breast cancer [73,74]. The term neoadjuvant chemotherapy (NAC) refers to chemotherapy given before locoregional therapy, which was shown to be effective in the management of buccal carcinoma more than 3 decades ago [75,76]. In the context of breast cancer, the initial aim of NAC was to achieve an immediate reduction in tumor burden, thereby expediting subsequent radical mastectomy or radiotherapy [77]. Eventually, with several studies pointing to no difference in survival between breast-conserving surgery and radiotherapy versus mastectomy, the use of NAC was extended to patients with locally advanced breast cancer, in view of increasing breast conservation rates [78–80]. On the other hand, post-operative chemotherapy, also known as adjuvant chemotherapy (AC), is increasingly advocated in the eradication of micro-metastatic disease (already present at the time

of surgery), with an accompanying reduction in recurrence rates and an improved long-term overall survival [81–83]. However, whether AC or NAC offers a more enhanced survival benefit in breast cancer patients, remains controversial [84,85] and several landmark studies have found that regardless of the sequence of chemotherapy (AC or NAC), there has been no significant difference in disease progression, disease-free survival or overall survival for any breast cancer subtype [84,86–88].

Cytotoxic chemotherapy for breast cancer has been used consistently in the 1970s, leading to the identification of several groups of antitumor compounds including alkylating agents (cyclophosphamide, thiotepa, L-phenylalanine mustard), antimetabolites (5-fluorouracil, methotrexate), vinca alkaloids (vincristine, vinblastine) and anthracyclines or antitumor antibiotics (doxorubicin, mitomycin), amongst others [89,90]. For early breast cancer, the current chemotherapy standards are the anthracyclines and taxanes, administered in combination or in sequence over a period of 18-24 weeks [91]. However, in the adjuvant setting, treatment with these 2 compounds, resulted in a rising number of female patients being pre-exposed to these agents, while presenting with metastatic disease, thus further complicating disease management [83]. For patients with TNBC, neoadjuvant anthracycline-taxane therapy is recommended, with the addition of platinum to further improve pathological complete response [91–93].

Interestingly, anthracyclines are among the most active chemotherapeutic agents for the treatment of breast cancer, as illustrated by multiple trials demonstrating its association with lower rates of breast cancer recurrence and improved survival as compared with chemotherapeutic regimens employing cyclophosphamide, methotrexate and fluorouracil [94]. By the year 2000, it was reported that the use of adjuvant anthracyclines was prominent in 70-80% of women younger than 70 years old [95]. Nonetheless, given its association with cardiac toxicity, there has been a decline in the use of anthracycline-based chemotherapy [96]. Although rare, this resulting congestive heart failure is known to be irreversible and may increase as the treatment progresses [97]. Based on these overriding drawbacks, there has been a general trend towards the investigation of taxane-based regimens as an alternative to anthracycline treatment [98]. Taxanes (paclitaxel, docetaxel) generally work by inhibiting microtubule disassembly, which in turn halts mitotic activity in

malignant cells [83]. While paclitaxel was identified to have significant activity against metastatic breast cancers in the 1990s, docetaxel appears to be the more active taxane, with a longer half-life, rapid cellular uptake and longer intracellular retention [83,99]. Unfortunately, taxane-based therapy is prone to drug resistance, particularly due to the overexpression of p-glycoprotein efflux pumps [100].

1.3.2 Surgery

Cancer surgery represents the oldest oncological discipline, dating back as far as ancient Egypt [101] and probably remains one of the frontline treatment modality for most cancers. With the introduction of robotics, laparoscopy and reconstructive surgical procedures to combat morbidity and mortality, there has been a major shift towards the preservation of form, function and quality of life [102]. More explicitly, modern cancer surgery aims to excise the tumor with a surrounding margin of healthy tissue, rather than cutting directly into the cancerous mass [102]. Unfortunately, such a delicate procedure necessitates the selection and integration of appropriate diagnostic methods and currently, x-rays, radiography and computerized tomography (CT) scanning are being used to allow determination of the exact location and extent of the tumor [103]. Undoubtedly, the challenge for surgeons has been to facilitate local control, while achieving optimum cosmesis and minimal rates of recurrence [102]. To this end, progress in surgical advances, coupled with the popular usage of AC and NAC, provides an optimistic climate that reduces morbidity and encourages the rate of breast-conservation and breast reconstruction for those undergoing mastectomy (complete removal of the entire breast) [84].

In the 1980s, most women with breast cancer were subjected to mastectomy (usually with axillary lymph node dissection), which resulted in a permanent disfiguring scar, forcing women to resort to the wearing of prosthesis, both of which had considerable repercussions on sexuality and femininity [102]. Furthermore, it is recognized that body disfigurement caused by surgery, will affect the emotional and psychological state of breast cancer patients, making them more prone to depression [104,105]. Common post-surgical morbidities include lymphedema, impaired shoulder mobility, and decreased upper extremity flexibility and strength [106,107]. Strikingly enough, some women with unilateral disease (cancer in one breast), opt for bilateral mastectomy to prevent

cancer development in the other breast, despite no clinical proof warranting additional survival benefit [108,109]. Several factors can affect the decision-making process and women's preferences for breast-conserving surgery (also known as lumpectomy) or mastectomy; these include tumor size, location, access to radiotherapy, socio-economic status, educational level, ethnicity, BRCA status and family history [110–115].

With the expanding arena of reconstructive techniques and the relentless innovation in plastic surgery, the rates of breast reconstruction following mastectomy are improving steadily, especially with several studies attesting to better quality of life and mental health experienced by women who adopted this procedure after mastectomy [116,117]. Nonetheless, these women showed higher levels of physical discomfort [118]. In contrast, breast-conservation surgery, which was made possible through the pioneering work of Fisher and Veronesi [78,119], has evolved and is now recognized as a safer alternative to mastectomy [120]. Early attempts at breast conservation involved wide excision of the tumor, often by removing a whole breast quadrant, without any restoration of breast contour [102]. However, with modern oncoplastic techniques, breast-conservation surgery is brimming with promise; surgeons are now able to excise up to 50% of the volume of the breast and still maintain breast shape and aesthetics through a complex array of intramammary flaps and pedicles [121].

As a consequence of such developments, cancer surgery is undergoing a period of renaissance, especially with the inception of personalized surgery. Precision surgery guided by intraoperative molecular imaging involving the use of dyes and isotopes, is in ebullition [122]. Whether or not these technologies will be affordable for routine clinical practice, however, remains to be seen.

1.3.3 Radiation therapy

With much credit attributed to Wilhelm Röntgen and Marie Curie for the discovery of x-rays and radioactive elements respectively, radiation therapy for the treatment of breast cancer was first made possible in the 1930s, with the use of radium needles and external-beam radiation therapy with orthovoltage x-rays [123,124]. It was initially either added to mastectomy to eradicate possible residual disease (in the breast, chest wall or underarm area), or used as an alternative to

surgery, particularly in high-risk areas where surgery could affect function and cosmesis [125]. Nowadays, breast-conservation surgery followed by radiation therapy, is a widely accepted standard approach, which has shown to reduce the risk of cancer recurrence by 50% at 10 years and the risk of breast cancer deaths by almost 20% at 15 years [120,126,127]. Moreover, women treated with this combination approach, had a greater likelihood of bilateral breast preservation at 10 years, as compared to women treated by breast-conservation surgery alone [128]. Despite these benefits, Hughes and colleagues have demonstrated that radiation therapy does not improve survival for older breast cancer patients (70 years of age and above) who have recourse to hormonal therapy, although it does reduce the risk of local recurrence [129]. Interestingly enough, studies have shown that there is an underuse of radiation therapy among younger women with early breast cancer; rates of radiation therapy receipt were around 85%, suggesting that 15% (or more than 1 in 8) women, do not receive standard of care treatment [130,131]. Some of the common reasons behind this tendency, range from improper patient selection, completion mastectomy (patients who received breast-conservation surgery and later a mastectomy), transportation/ambulatory issues and fear surrounding radiation toxicity [132].

In contrast, postmastectomy radiation therapy remains a popular approach in the management of advanced-stage breast cancer [133,134]. Although radiation is recommended for tumors greater than 5 cm or with more than 4 involved lymph nodes, postmastectomy radiation therapy is being applied more broadly, given its potential in preventing local recurrence [94,135]. However, despite the reduction in local and regional disease progression, the addition of radiation to mastectomy, has failed to provide the much-needed increase in survival and freedom from distant metastases [125]. Several important bottlenecks are associated with the use of postmastectomy radiation therapy; with the lack of advanced imaging technologies to detect local-regional disease progression, there is no way to ensure coverage of critical breast cancer targets or determine what volume of critical organs is exposed to radiation [125]. Unfortunately, non-targeted radiation therapy induces tissue injury on the chest wall, which can manifest as radiation dermatitis, edema, breast shrinkage, pulmonary fibrosis, secondary solid cancers and ischemic heart disease [136–140]. To this end, achieving the required clinical ideal, has resulted in the harnessing of three-dimensional CT imaging for the treatment planning of radiation therapy, while allowing the

development of new techniques that can deliver radiation to tumor cells more accurately, with fewer side effects and improved survival [141].

Accelerated partial-breast irradiation, which refers to radiation therapy given at higher doses over fewer days, may be effective as conventional therapy [142]. It can be administered as an external-beam, catheter-based (brachytherapy) or intraoperative radiation therapy [143]. External-beam radiation therapy (where radiation from an outside source is focused on the cancerous area) offers excellent target coverage and dose heterogeneity, but low conformality as compared to brachytherapy, which may increase radiation exposure to the uninvolved ipsilateral breast, skin, heart and lungs [144]. Fortunately, intensity-modulated radiotherapy and tomotherapy for CT guidance may assist in resolving these issues [145]. Brachytherapy, on the other hand, employs the use of catheters that can be inserted in the excision cavity remaining after breast-conservation surgery and while they reduce exposure to normal tissues, infection associated with such treatment, is not completely avoided [143]. Intraoperative radiation therapy represents the ability to deliver a single large therapeutic dose of radiation directly to the tumor bed during surgery [144]. Its advantages are manifold; it alleviates the need for a prolonged course of treatment, which ultimately reduces financial burden and psychological distress caused to patients [146]. The rationale for such a procedure, is based on the finding that approximately 85% of breast relapses are confined to the same quadrant of the breast as the primary tumor [147]. In spite of showing no increase in postsurgical complication rates following the use of intraoperative radiation therapy, Veronesi *et al*. (2003) suggest that longer follow-ups are needed to assess cosmetic outcomes, which may be impaired by fibrotic changes in the breast tissue after a high-dose irradiation [146].

1.3.4 Photodynamic therapy

Photodynamic therapy (PDT) is a minimally invasive therapeutic modality used for the management of a variety of cancers and benign diseases [148]. It relies primarily on the uptake of a light-absorbing chemical substance, also known as a photosensitizer (PS), which upon being excited by light at a defined wavelength, reacts with oxygen to generate oxidant species (such as radicals, singlet oxygen and triplet species) in target tissues, leading to cell death [149,150]. The overarching cytotoxic potential of PDT has been established to arise from the oxidation of a large

array of biomolecules in cells (nucleic acids, lipids and proteins), culminating to severe alteration in cell signaling cascades or gene expression regulation [151,152]. Nowadays, new evidence is underscoring the potential of PDT in inducing immunity against recurrence, while destroying distant metastases with minimal side-effects and reduced long-term morbidity, thus providing additional advantages over existing treatments such as chemotherapy and radiotherapy [153,154].

As mentioned previously, the successful use of PDT requires the simultaneous presence of 3 important components: the PS, molecular oxygen present in the tissues and visible or near-infrared radiation, none of which is particularly toxic or cell-damaging on its own [148]. Following systemic or topical administration of the PS, its uptake into malignant tissue remains crucial; without achieving optimum tissue concentration, exposure to light (usually done over a pre-determined period) will not ensure effective treatment [154]. Interestingly, PDT can exert its oxidative effects through 2 distinct mechanisms (Figure 2). The absorption of a photon of light by the PS leads to a photochemical reaction, which allows elevation of the PS molecule from its ground state (S_o) to an excited state (S_1) [153–155]. For this purpose, the optimum wavelengths for the transmission of light to the desired area, lie between 600-800 nm; across this range, major components of living tissue (water, haemoglobin in blood and protein) have low absorption, which allows more efficient light transmission [154,156]. Subsequently, transition of the PS from the singlet S_1 state to the triplet T_1 excitable state, allows the PS to transfer this energy to biomolecules or to oxygen molecules, to generate reactive oxygen species (ROS) (Type I mechanism) or highly reactive singlet oxygen (Type II mechanism) respectively [154,157].

Strangely enough, it is assumed that type II reaction is the most important process governing the efficiency of PDT [157]. However, several factors may affect the ratio of contribution of both mechanisms, including oxygen concentration, pH, tissue dielectric constant and PS structure [157]. As the oxygen starts to deplete, the first type of mechanism begins to prevail [158]. Through the generation of a diverse palette of oxygen species, destruction of tumor cells is achievable through the synergistic action of different types of cell death. Nonetheless, this is highly dependent on the intracellular location of the PS; mitochondrial damage can lead to apoptosis, cell membrane destruction induces necrosis, and damage to lysosomes or endoplasmic reticulum can give rise to

autophagy [159–161]. Additionally, damage to tumor vasculature can compromise the supply of oxygen and essential nutrients, as well as activate the immune system by inducing an inflammatory and immune response against tumor cells [157,162,163]. In other words, the induction of multiple cell killing mechanisms, represents a formidable characteristic of PDT, since it can increase photodestruction of tumor cells harboring resistance to a particular cell death pathway [164].

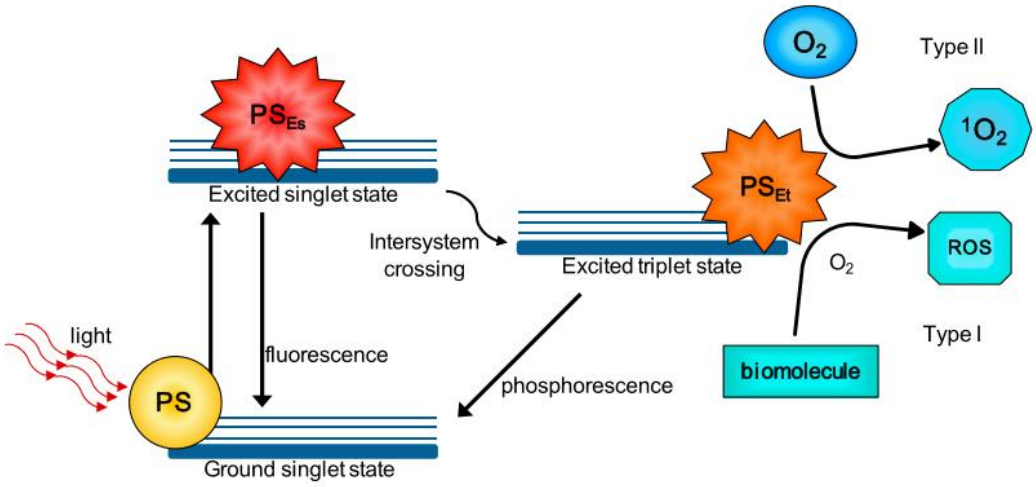

Figure 2: Principle of photodynamic therapy. Following light absorption, the photosensitizer reaches an excited singlet state. Transition to the triplet excited state, allows (1) reaction with biomolecules to generate radicals, which react with molecular oxygen to generate reactive oxygen species through type I reaction, or (2) direct reaction with oxygen to form singlet oxygen species via type II mechanism [155].

Fortunately, the described photocytotoxic reactions occur primarily in the area of PS distribution, thereby enabling selective destruction [165]. Moreover, as compared to normal tissues, tumors can preferentially retain a larger concentration of the PS when administered intravenously [154]. Reasons for such biodistribution may be the leaky vasculature and poorer lymphatic drainage of tumors, or the tendency of PSs to combine with low density lipoproteins which are abundant in actively dividing cancer cells [154,157,166]. Due to their photochemistry and uptake properties, currently only a few PSs are officially approved worldwide and used clinically [153]. As such, PSs used for preclinical and clinical application in the context of breast cancer, are listed in Table 1. In 1993, Porfimer sodium (sold as Photofrin), was the first PS approved for PDT of bladder cancer by the Canadian Health Agency [153]. Eventually, it was approved by the Food and Drug Administration (FDA) for the treatment of various types of malignancies, including lung, esophageal, gastric, cervical and breast cancer [167,168]. Despite showing efficacy as a good PS,

Photofrin exhibits certain shortcomings that limit its clinical application; it has low chemical purity (it is a mixture of over 60 molecules), poor tumor penetration, long half-life and high accumulation, which results in skin hypersensitivity to light for several weeks [157,169,170]. The disadvantages of 1st generation PSs thus provided an incentive for the investigation of new compounds, which led to the development of second generation PSs [171–173].

Table 1: Photosensitizers investigated for use in breast cancer treatment

Photosensitizer (PS)	Treatment wavelength (nm)	Stage of development	References
Porfimer sodium (Photofrin)	630	*1st generation PS* FDA approved but in clinical trial for breast cancer skin metastases	[168,174]
Verteporfin (Visudyne)	690	*2nd generation PS* Clinical trial for primary breast cancer	[172,175]
SnEt2 (Purlytin)	660	*2nd generation PS* Phase II clinical trial	[171]
Motexafin lutetium (Lutex)	720	*2nd generation PS* Phase I clinical trial	[172]
mTHPC (Temoporfin)	652	*2nd generation PS* Approved for the treatment of squamous cell carcinoma and lung cancers	[154,156]
NPe6 (Talaporfin)	660	*2nd generation PS* Clinical trial for breast cancer skin metastases	[173]
Zinc phthalocyanine	675	*2nd generation PS* Not currently used	[176]

Temoporfin (mTHPC) was the second PS to be granted approval for the treatment of advanced head and neck squamous cell carcinomas [177,178]. Given its promising activity, it was tested in various other cancers (breast, pancreatic and prostate) but the results varied considerably [179–181]. For breast cancer patients, Temoporfin-based PDT seemed effective, coupled with minimal-invasive and few side effects [180]. Similarly, Visudyne is another 2nd generation compound indicated for the treatment of cutaneous metastases in breast cancer [172,175]. Despite its poor water solubility, Visudyne exhibits high tissue penetration at 690 nm, with an optimum concentration lasting between 30-150 minutes and complete clearance at 48 hours [154]. Purlytin (a chlorine PS), Talaporfin and Lutex have also been assessed in the treatment of breast cancer metastases, recurrence and mammary skin lesions [171–173].

Another area of active interest has been the investigation of PDT treatment in combination with adjuvant radiotherapy and chemotherapy. For instance, several *in vitro* studies warrant a synergism between PDT and ionizing radiation in killing breast tumor cells [174,182]. The use of indocyanine green as a PS in conjunction with low dose radiotherapy, has shown to be effective at reducing the percentage of viable cancer cells, while partially abating the adverse effects of PDT [182]. Following this same strategy, PDT has been combined with traditional chemotherapy, in view of potentiating therapeutic outcomes associated with the use of low-dose treatments, thus concurrently minimizing side effects and reducing the risk of drug resistance [162]. For example, cisplatin, a chemotherapeutic drug which is infamous for its severe adverse reactions, has been combined (in low doses) with indocyanine green-based PDT and the results demonstrated reinforcement of therapeutic efficacy as compared to each therapy alone [183]. Likewise, the combination of Temoporfin and 5-fluoro-2'-deoxyuridine gave rise to lower cell survival in MCF-7 breast cancer cells as opposed to the corresponding single-mode therapy [184]. Research conducted by two independent groups on the *in vitro* and *in vivo* effects of doxorubicin and PDT on breast cancer, further supports the concept of the enhanced antitumor effects arising from this combination strategy [185,186].

PDT as a therapeutic intervention has been shown to improve patient's quality of life and reduce medical costs as compared to palliative surgery and chemotherapy regimens [187,188]. However,

several factors may considerably hamper PDT treatment outcomes and its transition into clinical practice. These include: rapid depletion of oxygen levels in tumorigenic tissues [189,190], limited penetration of light [153], finding the optimal light dose regimes [162,191], avoiding skin photosensitivity [154] and pain [162], incomplete tumor elimination and presence of PDT-resistant tumors [153]. Therefore, it comes as no surprise that PDT in breast cancer is still at preliminary stages of research [154]. Further clinical studies are thus required for PDT to be accepted as a standard first-line treatment (either alone or in combination) for a wide variety of tumors, including breast cancer.

1.4 Targeted (antibody-based) therapy of breast cancer

1.4.1 Overview: Monoclonal antibodies as therapeutic agents in oncology

More than a century ago, Paul Ehrlich postulated that a 'magic bullet' could be used to selectively target disease [192]. This vision became more practical with the advent of hybridoma technology (by Köhler and Milstein in 1975), which allowed the production and engineering of unlimited quantities of highly specific monoclonal antibodies (mAbs) [193]. Indeed, the use of mAbs as therapeutics has been receiving considerable attention by the pharmaceutical industry, with approximately 80 mAbs approved by the FDA (as of May 2018) for various indications, including cancer and immunological diseases [194,195]. These therapeutic antibodies are generally of the immunoglobulin G (IgG) isotype and possess the same basic structure (Figure 3). IgG molecules are large heterodimeric proteins with a molecular weight of ~150 kDa and are comprised of 2 identical heavy chains and 2 identical light chains (held together by disulfide bonds), each composed of variable (V_H and V_L) and constant domains (C_H and C_L) [196]. The variable region contains the complementarity determining regions (CDRs) which are the major site of interaction with the target antigen [197]. Altogether, the IgG molecule is divided into 3 functional domains; 2 antigen-binding domains (Fab) connected by a highly flexible hinge domain to the fragment crystallizable (Fc or effector) domain of the antibody, which can interact with a variety of cell surface receptors, as well as components of the complement system [196,197]. Through the selective recognition of antigens that are preferentially expressed on tumor cells, mAbs may exert antitumor effects through various mechanisms, including apoptosis, antibody-dependent cellular

cytotoxicity (ADCC), blocking growth factor receptors and complement-mediated cytotoxicity [198].

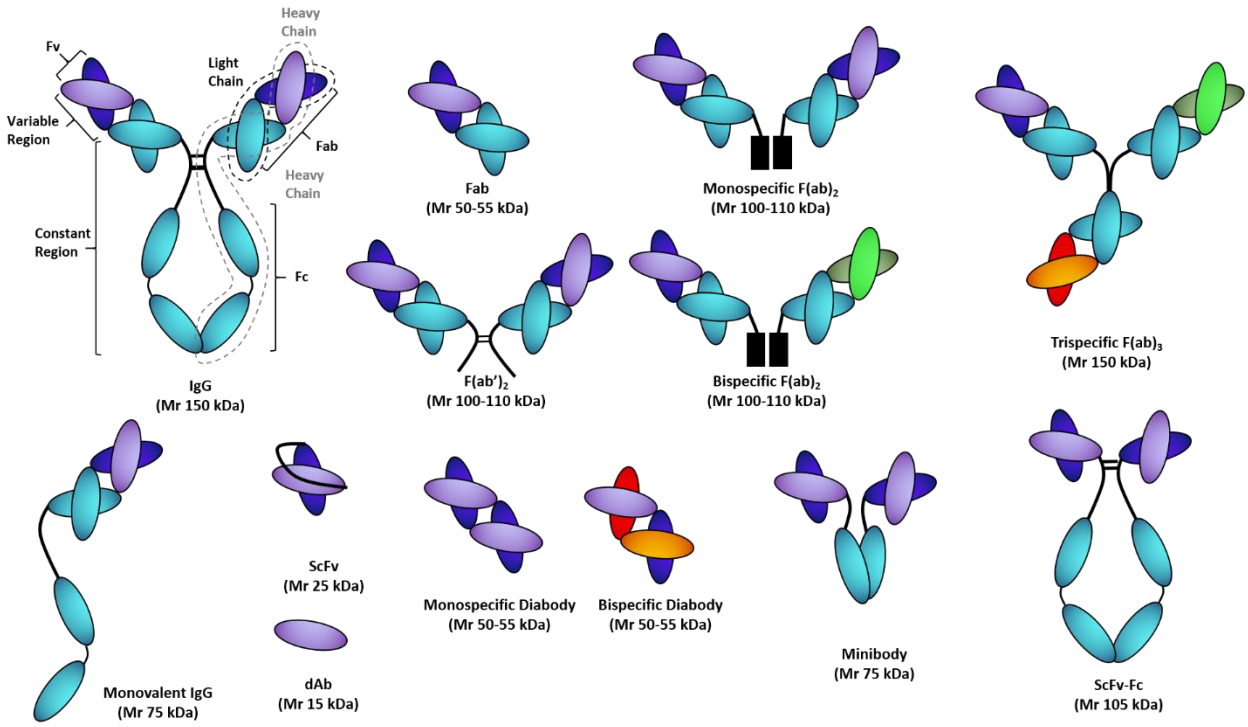

Figure 3: Schematic diagram depicting structure of an IgG molecule and a variety of engineered antibody formats. Recombinant antibody technology and phage display techniques have allowed the generation of various antibody formats with varied affinity and specificity (Source: tebu-bio.com, 2018).

While initial trials with mAbs produced quite startling results [199], various challenges became apparent. Most of these mAbs were derived from mice and patients exposed to them developed human anti-mouse antibody (HAMA) responses, which considerably restricted the number of treatments that could be safely administered [200]. To mitigate these shortcomings, molecular engineering techniques enabled CDR-grafting to generate chimeric and fully humanized antibodies [197]. Moreover, alleviating barriers to antibody distribution in tumor cells, encouraged the enzymatic cleavage of IgG molecules into smaller functional fragments (Fab and $F(ab')_2$), as well as harnessing the advantages of antibody technology to engineer a variety of recombinant antibody formats (Figure 3) [197]. As such, single-chain variable fragments (scFvs) (composed of peptide-linked V_H and V_L domains) – known for their small size (~25 kDa), rapid renal elimination and highly specific tumor localization – are emerging as key players in the field of targeted anticancer therapeutics by fostering the development of immunotoxins (ITs) and human cytolytic

fusion proteins (hCFPs) [71,201]. In contrast, to improve their killing activity, mAbs are being armed with potent cytotoxic drugs, giving rise to antibody-drug conjugates (ADCs) [202].

1.4.2 Anti-HER2 antibody-based therapies

For a long time, only ER and PR were available as biological markers guiding targeted treatment options in breast cancer and the use of endocrine therapy (involving chemical compounds acting as receptor agonists or antagonists) in combination with chemotherapy, failed to show considerable utility in the management of cancer [203]. These limitations aroused significant research interest in the discovery of potential therapeutic markers and one such promising marker is the HER2 oncogene. HER2 (also known as c-erbB-2) is a transmembrane receptor which belongs to a family of epidermal growth factor receptors (EGFRs) with tyrosine kinase activity [204]. This family of receptors is responsible for the growth and differentiation of many normal and transformed epithelial cell types [205]. HER2 is an attractive target since it is overexpressed in 20-30% of ductal breast tumors and this overexpression is associated with reduced median survival as compared to women with normal tumor expression of HER2 [37]. In September 1998, Trastuzumab (Herceptin), a humanized mAb directed against the extracellular domain of HER2, was approved for the treatment of metastatic breast cancer patients (exhibiting HER2 overexpression) and therefore marked an important milestone in breast cancer treatment [206,207]. After binding to HER2, Trastuzumab induces its antitumor effects via the activation of ADCC and the suppression of HER2 homodimer signaling [204]. Additionally, its binding may interfere with HER2-mediated downstream signaling processes such as cell proliferation, angiogenesis and DNA repair [208]. Trastuzumab therapy is generally well-tolerated and produces a significant clinical benefit when used in combination with chemotherapy in the adjuvant and neoadjuvant settings [209,210]. Unfortunately, its concurrent use with anthracyclines resulted in an increase in cardiac dysfunction [211]. Moreover, when used as a single agent or in combination therapies, Trastuzumab resistance is not avoided [204]. While this phenomenon is not completely understood [204], an additional mAb-based approach against HER2 was developed (Pertuzumab), along with a myriad of small-molecule (kinase) inhibitors including Lapatinib, Neratinib, Gefitinib and Afatinib [212–216]. Despite significant clinical responses reported with the combined application of Trastuzumab and Pertuzumab [217,218], the growing list of adverse reactions (Table 2) are

pointing to the need to capitalize on the development of ADCs (example: Kadcyla) and bispecific antibodies such as Ertumaxomab (bispecific antibody targeting HER2 and CD3) [219].

Table 2: FDA-approved monoclonal antibody-based therapy for breast cancer

Type of mAb therapy	Name of drug	Most common treatment-related adverse reactions	References
Anti-HER2 antibody therapies	Trastuzumab	Chills, fever, pain, nausea, asthenia, cardiac dysfunction	[220]
	Pertuzumab	Diarrhoea, nausea, fatigue, vomiting, asthenia, back pain	[218]
Immune checkpoint inhibition	Atezolizumab (Tecentriq)	Pneumonitis, hepatitis, colitis, endocrinopathies, fatigue, nausea, diarrhoea, vomiting, constipation, cough, decreased appetite	[221]
Antibody-drug conjugates	Trastuzumab emtansine (Kadcyla)	Severe thrombocytopenia, fatigue, anaemia, nausea, haemorrhage, abdominal pain, pyrexia, pain, vomiting, dyspnoea	[222,223]
	Trastuzumab deruxtecan (Enhertu)	Nausea, fatigue, vomiting, alopecia, constipation, decreased appetite, anaemia, neutropenia, diarrhoea, leukopenia, cough, thrombocytopenia	[224]

1.4.3 Immune checkpoint blockade

The immune system can be regarded as a double-edged sword in cancer; on the one hand, immune cells can mediate antitumor immunity and on the other hand, they can also promote tumor progression and shape malignant disease [225]. Given their ability to recognize and destroy pathogen-infected or aberrant cells (such as cancer cells), activated CD8+ (cytotoxic) T-cells are

considered as the main effectors of cell-mediated immunity [212]. Their activation and maturation are dependent on 2 critical signals: (1) an antigen-specific signal provided through the interaction of the T-cell receptor (TCR) with major histocompatibility complex (MHC) class II expressed on the surface of antigen-presenting cells (APCs), and (2) co-stimulatory signals resulting from the engagement of T-cells with co-stimulatory molecules present on the membrane of APCs [226]. The resulting response and specifically its amplitude and duration, are tightly regulated by a balance between co-stimulatory and inhibitory signals [227,228]. These inhibitory pathways, also known as immune checkpoints, are central to the maintenance of self-tolerance and the reduction of collateral tissue damage [204]. Unfortunately, tumors can resist (or evade) immune attack through the dysregulation of these immune checkpoints within the tumor microenvironment [204,212]. Therefore, immune checkpoint blockade represents one of the most promising approaches to activate therapeutic antitumor immunity [227,229].

On account of their pivotal role during immune response and peripheral tolerance, both cytotoxic T-lymphocyte-associated protein 4 (CTLA-4) and programmed cell death protein 1 (PD-1)/programmed-death ligand 1 (PD-L1) pathways have been actively studied, resulting in the approval of a number of CTLA-4 and PD-1/PD-L1 checkpoint inhibitors [212]. Ipilimumab, an IgG1 antagonistic CTLA-4 antibody, was the first to receive FDA approval as monotherapy for the management of advanced melanoma [212,230]. Nonetheless, it is still being actively evaluated for its safety and clinical efficacy in early and advanced-stage breast cancers [231,232]. In March 2019, the humanized anti-PD-L1 mAb Atezolizumab or Tecentriq (when used in combination with the chemotherapeutic drug Abraxane), was approved for the treatment of triple-negative, metastatic breast cancer patients demonstrating PD-L1 protein expression [212,233]. The overarching principle for such therapy, relies primarily on the fact that PD-1 (expressed on immune cells) binding to its ligand PD-L1 (expressed on tumor cells), promotes the dephosphorylation of T-cell receptor proximal signal components and leads to the inhibition of signaling pathways regulated by protein kinases (PI3K/PTEN/CK2/RAS/MEK/ERK), culminating in decreased T-cell proliferation, survival and cytokine production [234]. Therefore, by disrupting the interaction between PD-1 and PD-L1, checkpoint inhibitors can restore antitumor immune responses and promote the elimination of tumor cells [235].

Approximately 20% of TNBC patients overexpress PD-L1, indicating that PD-1/PD-L1 signaling is indeed a promising therapeutic target in breast cancer [236]. However, despite the addition of Atezolizumab to the armamentarium of approved breast cancer therapies, it is important to note that modest objective response rates were observed with this anti-PD-L1 checkpoint inhibitor (53% versus 33% for the placebo group), including immune-mediated serious adverse events (Table 2) that could cause treatment discontinuation [221,237]. Consequently, the future of immune checkpoint blockade in breast cancer will undoubtedly depend on the identification of reliable biomarkers that play an important role in immune evasion, along with the combination of immune checkpoint modulators with more traditional anticancer therapies (chemotherapy and radiation therapy), in order to achieve more favorable treatment outcomes [225].

1.4.4 Antibody-drug conjugates

ADCs are complex engineered therapeutics, designed as a pharmaceutical answer to the oncologists' demand for high precision weapons that can target tumor cells with reasonable efficiency and specificity [238]. They are composed of mAbs (which recognize tumor-associated antigens on target cells) conjugated to a cytotoxic payload via a chemical linker [239]. This intelligent delivery system thus allows harnessing of the cytocidal activity of chemotherapeutic agents (which are generally too toxic on their own to be systemically administered), while reducing off-target toxicities by limiting drug exposure to normal tissues [240]. Early work in ADC development was hampered by a number of pharmacological and safety considerations, culminating in a decline in the popularity of this approach [238,241,242]. With the realization that diverse aspects of ADC design were initially overlooked [243], substantial technological advancements are now prompting renewed enthusiasm for this class of therapeutics, through improvement of the antibody moiety, the chemical linker and the toxic payload [244,245]. Indeed, an eloquent testament underpinning the challenges faced in ADC development, is the result of approximately over 3 decades of research which has resulted in the clinical approval of only 11 ADCs: Gemtuzumab ozogamicin (Mylotarg), Brentuximab vedotin (Adcetris), Trastuzumab emtansine (Kadcyla/T-DM1), Inotuzumab ozogamicin (Besponsa), Polatuzumab vedotin-piiq (Polivy), Enfortumab vedotin (Padcev), Trastuzumab deruxtecan (Enhertu), Moxetumomab pasudotox (Lumoxiti), Sacituzumab govitecan (Trodelvy), Belantamab mafodotin-blmf (Blenrep)

and Loncastuximab tesirine-lpyl (Zynlonta) [246]. Among these agents, Trastuzumab emtansine and Trastuzumab deruxtecan have been approved (in 2013 and 2019 respectively) for unresectable or metastatic HER2-positive breast cancer patients who do not respond to prior anti-HER2-based regimens or to chemotherapy [247,248].

The 3 structural components of an ADC (Figure 4), namely the antibody, the linker and the cytotoxic warhead (as well as the bioconjugation method or the way the components are assembled), altogether dictate the overall biophysical and physiological properties of the ADC molecule, highlighting their significance in effective ADC design [238,240]. Firstly, selection of the mAb moiety, is highly dependent on the identification of unique target antigens that should fulfill several important requirements: (1) high expression in tumor cells and minimal or no expression in healthy tissues, (2) surface expression on tumor cells for ease of access to the circulated mAb, and (3) possess internalization properties to facilitate ADC transport into the cell and enhance efficacy of the toxic payload [249–251]. In contrast, the mAb should display high specificity and binding affinity to the tumor cell-surface antigens, good retention, low immunogenicity and low cross-reactivity [252–254]. Similarly, the chemical linker represents an essential structural component of ADCs; it is instrumental in forming the connection between the antibody and the toxic payload. Therefore, the linker should be stable in circulation to prevent premature release of the drug in off-target tissues, yet permit effective release of the killing agent after internalization and trafficking in specific subcellular compartments have occurred [255–257]. Linkers can be broadly classified into 2 main groups; cleavable and non-cleavable linkers [258]. More explicitly, non-cleavable linkers (often containing a thioether bond) require complete lysosomal proteolytic degradation of the mAb before release of the drug into the cytosol [242]. Trastuzumab emtansine, consisting of Trastuzumab conjugated via a non-reducible thioether linkage to the DM1 cytotoxic drug, demonstrates one of the successful examples of ADCs using a non-cleavable linker [259]. On the other hand, cleavable linkers contain a site between the payload and the point of antibody attachment, where cleavage will occur based on environmental differences (redox potential, pH) and the action of specific lysosomal enzymes [244,258]. As outlined by Khongorzul and colleagues (2019), there are various types of cleavable linkers [254], but most importantly, Trastuzumab deruxtecan encompasses a tetrapeptide-based cleavable linker,

which accounts for better stability in systemic circulation [260]. The choice of the ADC cytotoxic payload is also not random; the ideal ADC warhead should exhibit *in vitro* subnanomolar half maximal inhibitory concentration (IC_{50}) values, sufficient solubility in aqueous environments, low molecular weight, long half-life and low immunogenicity, while allowing for proper conjugation to the linker without abrogating the internalization property of the mAb (but instead promote its antitumor effects) [261–263]. There are essentially 2 main categories of warheads employed in ADC configuration; these are microtubule-disrupting agents (auristatins, maytansinoids) and DNA-damaging agents (calicheamicin, duocarmycin, doxorubicin) [254]. As such, Trastuzumab emtansine exploits the activity of DM1 (also known as mertansine, a derivative of maytansine), which has the ability to inhibit tubulin polymerization, resulting in mitotic arrest and cell death [264]. In opposition, Trastuzumab deruxtecan consists of Trastuzumab covalently linked to a topoisomerase I inhibitor payload (DXd, a derivative of the camptothecin analogue exatecan) [248]. The increasing success rate of such agents are based on their ability to inhibit topoisomerase-DNA complexes, leading to the inhibition of DNA replication, cell cycle arrest and ultimately apoptosis [260].

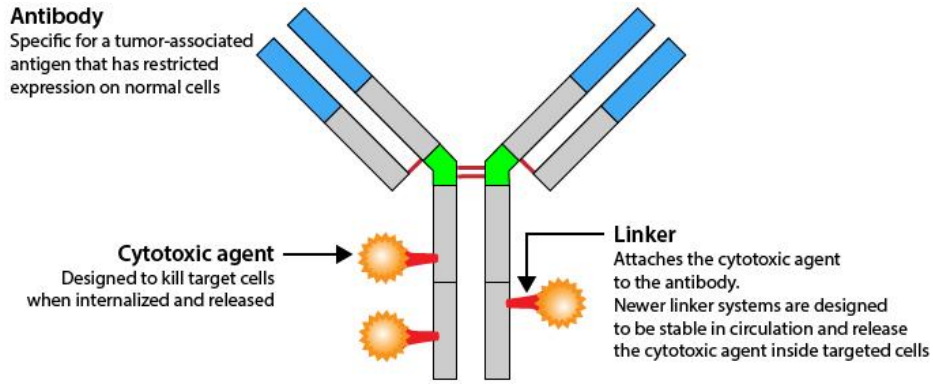

Figure 4: Structural composition of an antibody-drug conjugate. Antibody-drug conjugates are generally composed of 3 critical components: a humanized monoclonal antibody, bound to a cytotoxic drug, using a cleavable/non-cleavable chemical linker. Also shown are key properties of each structural component (Source: chromacademy.com, 2020).

Trastuzumab emtansine was first approved on the basis of 2 phase III randomized clinical trials, which provided enough data to corroborate the increase in progression-free survival and overall survival associated with its use in metastatic breast cancer patients [265,266]. The linkage of DM1 to Trastuzumab, with an average of 3.5 drug-to-antibody ratio (DAR), allows the selective

targeting of malignant cells over a wider therapeutic window [259]. In fact, in addition to DM1-mediated tubulin inhibition, Trastuzumab emtansine has also been shown to retain the activities of Trastuzumab mAb, which includes the abolition the HER2 signaling pathways, inhibition of HER2 ectodomain shedding and Fc-mediated immune responses (Figure 5) [267,268]. However, despite significant improvement in treatment outcomes, several adverse effects are common (Table 2) and a substantial fraction of patients are refractory to Trastuzumab emtansine therapy, owing to the phenomenon of inherent and acquired resistance [222,223,265,266]. As extensively described by Hunter *et al*. (2019), various potential resistance mechanisms have been recognized; reduced HER2 expression, reduced T-DM1 binding, dysregulated PI3K signaling and the increased expression of drug efflux transporters, amongst others [268].

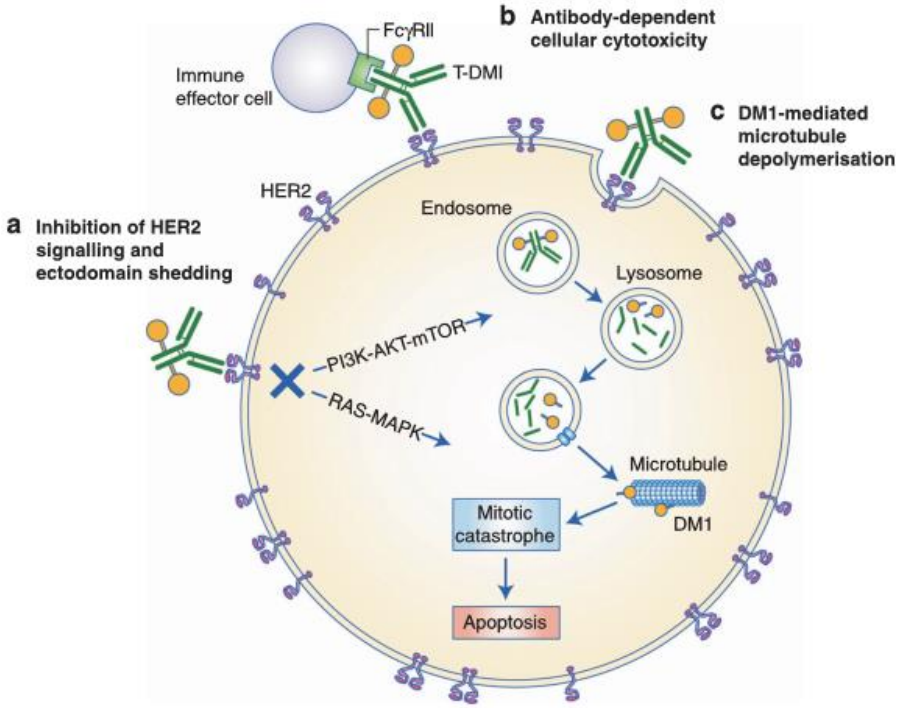

Figure 5: Mechanism of action of Trastuzumab emtansine. Trastuzumab-DM1 exerts its antitumor effects via at least 3 distinct types of mechanisms: (a) HER2 signaling blockade and inhibition of ectodomain shedding, (b) Fc-mediated immune responses (example: antibody-dependent cellular cytotoxicity) and (c) DM1 payload-mediated microtubule poisoning [268].

To this end, various strategies have been implemented to obviate T-DM1 resistance, including the use of combination therapies (tyrosine kinase inhibitors and immune checkpoint blockade) to target molecules implicated in the loss of DM1 sensitivity [269]. Most importantly, alternative

linker-payload chemistries have been sought to generate more effective 2nd generation anti-HER2 ADCs (example: Trastuzumab deruxtecan and Trastuzumab duocarmazine) [268]. Trastuzumab deruxtecan achieves a higher DAR than T-DM1 (7.7 versus 3.5) which allows for greater payload delivery per antigen engagement, together with improved homogeneity in conjugation [260]. Moreover, Trastuzumab deruxtecan has shown promising activity in T-DM1-resistant cell lines and patient-derived xenograft models, as well as in tumors exhibiting low sensitivity to T-DM1 because of their reduced HER2 expression [270,271]. Despite the occurrence of adverse reactions (Table 2), Trastuzumab deruxtecan is being venerated for its activity in tumors that have progressed despite prior T-DM1 therapy. Plausible explanations for this robustness might be firstly the difference in linker-payload chemistry which would reduce the likelihood of resistance mechanisms that are specific to DM1 [272]. Secondly, the DXd payload might not be efficiently removed from the cell by drug efflux pumps (as compared to DM1) [270]. Thirdly, Trastuzumab deruxtecan (but not T-DM1) is known for its bystander effect, whereby neighbouring HER2-negative cells can be subjected to DXd cytotoxicity [273]. This process may also be effective in the destruction of resistant clones that would otherwise require a targeted delivery approach for their removal [268].

1.5 SNAP-tag technology as a novel antibody-drug conjugation method

In the ADC development landscape, most conjugation methods available to arm mAbs to effector molecules rely on the direct functionalization of lysine side chains or the reduction of disulfide bonds to generate reactive sulfhydryl groups [274]. Although these methods are widely used, they give rise to a heterogeneous mixture of ADC products (ranging from 0 to 8 DAR), each with different pharmacokinetic and toxicity profiles [275]. This is primarily due to the abundance of cysteine and lysine side chains in a typical antibody, which may give rise to hundreds and millions of conjugation variants respectively [274,276]. As demonstrated by Hamblett and colleagues (2004) who studied the therapeutic efficacy of heterogeneous ADCs, the key design parameter for ADCs is the number of drug molecules attached to the antibody [277]. Based on these premises, several site-specific conjugation methods have been developed, which could easily be implemented as a result of the impact of genetic engineering in the production of various recombinant antibody formats bearing unique modifications to allow for specific coupling

reactions [278–280]. To this end, self-labeling proteins such as human alkylguanine-DNA alkyltransferase (AGT) (SNAP-tag and CLIP-tag) and bacterial haloalkane dehalogenase enzymes (Halo-tag), have emerged as efficient site-specific conjugation strategies that allow the sustainable production of homogeneous conjugate preparations [281,282].

SNAP-tag is an engineered version of the human DNA repair enzyme AGT which can react specifically with O(6)-benzylguanine (BG)-modified substrates via irreversible transfer of an alkyl group to a cysteine residue (Figure 6) [283,284]. In a normal setting, wild type AGT serves as a protection mechanism by maintaining DNA integrity; it scans DNA for alkyl adducts and removes them from the O^6 position of guanines and the O^4 position of thymine, resulting in its degradation [285]. Exploiting this activity thus led to the application of phage display to select for an AGT mutant (SNAP-tag) with higher reactivity towards O(6)-BG-modified molecules [286]. Further optimization of its properties was also carried out as follows: (1) incorporation of additional mutations to reduce its natural binding to DNA, (2) deletions were made to reduce its size and (3) removal of 2 non-fundamental cysteines to facilitate folding under oxidative conditions [285,287]. Therefore, the resulting product, most commonly known as SNAP-tag, is composed of 182 amino acids and its activity is at least 50 times higher than wild type AGT [286–288]. On that account, SNAP-tag can be fused to virtually any protein of interest (from the N- or C-terminus [289]) to allow for the rapid and well-defined autocatalytic labeling (under physiological conditions) with a predictable 1:1 stoichiometry [287,290].

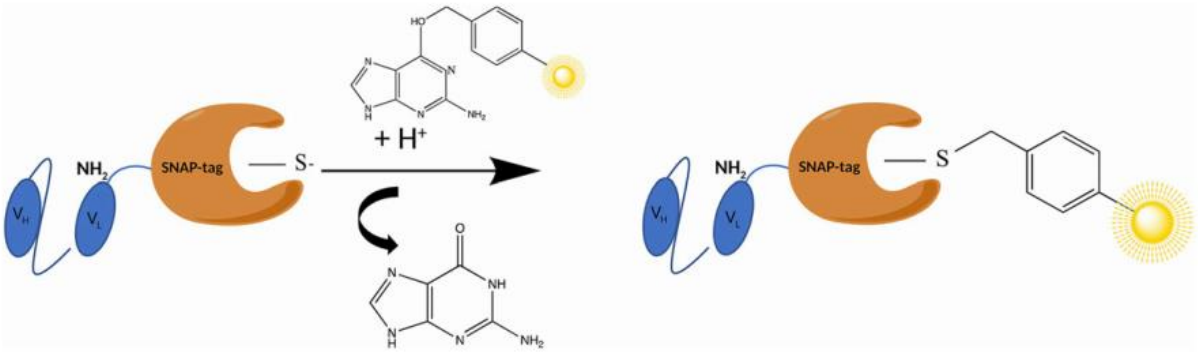

Figure 6: Site-directed modification of a recombinant single-chain antibody fragment using SNAP-tag technology. SNAP-tag reacts with para-substituted O(6)-BG derivatives (example: BG-modified photosensitizers) through a nucleophilic substitution reaction while releasing free guanine [291].

The advantages of using this technology are manifold: (1) being derived from a human enzyme, SNAP-tag reduces the risk of immunogenicity-related unwanted immune responses, (2) the simplicity of the reaction conditions (can be carried out under physiological conditions at room temperature with no additional activating substances), (3) the selective nature of the conjugation (reacts only with BG substrates) and (4) the availability of a wide range of BG linkers and molecules [285–287,290,292]. SNAP-tag has thus been applied in a variety of experimental systems, including *in vitro* imaging, live animal imaging, protein isolation and purification, determination of protein-protein interactions and the generation of recombinant ADCs, amongst others [274,286,293–295]. In the last 15 years, SNAP-tag has been genetically fused to ligands binding to specific cell-surface receptors, as well as recombinant antibodies (scFvs) targeting tumor-associated antigens [285,296]. Results from these studies indicated that these SNAP-tag fusions could be expressed efficiently (in large quantities) in mammalian systems, with retention of their antigen-binding properties [296]. After conjugation with BG-modified fluorescent dyes (example: BG-Vista Green, BG-Alexa Fluor 647, BG-Alexa Fluor 488), the authors were able to show specific accumulation of the resulting imaging probe at the tumor site at 10 hours post-injection [296]. Additionally, the relatively small size of such probes, fosters rapid and efficient renal clearance, which is considered advantageous for imaging and diagnostic applications [297]. As exemplified by Hussain *et al*. (2011) with the use of BG-chlorin e6 (a potent PS), this technology is not limited to a single class of effector molecule and undoubtedly represents an attractive agent for cancer detection and cell-specific drug delivery [298].

1.6 Auristatin F: A potent microtubule-targeting agent in recombinant ADCs

In the late 1970s, extensive research of marine life forms resulted in the discovery of dolastatin 10, a powerful antineoplastic agent and microtubule inhibitor, which was extracted from the sea hare *Dolabella auricularia* [299]. Dolastatin 10 showed the highest cytotoxic activities against human cancer cell lines, which spurred its advancement in a number of clinical studies [300,301]. However, with no significant activity observed at the maximum tolerated dose (MTD) [302–304], improving its *in vivo* efficacy led to the development of fully synthetic dolastatin 10 derivatives, termed auristatins. Auristatins are important payloads used in the burgeoning ADC pipeline; approximately one third of ADCs in clinical trials employ the monomethyl auristatin analogues E

and F (MMAE and MMAF/AURIF) [305,306]. In contrast to MMAE, AURIF exhibits lower membrane permeability and can be conjugated via non-cleavable linkers, without abrogating the cytotoxic activity [307]. They usually exhibit 10 times higher potency than doxorubicin or vinblastine, with robust activity towards multi-drug resistant tumors [308]. These agents have the ability to inhibit microtubule assembly and tubulin-dependent guanosine triphosphate (GTP) hydrolysis, resulting in cell cycle arrest (in the G2/M phase) and apoptosis [309,310]. Additionally, they can stimulate an immune response towards cancerous cells, induce immunogenic cell death and also promote intratumoral vascular damage [311]. The quest of harnessing these advantages while overcoming the bottlenecks of ADC production, thus led to the application of SNAP-tag technology in the preparation of novel recombinant ADCs, consisting of SNAP-tagged scFvs conjugated to BG-modified AURIF (Table 3) [312,313].

In these studies, Woitok *et al*. were able to demonstrate the economic production of recombinant ADCs, as well as efficient conjugation with only a 2-fold molar excess of the BG-modified substrate [298,312,314]. Efficient binding and internalization (after incubation for 4 hours at 37^{o}C) of the anti-EGFR (425(scFv)-SNAP-AURIF) and anti-HER2 (αHER2(scFv)-SNAP-AURIF) immunoconjugates, were confirmed on target cells, supporting the fact that conjugation to BG-AURIF, has no impact on the binding ability of the fusion protein [312]. Moreover, the unconjugated scFv-SNAP and the non-binding SNAP fusion (Ki4(scFv)-SNAP-AURIF), did not affect the viability of any cell line, highlighting the specific delivery of AURIF to EGFR^{+}/HER2^{+} cells [312]. Interestingly, auristatins on their own usually display potent cytotoxicity in the lower nanomolar range (~1 nM) [315]. The authors were able to show comparable cytotoxicity, ranging from 3-21 nM, indicating that AURIF retained its functionality even after being linked to BG [312,313]. The stability of ADCs in circulation, represents an important prerequisite for the safe administration of these agents. To this end, the authors were able to confirm that αHER2(scFv)-SNAP-AURIF maintained full activity, while 425(scFv)-SNAP-AURIF retained at least 50% of its cytotoxicity after 48 hours incubation in serum [312]. They also speculate that conjugating more than one molecule of drug via SNAP-tag, could be the next uncharted territory to be explored to further increase the efficacy of recombinant ADCs [312,313].

1.7 Theranostic near-infrared photoimmunotherapy

One of the main drawbacks of PDT is the scattergun effect of the activated PS, which causes significant damage to surrounding healthy cells [298]. Efforts to bypass this lack of specificity may have resulted in the use of various combinations of conventional PSs and mAbs, but only a limited success rate was observed [316–319]. Reasons explaining the difficulties in generating targeted PSs were as follows: (1) conventional PSs demonstrate low extinction coefficients, which necessitates conjugation of a large number of PSs to a single antibody molecule for effective therapy, thus potentially reducing the binding affinity, (2) conventional PSs are generally hydrophobic (they can permeate into cells and lead to cell death), which makes their conjugation to antibodies more complex while trying to avoid compromising the activity and *in vivo* target accumulation, and (3) conventional PSs usually absorb light in the visible range, thereby reducing tissue penetration [320]. Given these challenges, Mitsunaga *et al*. (2011) developed a new form of molecular targeted cancer therapy – termed photoimmunotherapy (PIT) – consisting of a mAb (targeting an expressed antigen on the cancer cell surface) attached to a photoabsorbing near-infrared (NIR) phthalocyanine-based chemical called IRDye700DX (IR700) [320,321]. After irradiation with NIR light of 690 nm wavelength, the IR700 part of the molecule becomes activated and splits (turning hydrophobic), resulting in immediate cell death [320,322]. Since 690 nm NIR light can penetrate the skin and tissues to several centimeters in depth without harming normal cells, this technology can access deeply-seated tumors via endoscopes or catheter needles, both of which can be easily adapted for clinical practice [322–324]. Interestingly, the mAb-IR700 conjugates were most effective when bound to the cell membrane (no phototoxicity observed when not bound), implying a different killing mechanism for PIT as compared to traditional PDT [320]. Indeed, it has been reported that IR700 activation causes increased water diffusion into treated cells, resulting in an expansion of the cell to its maximum size, ultimately causing membrane rupture and inducing necrosis [325]. Furthermore, this mode of cell death can promote an immune response, culminating in the release of immune mediators and the stimulation of neutrophils, macrophages and CD8+ T-cells which play a long-term role in the elimination of neoplastic cells [295,321,326].

NIR-PIT can be applied to a broad array of cancer-specific target molecules, as illustrated for EGFR [327–330], HER2 [331,332], carcinoembryonic antigen (CEA) [333], as well as cancer stem cell (CSC) markers (of breast cancer and glioblastoma) such as cluster of differentiation (CD) 44 [334] and CD133 [335]. Using this approach, tumor shrinkage can be achieved even with a single administration of mAb-IR700, followed by a single exposure to NIR light *in vivo* [320,336]. While conventional PDT requires internalization of the PS into the mitochondria or lysosomes, intracellular delivery is not required for mAb-IR700-mediated phototoxicity [320,334]. Furthermore, treatment with ROS scavengers (example: sodium azide), did not eliminate the effectiveness of the conjugate, indicating that ROS generation forms a minor part of the phototoxic activity and that these agents could be suitable for targeting hypoxic tumor cells that are resistant to chemotherapy and radiotherapy [320,337]. Another interesting aspect of NIR-PIT is that tumor vessels become very leaky for several hours after treatment [338]. This phenomenon, most commonly known as super enhanced permeability and retention (SUPR) effect, allows the homogeneous redistribution of the antibody-IR700 conjugate within the already-treated tumor space [339].

Among all the clinically useful PSs, IR700 seems to have the most favorable chemical properties for PIT. For example, as opposed to conventional PSs which emit fluorescence at visible wavelengths, next-generation NIR dyes such as IR700, exhibit less background interference (caused by light absorbance and scattering by haemoglobin, melanin and lipids) and improved tissue penetration [340]. It is considerably less sensitive to photobleaching, has excellent water solubility and can be covalently conjugated to the targeting moiety via an *N*-hydroxysuccinimide (NHS) ester or maleimide [320]. The highly hydrophilic nature of IR700, implies that the antibody is crucial for targeting; this enables targeted accumulation at the tumor site, with minimal uptake in non-target tissues [330]. Indeed, IR700 offers a fail-safe system for preventing off-target effects; in its free and catabolized forms, IR700 is readily excreted into urine within 1 hour after administration (without accumulation in any specific organ) [320]. Additionally, IR700 also emits fluorescence, which can be harnessed to monitor body distribution, phototoxic effects, tumor accumulation and to select for the optimum timing for photo-irradiation [334,341]. Therefore, the ability to combine potent therapeutic and diagnostic properties with the specificity of various cell

receptor ligands (all in one product), makes IR700 an instrumental tool in the development of targeted theranostics.

As recently reviewed by Sandland and Boyle (2019), there are various physicochemical properties that tetrapyrroles (example: phthalocyanine) need to possess in order to be viable PSs for conjugation to antibodies [342]. Conjugation reactions must be feasible in biologically compatible solutions, with minimal modification of the antibody component, while ensuing uniform stoichiometry, high yield and easy purification [343]. Moreover, several challenges need to be tackled in order to generate pharmaceutically acceptable photoimmunoconjugates that are well-suited for administration in patients [344]. As a step closer to achieving these clinical ideals, von Felbert *et al*. (2016) demonstrated the potential of SNAP-tag in the generation of scFv(425)-SNAP-IR700 for the detection and elimination of skin cancer cells overexpressing EGFR [345]. Soon enough, this platform was extended to other malignancies (such as ovarian and breast cancers) with the creation of homogeneous photoimmunotheranostic agents displaying potent phototherapeutic activities in the nanomolar range (Table 3), along with powerful imaging properties [295,340]. Of note, there are several key differences between this technology and the aforementioned mAb-IR700 conjugates (pioneered by Mitsunaga *et al*. [320]). Firstly, the conjugation method is different; to engineer mAb-IR700, IR700 molecules were randomly conjugated to antibodies using the amino groups of lysine side chains, producing products with varying DARs [346]. On the other hand, although requiring that IR700 NHS be modified with BG using BG-PEG_{24}-NH_2, SNAP-tag (genetically fused to antibodies) provides a method to generate standardized photoimmunotheranostics with a DAR of 1 (thus ensuring unified pharmacokinetics) [295,346]. Furthermore, there are several advantages of using antibody fragments (scFvs) over mAbs. It is known that size can affect a probe's capacity to penetrate tissues, as well as its clearance rate from circulation and non-target tissues [347,348]. To this end, scFvs are endowed with the ability to accumulate rapidly in tumor tissues (can penetrate solid tumors) and their small size ensures that they are cleared within minutes or hours from the body [349]. Meanwhile, the large hydrodynamic diameter (~10 nm) of full-length antibodies prevents glomerular filtration and their high serum stability leads to prolonged circulation, which promotes high background signals in radio or optical imaging [297].

Table 3: Cytotoxic activity of Auristatin F-based recombinant ADCs and SNAP-tag based photoimmunotheranostic agents using IR700

Targeted therapy	Construct name	Disease model	IC_{50} (nM)	References
Recombinant antibody-drug conjugates	425(scFv)-SNAP-AURIF	Epidermoid carcinoma TNBC Rhabdomyosarcoma	8 2.6-4 8	[312,313]
	1711(scFv)-SNAP-AURIF	Epidermoid carcinoma TNBC Rhabdomyosarcoma	12 4 4	[313]
	αHER2(scFv)-SNAP-AURIF	$HER2^+$ breast cancer	0.6	[312]
Photoimmuno-theranostics	scFv(425)-SNAP-IR700	Ovarian cancer TNBC Skin cancers	45-66 26-61 32-55	[340] [295] [345]
	αCSPG4(scFv)-SNAP-IR700	TNBC	128-131	[295]
	αEpCAM(scFv)-SNAP-IR700	TNBC ER^+ breast cancer	40-165 56	[295]

1.8 Potential biomarkers for TNBC detection and treatment

1.8.1 Chondroitin sulfate proteoglycan 4

Chondroitin sulfate proteoglycan 4 (CSPG4), also known as melanoma-associated chondroitin sulfate proteoglycan (MCSP) or high molecular weight melanoma-associated antigen (HMW-MAA), is a highly glycosylated transmembrane protein and a member of the chondroitin sulfate

group of glycosaminoglycans (GAGs) [350]. CSPG4 was first characterized on human melanoma cells and subsequently shown to be implicated in the pathology of other solid tumors, as well as haematological malignancies [351,352]. CSPG4 has conserved its structural and functional properties through phylogenetic evolution; it shows over 80% homology with the rat neural/glial antigen 2 (NG2) and the mouse aniridia type II (AN2) proteoglycans [353,354]. Structurally, CSPG4 is composed of an *N*-linked 280 kDa glycoprotein and a 450 kDa chondroitin sulfate proteoglycan [71]. Its extracellular portion consists of 3 main domains: (1) the N-terminal domain D1 contains 2 laminin G-type subdomains and might be involved in mediating interactions with the extracellular matrix, as well as ensuring the stability of the tertiary structure, (2) domain D2 contains several glycosylation and chondroitin sulfate binding sites which may enable the activation of integrins and metalloproteases, and (3) domain D3 (a small globular region proximal to the cell membrane) encompasses several protease cleavage sites and might be important in interacting with lectins and integrins [350,355–358]. The intracellular portion of CSPG4 includes a threonine and proline-rich motif, as well as a PDZ (postsynaptic density protein 95 – *Drosophila* disc large tumor suppressor – Zona occludens 1) domain [359]. Threonine phosphorylation of this region (by ERK/PKCα) causes the activation of downstream cell proliferation and survival pathways (example: PI3K/Akt/mTOR pathway), increases cell motility and epithelial-to-mesenchymal transition, while promoting chemoresistance [360–362]. By virtue of these abilities, including promoting migration and metastasis, Wang *et al*. (2010) suggest that CSPG4 is likely to be involved in the functional properties of CSCs [353]. CSPG4 is also recognized for its role in angiogenesis, vascularization, multiple tissue development and homeostasis, depending on the nature of the tissue microenvironment [363–365]. Strikingly enough, despite the versatile functions of CSPG4, studies with NG2 knockout mice point to the fact that deletion of this antigen is not lethal [366]. However, the involvement of CSPG4 in cancer initiation or its accumulation as a secondary tumor-associated event, is still poorly understood [350,360]. CSPG4 is known to be heterogeneously expressed on normal tissues (such as mesenchymal stem cells), which lose their expression during terminal differentiation [367]. In the context of breast cancer, CSPG4-specific mAbs have shown that CSPG4 is expressed on nearly 73% of TNBC lesions and cell lines, which correlates with an aggressive clinical phenotype and poor treatment outcomes [368,369]. Therefore, the restricted distribution of CSPG4 in normal tissues (as compared to malignant cells)

warrants its use as a potential biomarker for imaging and therapeutic applications in TNBC. For instance, through the inhibition of neoangiogenesis and signal transduction pathways [353], mAbs targeting CSPG4 are able to inhibit cell growth, adhesion and migration in several TNBC tumor models [369]. These promising results are thus leading to the development of various antibody-based therapies specific for CSPG4, including *Pseudomonas aeruginosa* exotoxin A-based ITs, hCFPs, radioimmunoconjugates, theranostic agents, chimeric antigen receptor T-cell (CAR-T) therapy and bispecific T-cell engagers (BiTEs) [295,350,370–372].

1.8.2 The CD44 antigen

According to the CSC hypothesis, small populations of tumor stem cells play a major role in promoting malignant formation, growth, invasion, metastasis and recurrence [373,374]. In recent years, several studies have disclosed a small number of highly tumorigenic cell populations in breast cancer (also known as breast cancer stem cells), which demonstrate stem cell-like properties such as indefinite potential for self-renewal and longevity [375–378]. In TNBC, the majority of deaths arise from these notoriously resistant CSCs [379,380], which were shown to be enriched after chemotherapy [381]. Therefore, CSCs represent a druggable Achilles' heel for the targeted therapy of TNBCs. To this end, several breast cancer stemness markers were identified including CD44, CD24, CD133, epithelial cell adhesion molecule (EpCAM) and CD166 [382,383]. Among these CSC markers, the $CD44^{high}/CD24^{-/low}$ phenotype is more abundant in TNBC patients and correlates with poor treatment outcomes and worse prognosis [384]. CD44 is a non-kinase transmembrane glycoprotein, which is encoded by the highly conserved CD44 gene on chromosome 11 in humans [385,386]. As compared to its standard form (CD44s), its alternative spliced variants (CD44v) are thought to play a role in cancer development and progression [385]; CD44v isoforms can act as co-receptors for growth factors and they possess additional binding motifs that enable the interaction of CD44 with molecules in the microenvironment [387,388]. Nonetheless, CD44s has been found to be essential for cells undergoing epithelial-mesenchymal transition, especially in the progression and recurrence of breast cancer [389]. Even more conflicting is the fact that some studies warrant a protumorigenic role for CD44 (promotes breast cancer metastasis [390]), while others report its protective role in breast cancer [391], suggesting that CD44 may affect tumor growth and metastasis differently at different phases of tumor

progression [392]. Similar to CSPG4, CD44 consists of 3 domains: an extracellular domain, a transmembrane domain and an intracellular domain [393]. In brief, the extracellular domain contains the amino terminal globular domain which provides binding sites for hyaluronic acid (HA, the most specific ligand for CD44 activation), GAGs and other ligands [394]. HA is a major extracellular matrix component (expressed by stromal and tumor cells) [385], which binds to CD44 and induces conformational changes that activate cell signaling pathways (Ras, mitogen-activated protein kinase (MAPK), PI3K) to promote cell adhesion, migration and proliferation [395,396]. Interestingly, in breast cancer, the activation of CD44 by HA culminates in the expression of multidrug resistance genes (P-glycoprotein) and the anti-apoptotic gene Bcl, which promote tumor cell proliferation and survival [397]. On the other hand, the intracellular domain has an important role to play in the subcellular localization of CD44, cell migration, signaling, cytoskeletal organization and gene transcription [398,399]. Lastly, the transmembrane region, which carries hydrophobic amino acids and a cysteine residue, is deemed to be involved in CD44 oligomerization and its association with lipid rafts [400,401]. In summary, the overexpression of CD44 on CSCs, as well as its multifunctional role in tumorigenesis, reinforces its potential as a diagnostic and therapeutic target.

1.8.3 Aspartate (aspartyl/asparaginyl) β-hydroxylase

Being first described in 1989, aspartate (aspartyl/asparaginyl) β-hydroxylase (ASPH) is a type II transmembrane protein which is highly conserved and belongs to the α-ketoglutarate-dependent dioxygenase family [402–404]. It catalyzes the β-hydroxylation of aspartyl and asparaginyl residues in EGF-like repeats of certain proteins (which are important in cell motility and adhesion), including clotting factors, extracellular matrix proteins, as well as Notch, its homologues and its ligands (example: Jagged and Delta-like) [404–407]. Interestingly, the ASPH protein is divided into 4 distinct domains: an amino or N-terminal cytoplasmic domain, a transmembrane domain, a negatively charged domain that projects into the lumen of the endoplasmic reticulum and a COOH-terminal catalytic domain, all of which have been demonstrated to be critical for ASPH's catalytic activity [404,408,409]. ASPH has garnered significant attention due to its overexpression in a broad range of human malignancies, such as those of the breast, colon, pulmonary, pancreatic, hepatic and neural origin [410–413]. As reported by Yang and colleagues (2010), this

overexpression is closely associated with tumor cell formation, proliferation, invasion, metastasis and other hallmarks that promote propagation of the malignant phenotype [413]. In normal tissues, the expression of ASPH is minimal, with primary localization in internal compartments (such as the endoplasmic reticulum) and upon malignant transformation, ASPH is overexpressed and translocated to the tumor cell surface, thus making it a specific tumor-associated surface antigen [414]. This peculiar phenomenon accounts for the detection of ASPH in the sera of patients with breast, colon, lung and prostate cancers [404], which emphasizes the need for an efficient detection method. In breast cancer, it has been reported that the upregulation of ASPH (most specifically in ER-positive and tamoxifen-resistant breast cancers) is mediated by the MAPK and PI3K pathways, thereby causing resistance to endocrine therapy in these tumors [415]. In a recent study by Lin *et al*. (2019), it was shown that moderate to high level expression of ASPH is associated with more aggressive molecular subtypes of breast cancers (such as TNBC and HER2+ tumors), multiple-organ metastasis, early recurrence, rapid progression and reduced overall and disease-free survival [416]. Additionally, the ASPH-Notch axis was determined to be a major molecular mechanism responsible for the generation and maintenance of malignant cell behavior in breast cancer [416]. Indeed, ASPH is known to induce tumorigenesis through activation of the Notch signaling pathway, disruption of mitochondrial functions and suppression of natural killer cell surveillance activity [417,418]. Most importantly, the Notch pathway is important for differentiation, cell fate determination, adhesion, migration, invasion and stemness [419]; after the induction of ASPH overexpression, the enzyme interacts with EGF-like repeats in the extracellular domain of Notch, resulting in conformational changes that activate the transcription of downstream target genes involved in cancerous formation [418]. Based on the above premises, the role of ASPH as a potential tumor biomarker and therapeutic target is becoming more evident. Several mAbs targeting ASPH were developed with promising results: (1) the mAbs demonstrated high efficiency and specificity, (2) the level of ASPH expression was determined in various tumor tissues and cell lines and (3) it was shown that the protein expression of ASPH was parallel with mRNA expression, suggesting that ASPH expression is regulated at the transcriptional level [404,413,420]. Moreover, anti-ASPH mAbs are being studied for their use as vehicles in the delivery of cytotoxic moieties, including plant toxins and radioactive agents [414,421].

1.9 Aims and objectives of project

Throughout history, there has been a piqued interest in understanding the link between the etiology of cancer and its fundamental biological nature [7]. With the inception of molecular and genetic profiling platforms, increased insights into the minutiae governing the biochemical differences between normal and tumor cells, have been made possible. Continued unraveling of the multifaceted nature of cancer cells, has thus probed a major shift from non-targeted to more targeted therapies [201]. Indeed, with the notion that a 'one-size-fits-all' approach is not adequate, a more rational perspective is being adopted to streamline and personalize the development of new regimens for those who are unlikely to benefit from existing therapies [83]. Ideally, while achieving precision medicine where only cancer cells are eliminated (with minimal collateral damage to normal tissues), heralds a better future for cancer patients, it continues to remain a research area that is still in its infancy [334]. For notoriously aggressive and persistent cancers such as TNBCs, the lack of druggable targets, is increasing the dependency on standard treatment options (chemotherapy, surgery, radiotherapy) that are often associated with a high risk of local and systemic relapses [46]. The heterogeneity of this disease implies that there is a lack of tools available for its proper detection and prognosis [52]. No effective targeted therapy is currently available and no single receptor can be expected to target all TNBCs [72]. Therefore, at the Medical Biotechnology and Immunotherapy Research Unit, we propose to develop a panel of companion recombinant immunodiagnostics, which when combined together, could enable the detection and classification of the vast majority of TNBCs (via multiplex immunofluorescence imaging of African patient-derived biopsies (supported by the work of PhD student Natasha Hardcastle)), thereby providing a much-needed incentive for the tailoring of according therapies best suited for the particular needs and disease profiles of each patient. To this end, this project will focus primarily on 3 important surface receptors (CSPG4, CD44 and ASPH) that are typically overexpressed in TNBCs. More explicitly, the proposed research aims are as follows (Figure 7):

1. Generate SNAP-tag based fusion proteins consisting of scFvs targeting CSPG4, CD44 and ASPH, and validate their utility in the screening of TNBC cell lines (through conjugation with BG-Alexa Fluor 488 fluorophore).

2. Despite showing great promise as molecularly targeted therapies for cancer [422], ADCs suffer from various limitations [312,313,423,424]. SNAP-tag technology alleviates these challenges by allowing the specific covalent conjugation of drugs in a defined 1:1 stoichiometry [313]. The SNAP-tag fusion proteins generated in this research will be made to react specifically with BG-modified AURIF to generate novel AURIF-based immunoconjugates, whose cytotoxic activities will be assessed on target TNBC cell lines.

3. Efforts put forward to bypass the lack of specificity associated with PDT, may have resulted in the creation of NIR photoimmunotheranostic agents, however their generation is not always an easy process [320,343,344]. Using the same principle outlined by von Felbert *et al.* (2016) [345], scFv-SNAP-tag fusions bearing IR700 as a potent NIR PS, will be engineered and their specific and dose-dependent biological activities will be determined *in vitro*.

Consequently, the specific objectives of this study will entail the *in silico* design of the mammalian expression vectors, followed by molecular cloning of the respective scFv DNA sequences in fusion with SNAP-tag. Protein expression will be carried out using HEK293T cells as a transient secretory mammalian expression system. After harvesting of the cell culture supernatant, the resulting fusion proteins will be purified by immobilized metal affinity chromatography and analyzed using SDS-PAGE and western blot. Binding of the fusion proteins to TNBC cell lines will be validated both quantitatively by flow cytometry and qualitatively by confocal microscopy. Finally, the cytotoxicity of the resulting scFv-SNAP conjugates (AURIF/IR700) will be determined based on their ability to specifically target and destroy TNBC cells which express their target antigens.

Overall, the results of this study will provide comparative data on non-invasive and safe methods that could be used to localize and target triple-negative breast tumors. Therefore, the combination of such therapeutic agents with a robust companion diagnostic portfolio provided by SNAP-tag technology, represents the first step towards the effective management of African TNBC.

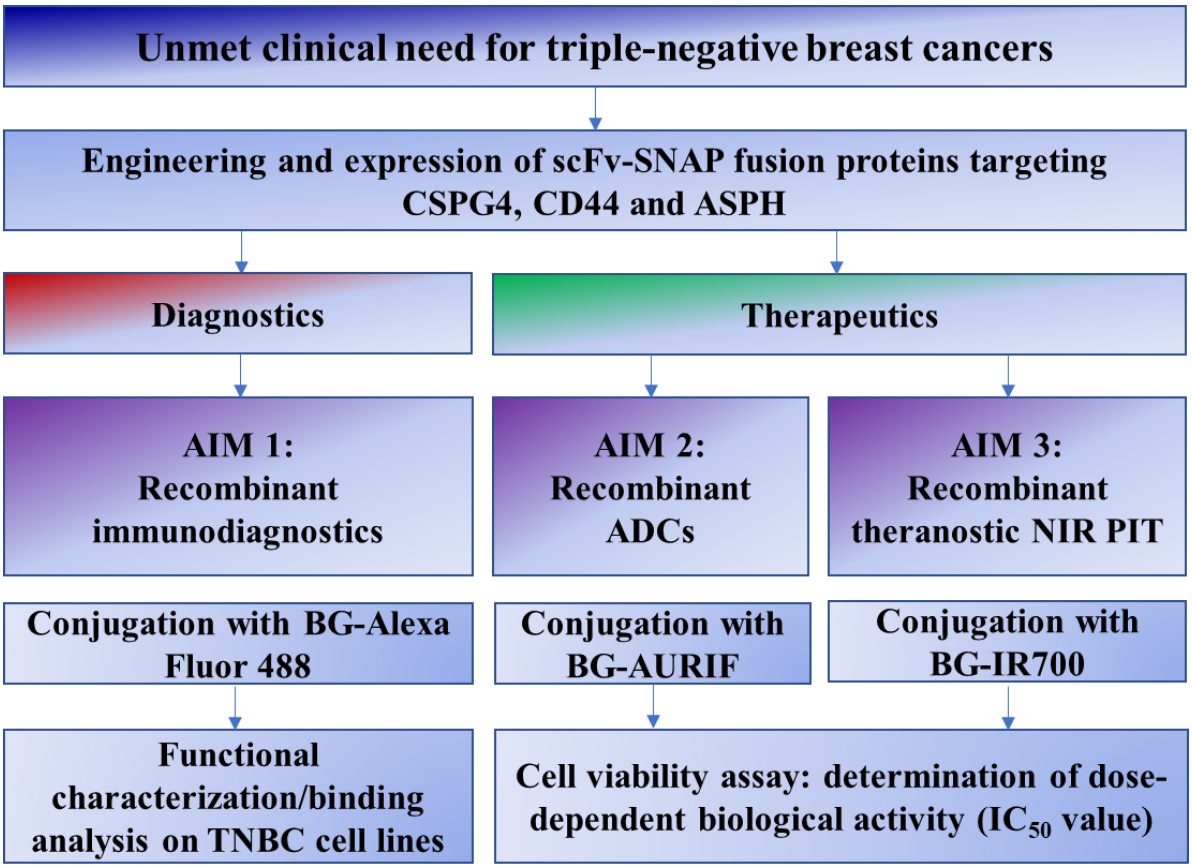

Figure 7: Flow chart of current research. TNBCs represent an important and unmet clinical need in oncology. This research proposes to use the differential expression of tumor-associated antigens and exploit them as guiding mechanisms for the diagnosis and the specific delivery of cytotoxic compounds or PSs to diseased TNBC cells.

Chapter 2: Materials and Methods

2.1 Cell culture

Human embryonic kidney cells (HEK293T) (ATCC: CRL-11268) and the human melanoma cell line SK-Mel-28 (ATCC: HTB-72) were cultured in RPMI-1640 medium (containing 2 mM L-glutamine, 3.7 g/L $NaHCO_3$ and 15 mg/L phenol red), supplemented with 10% (v/v) heat-inactivated fetal bovine serum (FBS) and 1% (v/v) 100 U/ml penicillin-streptomycin. Similarly, the human breast cancer cell lines, Hs578T (ATCC: HTB-126), MDA-MB-468 (ATCC: HTB-132), MDA-MB-231 (ATCC: HTB-26) (note: Hs578T, MDA-MB-231 and MDA-MB-468 are TNBC cells) and MCF-7 (ATCC: HTB-22) were all cultured in Dulbecco's Modified Eagle Medium (DMEM) (containing 2 mM L-glutamine, 3.7 g/L $C_3H_3NaO_3$ and 16 mg/L phenol red), supplemented with 10% (v/v) heat-inactivated FBS and 1% (v/v) 100 U/ml penicillin-streptomycin. The cells were maintained in a 5% CO_2 incubator with 95% humidity at 37^{o}C. Medium was changed every 3-4 days and cells were passaged when 90% confluent. All products were purchased from Gibco by Life Technologies® (RPMI-1640: Gibco #10566 and DMEM: Gibco #61870), supplied by Thermo Fisher Scientific, South Africa.

2.2 In silico design of mammalian expression vectors

In order to design the SNAP-tag based fusion proteins, scFv gene sequences were obtained from the following patents and collaborators: CD44 (US 20030103985A1), ASPH (US 7413737B2) and CSPG4 (German collaborators from University Hospital RWTH Aachen [372]). These sequences were then analyzed on IgBLAST (available at: https://www.ncbi.nlm.nih.gov/igblast/) and compared to existing immunoglobulin germline variable region gene sequences. Once the framework regions (FR) and complementarity determining regions (CDRs) were identified for each, each scFv variable heavy chain (V_H) was linked to its corresponding variable light chain (V_L), and each resulting CDR was then aligned to its parental sequence using CLC genomic workbench v12 software. The newly designed scFv sequences were then inserted into the prototype pCB-AnnexinV-SNAPf expression plasmid shown in Figure 8 (previously generated at MB&I) between *Sfi*I and *Not*I restriction sites, using SnapGene software (version 3.1.1, GSL Biotech, Chicago).

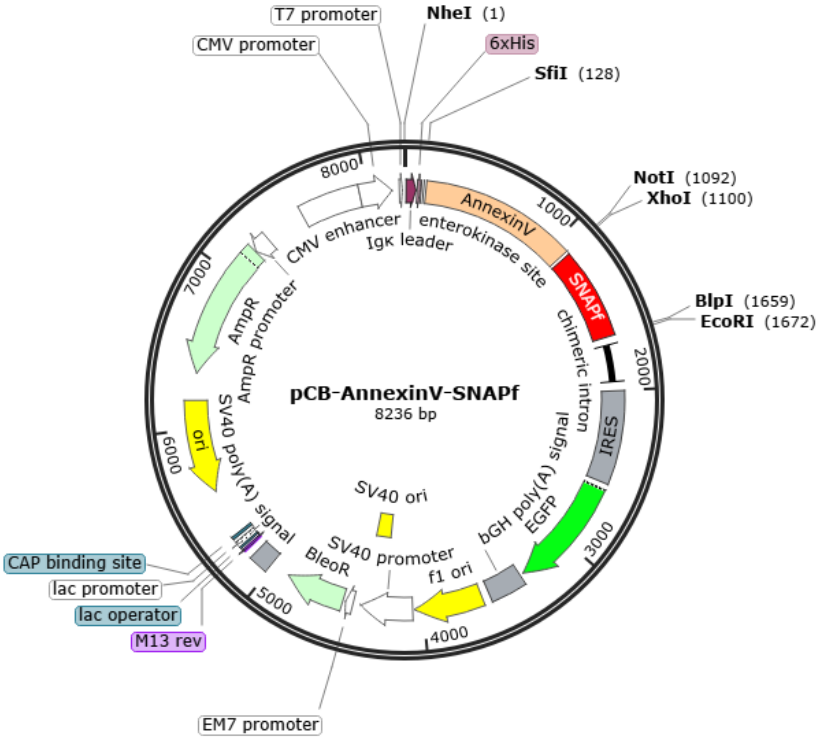

Figure 8: Vector map of pCB-AnnexinV-SNAPf. Crucial components of this mammalian expression plasmid are indicated in Table 4 below. *Sfi*I and *Not*I restriction sites were used to clone in the scFv sequence for CD44.

Important components of the MB&I pCB-AnnexinV-SNAPf mammalian expression plasmid are summarized in Table 4. After confirming the integrity of the open reading frame (ORF), the scFv sequences (with *Sfi*I/*Not*I restriction sites) were sent to be synthesized in a pUC57 plasmid from Genescript (USA). The cloning of pCB-αCSPG4(scFv)-SNAP (mAb9.2.27-SNAP) was carried out in 2016 (Honours project) and the cloning of αASPH(scFv)-SNAP was carried out by Dr. Krupa Naran (Postdoctoral fellow). Therefore, detailed results of their molecular cloning, will not be included as part of this PhD dissertation.

Table 4: Important components of the mammalian expression plasmid and their function

Component	Function
Cytomegalovirus (CMV) promoter	Induces high-level expression of the fusion protein [425]

T7 promoter	Allows *in vivo* transcription in the sense orientation
Ig-*Kappa* leader	Crucial for the secretion of the fusion protein into the supernatant of HEK293T cells [426]
N-terminal polyhistidine tags (His x 6)	Useful for protein purification using immobilized metal affinity chromatography (IMAC) [427] and for detection of fusion proteins using an anti-His antibody
Enterokinase (EKS) cleavage site	Allows removal of the N-terminal his-tags and isolation of the fusion protein
SNAPf	A fast-labeling variant of SNAP-tag, which displays up to a tenfold increase in its reactivity towards benzylguanine (BG) substrates [428]
Chimeric intron	Enhances mRNA processing and increases the expression levels of the protein coding genes [429]
bGH poly(A) signal	Allows efficient transcription termination and polyadenylation of mRNA
F1 origin	Allows rescue of single-stranded DNA
SV40 Ori	Origin of replication
Internal ribosome entry site (IRES)	mRNA sequence which mediates expression of green fluorescent protein (GFP)
Green fluorescent protein (GFP)	Reporter protein showing successful transfection in mammalian cells, as well as *in cis* expression of the putative fusion protein
BleoR	Allows selection of transient transfectants in mammalian cells (using Zeocin)

Lac operator	A short region of DNA that interacts with the lac repressor to inhibit transcription of lac genes in the absence of lactose
Lac promoter	Modulates transcription of lac operon genes involved in the metabolism and absorption of lactose in bacteria [430]
SV40 promoter	Allows high-level expression and replication in cell lines which express the large T antigen
Ampicillin resistance gene	Allows selection in *E. coli*
M13 rev	Single-stranded oligonucleotide sequence (5′-CAG GAA ACA GCT ATG ACC-3′) which can be used in polymerase chain reactions [431]
CAP binding site	Binding site for catabolite activator protein (CAP), which is involved in the transcription of several genes, including enzymes involved in sugar metabolism [432]
*Sfi*I/*Not*I	Restriction sites

2.3 Molecular cloning of SNAP-tag based fusion proteins

2.3.1 Transformation of *E. coli* with plasmid DNA

The exogenous DNA of interest (pCB-AnnexinV-SNAPf and pUC57-αCD44(scFv)) was incorporated into chemically (calcium) competent DH5α *E. coli* cells (K12 strain, genotype: fhuA2 (argF-lacZ)U169 phoA glnV44 80 (lacZ)M15 gyrA96 recA1 relA1 endA1 thi-1 hsdR17, New England Biolabs, USA) using the heat shock method. The bacterial cells were firstly thawed on ice for 10 minutes. Thereafter, 0.5 µl of plasmid DNA (100 ng/µl) (resuspended in molecular grade water) was added to 50 µl of bacterial cells. The mixture was carefully mixed by flicking the tube, which was then placed on ice for 30 minutes and heat shocked at 42^{o}C for 60 seconds in a water bath. The tube was then placed on ice for 5 minutes and 950 µl of SOC (Super Optimal broth with

Catabolite repression, containing 2% (w/v) vegetable peptone, 0.5% (w/v) yeast extract, 10 mM NaCl, 2.5 mM KCl, 10 mM $MgCl_2$, 10 mM $MgSO_4$ and 20 mM glucose) outgrowth medium was added to the mixture to help in the recovery of the cells. The full 1 ml mixture was then inoculated in 50 ml LB (Luria broth, containing 1% (w/v) Casein Peptone, 0.5% (w/v) yeast extract and 1.0% (w/v) NaCl) liquid medium (Thermo Fisher Scientific, South Africa) supplemented with 200 µg/ml ampicillin antibiotic and placed on a shaker at 37^{o}C overnight.

2.3.2 Isolation of plasmid DNA from *E. coli*

The plasmid DNA was isolated from *E. coli* and purified using the NucleoBond® plasmid purification kit (Product number: 740573, Macherey-Nagel, United Kingdom) according to the manufacturer's instructions. The principle of this assay relies on the alkaline lysis of bacterial cells for the extraction of plasmid DNA. The DNA is then bound to an anion-exchange resin in the NucleoBond® column, from where it is eluted off and precipitated using isopropanol. In the last step, 30 µl of molecular grade water (pre-heated at 50^{o}C for 10 minutes) was used to resuspend the DNA pellet instead of TE buffer. This step was done because the presence of chemicals in TE buffer (EDTA and Tris) can affect the quality of the DNA samples that are meant to be used in downstream applications. The amount of DNA recovered was then quantified using a NanoDrop ND-2000 (Thermo Fisher Scientific, USA).

2.3.3 Restriction enzyme digest

Restriction digest was used for the generation of compatible ends suitable for ligation. Starter plasmid DNA (pCB-AnnexinV-SNAPf and pUC57-αCD44(scFv)) (in molecular grade water) was incubated successively with New England Biolabs (NEB, USA) restriction enzymes *Sfi*I (for 4 hours at 50^{o}C), followed by *Not*I (overnight at 37^{o}C) as indicated in Table 5 below.

Table 5: Setting up the restriction enzyme digest reaction mixture

Reagents	Amount required
*Sfi*I (2000 units/ml)	0.5 µl
*Not*I (2000 units/ml)	0.5 µl

10x NEB Cutsmart buffer	5 µl
Plasmid DNA (added last)	2 µg
Molecular grade water	Adjust to final volume of 50 µl

2.3.4 Agarose gel electrophoresis

Following restriction digest, the DNA fragments were separated using agarose gel electrophoresis. A 1.2% (w/v) agarose gel was made using a 1x TAE buffer (40 mM Tris, 20 mM acetic acid, 1 mM EDTA, pH 8.5). For visualization and tracking of the DNA bands, the agarose gel was mixed with SYBR® Safe DNA gel stain (Thermo Fisher Scientific, South Africa). Additionally, the DNA samples were mixed with 6x Orange DNA Loading Dye (Thermo Fisher Scientific, USA) before loading into the wells. Electrophoresis was performed at 100 volts for 60 minutes using Wide Mini Sub-Cell systems (Bio-Rad, USA) and the DNA fragments were visualized upon exposure to blue light excitation (using a Dark Reader Transilluminator from Clare Chemical Research, USA).

2.3.5 Recovery of DNA fragments from agarose gels

The digested DNA fragments were excised from the agarose gels and purified using the QIAquick® Gel Extraction Kit (Product number: 28704, Qiagen, Netherlands) according to the manufacturer's instructions. This gel extraction method relies primarily on the binding of DNA fragments to a silica-membrane-based column. The DNA was eluted by adding 20 µl of distilled water (pre-heated at 50^{o}C) to the center of the membrane, before centrifuging the samples for 2 minutes at 14,000 rpm. Thereafter, the DNA recovered was quantified (as described above) and stored at 4^{o}C until ready for use.

2.3.6 Ligation reactions and transformation of recombinant plasmids in *E. coli*

Ligation of the DNA fragments to the pCB-SNAPf vector backbone was carried out using T4 DNA ligase (400,000 units/ml) and 10x ligation buffer (both from New England Biolabs, USA) according to the manufacturer's instructions. Reactions were set up as indicated in Table 6 and incubated overnight at 16^{o}C. The amount of insert required for a 1:1, 1:2 and 1:3 (vector: insert) ratio was calculated using the NEBioCalculator (https://nebiocalculator.neb.com/#!/ligation). This was done to maximize the success rate of the ligation experiments. A 'vector only' control (*Sfi*I/*Not*I

double digested pCB-AnnexinV-SNAPf DNA) was also set up to assess any possible vector re-ligation. Next day, the reaction mixture was heat-inactivated at 65°C for 10 minutes and 5 µl of the recombinant DNA was then transformed into 50 µl of chemically competent DH5α *E. coli* cells (New England Biolabs, USA). The mixture was incubated on ice for 30 minutes, heat shocked for 60 seconds at 42°C in a water bath and cooled on ice for a further 5 minutes. Thereafter, 950 µl of SOC solution was added to the mixture, which was then incubated at 37°C for 1 hour in a heating block. The cells were then mixed thoroughly, centrifuged (14,000 rpm for 2 minutes) and 900 µl of supernatant was removed. The remaining pellet was resuspended in a final volume of 200 µl with LB liquid medium and 100 µl of cells were plated on LB agar plates (1% (w/v) Casein Peptone, 0.5% (w/v) yeast extract, 1% (w/v) NaCl and 1.2% (w/v) agar) supplemented with 200 µg/ml ampicillin (including 'vector only' and bacterial controls). The plates were left overnight at 37°C. The next day, 3 single colonies were picked from each plate and grown overnight in 2 ml of LB medium containing ampicillin (200 µg/ml). The transformation efficiency in colony forming units (cfu) per µg of DNA was calculated using the following formulae:

$$Transformation\ efficiency\ \left(\frac{cfu}{\mu g}\right) = \frac{Number\ of\ transformed\ colonies}{Amount\ of\ DNA\ spread\ on\ the\ plate\ (\mu g)}$$

Table 6: Setting up ligation reactions of digested insert with vector backbone

Component	Amount required
Vector DNA	50 ng
Insert DNA	Varies depending on fragment size (use NEBioCalculator)
T4 DNA ligase buffer (10x)	2 µl
T4 DNA ligase (400,000 units/ml)	1 µl (added last)
Molecular grade water	Adjust to final volume of 20 µl

2.3.7 Small-scale DNA isolation, restriction mapping and DNA sequencing

The recombinant DNA plasmids were isolated and purified from *E. coli* using the Zyppy™ Plasmid Miniprep Kit (Product number: D4036, Zymo Research, USA) according to the manufacturer's instructions, with minor alterations. In the first step, 1.2 ml of the bacterial culture was centrifuged (14,000 rpm for 2 minutes), 600 µl of supernatant was removed and the pellet was resuspended in the remaining 600 µl of LB medium. This was done to maximize the number of bacterial cells present and thus increase the resulting DNA yield. Furthermore, in order to avoid contamination of plasmid DNA with chemicals present in the Zyppy™ elution buffer, the DNA was eluted in 20 µl of distilled water (pre-heated at 50°C). The remaining 800 µl of ligation product was stored at 4°C for potential large-scale DNA purification before sending for sequencing. Single restriction enzyme digest simulations were carried out on SnapGene software (version 3.1.1, GSL Biotech, Chicago) to predict the cutting patterns of *Bam*HI-HF and *Pvu*II-HF for pCB-AnnexinV-SNAPf against pCB-αCD44(scFv)-SNAPf. Digestion reactions were then set up with 5 µl of purified DNA, 1 µl of 10x NEB Cutsmart buffer, 0.5 µl of restriction enzyme and topped up to 10 µl with molecular grade water. Samples were incubated at 37°C overnight and analyzed the next day using agarose gel electrophoresis as described above. This allowed to identify and confirm correct ligation of recombinant plasmids, by comparing with the SnapGene simulations. Correct recombinant clones were then grown in LB media and purified using the NucleoBond® plasmid purification kit as mentioned before (section 2.3.2). Samples were then sent to Inqaba Biotechnical Industries (Pretoria, South Africa) for DNA sequencing using the Sanger sequencing method. For this purpose, a universal T7 primer (AATACGACTCACTATAG), as well as specific internal primers (CMV forward: CGCAAATGGGCGGTAGGCGTG and SNAPf internal: CCTCGCCGAACTTCACCACCTTC) were used to help in the sequencing of the cloned product. SnapGene (version 3.1.1, GSL Biotech, Chicago) was used to confirm successful insertion of the scFv sequences in the pCB-SNAPf backbone by aligning them with the original *in silico* sequence.

2.4 Expression and purification of the SNAP-tag based fusion proteins

2.4.1 Expression of the fusion proteins in HEK293T cells

Upon confirmation of the DNA sequences, the eukaryotic expression vector systems (1 µg/µl) were transiently transfected into HEK293T cells (at 70-80% confluency) using XtremeGene™

transfection reagent (Sigma-Aldrich, South Africa) according to the manufacturer's instructions. This procedure utilizes lipids and polymers that are capable of complexing with DNA to form micelles, which in turn facilitate the uptake of DNA into mammalian cells. A 1:3 ratio of DNA to transfection reagent was used (3 µl of DNA and 9 µl of transfection reagent) and mixed with 188 µl of serum-free and antibiotic-free RPMI-1640 (Gibco #10566, containing 2 mM L-glutamine, 3.7 g/L $NaHCO_3$ and 15 mg/L phenol red). Untransfected HEK293T cells were included as a negative control. The transfected cells were then grown in RPMI-1640 culture medium (Gibco #10566) supplemented with 10% (v/v) FBS and 1% (v/v) 100 U/ml penicillin-streptomycin. Plasmid uptake was then assessed after 3 days, through the microscopic visualization of enhanced green fluorescent protein (eGFP) expressed by the transfected cells, using a ZOE™ Fluorescent Cell Imager (Bio-Rad Laboratories, UK). To determine the transfection efficiency, 2 ml of the transfected cells and controls were subjected to flow cytometry using the BD™ LSR II flow cytometer (BD Biosciences, USA). Transfection efficiency was expressed as a percentage of the eGFP-positive cells present within the total population. Zeocin selection (100 µg/ml) was then applied to enrich the eGFP-positive cells containing the recombinant plasmids. These cells were then grown at 90% confluency and the cell culture supernatant containing the secreted protein of interest, was harvested every 4 days, for a period of ±6 months or until sufficient protein (> 1 mg/ml) was obtained. The collected supernatant was pooled, centrifuged at 2500 rpm for 3 minutes to remove cellular debris, and then stored at 4°C until protein purification.

2.4.2 Protein purification using Immobilized Metal Affinity Chromatography (IMAC)

The cell culture supernatant (1 part of cell culture supernatant was mixed with 3 parts of 4x incubation buffer (200 mM NaH_2PO_4, 1.2 M NaCl, 40 mM imidazole, pH 8.0) to ensure optimal binding conditions) of each recombinant fusion protein (αCD44(scFv)-SNAPf, αASPH(scFv)-SNAP and αCSPG4(scFv)-SNAP) was first filtered using the Nalgene™ vacuum filtration system (Sigma-Aldrich, South Africa) containing a 0.45 µm Durapore® membrane filter (Millipore, USA) to exclude any microcellular debris, before purification by Immobilized Metal Affinity Chromatography (IMAC). IMAC was carried out by using a Ni^{2+} sepharose affinity resin (packed in a HisTrap™ Excel column, GE Healthcare, USA) on an ÄKTA Avant protein purification system (GE Healthcare, USA). Initially, each clarified cell culture supernatant was applied on a

pre-equilibrated HisTrap^{TM} Excel column at a flow rate of 5 ml/minute. Thereafter, the column was washed with 20 column volumes of equilibration buffer (50 mM NaH_2PO_4, 300 mM NaCl, pH 8.0) and the bound fusion proteins were eluted using elution buffer (50 mM NaH_2PO_4, 300 mM NaCl, 500 mM imidazole, pH 8.0) containing a high concentration of imidazole. In principle, fractional elution of the his-tagged fusion proteins is made possible by increasing the concentration of imidazole, which competes with histidine for binding to the metal-charged resin. As illustrated by Figure 9, the combination of a gradient (0-30% imidazole) and step (100% imidazole) elution process (green graph), allows complete removal of the fusion proteins from the column, as observed in the form of 2 distinct peaks on the chromatogram (blue graph).

Thereafter, in order to concentrate the eluted fractions (as well as remove residual imidazole), 10K-sized Amicon filters (Sigma-Aldrich, South Africa) were used. The samples were centrifuged at 4500 x g for 20 minutes at 4^{o}C and washed in 1x phosphate buffered saline (pH 7.4) (henceforth referred to as 1x PBS, containing 137 mM NaCl, 8.8 mM Na_2HPO_4, 2.7 mM KCl and 1.75 mM KH_2PO_4) thrice prior to downstream assays (note: 1x PBS was also used as the protein storage buffer at -20^{o}C). Protein quantification was assessed by UV spectrophotometry, using a DeNovix DS-11 (DeNovix, USA), prior to further characterization.

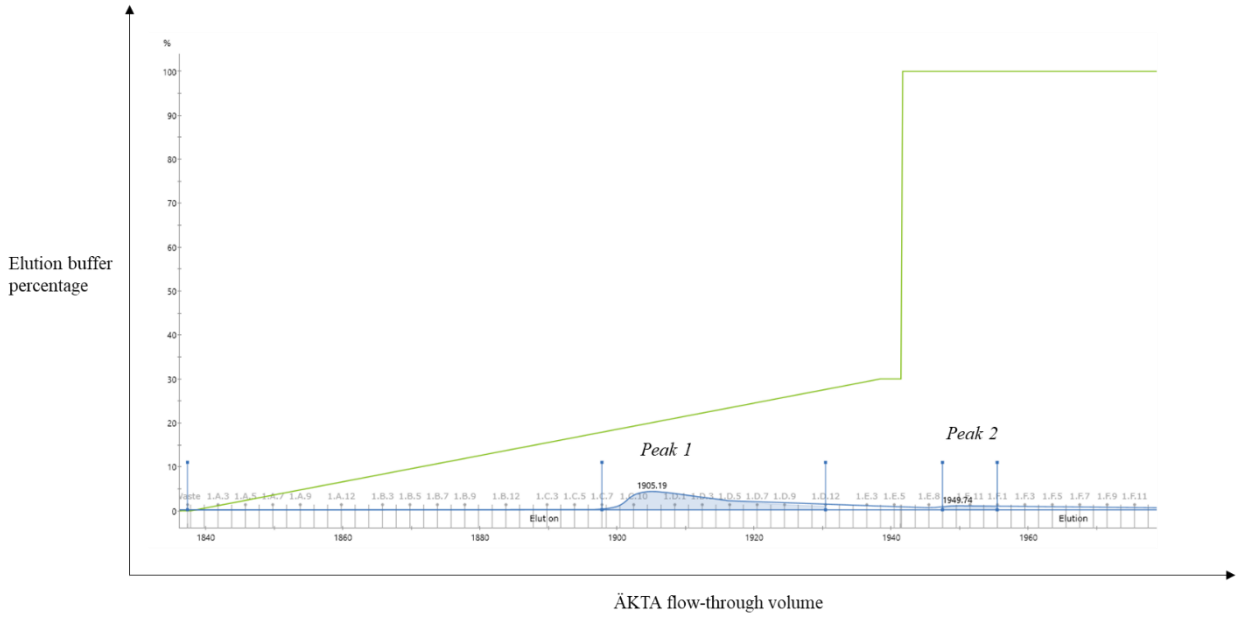

Figure 9: Chromatogram exemplifying the applied imidazole concentrations and the expected elution peaks. After application of the clarified cell culture supernatant onto the Ni^{2+} sepharose column and the washing of low affinity proteins, the high affinity his-tagged fusion proteins were eluted using a high concentration of imidazole. This was done via combination of a gradient (0-30% imidazole) and step elution process (100%) (green graph), resulting in the formation of 2 distinct protein peaks on the chromatogram (blue graph).

2.4.3 Sodium dodecyl sulfate-polyacrylamide gel electrophoresis (SDS-PAGE) and western blot analysis of recombinant protein fractions

A discontinuous 10% SDS-PAGE gel was used to resolve proteins electrophoretically on the basis of their molecular weights. For sample preparation, 15 µl of the recombinant protein samples was mixed with 5 µl of 4x Laemmli protein sample buffer (Bio-Rad, USA) supplemented with 10% (v/v) 2-mercaptoethanol (Sigma-Aldrich, South Africa), and heated at 95^{o}C for 5 minutes. After loading the protein samples and the Page Ruler prestained protein ladder (5 µl) (Thermo Fisher Scientific, South Africa), the SDS-PAGE gel was run at 100 volts for 95 minutes on the Mini-Protean Tetra Cell system (Bio-Rad, USA). The protein bands were visualized by staining the gel with Aqua Staining Solution (Vacutec, South Africa). Densitometry measurements were carried out using ImageJ v1.52a software (https://imagej.nih.gov/ij/download.html), which compares the optical densities of the target band of interest, against positive control bands (Bovine serum albumin (BSA)) on the same gel. Two-fold serial dilutions of BSA (Thermo Fisher Scientific, South Africa) were used for the generation of a standard curve of optical colour intensity against the quantity of protein (µg), allowing for the yield of the SNAP-tag fusion proteins to be estimated from the total protein concentration. Subsequently, western blotting was used to confirm the functionality and integrity of the recombinant his-tagged fusion proteins. Protein bands were transferred from an unstained SDS-PAGE gel to a nitrocellulose membrane (PVDF transfer membrane, Roche, Switzerland) using a Mini Trans-Blot Cell system (Bio-Rad, USA) set at 100 volts for 75 minutes. The membrane was then blocked with non-fat milk for 1 hour at room temperature and incubated with a 1:1000 dilution of an anti-his rabbit primary antibody (Qiagen, Hilden, Germany) and a 1:5000 dilution of a goat anti-rabbit horseradish peroxidase (HRP)-conjugate antibody (Bio-Rad, USA). Clarity^{TM} Western ECL substrate (Bio-Rad, USA) was added to the blot, prior to visualization using a Gel Doc^{TM} XR Gel Documentation System (Bio-Rad,

USA). A chemiluminescent ladder (5 µl) (SuperSignal™ Molecular Weight Protein Ladder, Thermo Fisher Scientific, South Africa) was used to assess the size of the protein bands.

2.5 Conjugation of SNAP-tag based fusion proteins to BG-modified substrates

2.5.1 Conjugation to BG-modified Alexa Fluor 488

The purified SNAP-tag based fusion proteins (5 µM) (in 1x PBS as the buffer system) were mixed with 10 µM of SNAP-Surface® Alexa Fluor® 488 (BG-Alexa Fluor 488, New England Biolabs, USA), 1 mM dithiothreitol (DTT, a reducing agent that improves the stability of SNAP-tag) (Sigma-Aldrich, South Africa) and made up to a final volume of 50 µl with 1x PBS. Conjugation was carried out at 37^{o}C in the dark for 60 minutes. The labeled proteins were resolved on an SDS-PAGE gel and visualization of the fluorescent signal was made possible upon exposure to blue light excitation, using a Dark Reader Transilluminator (Clare Chemical Research, USA). The coupling efficiency was photometrically determined (as outlined by Hussain *et al*. (2019) [274]), using the theoretical extinction coefficients of the proteins and the extinction coefficients of the fluorescent dyes.

2.5.2 Generation of monomethyl auristatin F-containing immunoconjugates

AURIF was sourced from BrightGene Bio-Medical Technology (China) and the compound was BG-modified by MSc student Allan Huysamen (Professor Roger Hunter's group, Department of Chemistry, University of Cape Town, South Africa). The purified recombinant fusion proteins were incubated for 4 hours at room temperature, with a 3-fold molar excess of BG-modified AURIF (initially in lyophilized form, BG-AURIF was solubilized in 100% (v/v) dimethyl sulfoxide (DMSO) (Sigma-Aldrich, South Africa)), 1 M ectoine (a protein-stabilizing compatible solute [433]) (Sigma-Aldrich, South Africa) in 1x PBS and 1 mM DTT. The unconjugated BG-modified AURIF was removed using 10K-sized Amicon filters (Sigma-Aldrich, South Africa) according to the manufacturer's instructions. Since the resulting product cannot be directly visualized, saturation of the binding domain of SNAP-tag with BG-AURIF, was ascertained by post-incubation (double conjugation) with a 2-fold molar excess of BG-Alexa Fluor 488 for 1 hour

at 37^{o}C. Next, SDS-PAGE analysis was conducted and visualization of any potential fluorescence signal was carried out as described previously.

2.5.3 Conjugation to BG-modified IR700

Lyophilized BG-modified IRDye®700DX phthalocyanine (BG-PEG_{24}-IR700, henceforth referred to as BG-IR700) was kindly provided by Professor Matthias Peipp (University of Kiel, Germany). Following the solubilization of this compound in 50% (v/v) DMSO (Sigma-Aldrich, South Africa), the SNAP-tag based fusion proteins were then incubated with a 3-fold molar excess of BG-IR700 in the dark, for 4 hours at room temperature. In order to confirm successful conjugation with BG-IR700, the labeled fusion proteins were then resolved on an SDS-PAGE gel and visualization of the fluorescence signal was carried out using an iBright FL1000 Imaging System (Invitrogen, Thermo Fisher Scientific, South Africa). Subsequently, the unbound dye was removed using 10K-sized Amicon filters (Sigma-Aldrich, South Africa) according to the manufacturer's instructions. Interestingly, while the IR700 dye has proven to be a valuable tool for *in vivo* optical imaging, its narrow NIR fluorescence peak cannot be effectively detected by most traditional *in vitro* imaging devices, such as confocal microscopy and flow cytometry [345]. On this basis, the fusion proteins were therefore conjugated to BG-Alexa Fluor 488, as a surrogate for use in the confocal microscopy and flow cytometry experiments (section 2.6).

2.6 Binding analysis of the SNAP-tag based fusion proteins

2.6.1 Screening of target cells and validation of surface binding by confocal microscopy

In addition to its propriety as a qualitative method to validate surface binding, confocal microscopy was implemented as an initial screening strategy in the identification of antigen-positive TNBC cell lines available at MB&I (since the genetic makeup of cells can differ from those described in literature). Therefore, target cell lines (1 x 10^4 cells) were seeded on a coverslip in a 35 mm dish and incubated in RPMI-1640 (Gibco #10566) or DMEM medium (Gibco #61870) (both supplemented with 10% (v/v) heat-inactivated FBS and 1% (v/v) 100 U/ml penicillin-streptomycin) overnight in a 5% CO_2 incubator with 95% humidity at 37^{o}C. The next day, cells were incubated for 15-20 minutes with 15 µM of Alexa488-conjugated fusion protein in 100 µl of

serum-free medium and 200 µl of 1:5000 Hoechst stain (Thermo Fisher Scientific, South Africa). Excess dye was removed by washing the cells three times with 1x PBS, before fixing with 4% (v/v) paraformaldehyde (PFA) (Sigma-Aldrich, South Africa) for 20 minutes at room temperature. The cells were then washed one more time with 1x PBS and the coverslip was mounted on a microscope slide (using Mowiol mounting medium from Merck, USA). The slides were left to dry in the dark at room temperature for 24 hours, before images were captured on the Zeiss confocal-scanner microscope (LSM880) with Airyscan (Confocal and Light Microscope Imaging Facility, University of Cape Town, South Africa) on the 40X air objective.

2.6.2 Binding analysis and flow cytometric determination of receptor density on tumor cells

Flow cytometry was used to further verify the functionality (or binding potential) of the antibody moiety of the SNAP-tag based fusion proteins, while simultaneously allowing the relative quantitation of antigen/receptor expression status in a population of tumor cells.

2.6.2.1 Staining of cells

Briefly, adherent cells were lifted using Accutase® solution (Sigma-Aldrich, South Africa), a mild detachment reagent suitable for use in the analysis of cell surface markers. Approximately 2 x 10^6 cells were aliquoted per sample tube and centrifuged at 800 x g for 7 minutes at 4^{o}C. Thereafter, the supernatant was discarded and the cells were washed twice in 2 ml of 1x PBS to ensure complete removal of unspecific proteins in solution. After decanting the supernatant, the cell pellet was resuspended in 50 µl of a 1:2000 dilution of LIVE/DEAD^{TM} Fixable Violet Dead Cell Stain Kit (also known as ViViD) (Product number: L34963, Thermo Fisher Scientific, South Africa) and incubated at room temperature for 20 minutes in the dark. Of note, ViViD, an amine-reactive dye, works by crossing the cell membranes of dead cells and reacting irreversibly with free amines in their cytoplasm [434]. Dead cells can thus be identified by flow cytometry since live cells do not take up ViViD. Next, the cells were washed twice with 2 ml of FACS buffer (containing 2% (v/v) FBS and 0.1% (v/v) sodium azide (prevents antibody-antigen complex internalization that can cause loss of fluorescence intensity) in 1x PBS) and centrifuged at 800 x g for 7 minutes at 4^{o}C. The cells were then resuspended in the dead volume, incubated with 50 µl of Alexa Fluor 488-conjugated protein for 30 minutes at room temperature and washed twice with FACS buffer

as previously described. Here, an antibody titration was carried out (in duplicate), with various serial dilutions of scFv-SNAP-Alexa488 (0, 1, 5, 10, 25, 50, 100, 250, 500 and 1000 µg/ml). This was done to enable determination of the optimal antibody concentration to use in each experiment, to allow the best separation between the negative and positive populations, while excluding the maximum background fluorescence achievable [435]. Subsequently, to fix the cells, each cell pellet was resuspended in 300 µl of 1% (v/v) PFA solution and incubated for 10 minutes at room temperature in the dark. The cells were then washed twice with 2 ml of 1x PBS, resuspended in 300 µl of 1x PBS and kept in the dark at 4^{o}C until data acquisition.

2.6.2.2 Compensation controls

Compensation controls were prepared for every flow cytometry session. Compensation is an important prerequisite in multicolor flow cytometric analysis; it corrects for spectral overlap which arises from the use of fluorescent dyes that are perceivable by more than one detector [436,437]. A total of 3 compensation tubes were used in this study: (1) unstained anti-mouse Ig-*Kappa* compensation beads (Becton-Dickinson (BD) Biosciences, USA) (negative compensation control), (2) anti-mouse Ig-*Kappa* compensation beads stained with 5 µl of 1:10 dilution of FITC mouse anti-human CD107 (BD Biosciences, USA) (single stain FITC/Alexa488 compensation control) and (3) ArC^{TM} amine reactive compensation beads (Thermo Fisher Scientific, South Africa) stained with 1 µl of 1:40 dilution of ViViD (Pacific Blue/ViViD compensation control). The compensation beads were vortexed thoroughly before use (to avoid clumping) and thereafter, 1 full drop of the relevant compensation bead was added to each tube. The corresponding stain was added directly to the bead suspension and the samples were incubated for 30 minutes in the dark at room temperature. Next, the beads were washed with 2 ml of 1x PBS and centrifuged at 800 x g for 5 minutes at 4^{o}C. The supernatant was discarded and the beads were then resuspended in 150 µl of 1x PBS and stored at 4^{o}C in the dark until acquisition.

2.6.2.3 Acquisition

Samples were acquired using FACSDiva^{TM} software (v8.0.1) (BD Biosciences, USA) on a BD^{TM} LSR II flow cytometer equipped with a fluorescein isothiocyanate (FITC)/Alexa488 and Brilliant Violet 421/Pacific Blue laser lines (provided by the IDM Flow Cytometry Core Facility,

University of Cape Town, South Africa). For each cell sample, 5 x 10^4 events were acquired. Additionally, 2 x 10^4 events were acquired for each compensation control.

2.6.2.4 Analysis

Data analysis was carried out using FlowJo™ software (v10.6.1) (BD Biosciences, USA) and involved the generation of pseudocolor plots, whereby an appropriate gating strategy was devised to allow determination of the level of receptor expression on the surface of target cells (Figure 10).

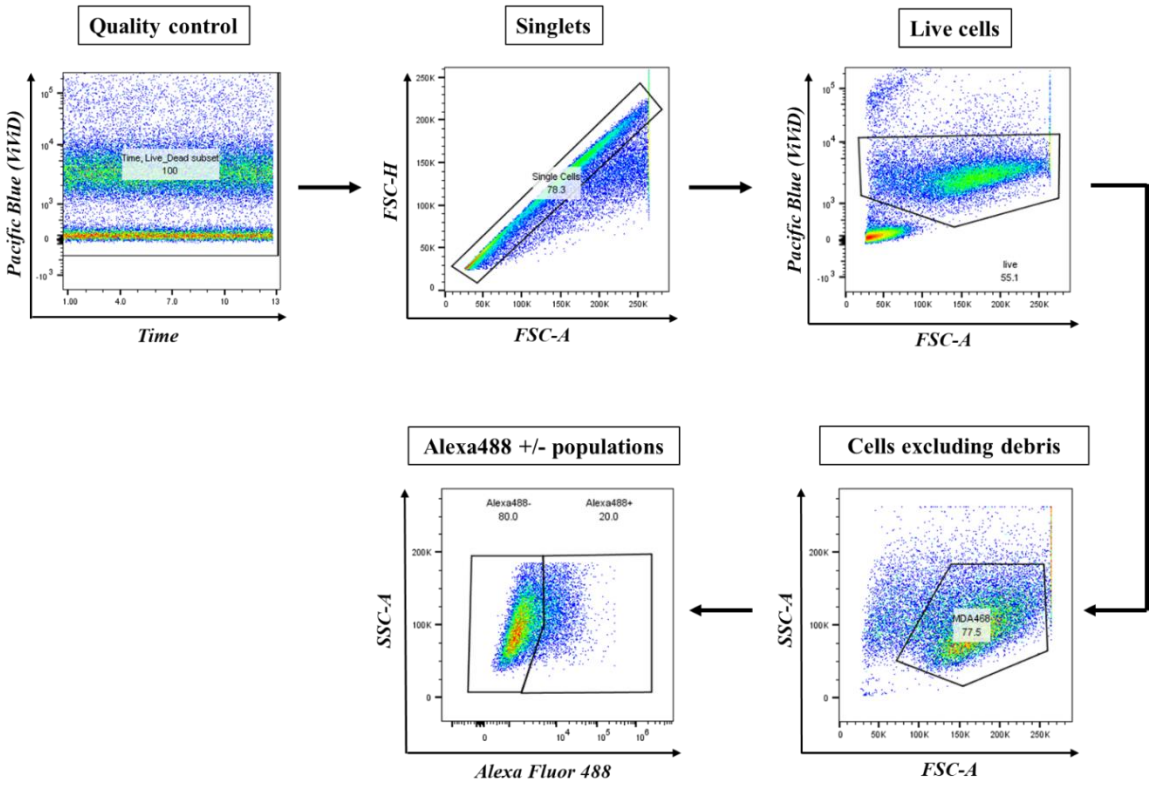

Figure 10: Representative pseudocolor plots indicating the gating strategy employed in the determination of the receptor expression status. Target cell lines were incubated with the Alexa488-conjugated scFv-SNAP fusion protein and acquired on a BD™ LSR II flow cytometer. Gating the cells on the basis of time served as an initial quality control step. Singlets were then identified in the forward scatter plots and dead cells were excluded by ViViD. After identifying the cell population of interest by ruling out the presence of debris, gates were applied for the identification of the Alexa488-positive/negative cell populations.

This also allowed the generation of antibody titration curves (using GraphPad Prism v5) for each cell line and scFv-SNAP-Alexa488 combinations, depicting the change in (1) signal-to-noise ratio, (2) staining index and (3) median fluorescence intensity (MFI) of the Alexa488-positive

population. The signal-to-noise ratio measures the difference in fluorescence between the positive and negative populations, whereas the staining index measures the relative brightness of the fluorochrome detected by the flow cytometer [435,438]. The below equations were used to compute these 2 parameters:

$$Signal-to-noise\ ratio = \frac{MFI\ (positive\ population)}{MFI\ (negative\ population)}$$

$$Staining\ index = \frac{MFI\ (positive\ population) - MFI\ (negative\ population)}{2\ X\ robust\ standard\ deviation\ (negative\ population)}$$

After selection of the optimal antibody titer, histograms and bar graph were generated, to compare the distribution of CSPG4, CD44 and ASPH across target cell lines. Statistical analyses were performed using GraphPad Prism v5; Student's *t*-tests (relative to the negative cell line) were calculated to show any statistical difference. A *p*-value of < 0.05 was considered to be statistically significant.

2.7 Cytotoxicity studies

2.7.1 Cytotoxic analysis of SNAP-tag based fusion proteins conjugated to BG-AURIF

Cells (5 x 10^3) were seeded in a 96-well plate (in either RPMI-1640 (Gibco #10566) or DMEM medium (Gibco #61870), supplemented with 10% (v/v) heat-inactivated FBS and 1% (v/v) 100 U/ml penicillin-streptomycin) and allowed to adhere overnight under standard tissue culture conditions (37ºC, 5% CO_2 and 95% humidity). The next day, they were treated with 3-fold serially diluted concentrations of AURIF (unmodified), BG-AURIF, scFv-SNAP (unconjugated) or scFv-SNAP-AURIF and incubated for 72 hours in a 5% CO_2 incubator with 95% humidity at 37ºC. Untreated cells served as negative controls (100% cell viability), while Zeocin-treated (100 µg/ml) cells were used as positive controls (0% cell viability). The Cell Proliferation Kit II (XTT) (Product number: 11465015001, Roche, Switzerland) was used (according to the manufacturer's protocol) to assess cytotoxicity. In this assay, cleavage of the tetrazolium salt XTT occurs in the presence of metabolically active cells and results in the formation of orange formazan crystals, which absorb

light at 450 nm. Thus, at 68 hours post-treatment, cells were treated with the XTT reagent and at 72 hours, absorbance readings (at 450 nm as the measurement filter and 650 nm as the reference filter) were taken using a spectrophotometer (iMark^{TM} Microplate Absorbance Reader, Bio-Rad, USA). All experiments were carried out in triplicate (n=3), with 3 technical repeats. The absorbance values were normalized with respect to the untreated and Zeocin controls, and the results were presented as a percentage of cell viability. The concentration required to achieve a 50% reduction in cell viability (IC_{50} value) was calculated using GraphPad Prism v5 software.

2.7.2 Evaluation of photoimmunotoxicity of IR700-conjugated fusion proteins

Target cell lines (5 x 10^3) were seeded in a 96-well plate (in either RPMI-1640 (Gibco #10566) or DMEM medium (Gibco #61870), supplemented with 10% (v/v) heat-inactivated FBS and 1% (v/v) 100 U/ml penicillin-streptomycin) and allowed to adhere overnight at 37°C in a 5% CO_2 atmosphere at 95% humidity. The following day, cells were incubated with 3-fold serially diluted concentrations of BG-IR700 or scFv-SNAP-IR700 and incubated for 3 hours at 37°C in the dark (negative control: untreated cells and positive control: Zeocin (100 µg/ml)). Concurrently, to assess whether the heat generated by the laser could potentially affect cell viability and compromise the reliability of the data, untreated (and treated) cells were either exposed to NIR light or left in the dark. Thereafter, the cells were washed in 1x PBS and incubated in 200 µl of phenol red-free media supplemented with 10% (v/v) heat-inactivated FBS and 1% (v/v) 100 U/ml penicillin-streptomycin (RPMI-1640: Gibco #11835-030 or DMEM: Gibco #21063-029), before being irradiated with a BioLambda LEDbox laser (São Paulo, Brazil) of 690 nm wavelength, set at 14 mW/cm^2 power density, 25 J/cm^2 dose and exposure time of 30 minutes. The following equation was used to determine the irradiation time:

$$Time\ (seconds) = \frac{Dose\ \left(\frac{J}{cm^2}\right)}{Power\ density\ \left(\frac{W}{cm^2}\right)}$$

Following light activation of IR700, the cells were left to recover for 24 hours in complete media in a 5% CO_2 incubator with 95% humidity at 37°C. At 20 hours post-recovery, XTT reagent was

added, absorbance readings were taken at 24 hours and the results were analyzed as described in section 2.7.1. All dose-response experiments were performed 3 times, with 3 technical repeats. Student's *t*-tests were also carried out to demonstrate any temperature-related changes in the growth of untreated cells (n=48) subjected to NIR light irradiation or left in the dark. Statistical significance was demonstrated by a *p*-value of < 0.05 (calculated using GraphPad Prism v5).

Chapter 3: Results

Given their cardinal roles in promoting tumor growth, proliferation, resistance and metastasis, CSPG4, CD44 and ASPH represent promising target antigens in the management of TNBCs [353,368,384,413,416]. This clinically aggressive and heterogeneous disease warrants the need for a cornucopia of reliable medical tools, which when combined, ensures the coverage, detection and targeting of the vast majority of triple-negative breast tumors, thereby enabling the expansion of precision medicine. Consequently, the fundamental purpose of the present work pertains to the development of novel antibody-based diagnostic and therapeutic approaches that form an important first step in responding to the medical urgency of TNBCs. More precisely, this study aimed to harness the versatility of SNAP-tag technology to engineer and assess the *in vitro* functionality of CSPG4, CD44 and ASPH-targeting (1) recombinant immunodiagnostics, (2) homogeneous AURIF-containing ADC products and (3) IR700-based photoimmunotheranostic agents. Therefore, the results chapter is divided as follows: the first 2 sections (sections 3.1 – 3.2) describe the *in silico* design and molecular cloning strategies employed (as exemplified for αCD44(scFv)-SNAPf), the next 3 sections (sections 3.3 – 3.5) summarize the generation and characterization of the fusion proteins, while the last 2 sections (sections 3.6 – 3.7) demonstrate the comparative binding and cytotoxic activities of the immunoconjugates on TNBC cells.

3.1 In silico design of mammalian expression vectors

In view of developing a panel of diagnostic tools, as well as a reliable strategy for the targeted delivery of cytotoxic warheads (AURIF/IR700), scFv gene sequences specifically targeting the 3 receptors, were subjected to IgBLAST analysis (section 2.2). As an *in silico* quality control tool, IgBLAST confirmed the presence of intact CDRs and FR regions in the scFv sequence (as illustrated for αCD44(scFv) in Figure 11A). The CLC genomics workbench application was then used to align and compare the reliability of the V genes before proceeding to *in silico* cloning. Next, each scFv was genetically modified through the insertion of *Sfi*I and *Not*I restriction enzyme cutting sites. The ORF for each construct was accordingly generated through insertion of the scFv sequences into the pCB-SNAP backbone, which includes an enterokinase recognition sequence for removal of the N-terminal pre-peptide in order to generate the final active product (Figure 11B-

D). The scFv portion is located 3' to SNAP-tag, while the polyhistidine tag [426] and the Ig-*Kappa* leader sequence [427], are located at the N-terminus. After generation of the recombinant plasmids and ensuring the absence of stop codon interference, the scFv sequences were aligned to their parental (patent) sequences to validate the integrity of the CDRs and FR regions. Finally, the confirmed scFv sequences were sent to Genescript (USA) for synthesis into a commercial pUC57 vector, with *Sfi*I and *Not*I as unique restriction sites.

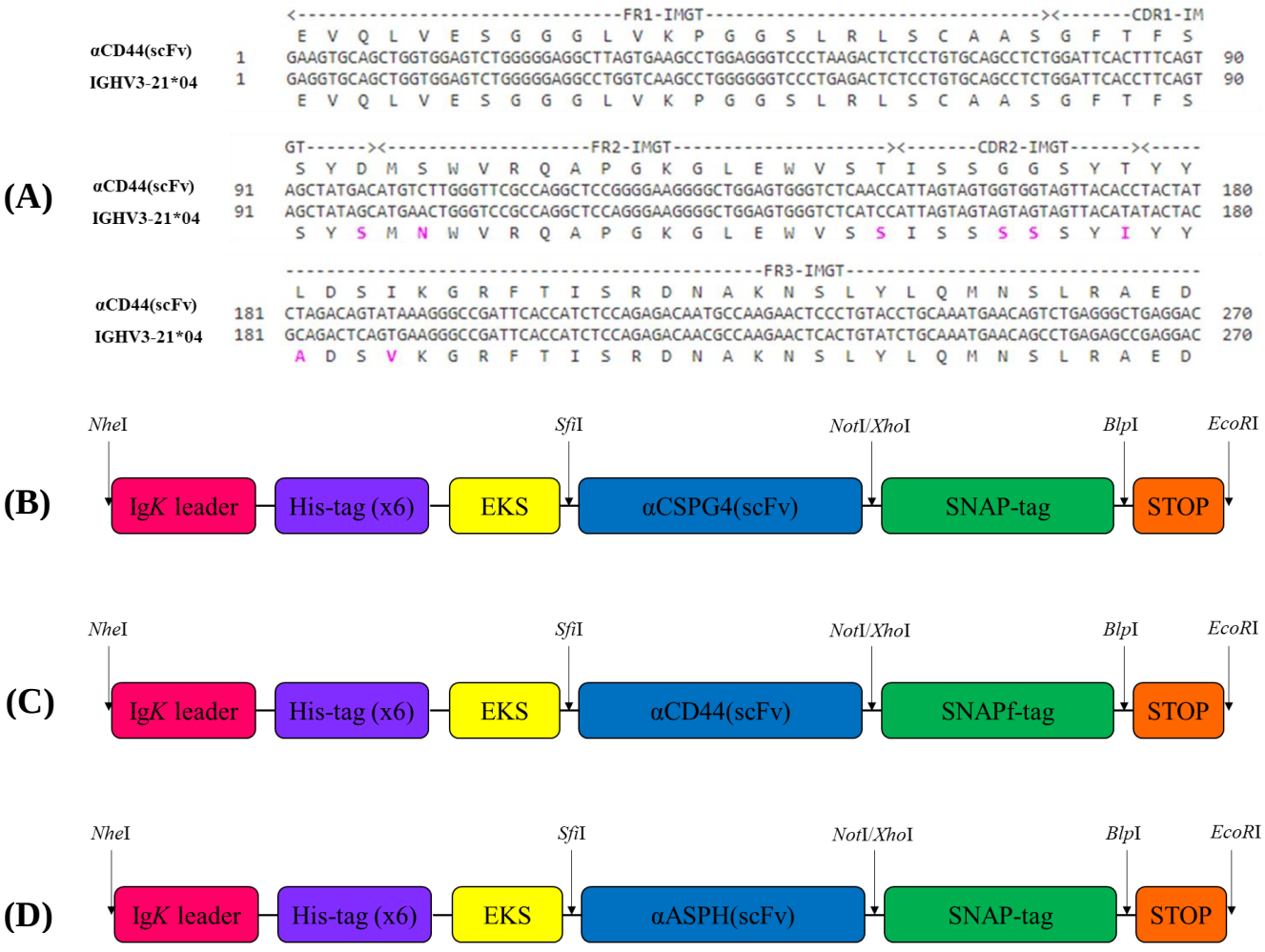

Figure 11: *In silico* design of mammalian expression plasmids for CSPG4/CD44/ASPH-targeting SNAP-tag based fusion proteins. (A) IgBLAST analysis of αCD44(scFv) comparing the extracted scFv sequences against existing immunoglobulin germline variable region gene sequences. Intact (no stop codon) CDRs and FR regions were identified. Variations from the germline sequence are represented in pink. ORFs coding for (B) αCSPG4(scFv)-SNAP, (C) αCD44(scFv)-SNAPf and (D) αASPH(scFv)-SNAP. Here, *Sfi*I and *Not*I restriction sites were used in the cloning of the scFv genes into the pCB-SNAP backbone. Important components of the ORFs are indicated in the figure legend (Ig*K* leader: Ig-*Kappa* leader sequence for secretion of the fusion protein expressed by host cells, His-tag (x6): 6 histidine tags for protein

purification by IMAC and detection in western blot analysis, EKS: enterokinase cleavage site for the enzymatic removal of the N-terminal elements and STOP: stop codon for halting protein synthesis).

3.2 Generation of pCB-αCD44(scFv)-SNAPf using molecular cloning

3.2.1 Ligation of αCD44(scFv) to the pCB-SNAPf backbone

Following restriction enzyme digest of the starter plasmids (pCB-AnnexinV-SNAPf and pUC57-αCD44(scFv)), the insert and the vector DNA fragments were excised from agarose gels and purified in preparation for ligation (section 2.3.6). The ligation products were then transformed into chemically competent DH5α *E. coli* cells and plated onto LB agar plates supplemented with 200 µg/ml ampicillin, which provided a stable and controlled environment for the growth of bacteria possessing the ampicillin resistance gene (from the transformed recombinant plasmids). Therefore, bacterial clones encompassing the pCB-αCD44(scFv)-SNAPf plasmids were able to grow due to their capacity to express β-lactamase, which catalyzes the hydrolysis of the β-lactam ring of ampicillin [439]. No bacterial growth was observed on the contamination (control) plate (Figure 12E). However, the 'vector only' plate showed the presence of bacterial colonies, indicating vector re-ligation (Figure 12D). The calculated transformation efficiencies of the pCB-αCD44(scFv)-SNAPf plates for 1:1, 1:2 and 1:3 ratios of vector to insert, were 2.40 x 10^5 cfu/µg, 2.68 x 10^5 cfu/µg and 2.98 x 10^5 cfu/µg respectively.

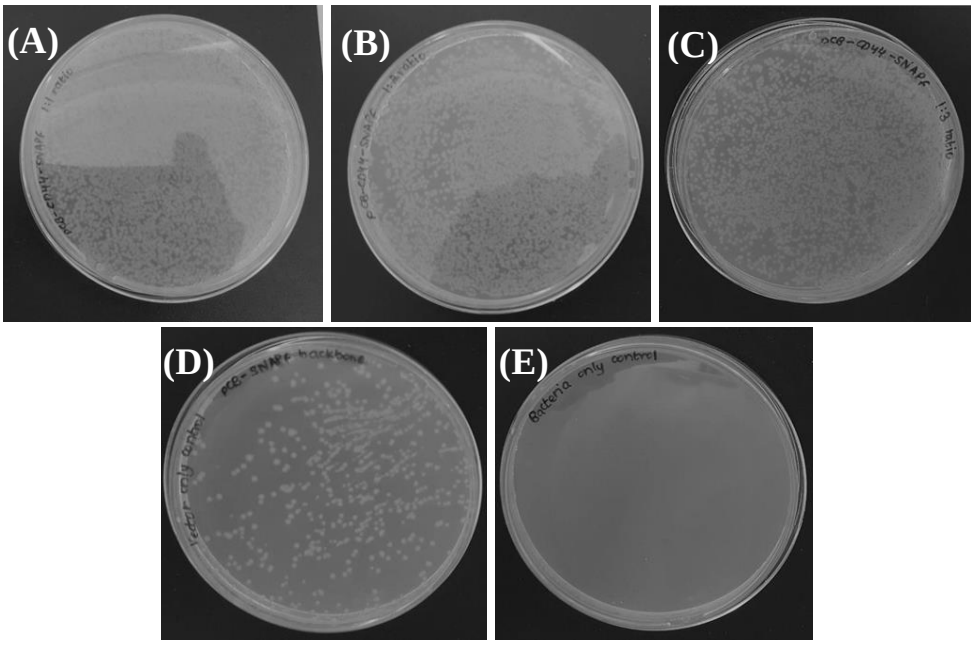

Figure 12: Growth of *E. coli* cells transformed with potential recombinant pCB-αCD44(scFv)-SNAPf plasmid DNA. Following transformation, 100 µl of bacterial mixture was plated onto LB agar plates, which were then incubated overnight at 37˚C (section 2.3.6). The concentration of ampicillin used was 200 µg/ml. (A) 1:1 ratio of vector to insert, (B) 1:2 ratio of vector to insert, (C) 1:3 ratio of vector to insert, (D) vector only plate and (E) contamination control.

3.2.2 Restriction mapping on selected pCB-αCD44(scFv)-SNAPf clones

Restriction mapping was used to confirm successful ligation of the αCD44(scFv) into the pCB-SNAPf backbone (section 2.3.7). To this end, a virtual simulation was first carried out on SnapGene software, in order to determine whether the selected enzymes would produce differential fragmentation of the recombinant and parental plasmids (Figure 13A). In this experiment, both pCB-αCD44(scFv)-SNAPf recombinant clones and the pCB-AnnexinV-SNAPf parental clone, were singly digested with *Bam*HI-HF and *Pvu*II-HF (Figure 13B), resulting in distinct fragment patterns that were in accordance with the theoretical agarose gel simulation. Therefore, while confirming successful cloning, this result ensures that re-ligated vector clones were not selected for DNA sequencing.

(A)

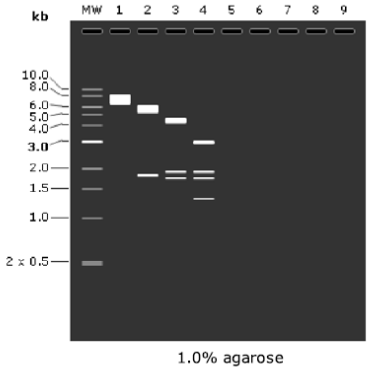

MW: 1 Kb DNA Ladder

1: pCB-AnnexinV-SNAPf
BamHI
1. 8236 bp = linearized at BamHI (2592)

2: pCB-CD44-SNAPf
BamHI
1. 6159 bp = BamHI (2340) – BamHI (515)
2. 1825 bp = BamHI (515) – BamHI (2340)

3: pCB-AnnexinV-SNAPf
PvuII
1. 4593 bp = PvuII (5350) – PvuII (1707)
2. 1895 bp = PvuII (1707) – PvuII (3602)
3. 1748 bp = PvuII (3602) – PvuII (5350)

4: pCB-CD44-SNAPf
PvuII
1. 3028 bp = PvuII (5098) – PvuII (142)
2. 1895 bp = PvuII (1455) – PvuII (3350)
3. 1748 bp = PvuII (3350) – PvuII (5098)
4. 1313 bp = PvuII (142) – PvuII (1455)

(B)

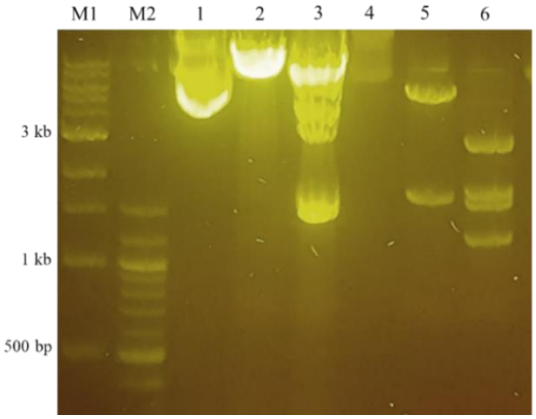

M1: 1 kb DNA ladder

M2: 100 bp DNA ladder

1: Undigested control
2: *Bam*HI-HF digest
3: *Pvu*II-HF digest
} pCB-AnnexinV-SNAPf

4: Undigested control
5: *Bam*HI-HF digest
6: *Pvu*II-HF digest
} pCB-αCD44(scFv)-SNAPf

Figure 13: Analysis of restriction mapping for pCB-αCD44(scFv)-SNAPf clones using agarose gel electrophoresis. All digestions were run overnight at 37˚C. DNA fragments were separated using a 1.2% (w/v) agarose gel ran for 1 hour at 100 volts. Digests on pCB-AnnexinV-SNAPf were used for comparison purposes (section 2.3.7). (A) Simulated digestion using SnapGene and (B) restriction mapping on pCB-AnnexinV-SNAPf and pCB-αCD44(scFv)-SNAPf clones.

3.2.3 Sequencing results of selected pCB-αCD44(scFv)-SNAPf clones

The selected recombinant plasmids were sent to Inqaba Biotechnical Industries (South Africa) for Sanger DNA sequencing. SnapGene was then used to confirm the integrity of the cloned product by aligning the resulting sequences with the original *in silico* sequence (section 2.3.7). As shown in Figure 14, the selected pCB-αCD44(scFv)-SNAPf clones showed approximately 100% homology with the *in silico* ORF sequence, thus confirming the credibility of the DNA sequence (successful incorporation of αCD44(scFv) into the pCB mammalian expression system) before proceeding to protein expression.

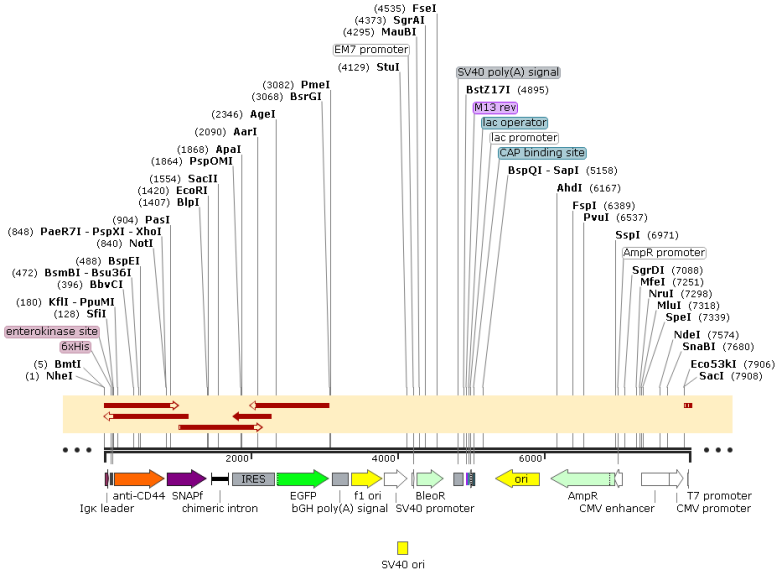

Figure 14: Map generated following alignment of trace sequences with the corresponding *in silico* sequence for pCB-αCD44(scFv)-SNAPf. The clones corresponded closely (approximately 100% homology) with the *in silico* ORF sequence (as indicated by the primers used (dark red arrows)).

3.3 Transfection into HEK293T cells for protein expression

Upon confirmation of the DNA sequences, the recombinant plasmids (pCB-αCSPG4(scFv)-SNAP, pCB-αCD44(scFv)-SNAPf and pCB-αASPH(scFv)-SNAP) were introduced into HEK293T cells for protein expression. Successfully transfected cells (potentially expressing the

putative fusion protein) were identified through microscopic visualization of eGFP using a ZOE™ Fluorescent Cell Imager (Bio-Rad Laboratories, UK). Using flow cytometry (section 2.4.1), the transfection efficiencies were determined as follows: 25.5%, 21.1% and 7.98%, for pCB-αCSPG4(scFv)-SNAP, pCB-αCD44(scFv)-SNAPf and pCB-αASPH(scFv)-SNAP respectively. Based on these values (transfection efficiencies < 70-80%), Zeocin selection (100 µg/ml) was applied to enrich the eGFP-positive cell population carrying the bleomycin resistance gene. These cells were then maintained in culture (ideally at 90% confluency) (Figure 15) until the cell culture supernatant (containing the fusion protein of interest) was ready for collection.

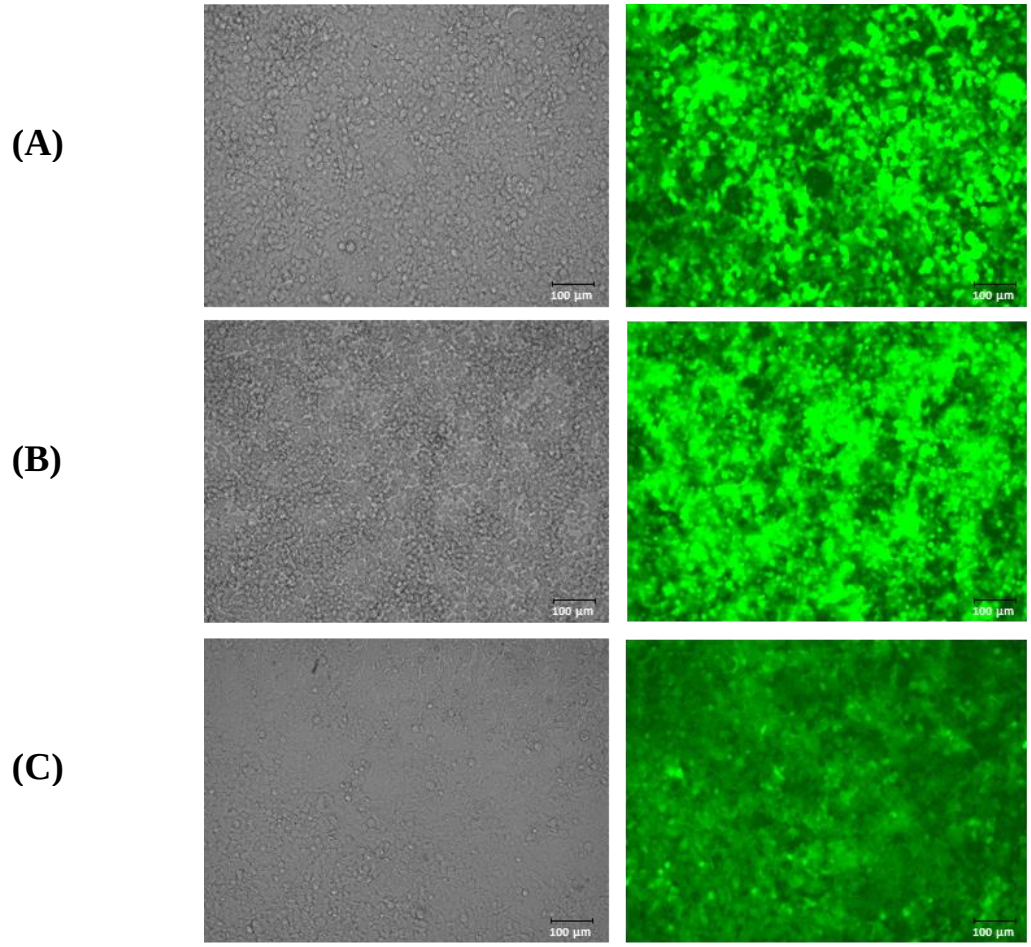

Figure 15: Microscopic visualization of eGFP in transfected HEK293T cells. (A) pCB-αCSPG4(scFv)-SNAP, (B) pCB-αCD44(scFv)-SNAPf and (C) pCB-αASPH(scFv)-SNAP. Transfection was carried out using XtremeGene™ transfection reagent (Sigma-Aldrich, South Africa) according to the manufacturer's instructions and eGFP enrichment was performed using 100 µg/ml of Zeocin (section 2.4.1). The green channel (right panel) was used to assess eGFP expression while the brightfield (or phase contrast) channel (left panel) showed the number of cells in a specific region. Images were taken using a ZOE™ Fluorescent Cell Imager at 100 µm magnification.

3.4 Purification of recombinant scFv-SNAP fusion proteins

3.4.1 SDS-PAGE analysis and densitometric quantification of purified protein fractions

Purification of the recombinant fusion proteins (from 1 litre of cell culture supernatant) was carried out using IMAC, whereby their elution was made possible through competitive binding between his-tag and imidazole for the Ni^{2+} column. The resulting elution profiles are shown in Figure 16, depicting the tendency of the purified SNAP-tag based fusion proteins being eluted from the column in the form of 2 distinct peaks, upon the application of increasing imidazole concentration via a gradient (0-30% imidazole) and step elution process (100% imidazole) (section 2.4.2).

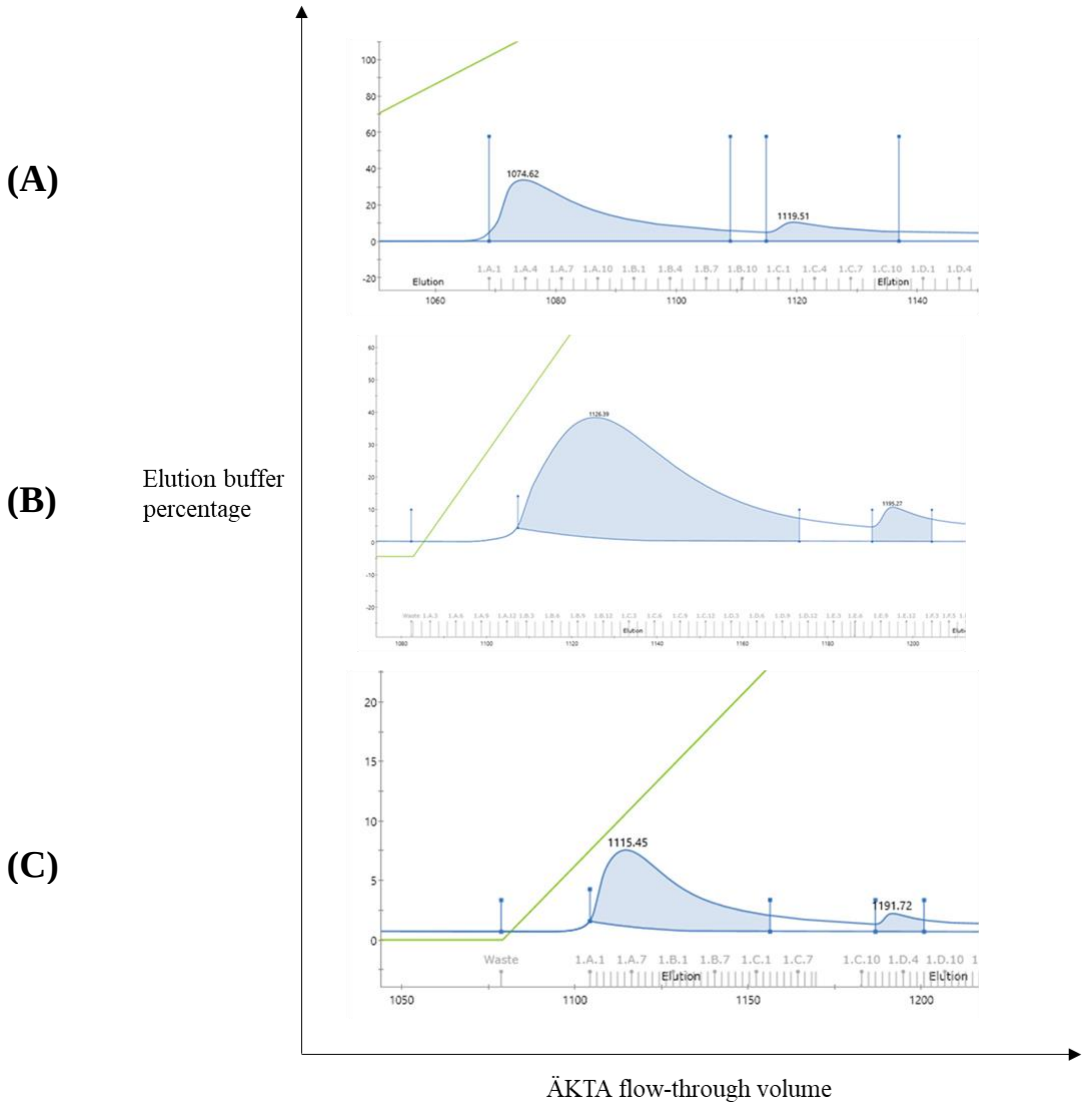

Figure 16: Chromatograms of (A) αCSPG4(scFv)-SNAP, (B) αCD44(scFv)-SNAPf and (C) αASPH(scFv)-SNAP after purification using IMAC. The *y*-axis is a measure of the elution buffer percentage, while the *x*-axis represents the ÄKTA flow-through volume with respect to increasing time. The blue line shows the elution profile of fusion protein and the green line demonstrates the concentration gradient of imidazole. Fractions were eluted in the form of 2 distinct peaks on the chromatogram.

Thereafter, each crude protein fraction was run on a 10% SDS-PAGE gel (Figure 17) that enabled the electrophoretic separation and identification of each fusion protein based on their molecular weights (as indicated by red arrow) (theoretical sizes for αCSPG4(scFv)-SNAP, αCD44(scFv)-SNAPf and αASPH(scFv)-SNAP are 51.1 kDa, 49.7 kDa and 51.2 kDa respectively). This step represents an important deciding factor in the subsequent pooling and enrichment of protein fractions (section 2.4.3); only fractions containing the putative fusion proteins were pooled, concentrated and desalted (removal of residual imidazole) prior to further characterization.

(A)

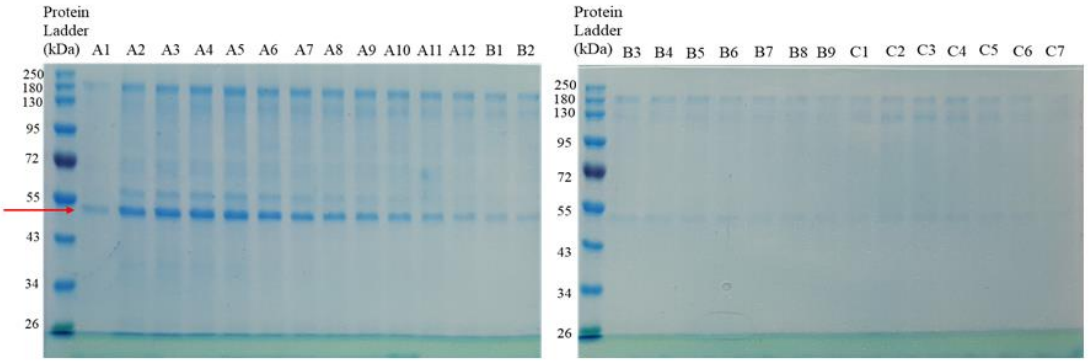

(B)

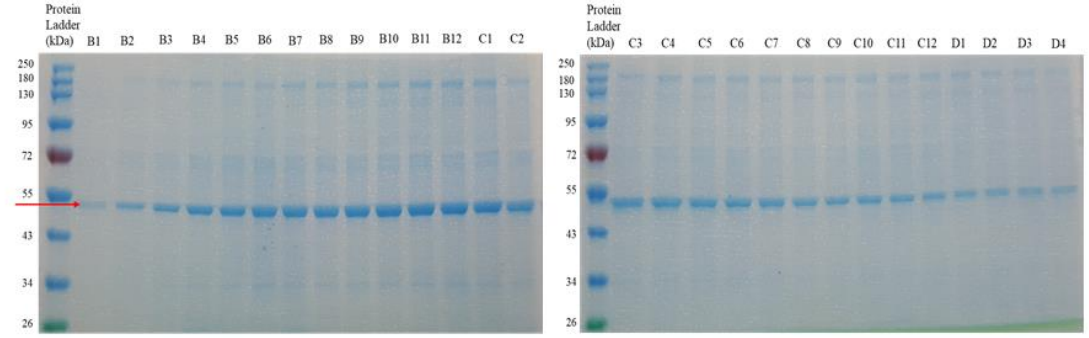

(C)

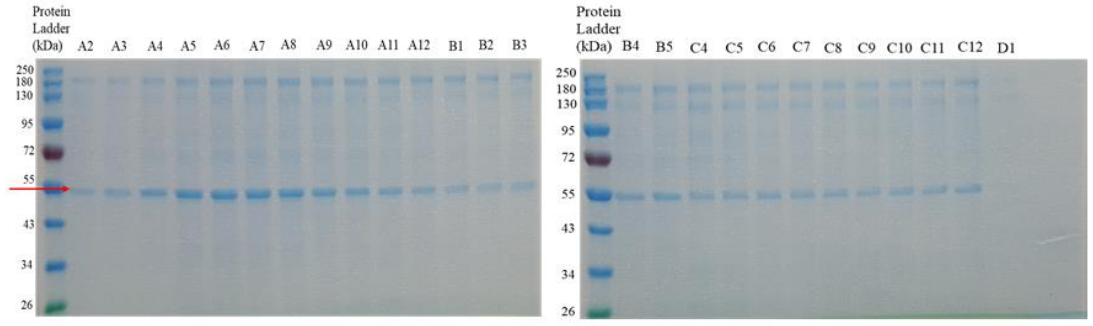

Figure 17: SDS-PAGE analysis of pre-concentrated IMAC eluate scFv-SNAP protein fractions. (A) αCSPG4(scFv)-SNAP (51.1 kDa), (B) αCD44(scFv)-SNAPf (49.7 kDa) and (C) αASPH(scFv)-SNAP (51.2 kDa). Following IMAC purification, a 10% SDS-PAGE gel was run to confirm expression of the fusion proteins and assess their purity (based on their differential molecular weights and rate of migration upon application of an electric field). The SDS-PAGE gel was run at 100 volts for 95 minutes and 15 µl of protein was loaded per well (fraction numbers are indicated at the top of each well). Thereafter, the protein bands were visualized by staining the gel with Aqua staining solution. Page Ruler prestained protein ladder from Thermo Fisher Scientific (South Africa) was used to determine the protein molecular weights.

Next, Amicon (10K molecular weight cut-off)-concentrated protein fractions (comprising peaks 1 and 2) were ran on a 10% SDS-PAGE gel. Two-fold serially diluted BSA standards were ran adjacent to the purified fusion protein, thus enabling protein quantification by densitometry. Presence of full-length scFv-SNAP fusion protein is indicated by red arrow (Figure 18).

(A)

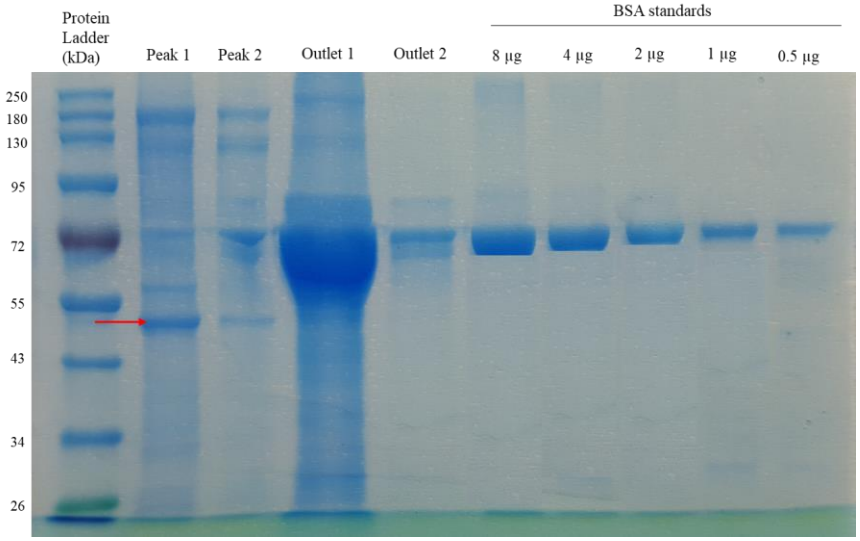

(B)

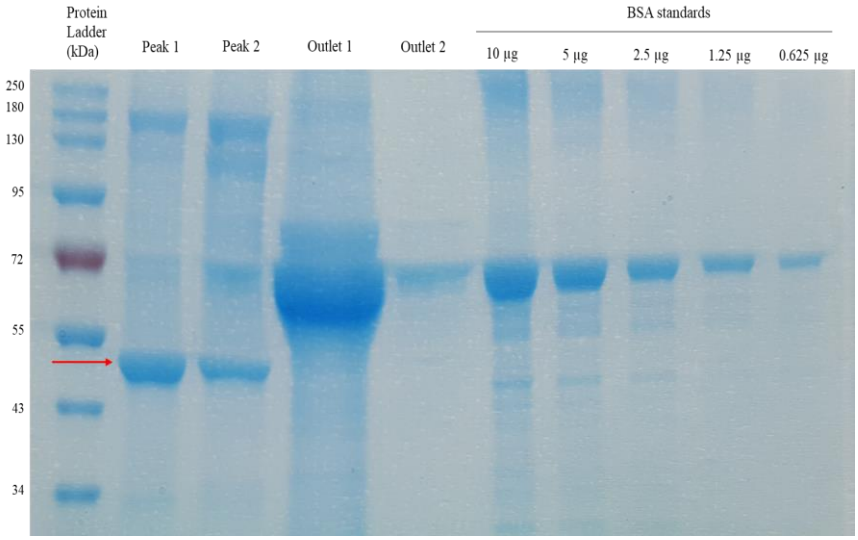

(C)

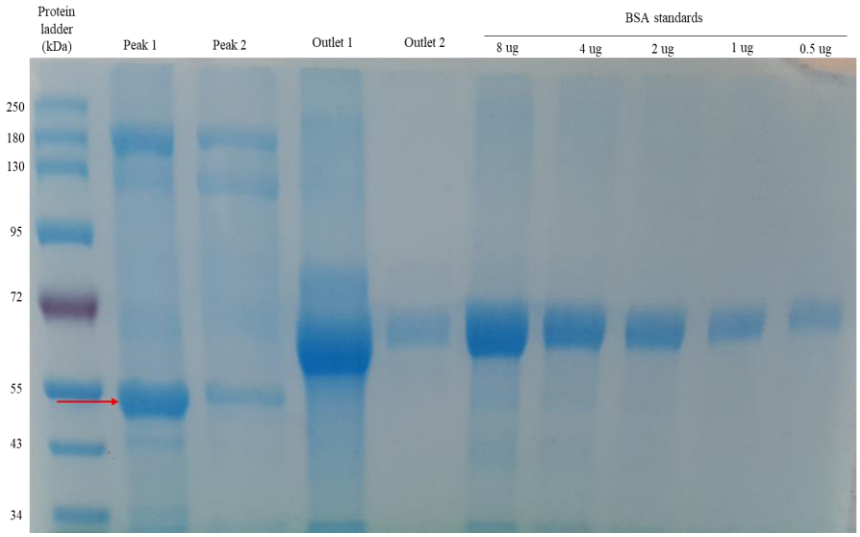

Figure 18: SDS-PAGE analysis of concentrated IMAC eluate scFv-SNAP protein fractions. (A) αCSPG4(scFv)-SNAP (51.1 kDa), (B) αCD44(scFv)-SNAPf (49.7 kDa) and (C) αASPH(scFv)-SNAP (51.2 kDa). Following Amicon (10K-sized) concentration, a 10% SDS-PAGE gel was run to re-confirm expression of the fusion proteins and assess their purity (section 2.4.3). The SDS-PAGE gel was run at 100 volts for 95 minutes and 20 µg of total protein from peaks 1 and 2, were loaded in lanes 2 and 3 respectively. Two-fold serially diluted BSA standards were ran in lanes 6-10 to allow protein quantification via densitometry. Outlets 1 and 2 (lanes 4 and 5) (usually containing BSA from the cell culture supernatant) represent the residual flow-through from the Ni^{2+} column following protein purification. Presence of full-length scFv-SNAP protein is indicated by red arrow. Thereafter, the protein bands were visualized by staining the gel with Aqua staining solution. Page Ruler prestained protein ladder from Thermo Fisher Scientific (South Africa) was used to determine the protein molecular weights.

Furthermore, to evaluate the efficacy of this protein purification step, residual flow-through from the Ni^{2+} sepharose column (outlets 1 and 2) were also inspected; while BSA from the cell culture supernatant was clearly visible, no remnant of scFv-SNAP was observed, confirming optimal performance of the metal-charged resin. Due to the presence of additional non-specific bands, especially at approximately 130-180 kDa (which denote a rate of purity of < 90%) (Figure 18), densitometry measurements (section 2.4.3) were carried out using ImageJ software to estimate the percentage of the total protein concentration (determined by UV spectrophotometry using a DeNovix DS-11) which corresponds to the scFv-SNAP fusion protein.

To this end, a standard curve was plotted, consisting of the optical colour intensity of the BSA standards (quantified by ImageJ software) on the *y*-axis, against the corresponding amount of protein on the *x*-axis (as illustrated in the case of αCSPG4(scFv)-SNAP in Figure 19). Therefore,

by extrapolating the measured colour intensity of the target bands to their protein quantity, the calculated yields and purity of each fusion protein were determined as shown in Table 7 below.

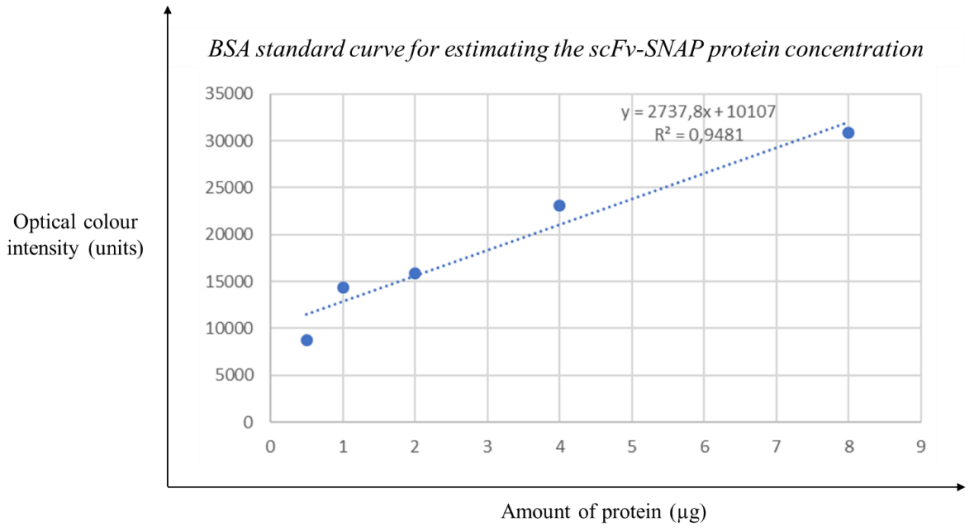

Figure 19: Generation of a BSA standard curve for the determination of αCSPG4(scFv)-SNAP protein concentration. Following measurement of optical colour intensity for the BSA standard bands (using ImageJ software), a graph of optical colour intensity (in units) was plotted against the corresponding amount of protein (in µg). Using the resulting graphical equation, the amount of scFv-SNAP protein in the total protein sample, was estimated, and allowed determination of the protein yield and percentage purity (as shown in Table 7).

Table 7: Densitometric quantification of the purified recombinant fusion proteins

scFv-SNAP fusion protein	[α]Total protein concentration in mg/L	[β]Calculated protein yield in mg/L	[γ]Percentage of scFv-SNAP in total IMAC purified protein sample	[δ]Absolute protein concentration in mg/L
αCSPG4(scFv)-SNAP peak 1	8.10	1.76	21.7%	2.35
αCSPG4(scFv)-SNAP peak 2	0.94	0.11	11.7%	0.75

αCD44(scFv)-SNAPf peak 1	9.84	2.28	23.2%	3.65
αCD44(scFv)-SNAPf peak 2	2.53	0.30	11.9%	0.20
αASPH(scFv)-SNAP peak 1	3.99	0.71	17.8%	1.23
αASPH(scFv)-SNAP peak 2	0.47	0.04	8.5%	0.02

α: quantified by UV spectrophotometry, β: determined by densitometry, γ: value from β divided by value from α (expressed as a percentage), and δ: based on calculated scFv-SNAP concentration (from β) and total volume of protein recovered from cell culture supernatant.

The data computed in the above table, indicate that the protein purity and absolute yield ranged from 8.5 – 23.2% and 0.02 – 3.65 mg/L respectively. Such prevailing poor yield and purity (< 90%) advocate the need for an additional or improved protein purification strategy. Nonetheless, since the lowest values were obtained from peak 2, peak 1 was rationally chosen for use in the downstream functional assays. Lastly, the disparities observed in the calculated values across the various fusion proteins, suggest that their expression could be influenced by various undefined *in vitro* environmental and physiological factors.

3.4.2 Western blot analysis of purified protein fractions

To further confirm successful expression and integrity (proper folding) of full-length recombinant fusion proteins bearing functional his-tags, a western blot was carried out by transferring the protein bands from an unstained SDS-PAGE gel to a nitrocellulose membrane (section 2.4.3). Thereafter, the proteins were incubated with an anti-his rabbit primary antibody which binds to the C-terminal histidine residues of the fusion proteins. A secondary antibody (goat anti-rabbit HRP-conjugate antibody) then allowed visualization of the his-tagged fusion proteins by reaction with a chemiluminescent substrate. From Figure 20, presence of intact full-length fusion protein observed on the SDS-PAGE gel (left panel), can be correlated to the same molecular size bands on the western blot (as indicated by red arrow on right panel). Clear signs of minor protein degradation can be observed in peak 1 and/or peak 2 for αCD44(scFv)-SNAPf and αASPH(scFv)-

SNAP (bands at ~20-35 kDa on western blot). While the exact cause for this phenomenon is open to speculation (for example: temperature, trace presence of proteases, protein misfolding), it can jeopardize future experimental setups if the degradation products encompass a functional SNAP-tag domain.

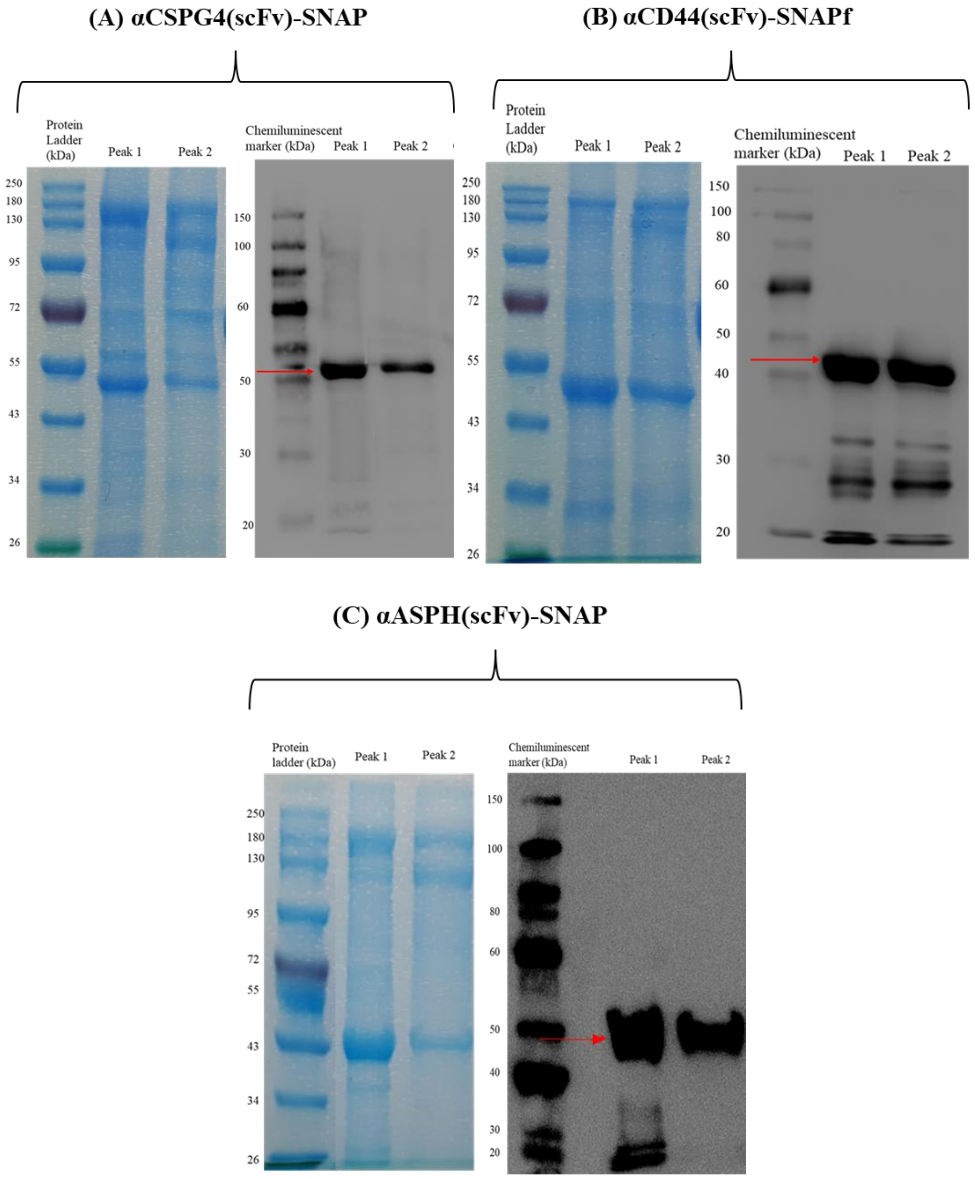

Figure 20: Western blot analysis of enriched scFv-SNAP fusion protein fractions. (A) αCSPG4(scFv)-SNAP (51.1 kDa), (B) αCD44(scFv)-SNAPf (49.7 kDa) and (C) αASPH(scFv)-SNAP (51.2 kDa). Left panel: Comparison of protein profiles on a 10% SDS-PAGE gel stained with Aqua staining solution. Right panel: Immunoblot of proteins transferred to a nitrocellulose membrane from a duplicate SDS-PAGE gel. Transfer was done at 100 volts for 75 minutes and 1 µg/µl protein was loaded per well. A chemiluminescent ladder (5 µl) (SuperSignal™ Molecular Weight Protein Ladder) was used to assess the size of the protein bands. An anti-his rabbit antibody (1:1000 primary antibody) and a goat anti-rabbit HRP-conjugate

antibody (1:5000 secondary antibody) were used. Red arrow indicates presence of full-length recombinant scFv-SNAP fusion protein. The membrane was visualized using a Gel Doc™ XR Gel Documentation System.

3.5 Conjugation of SNAP-tag based fusion proteins to BG-Alexa Fluor 488

After confirming the (N-terminal) integrity of the recombinant fusion proteins, the next step involved investigating the self-labeling activity of their SNAP-tag moiety. Therefore, the scFv-SNAP fusion proteins were conjugated with BG-Alexa Fluor 488 as described in section 2.5.1 and the resulting products were resolved on an SDS-PAGE gel, prior to visualization under blue light excitation (Figure 21). The observable fluorescent bands corresponded with the theoretical size of the fusion proteins, thus confirming the functionality and binding activity of SNAP-tag to BG-modified substrates such as BG-Alexa Fluor 488. Most importantly, the degraded protein bands (observed in Figure 20) showed no conjugation to the fluorophore. The bottom bands indicated the presence of unconjugated (excess) fluorescent substrate, which were removed using Zeba™ Spin Desalting Columns (40 kDa) (Thermo Fisher Scientific, South Africa) before proceeding to binding assays. The coupling efficiency was determined as described previously [274]; after 30 minutes incubation at 37°C, the labeling efficiency was 91, 95 and 86% for αCSPG4(scFv)-SNAP, αCD44(scFv)-SNAPf and αASPH(scFv)-SNAP respectively.

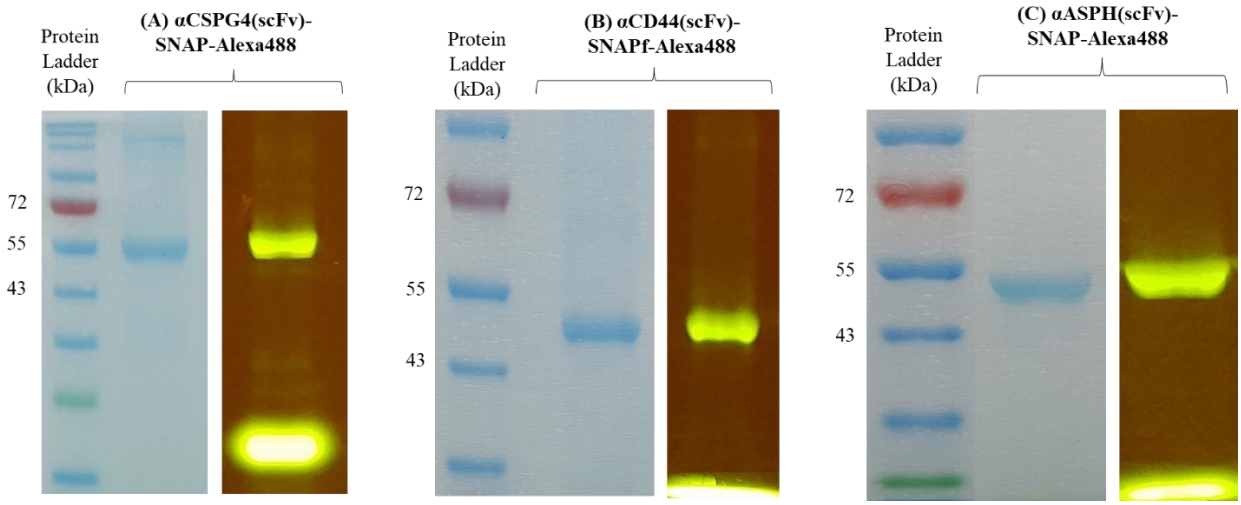

Figure 21: Assessing the binding activity of scFv-SNAP to BG-Alexa Fluor 488. A ratio of 1:2 of protein to BG-Alexa Fluor 488 was used in the conjugation reaction (5 µM to 10 µM). (A) αCSPG4(scFv)-SNAP (51.1 kDa), (B) αCD44(scFv)-SNAPf (49.7 kDa) and (C) αASPH(scFv)-SNAP (51.2 kDa). Left panel: Alexa488-conjugated protein ran on a 10% SDS-PAGE gel stained with Aqua staining solution. Right

panel: The same SDS-PAGE gel visualized under blue light for potential fluorescence. The SDS-PAGE gel was run at 100 volts for 95 minutes and 20 µl of conjugated protein sample was loaded per well. Page Ruler prestained protein ladder (Thermo Fisher Scientific, South Africa) was used to confirm the protein sizes. A Dark Reader Transilluminator was used for visualization of the fluorescent signal.

3.6 Investigating the binding activity of scFv-SNAP-Alexa Fluor 488 to target cells

3.6.1 Screening of target cells and validation of surface binding by confocal microscopy

The overarching working principle of targeted diagnostics and therapeutics relies heavily on the expression of accessible (often surface-bound) target antigens. Consequently, to fully assess the potential of the SNAP-tag based immunoconjugates as therapeutics for TNBCs, it became instrumental to assess the membrane expression of CSPG4, CD44 and ASPH on a panel of target cell lines (consisting of Hs578T, MDA-MB-231 and MDA-MB-468 as TNBC cells) using confocal microscopy (section 2.6.1). Simultaneously, this also allowed the binding ability (or functional integrity) of the antibody fragments to be evaluated. Membrane binding of αCSPG4(scFv)-SNAP-Alexa488 (Figure 22) (green signal) was confirmed on Hs578T, MDA-MB-468 and SK-Mel-28 cells (melanoma cells). Interestingly, the following observations were made: Hs578T and SK-Mel-28 cells displayed even membrane staining throughout most fields of view, MDA-MB-468 cells showed staining in certain areas only, and HEK293T and MDA-MB-231 cells exhibited no CSPG4-associated fluorescent signal. Therefore, the latter two cell lines were postulated to be negative for CSPG4.

(A) HEK293T **(B) Hs578T**

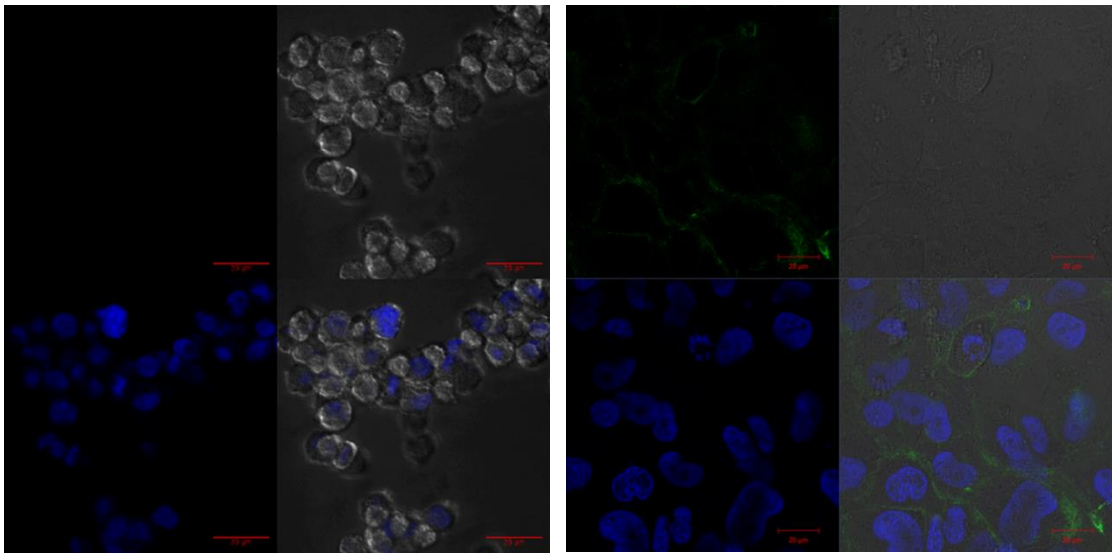

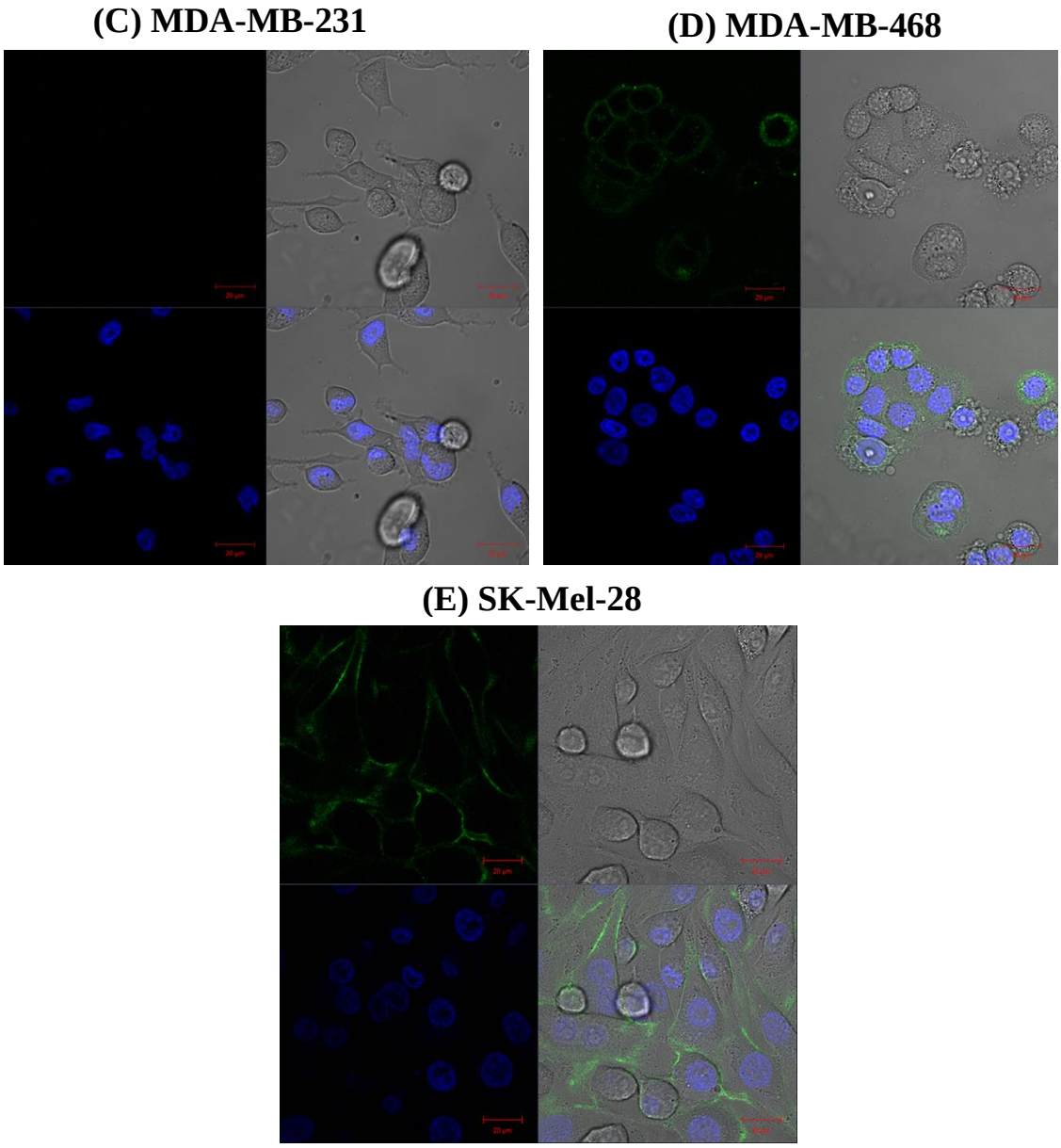

Figure 22: Assessing the binding activity of αCSPG4(scFv)-SNAP-Alexa488 by screening target cells for potential CSPG4 expression. (A) HEK293T, (B) Hs578T, (C) MDA-MB-231, (D) MDA-MB-468 and (E) SK-Mel-28. Cell lines were incubated with 15 µM of conjugated protein (green signal) for 15-20 minutes at 37ºC. Hoechst (1:5000 dilution in media) was used as a stain for the nuclei (blue signal). Washes were performed 3 times with 1x PBS, before fixing with 4% PFA and mounting the coverslips on a microscope slide. Images were captured using a Zeiss confocal-scanner microscope (LSM880) with Airyscan at 20 µm magnification.

Similarly, by using the same strategy, surface binding of αCD44(scFv)-SNAPf-Alexa488 was observed on Hs578T, MCF-7 and MDA-MB-468, but not on HEK293T or MDA-MB-231 cells

(Figure 23). As opposed to Hs578T cells which exhibited a more uniform membrane distribution of the CD44-bound label, MCF-7 and MDA-MB-468 cells were characterized by sporadic (and less intense) staining across their cell population. Additionally, the formation of membrane blebbing was discernible across all technical and biological repeats for MDA-MB-468 (Figure 23E), suggesting the highly sensitive nature of this cell line. Nonetheless, since the Hoechst staining ascertained the presence of intact cell nuclei (blue signal), the binding data was regarded as being reliable.

(A) HEK293T

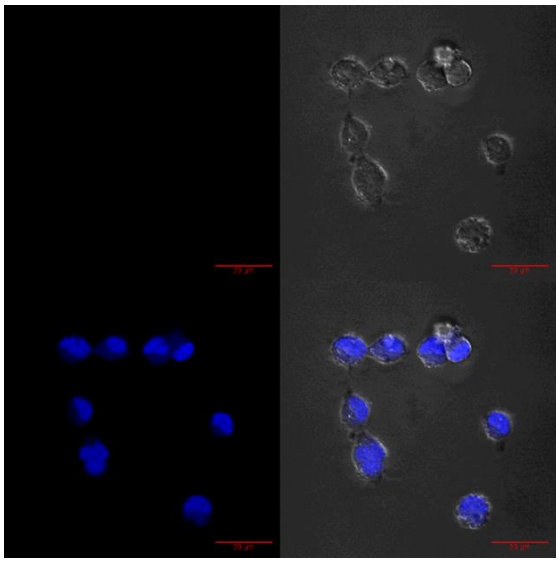

(B) Hs578T

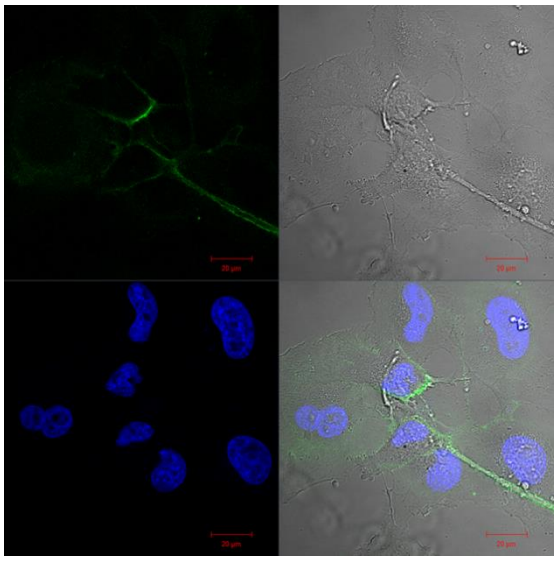

(C) MCF7

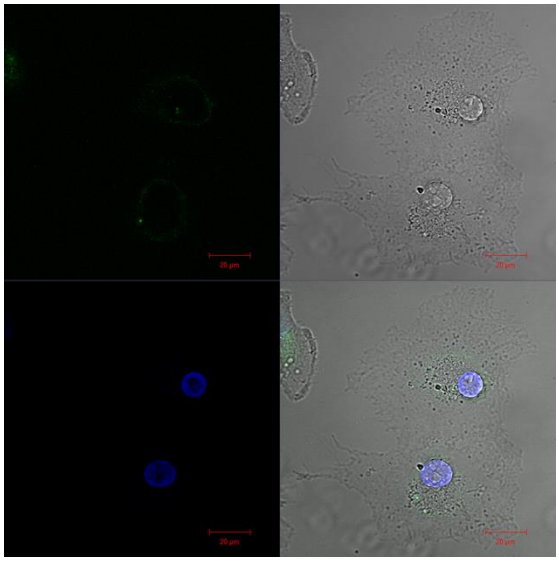

(D) MDA-MB-231

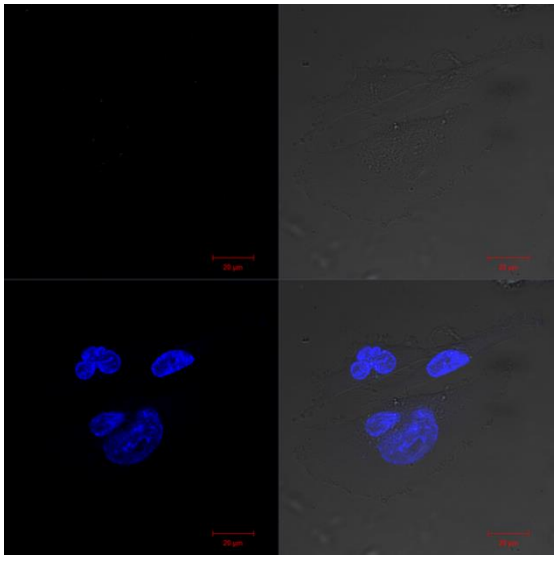

(E) MDA-MB-468

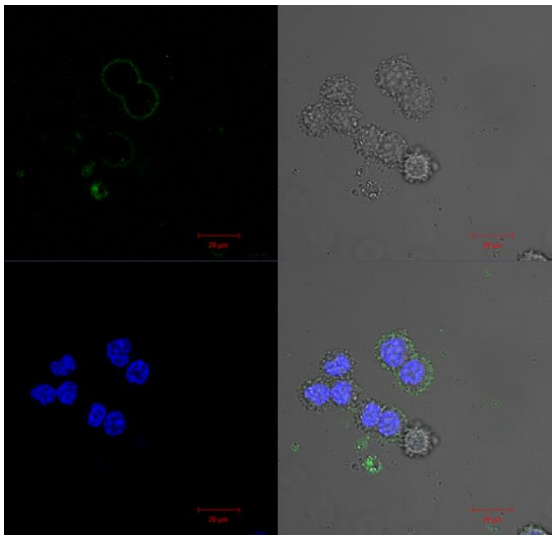

Figure 23: Assessing the binding activity of αCD44(scFv)-SNAPf-Alexa488 by screening target cells for potential CD44 expression. (A) HEK293T, (B) Hs578T, (C) MCF-7, (D) MDA-MB-231 and (E) MDA-MB-468. Cell lines were incubated with 15 µM of conjugated protein (green signal) for 15-20 minutes at 37°C. Hoechst (1:5000 dilution in media) was used as a stain for the nuclei (blue signal). Washes were performed 3 times with 1x PBS, before fixing with 4% PFA and mounting the coverslips on a microscope slide. Images were captured using a Zeiss confocal-scanner microscope (LSM880) with Airyscan at 20 µm magnification.

Lastly, the screening of TNBC cells with αASPH(scFv)-SNAP-Alexa488 was particularly challenging since most cell lines displayed no ASPH-related fluorescence staining. For this reason, only 2 TNBC cell lines were considered for further functional assays (Figure 24).

(A) Hs578T **(B) MDA-MB-468**

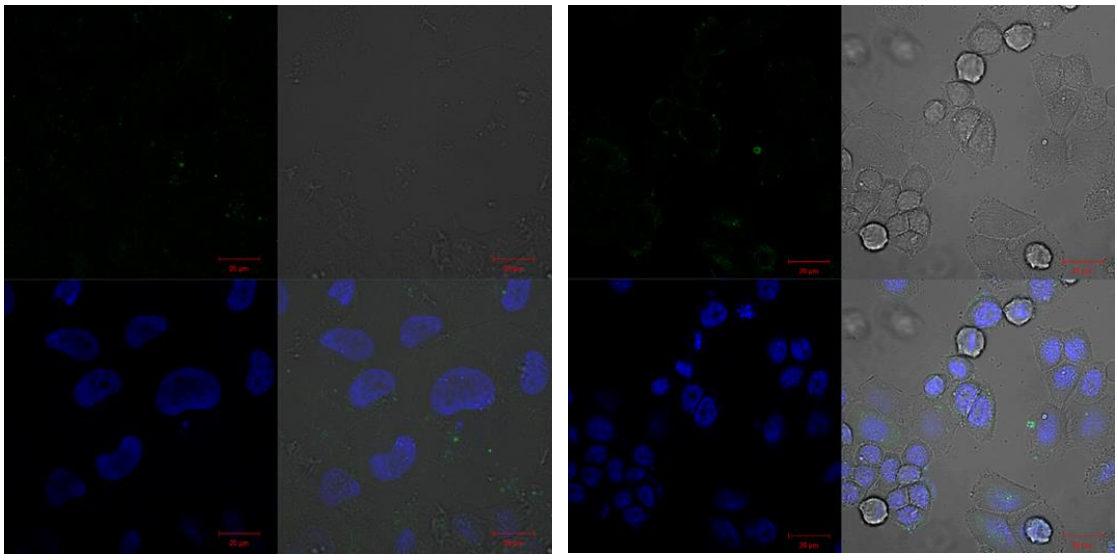

Figure 24: Assessing the binding activity of αASPH(scFv)-SNAP-Alexa488 by screening target cells for potential ASPH expression. (A) Hs578T and (B) MDA-MB-468. Cell lines were incubated with 15 µM of conjugated protein (green signal) for 15-20 minutes at 37ºC. Hoechst (1:5000 dilution in media) was used as a stain for the nuclei (blue signal). Washes were performed 3 times with 1x PBS, before fixing with 4% PFA and mounting the coverslips on a microscope slide. Images were captured using a Zeiss confocal-scanner microscope (LSM880) with Airyscan at 20 µm magnification.

As observed from Figure 24, very mild and sparse surface binding was observed on MDA-MB-468 cells and no binding was detected on Hs578T cells across all fields of view. Therefore, MDA-MB-468 was selected as the ASPH-positive cell line, with Hs578T cells as the negative control.

3.6.2 Binding analysis and flow cytometric determination of receptor density on tumor cells

Following confocal microscopy, flow cytometric analysis (section 2.6.2) was implemented to further confirm the binding specificity and capability of the scFv-SNAP fusion proteins, while synchronously quantifying surface expression of their cognate antigens within the live cell population. On this basis, the same panel of target cell lines used in section 3.6.1, was subjected to incubation with various serial dilutions of the according Alexa488-conjugated fusion protein, prior to acquisition on a BD^{TM} LSR II flow cytometer. Here, compensation [436,437] was applied to correct for spectral overlap arising from the use of BG-Alexa Fluor 488 and ViViD (live/dead marker), which were detectable in both the Alexa488 and Pacific Blue channels.

Thereafter, determination of the receptor expression status for each sample, required the design and implementation of an appropriate gating strategy. Figure 10 (section 2.6.2) depicts the gating strategy utilized in the analysis of all flow cytometric data acquired in this study. Initially, time gates were applied to ensure consistent fluorescence signal over time. This was done to exclude the presence of artefacts in the data, often resulting from the presence of microbubbles or clogs within the device's fluidic system. Similarly, in order to eliminate further irregularities in the data, a forward scatter height (FSC-H) against forward scatter area (FSC-A) plot was drawn to select for single cells only, since doublets and other cellular aggregates can give rise to inaccurate analysis. Subsequently, the Pacific Blue channel was used to identify live cells (negative for ViViD), which were then gated according to their size (FSC-A) and granularity (side scatter area (SSC-A)) to exclude cellular debris. Lastly, gates specific for the receptor-associated Alexa Fluor

488 fluorescence signal were applied, to delineate between (and allow quantification of) the antigen-positive and negative cell populations.

Moreover, as an essential optimization step in flow cytometry [435], antibody titrations were also carried out. In addition to the potential experimental repercussions of the observable low protein purity (< 90%) (Table 7), it became pertinent to estimate the optimal concentration of scFv-SNAP-Alexa488 needed to ensure the best segregation between the antigen-positive and negative populations for a given cell type. In other words, this strategy allowed determination of the antibody staining concentration to use to ensure the most accurate measure of expression levels, whilst limiting background interference. This was particularly important since even though antibodies will bind with high affinity to their target antigens, excess antibody can increase non-specific (low affinity) binding, which will promote background fluorescence (from the negative population) and reduce the ability to resolve populations [440]. Therefore, after application of the gating strategy (Figure 10), antibody titration curves were plotted for each scFv-SNAP-Alexa488 and cell line combinations; (from left to right) signal-to-noise ratio, staining index (SI), median fluorescence intensity (MFI) (for Alexa488-positive population) and concatenated pseudocolor plot (Figures 25 – 27).

As such, there are several factors to consider when selecting the optimal antibody dilution: (1) highest signal-to-noise ratio and SI, (2) MFI value of the antibody titer should be close to the saturation point and (3) the positioning of the negative population [441]. In this study, the saturation point (or point where curve plateaus) was not readily determinable and the highest MFI could not be assumed as the saturation point. While further increasing the scFv-SNAP-Alexa488 concentration was considered, it was observed that with the existing concentrations employed, most cells were already overstained. This occurrence was marked by high background signal (from unspecific binding and possible cell autofluorescence), with the negative population being shifted towards a higher fluorescence, thereby hampering the distinct identification of the negative and positive cell populations. Indeed, as observed from the concatenated pseudocolor plots (Figures 25 – 27), a ‘smear’ of the antigen-positive cells was observed, progressing to the top of the negative population. On this basis, choosing the appropriate fusion protein concentration to allow a reliable

estimation of receptor density, involved using the concatenated plots to gauge the right balance between a positive signal and an observable shift in the negative population. The selected antibody titer was then applied to the other titration curves (as indicated by red box). Therefore, for αCSPG4(scFv)-SNAP-Alexa488 (Figure 25), the chosen antibody concentrations were 100 µg/ml, 25 µg/ml, 100 µg/ml, 100 µg/ml and 1000 µg/ml for (A) HEK293T, (B) Hs578T, (C) MDA-MB-231, (D) MDA-MB-468 and (E) SK-Mel-28 cells respectively. Similarly, for αCD44(scFv)-SNAPf-Alexa488 (Figure 26), the optimal antibody titers were 100 µg/ml, 10 µg/ml, 100 µg/ml, 250 µg/ml and 250 µg/ml for (A) HEK293T, (B) Hs578T, (C) MCF-7, (D) MDA-MB-231 and (E) MDA-MB-468 cells respectively (Table 8).

Table 8: Summary of the chosen antibody titers and their associated signal-to-noise ratio, staining index (SI) and median fluorescence intensity (MFI) for each scFv-SNAP-Alexa Fluor 488 fusion protein on target cell lines

Treatment	Cell lines tested	Optimal antibody titer (µg/ml)	ᵅSignal-to-noise ratio	ᵅStaining index (SI)	ᵅMedian fluorescence intensity (MFI)
αCSPG4(scFv)-SNAP-Alexa488	HEK293T	100	10.8	4.21	12556
	Hs578T	25	2.54	1.36	4685
	MDA-MB-231	100	14.1	5.43	15763
	MDA-MB-468	100	4.17	3.38	2720
	SK-Mel-28	1000	7.36	6.47	23470
αCD44(scFv)-SNAPf-Alexa488	HEK293T	100	14.5	10.7	13021
	Hs578T	10	1.51	0.588	2265
	MCF-7	100	3.82	2.80	3210
	MDA-MB-231	250	18.3	6.42	28391
	MDA-MB-468	250	4.47	2.89	5666
αASPH(scFv)-SNAP-Alexa488	Hs578T	250	20.2	11.7	53835
	MDA-MB-468	500	5.23	4.21	6983

α: Data shown represent the average of 2 biological repeat experiments.

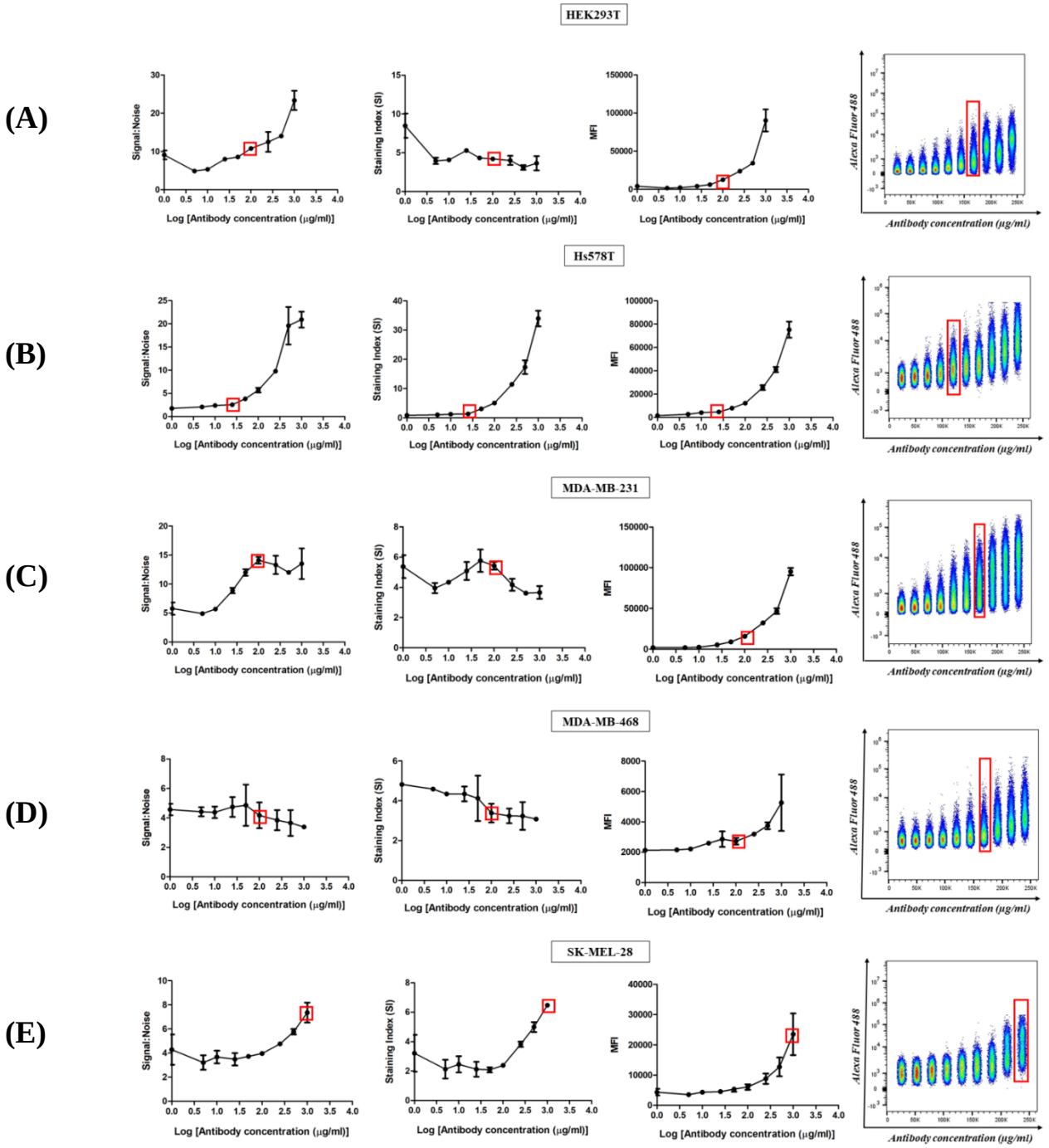

Figure 25: Determination of the optimal antibody concentration for αCSPG4(scFv)-SNAP-Alexa488 on target cell lines. Cells were treated with increasing protein concentrations and the corresponding antibody titration curves were plotted as follows: (from left to right) signal-to-noise ratio, staining index (SI), median fluorescence intensity (MFI) and concatenated pseudocolor plot. Data shown are representative of 2 biological repeat experiments. The chosen antibody concentrations (as indicated by the red box) were 100 µg/ml, 25 µg/ml, 100 µg/ml, 100 µg/ml and 1000 µg/ml for (A) HEK293T, (B) Hs578T, (C) MDA-MB-231, (D) MDA-MB-468 and (E) SK-Mel-28 respectively.

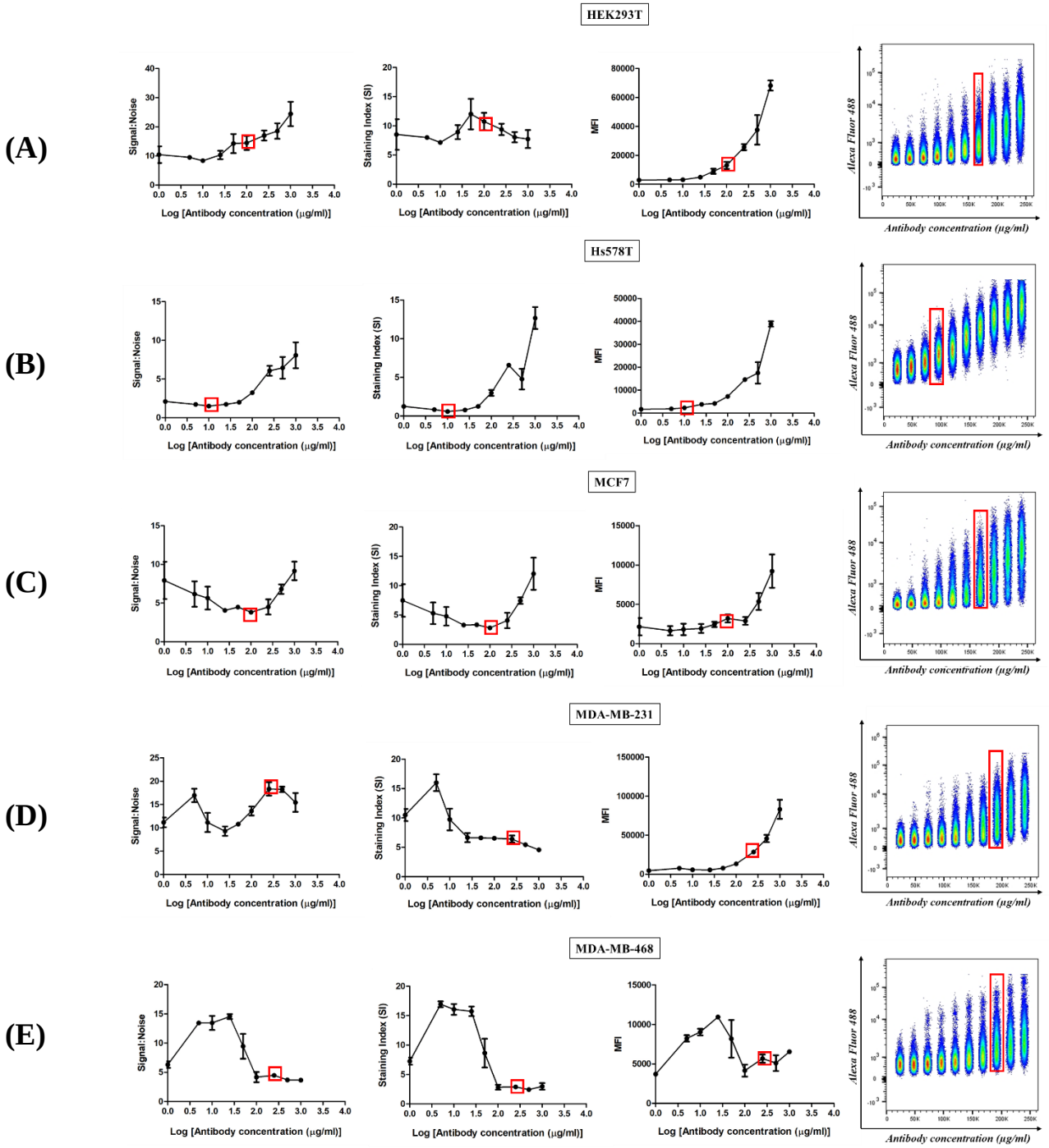

Figure 26: Determination of the optimal antibody concentration for αCD44(scFv)-SNAPf-Alexa488 on target cell lines. Cells were treated with increasing protein concentrations and the corresponding antibody titration curves were plotted as follows: (from left to right) signal-to-noise ratio, staining index (SI), median fluorescence intensity (MFI) and concatenated pseudocolor plot. Data shown are representative of 2 biological repeat experiments. The chosen antibody concentrations (as indicated by the red box) were 100 µg/ml, 10 µg/ml, 100 µg/ml, 250 µg/ml and 250 µg/ml for (A) HEK293T, (B) Hs578T, (C) MCF-7, (D) MDA-MB-231 and (E) MDA-MB-468 respectively.

Lastly, as shown in Figure 27, αASPH(scFv)-SNAP-Alexa488 exhibited optimal antibody concentrations at 250 µg/ml and 500 µg/ml for (A) Hs578T and (B) MDA-MB-468 respectively.

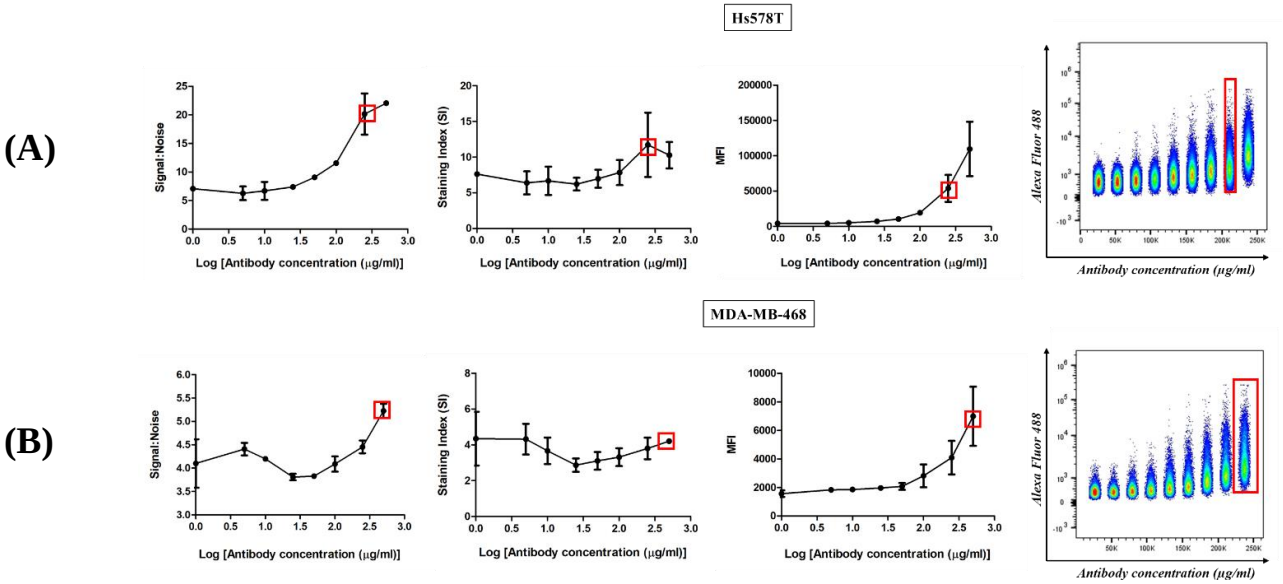

Figure 27: Determination of the optimal antibody concentration for αASPH(scFv)-SNAP-Alexa488 on target cell lines. Cells were treated with increasing protein concentrations and the corresponding antibody titration curves were plotted as follows: (from left to right) signal-to-noise ratio, staining index (SI), median fluorescence intensity (MFI) and concatenated pseudocolor plot. Data shown are representative of 2 biological repeat experiments. The chosen antibody concentrations (as indicated by the red box) were 250 µg/ml and 500 µg/ml for (A) Hs578T and (B) MDA-MB-468 respectively.

After selection of the most appropriate scFv-SNAP-Alexa488 concentration that would ensure maximal staining of the cellular marker in the sample (while minimizing background fluorescence), the next step was to (1) evaluate the percentage of antigen-positive cells present within the cell population, (2) quantify the receptor distribution per cell type (via the MFI) and (3) compare these values across the chosen panel of target cells (which includes TNBC cells) to confirm their suitability in cytotoxicity studies. To this end, representative pseudocolor plots were first drawn to show the position of the Alexa488-positive and negative cell populations, concurrently allowing the frequency (expressed as a percentage of the total live cell population) of the antigen-positive cells to be determined. For instance, the percentages of CSPG4-expressing cells were 1.04, 36.4, 1.80, 8.72 and 52.7% for HEK293T, Hs578T, MDA-MB-231, MDA-MB-468 and SK-Mel-28 cells respectively (Figures 28A and B). Likewise, the prevalence of CD44-positive cells was 0.84, 26.2, 19.6, 1.57 and 21.0% for HEK293T, Hs578T, MCF-7, MDA-MB-

231 and MDA-MB-468 cells (Figures 29A and B). On the other hand, ASPH showed an abundance rate of 19.8% in MDA-MB-468 cells and 0.44% in Hs578T cells (Figures 30A and B). Therefore, in the majority of cases, less than 50% of the cells expressed the putative target receptor.

Additionally, histograms were drawn to depict the relative fluorescence shift of the Alexa488-positive (green curve) and negative populations (blue curve), with respect to the untreated control (grey curve). As observed from Figures 28C and 29C, amongst the TNBC cell lines, Hs578T exhibited the highest count of CSPG4 and CD44-associated signal, whereas MDA-MB-468 and MDA-MB-231 cells were characterized by medium to low signals respectively. In contrast, MDA-MB-468 cells displayed a moderately positive shift in ASPH-specific Alexa488 fluorescence, whereas Hs578T cells were noticeably low in signal count number (Figure 30C). Therefore, reflecting the confocal microscopy observations made across the different fields of view, the frequency of the antigen-positive cells within the cell population, was as follows: (1) CSPG4: SK-Mel-28 > Hs578T > MDA-MB-468 > MDA-MB-231 > HEK293T, (2) CD44: Hs578T > MDA-MB-468 > MCF-7 > MDA-MB-231 > HEK293T and (3) ASPH: MDA-MB-468 > Hs578T. These results validated the concordance between the qualitative and quantitative binding data generated in this study (Table 9). Interestingly, statistical comparisons across cell lines revealed that the population of CSPG4 and CD44-positive cells was significantly lower in HEK293T cells (Figures 28D and 29D), making it an important negative control cell line for further functional assays. The same deduction was made in the case of Hs578T, which represented an $ASPH^{low\ frequency}$-expressing cell line (Figure 30D).

Similarly, MFI values were calculated to establish the levels of antigen expression within the Alexa488-positive population (Figures 28E – 30E). This is achievable since the intensity of the fluorescent signal is proportional to the amount of antibody bound per cell, which is in turn reflective of the number of antigen sites expressed [442,443]. Surprisingly, CSPG4/CD44-positive Hs578T cells showed a low distribution of receptors on their surface (Table 8), despite exhibiting a frequency of 36.4% (CSPG4) and 26.2% (CD44) in the overall cell population. Nonetheless, the low signal-to-noise ratio showcased by Hs578T (Figures 28F and 29F), was suggestive of potential background interference in the visible data. Conversely, although scarce in number, the

CSPG4/CD44-expressing HEK293T and MDA-MB-231 cells were marked by high to moderate receptor expression per cell (MFI range: 12556 – 28391) (Table 8). Furthermore, although non-significant, a similar phenomenon was apparent for MDA-MB-468 cells (Figure 30F), which showed positivity for ASPH in ~20% of its population. Unfortunately, the underlying causality behind these confounding observations is currently unknown and will require further investigation. Therefore, given its correlation with the confocal microscopy data, the computed frequency values were thus regarded as the best estimate of relative receptor abundance for each cell population.

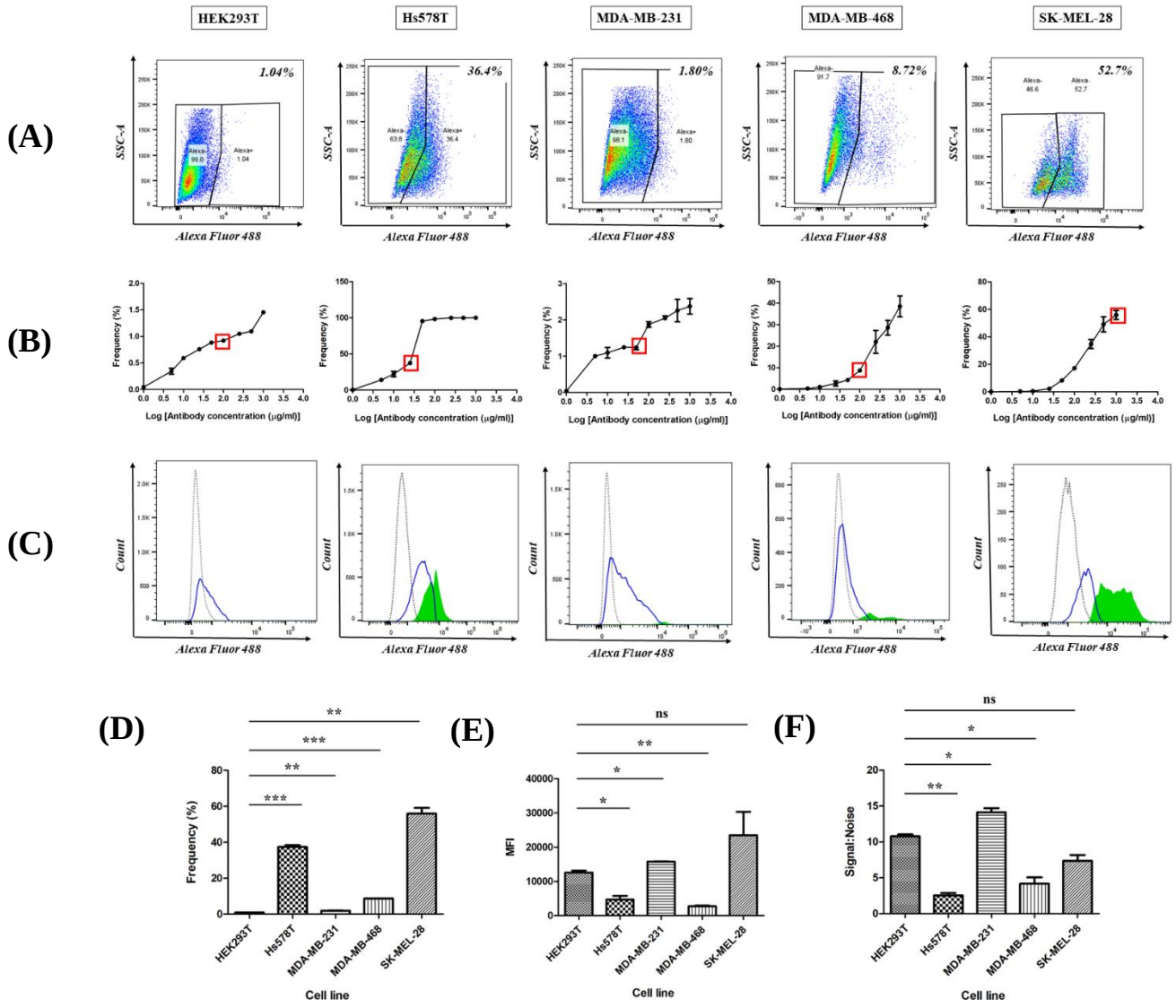

Figure 28: Comparison of the CSPG4 expression status across target cell lines. Cells were incubated with the optimal Alexa488-conjugated αCSPG4(scFv)-SNAP concentration and acquired on a BD™ LSR

II flow cytometer. Data shown are representative of 2 biological repeat experiments. (A) Representative pseudocolor plots with gates showing the position of the Alexa488-positive/negative cell populations at the optimal antibody titer. Frequencies of the Alexa488-positive populations (expressed as a percentage of the total population) are indicated at the top right-hand corner of the plots. (B) Antibody titration curves showing the frequencies of the Alexa488-positive population at the optimal antibody concentration (indicated by red box). (C) Histograms depicting the relative fluorescence of the Alexa488-positive/negative populations (grey curve: untreated cells, blue curve: Alexa488-negative cells at the optimal antibody concentration, green: Alexa488-positive cells at the optimal antibody concentration). Bar graphs demonstrating the (D) frequencies of the Alexa488-positive population, (E) median fluorescence intensity (MFI) and (F) signal-to-noise ratio across target cell lines. Statistical comparisons (relative to the CSPG4-negative HEK293T cell line) were calculated using Student's *t*-tests (**p* < 0.05, ***p* < 0.01, ****p* < 0.001, ns (not significant)).

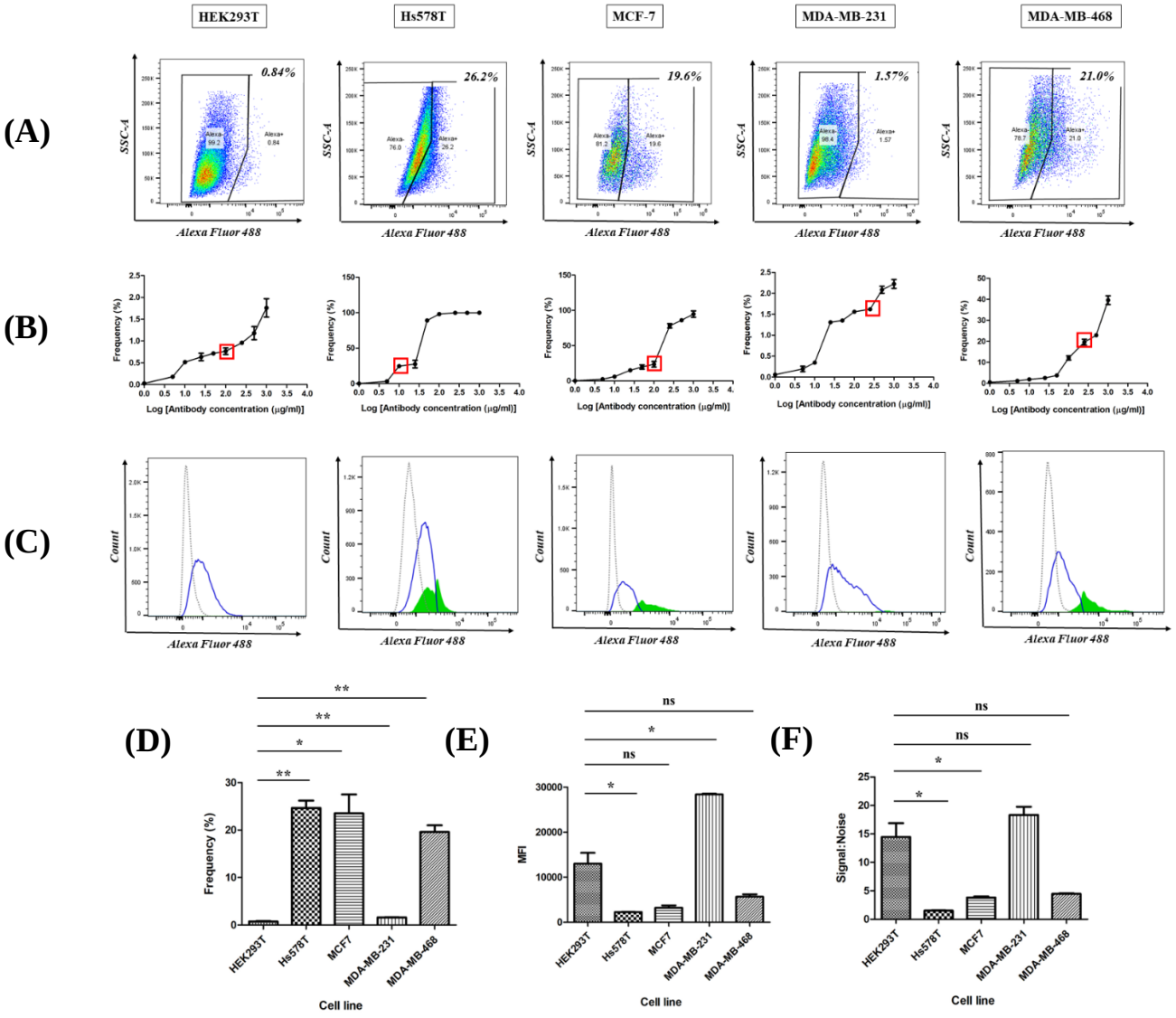

Figure 29: Comparison of the CD44 expression status across target cell lines. Cells were incubated with the optimal Alexa488-conjugated αCD44(scFv)-SNAPf concentration and acquired on a BD™ LSR II flow cytometer. Data shown are representative of 2 biological repeat experiments. (A) Representative pseudocolor plots with gates showing the position of the Alexa488-positive/negative cell populations at the optimal antibody titer. Frequencies of the Alexa488-positive populations (expressed as a percentage of the total population) are indicated at the top right-hand corner of the plots. (B) Antibody titration curves showing the frequencies of the Alexa488-positive population at the optimal antibody concentration (indicated by red box). (C) Histograms depicting the relative fluorescence of the Alexa488-positive/negative populations (grey curve: untreated cells, blue curve: Alexa488-negative cells at the optimal antibody concentration, green: Alexa488-positive cells at the optimal antibody concentration). Bar graphs demonstrating the (D) frequencies of the Alexa488-positive population, (E) median fluorescence intensity (MFI) and (F) signal-to-noise ratio across target cell lines. Statistical comparisons (relative to the CD44-negative HEK293T cell line) were calculated using Student's *t*-tests (*$p < 0.05$, **$p < 0.01$, ***$p < 0.001$, ns (not significant)).

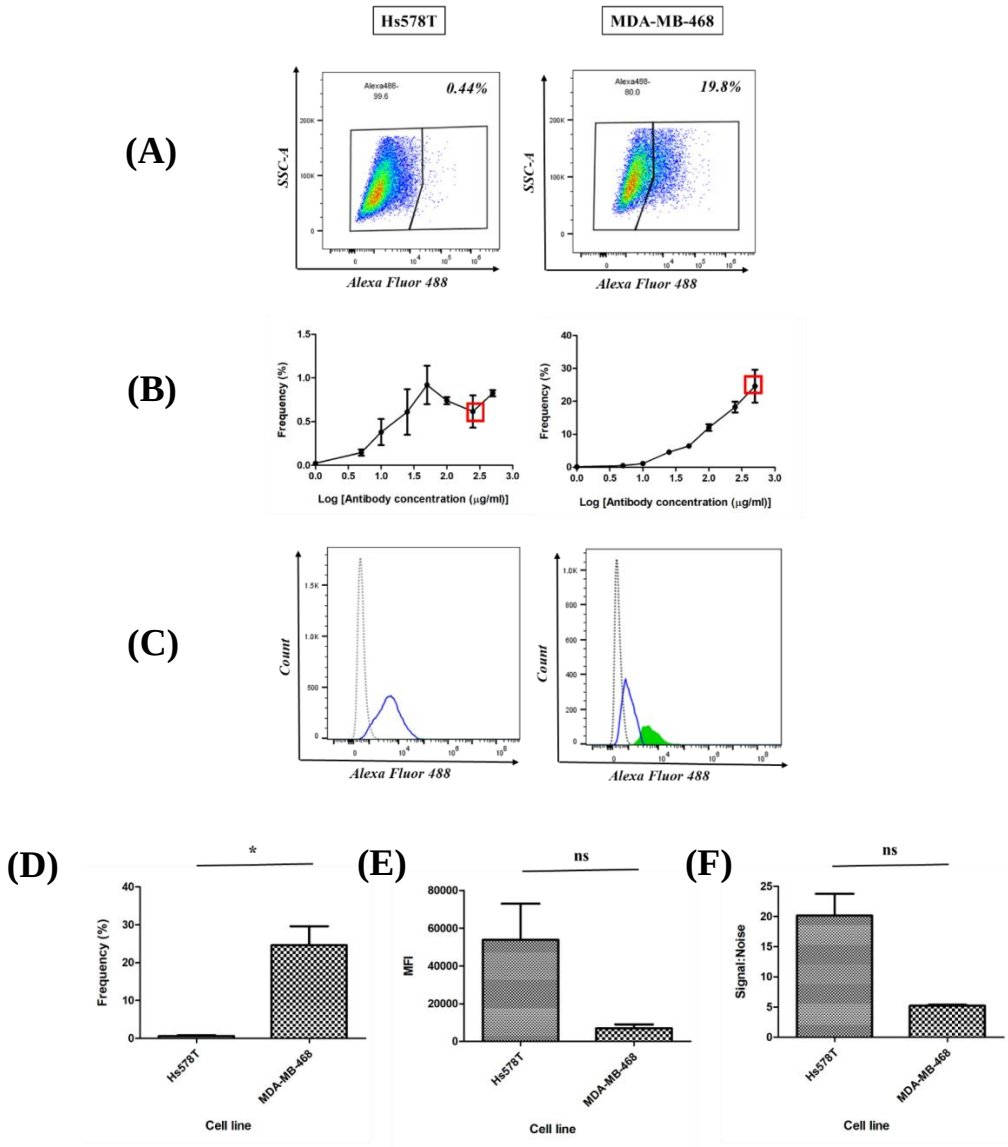

Figure 30: Comparison of the ASPH expression status across target cell lines. Cells were incubated with the optimal Alexa488-conjugated αASPH(scFv)-SNAP concentration and acquired on a BD™ LSR II flow cytometer. Data shown are representative of 2 biological repeat experiments. (A) Representative pseudocolor plots with gates showing the position of the Alexa488-positive/negative cell populations at the optimal antibody titer. Frequencies of the Alexa488-positive populations (expressed as a percentage of the total population) are indicated at the top right-hand corner of the plots. (B) Antibody titration curves showing the frequencies of the Alexa488-positive population at the optimal antibody concentration (indicated by red box). (C) Histograms depicting the relative fluorescence of the Alexa488-positive/negative populations (grey curve: untreated cells, blue curve: Alexa488-negative cells at the optimal antibody concentration, green: Alexa488-positive cells at the optimal antibody concentration). Bar graphs demonstrating the (D) frequencies of the Alexa488-positive population, (E) median fluorescence intensity (MFI) and (F) signal-to-noise ratio across target cell lines. Statistical comparisons (relative to the ASPH-negative Hs578T cell line) were calculated using Student's *t*-tests (*$p < 0.05$, **$p < 0.01$, ***$p < 0.001$, ns (not significant)).

In conclusion, the resulting specific binding activities of the scFv-SNAP-Alexa488 fusion proteins, as determined by confocal microscopy and flow cytometry, are summarized in Table 9 below.

Table 9: Overview of binding activities for Alexa Fluor 488-conjugated scFv-SNAP fusion proteins on target cell lines

Treatment	Cell lines tested	Surface binding as observed via confocal microscopy	Frequency of antigen-positive cells as determined by flow cytometry
αCSPG4(scFv)-SNAP-Alexa488	HEK293T	No binding	1.04%
	Hs578T	Uniform and intense	36.4%
	MDA-MB-231	No binding	1.80%
	MDA-MB-468	Mild and sparse	8.72%
	SK-Mel-28	Uniform and intense	52.7%
αCD44(scFv)-SNAPf-Alexa488	HEK293T	No binding	0.84%
	Hs578T	Uniform and intense	26.2%
	MCF-7	Mild and sparse	19.6%
	MDA-MB-231	No binding	1.57%
	MDA-MB-468	Mild and sparse	21.0%

αASPH(scFv)-SNAP-Alexa488	Hs578T MDA-MB-468	No binding Mild and sparse	0.44% 19.8%

3.7 Cytotoxicity studies

3.7.1 Cytotoxic analysis of SNAP-tag based fusion proteins conjugated to BG-AURIF

After confirming the functionality of the individual elements of the scFv-SNAP fusion proteins and determining the relative abundance of the antigen-positive cells across target cell lines, the next step involved establishing whether the fusion proteins can be used as a vehicle for the specific delivery of cytotoxic agents to TNBC cells. Initially, with BG-AURIF being synthesized from commercially available AURIF (BrightGene Bio-Medical Technology, China), an important requisite was to assess whether such chemical modifications had any impact on the cytotoxic activity of the resulting compound. To this end, all cell lines were treated with increasing concentrations of the drug and cell proliferation was measured using an XTT-based cell viability assay (section 2.7.1). The concentration of drug required to achieve 50% inhibition in cell viability was also calculated to assess drug efficacy.

Indeed, Figures 31 and 32 demonstrate that both AURIF and BG-modified AURIF were indiscriminately toxic towards all cell lines in a concentration-dependent fashion. This unspecific activity provided the rationale for using an antibody moiety as a guiding head for the targeted delivery of such warheads to tumor cells. Most importantly, AURIF displayed a more potent killing effect (IC_{50} range: 43-452.8 nM) as compared to BG-AURIF (IC_{50} range: 32.3 nM-17.1 µM) (Table 10). Consequently, despite this marginal reduction in activity (probably due to the smaller molecular size of AURIF which allows easier internalization into target cells), their overlapping range suggested that BG-AURIF retained most of its anti-mitotic properties and is therefore suitable for use in the generation of novel recombinant ADCs targeting CSPG4, CD44 and ASPH.

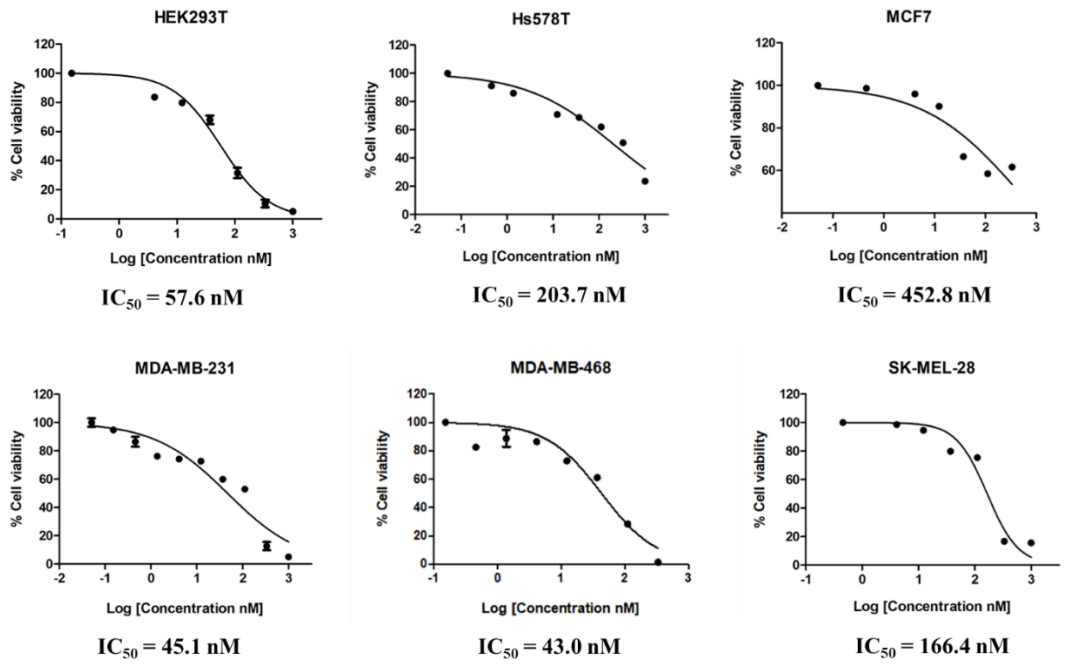

Figure 31: Dose-response curves demonstrating the cytotoxic activity of commercially sourced (unmodified) AURIF. The cytotoxic activity was assessed using an XTT-based viability assay after incubation with the drug for 72 hours. Cells were treated with (3-fold serially diluted) increasing concentrations of the drug and the IC_{50} values (relative to the untreated and Zeocin-treated (100 µg/ml) cells) were calculated using GraphPad Prism v5. Data are mean ± standard deviation (SD) of each measurement (presented as a percentage of cell viability), and the measurements were performed in triplicate at least 3 times.

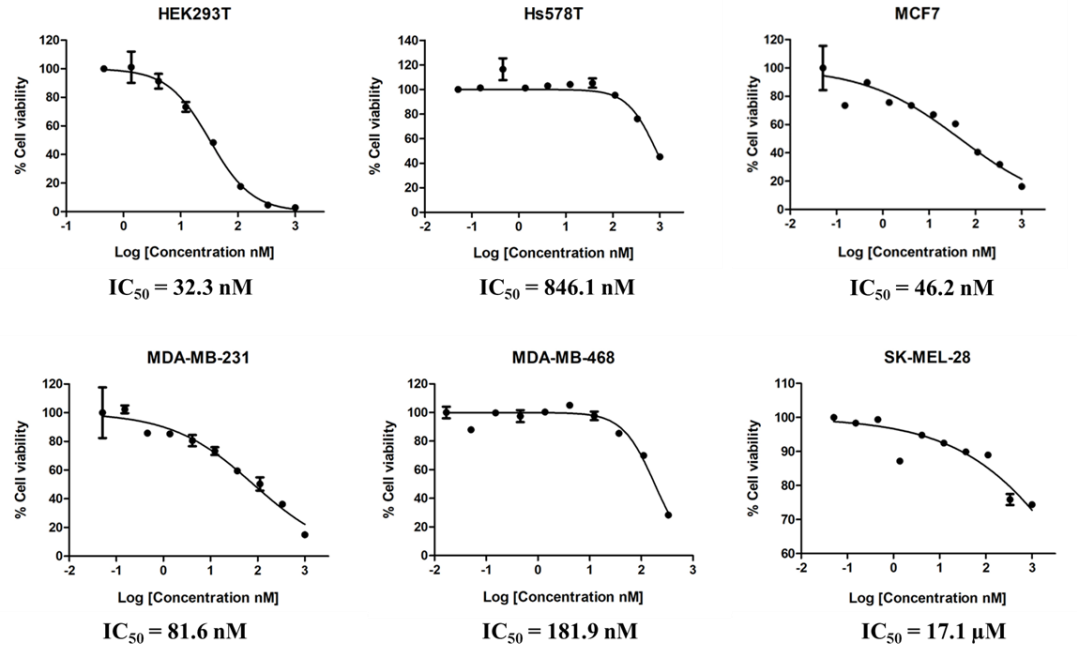

Figure 32: Dose-response curves demonstrating the cytotoxic activity of BG-modified AURIF. The cytotoxic activity was assessed using an XTT-based viability assay after incubation with the drug for 72 hours. Cells were treated with (3-fold serially diluted) increasing concentrations of the drug and the IC_{50} values (relative to the untreated and Zeocin-treated (100 µg/ml) cells) were calculated using GraphPad Prism v5. Data are mean ± standard deviation (SD) of each measurement (presented as a percentage of cell viability), and the measurements were performed in triplicate at least 3 times.

Subsequently, prior to conjugation with BG-modified AURIF, it was necessary to first ascertain that the unconjugated fusion proteins were not responsible for any visible lethal effect on the target cells. As expected, treatment with unconjugated αCSPG4(scFv)-SNAP fusion protein did not induce any palpable toxicity (Figure 33).

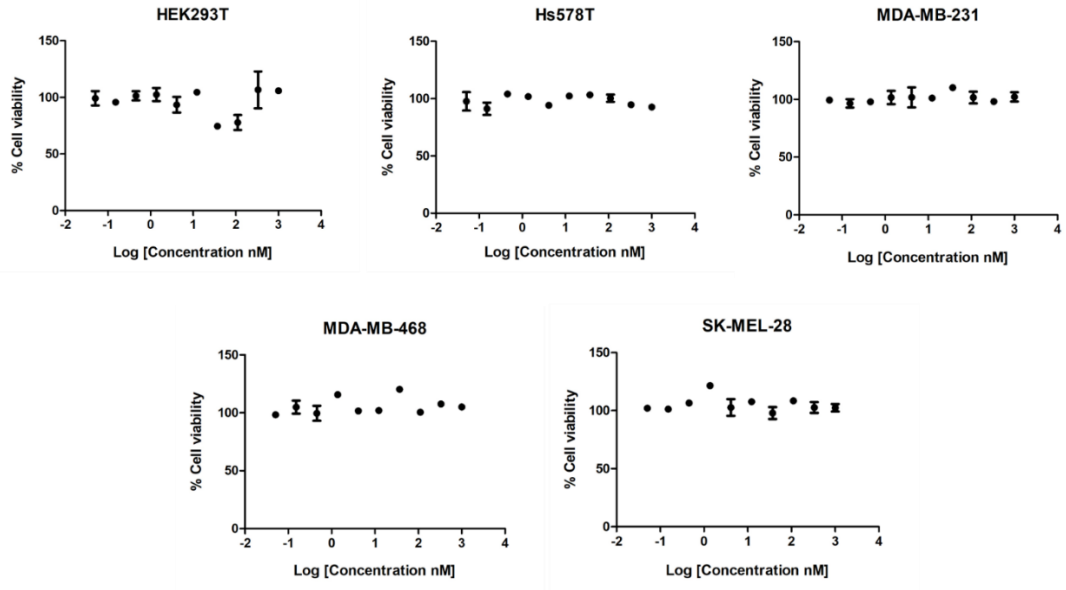

Figure 33: Investigating the cytotoxic activity of unconjugated αCSPG4(scFv)-SNAP fusion protein on target cell lines. The cytotoxic activity was assessed using an XTT-based viability assay after incubation with the protein for 72 hours. Cells were treated with (3-fold serially diluted) increasing concentrations of the protein and dose-response curves were generated using GraphPad Prism v5. Data are mean ± standard deviation (SD) of each measurement (presented as a percentage of cell viability), and the measurements were performed in triplicate at least 3 times.

Following the same trend, cells treated with increasing dilutions of αCD44(scFv)-SNAPf (Figure 34) and αASPH(scFv)-SNAP (Figure 35) remained unaffected across all cell types, indicating that the fusion proteins have no effect on cell proliferation despite the varying abundance levels of antigen-positive cells.

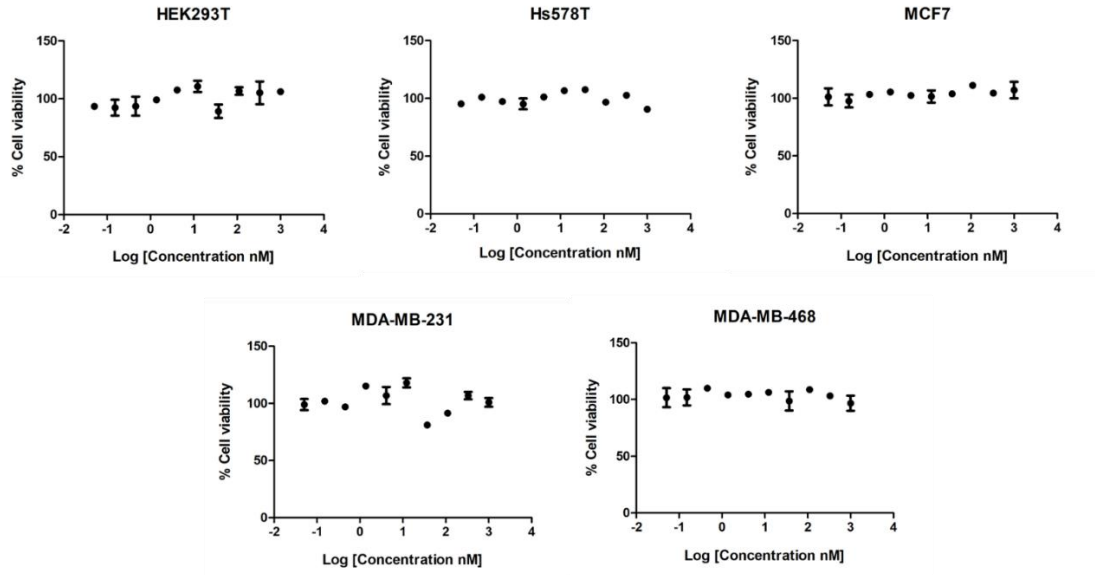

Figure 34: Investigating the cytotoxic activity of unconjugated αCD44(scFv)-SNAPf fusion protein on target cell lines. The cytotoxic activity was assessed using an XTT-based viability assay after incubation with the protein for 72 hours. Cells were treated with (3-fold serially diluted) increasing concentrations of the protein and dose-response curves were generated using GraphPad Prism v5. Data are mean ± standard deviation (SD) of each measurement (presented as a percentage of cell viability), and the measurements were performed in triplicate at least 3 times.

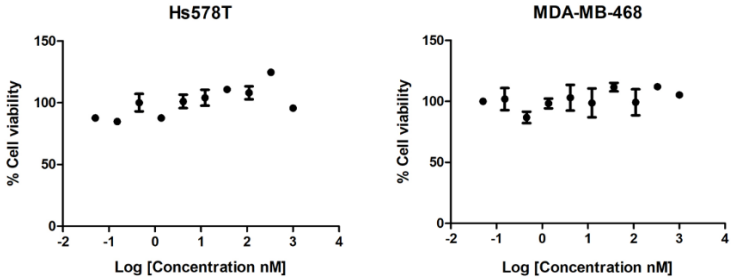

Figure 35: Investigating the cytotoxic activity of unconjugated αASPH(scFv)-SNAP fusion protein on target cell lines. The cytotoxic activity was assessed using an XTT-based viability assay after incubation with the protein for 72 hours. Cells were treated with (3-fold serially diluted) increasing concentrations of the protein and dose-response curves were generated using GraphPad Prism v5. Data are mean ± standard deviation (SD) of each measurement (presented as a percentage of cell viability), and the measurements were performed in triplicate at least 3 times.

Following conjugation to BG-AURIF, a second conjugation was performed with the addition of BG-Alexa Fluor 488, in order to confirm saturation of the scFv-SNAP with BG-AURIF prior to cytotoxicity studies (section 2.5.2). As shown in Figure 36, no fluorescent signal was detected (right panel), despite presence of the conjugated protein on the stained SDS-PAGE gel (left panel).

On this account, incubation of the fusion protein with a 3-fold molar excess of BG-AURIF for 4 hours at room temperature, was deemed to be sufficient to allow complete saturation of the binding domain of SNAP-tag with the antiproliferative drug. Thereafter, the killing effects of the resulting immunoconjugates were assessed using an XTT-based colorimetric cell viability assay as described previously.

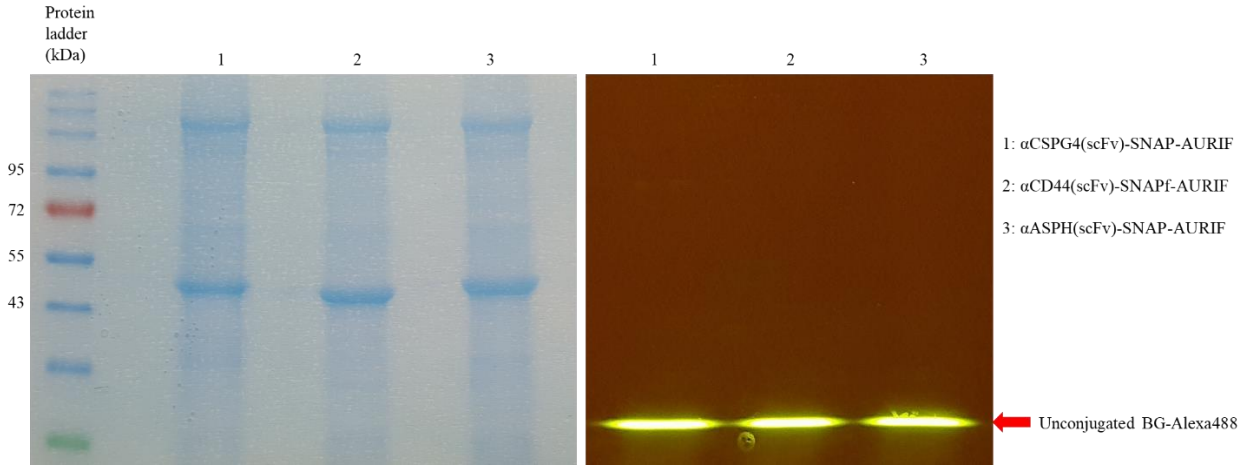

Figure 36: Confirming the saturation of scFv-SNAP fusion proteins with BG-AURIF through a double conjugation with BG-Alexa Fluor 488. After conjugation with BG-AURIF for 4 hours at room temperature, 5 µM of the conjugation reaction was incubated with 10 µM of BG-Alexa Fluor 488 for 60 minutes at 37°C, before being loaded on a 10% SDS-PAGE gel, which was visualized under blue light using a Dark Reader Transilluminator (right panel) and stained using Aqua staining solution (left panel). Unbound BG-Alexa Fluor 488 is indicated by red arrow.

After 72 hours incubation with incremental concentrations of αCSPG4(scFv)-SNAP-AURIF, cells that presented with a high frequency of CSPG4-expressing cells (Hs578T, MDA-MB-468 and SK-Mel-28) were reduced in a concentration-dependent manner (Figure 37). The concentration required to achieve a 50% reduction in TNBC cell viability (IC_{50} value) was as follows: 173.3 nM for Hs578T and 190.3 nM for MDA-MB-468 (Table 10). However, in the case of the melanoma cell line SK-Mel-28, higher drug concentrations would be required to generate a dose-response curve that would allow a reliable calculation of the IC_{50} value. Nonetheless, with the observable low protein yield (Table 7), extrapolation of the graph was favored (using GraphPad Prism v5), which allowed determination of an estimated IC_{50} value of 1.66 µM for SK-Mel-28. In contrast, cell lines that were less abundant in antigen-positive cells (HEK293T and MDA-MB-231 cells), were negligibly affected, thereby demonstrating that the resulting AURIF cytotoxicity is

dependent on the level of CSPG4-expression. Interestingly, although SK-Mel-28 cells exhibited the highest frequency (52.7%) of CSPG4-positive cells (Figure 28), they were less sensitive to the treatment as opposed to Hs578T and MDA-MB-468 cells. This unanticipated observation suggested that the biological activity and efficiency of such compounds were dictated by additional *in vitro* considerations.

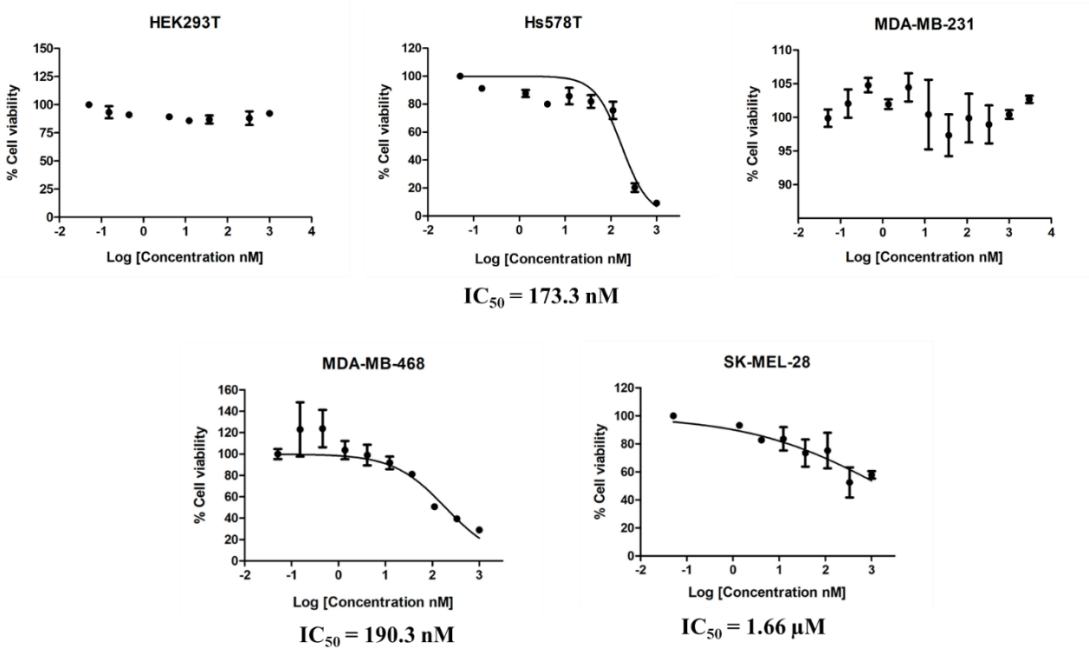

Figure 37: Dose-response curves demonstrating the cytotoxic activity of αCSPG4(scFv)-SNAP-AURIF *in vitro*. The cytotoxic activity was assessed using an XTT-based viability assay after incubation with the drug for 72 hours. Cells were treated with (3-fold serially diluted) increasing concentrations of the drug and the IC_{50} values (relative to the untreated and Zeocin-treated (100 µg/ml) cells) were calculated using GraphPad Prism v5. Data are mean ± standard deviation (SD) of each measurement (presented as a percentage of cell viability), and the measurements were performed in triplicate at least 3 times.

Further building on the selectivity of the engineered recombinant ADCs, it was demonstrated that only the $CD44^{high\ frequency}$-expressing cell lines (Hs578T, MCF-7 and MDA-MB-468) were susceptible to the immunoconjugate treatment, with IC_{50} values ranging from 100.4 nM to 1.27 µM (Figure 38). A similar pattern was perceived in the case of αASPH(scFv)-SNAP-AURIF (Figure 39). With HEK293T ($CD44^{low\ frequency}$), MDA-MB-231 ($CD44^{low\ frequency}$) and Hs578T ($ASPH^{low\ frequency}$) cells remaining unaffected even at the highest doses of the drug, such partiality towards receptor-abundant cells also indicated that conjugation of BG-AURIF to the scFv-SNAP

had no effect on the overall binding potential of the antibody moiety. Despite this, there was again no correlation between the percentage of antigen-positive cells in the population and the observable IC_{50} value, highlighting the complexity of targeted drug delivery.

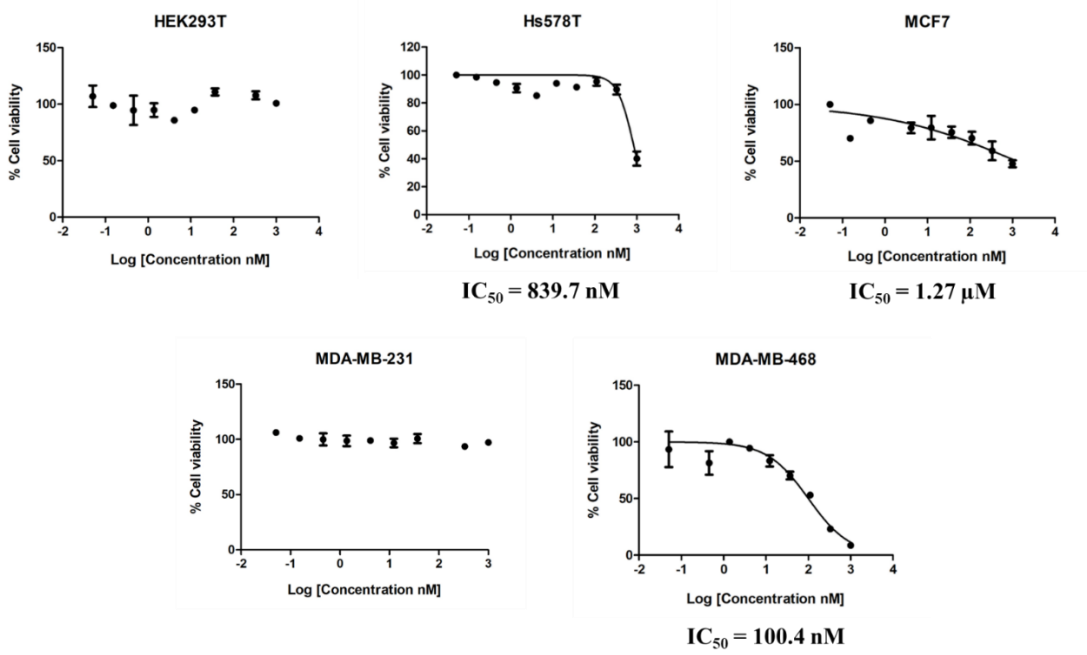

Figure 38: Dose-response curves demonstrating the cytotoxic activity of αCD44(scFv)-SNAPf-AURIF *in vitro*. The cytotoxic activity was assessed using an XTT-based viability assay after incubation with the drug for 72 hours. Cells were treated with (3-fold serially diluted) increasing concentrations of the drug and the IC_{50} values (relative to the untreated and Zeocin-treated (100 µg/ml) cells) were calculated using GraphPad Prism v5. Data are mean ± standard deviation (SD) of each measurement (presented as a percentage of cell viability), and the measurements were performed in triplicate at least 3 times.

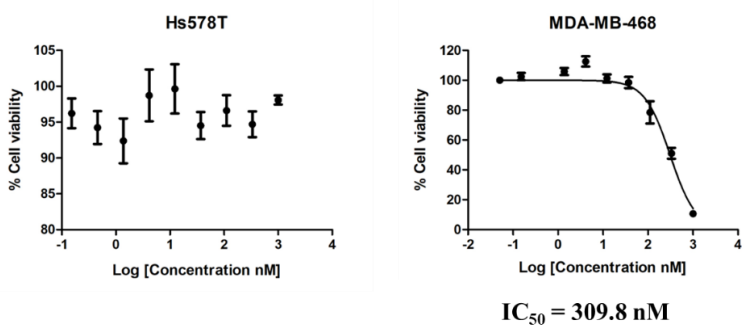

Figure 39: Dose-response curves demonstrating the cytotoxic activity of αASPH(scFv)-SNAP-AURIF *in vitro*. The cytotoxic activity was assessed using an XTT-based viability assay after incubation with the drug for 72 hours. Cells were treated with (3-fold serially diluted) increasing concentrations of the drug and the IC_{50} values (relative to the untreated and Zeocin-treated (100 µg/ml) cells) were calculated using

GraphPad Prism v5. Data are mean ± standard deviation (SD) of each measurement (presented as a percentage of cell viability), and the measurements were performed in triplicate at least 3 times.

Taken together, the resulting IC_{50} values generated from the AURIF-driven cytotoxicity studies in this section, are summarized in Table 10 below.

Table 10: Summary of IC_{50} values based on the cytocidal activity of scFv-SNAP-AURIF, unmodified AURIF and unconjugated BG-AURIF on target cell lines

Treatment	Cell lines tested	IC_{50} values (nM)
αCSPG4(scFv)-SNAP-AURIF	HEK293T	-
	Hs578T	173.3
	MDA-MB-231	-
	MDA-MB-468	190.3
	SK-Mel-28	1660
αCD44(scFv)-SNAPf-AURIF	HEK293T	-
	Hs578T	839.7
	MCF-7	1270
	MDA-MB-231	-
	MDA-MB-468	100.4
αASPH(scFv)-SNAP-AURIF	Hs578T	-
	MDA-MB-468	309.8
BG-AURIF	HEK293T	32.3
	Hs578T	846.1
	MCF-7	42.6
	MDA-MB-231	81.6
	MDA-MB-468	181.9
	SK-Mel-28	17100
AURIF	HEK293T	57.6
	Hs578T	203.7
	MCF-7	452.8

	MDA-MB-231	45.1
	MDA-MB-468	43.0
	SK-Mel-28	166.4

3.7.2 Evaluation of photoimmunotoxicity of IR700-conjugated fusion proteins

Investigation into the phototoxic activity of scFv-SNAP fusion proteins conjugated to BG-modified IR700, represents a proof of concept study demonstrating the ability of PIT to avoid the undesirable side-effects associated with PDT. Concurrently, by building on the cytotoxicity data observed via conjugation to the antimitotic drug AURIF, it showcases the versatility of SNAP-tag based fusion proteins as an efficient 'plug and play' approach in the generation of diverse diagnostic and therapeutic immunoconjugates. Therefore, the CSPG4, CD44 and ASPH-targeting scFv-SNAP fusion proteins generated in this research, were conjugated to the highly potent NIR PS called IR700 and administered to target cells. After irradiation with NIR light at 690 nm, the percentage of viable cells was determined using a formazan dye-based cell viability assay as described in section 2.7.2 and the corresponding IC_{50} values were computed using GraphPad Prism v5 software.

Most importantly, the source of NIR light and the IR700 PS (with and without light activation) on their own, should not induce any cell killing activity. Consequently, to ensure that the heat generated from the laser does not contribute to any detectable toxicity, untreated (media only) target cell lines were exposed to NIR light irradiation at 690 nm or left in the dark. As illustrated by Figure 40, treatment with NIR light had no impact on cell proliferation *in vitro*. Likewise, cells treated with the PS BG-IR700 only, did not experience any significant (or dose-dependent) reduction in cell viability, with or without light irradiation (Figures 41 and 42). These results implied that any potential photoimmunotoxic activities observed, would be due to the collaborative effect of the distinct functional elements of the IR700-conjugated fusion proteins.

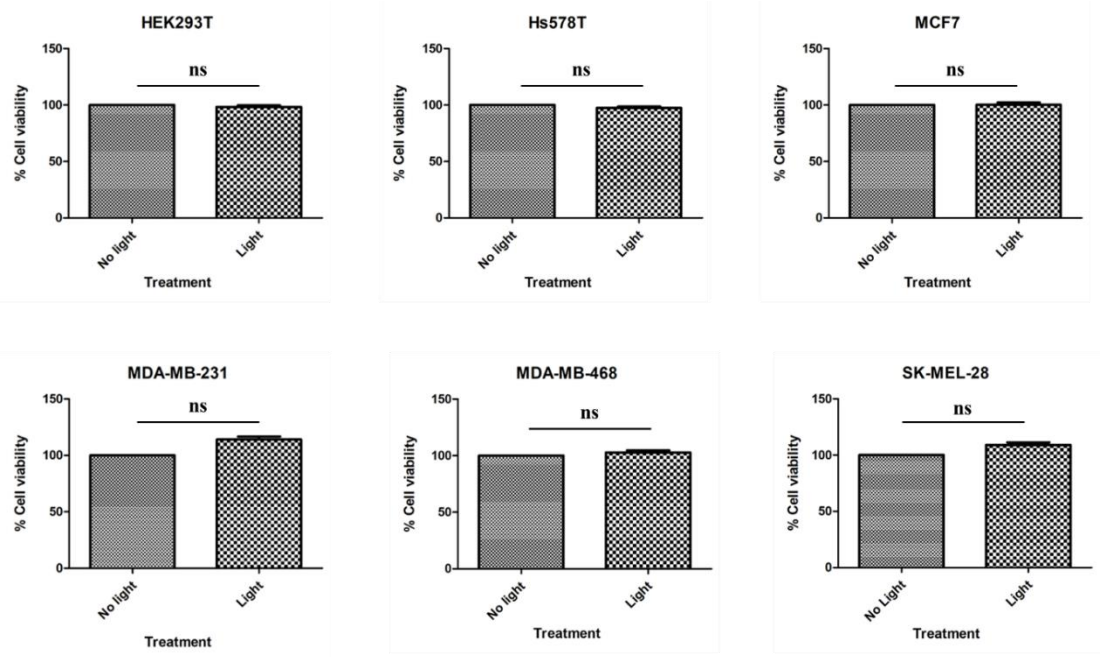

Figure 40: Evaluating the cytotoxic activity of 690 nm NIR light *in vitro*. The cytotoxic activity was assessed using an XTT-based viability assay after treatment with NIR light for 30 minutes. The percentage cell viability was normalized relative to the untreated cells and bar graphs were generated using GraphPad Prism v5. Data are mean ± standard deviation (SD) of each measurement (n=48). Student's *t*-tests were performed to determine statistical differences ($p < 0.05$) between no light and light irradiation (note: ns stands for 'not significant').

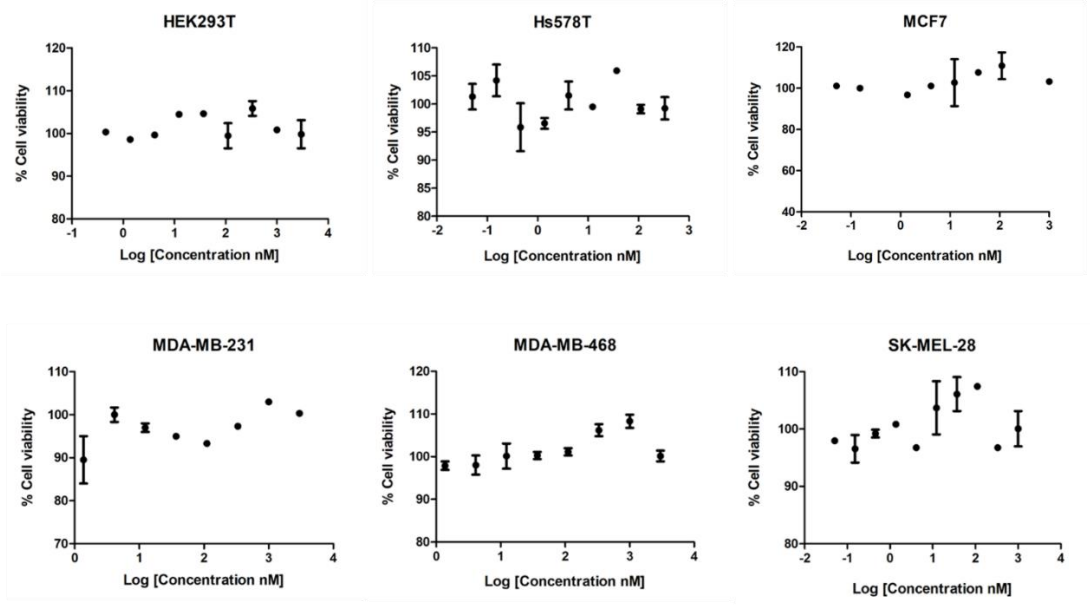

Figure 41: Investigating the cytotoxic activity of BG-IR700 on target cell lines, without exposure to NIR light at 690 nm. The cytotoxic activity was assessed using an XTT-based viability assay after

incubation with the PS for 3 hours. Cells were treated with (3-fold serially diluted) increasing concentrations of BG-IR700 and dose-response curves were generated using GraphPad Prism v5. Data are mean ± standard deviation (SD) of each measurement (expressed as a percentage of cell viability), and the measurements were performed in triplicate at least 3 times.

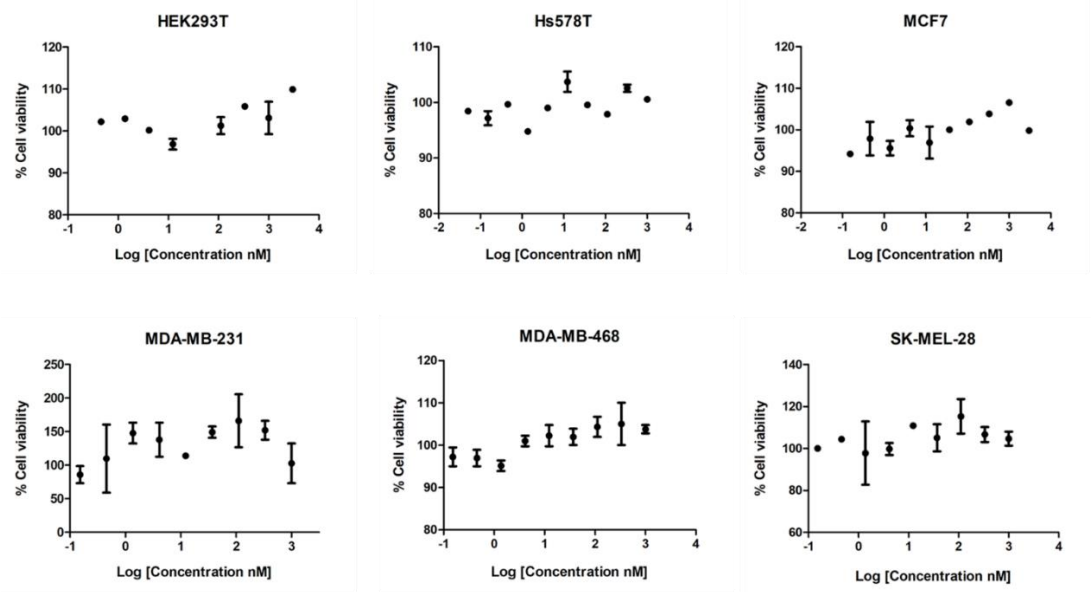

Figure 42: Investigating the cytotoxic activity of BG-IR700 on target cell lines, with exposure to NIR light at 690 nm. The cytotoxic activity was assessed using an XTT-based viability assay after incubation with the PS for 3 hours. Cells were treated with (3-fold serially diluted) increasing concentrations of BG-IR700 and dose-response curves were generated using GraphPad Prism v5. Data are mean ± standard deviation (SD) of each measurement (expressed as a percentage of cell viability), and the measurements were performed in triplicate at least 3 times.

Furthermore, as a pivotal aspect to the efficacy of these agents, it was necessary to ascertain successful site-specific coupling of BG-IR700 to SNAP-tag. Hence, following conjugation, the resulting combination products were resolved on a 10% SDS-PAGE gel and visualized using an iBright FL1000 Imaging System (Thermo Fisher Scientific, South Africa) before being stained for protein detection (section 2.5.3). This step enabled the discernment of red fluorescence signals (right panel) which corresponded to the appropriate theoretical sizes of the fusion proteins (left panel) (Figure 43). This inferred that incubation of the fusion protein with a 3-fold molar excess of BG-IR700 in the dark for 4 hours at room temperature, allowed efficient labeling of SNAP-tag with IR700. Additionally, prior to assessing the toxicity profiles of the putative compounds, the residual BG-IR700 dye (blue arrow) was removed by ultracentrifugation using Amicon filters (Sigma-Aldrich, South Africa) endowed with a 10K molecular weight cut-off pore size.

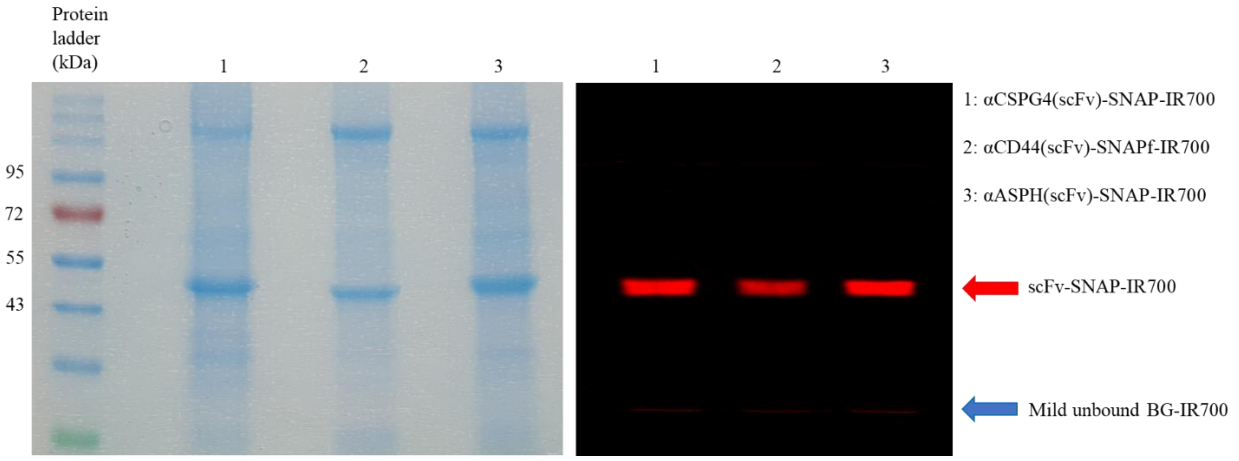

Figure 43: Confirming the saturation of scFv-SNAP fusion proteins with BG-IR700. The fusion proteins were incubated with a 3-fold molar excess of BG-IR700 in the dark for 4 hours at room temperature. The resulting samples were resolved on a 10% SDS-PAGE gel and fluorescence signals were visualized using an iBright FL1000 Imaging System (Invitrogen, Thermo Fisher Scientific, South Africa) (right panel). Thereafter, the same gel was stained using Aqua staining solution (left panel). Residual unbound dye was removed using 10K-sized Amicon filters (Sigma-Aldrich, South Africa) prior to phototoxicity studies. Red arrow: scFv-SNAP-IR700 and blue arrow: mild unbound BG-IR700 dye.

As such, by harnessing the selective nature of the antibody fragment, light-activated αCSPG4(scFv)-SNAP-IR700 was able to target and eliminate specific cell lines in a concentration-dependent manner (Figure 44).

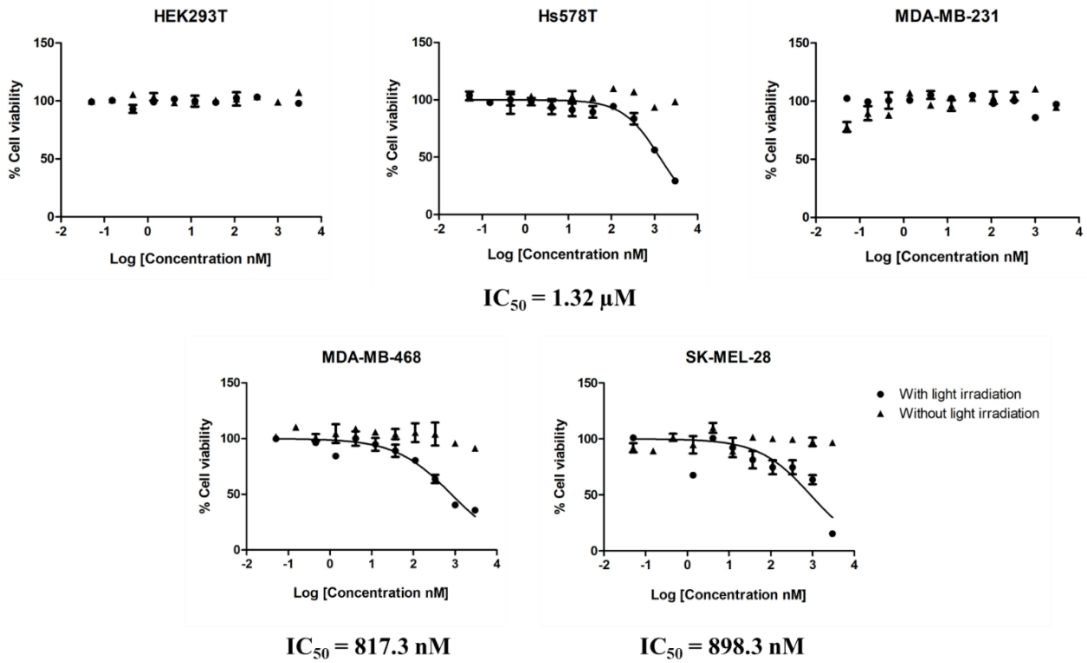

Figure 44: Dose-response curves demonstrating the photocytotoxic activity of αCSPG4(scFv)-SNAP-IR700 *in vitro*. The cytotoxic activity was assessed using an XTT-based viability assay after incubation with the drug for 3 hours. Cells were treated with (3-fold serially diluted) increasing concentrations of the drug (in the presence (●) and absence (▲) of NIR light at 690 nm) and the IC_{50} values (relative to the untreated and Zeocin-treated (100 µg/ml) cells) were calculated using GraphPad Prism v5. Data are mean ± standard deviation (SD) of each measurement (presented as a percentage of cell viability), and the measurements were performed in triplicate at least 3 times.

Among these CSPG4-abundant tumor cells, target TNBC cells – Hs578T and MDA-MB-468 – were affected with IC_{50} values numbered at 1.32 µM and 817.3 nM respectively. In contrast, the high frequency CSPG4-expressing cell line SK-Mel-28, exhibited an IC_{50} value of 898.3 nM. Therefore, reflecting the results obtained with the AURIF-based recombinant ADCs, cytotoxicity was again not dictated by the abundance of target receptors *in vitro*. Most importantly, αCSPG4(scFv)-SNAP-IR700 had no effect on: (1) $CSPG4^{low\ frequency}$-expressing cell lines (HEK293T and MDA-MB-231) and (2) all cell lines subjected to the absence of NIR light irradiation at 690 nm. These unique qualities warrant the use of such agents *in lieu* of PDT, to minimize the risk of detrimental side-effects inflicted to non-tumorigenic cells.

In congruence with the above findings, the CD44 and ASPH-targeting photoimmunotheranostic conjugates engineered in this study, showed for the first time, antigen and light-driven elimination of TNBC cells, with IC_{50} values ranging from 507 nM to 6.07 µM (Figures 45 and 46). This partiality towards high frequency receptor-expressing cell lines also suggested that conjugation of scFv-SNAP to BG-IR700 did not compromise the binding activity of the antibody moiety. However, a noteworthy observation pertained to the higher IC_{50} values (Table 11) obtained using this therapeutic approach as opposed to the targeted delivery of the antimitotic drug AURIF (Table 10). While the mechanism of action of the scFv-SNAP-IR700 combination products was not determinable in this study, this noticeable difference in activity highlighted the impact of distinct targeting strategies and their associated efficiencies when administered to the same panel of target cell lines.

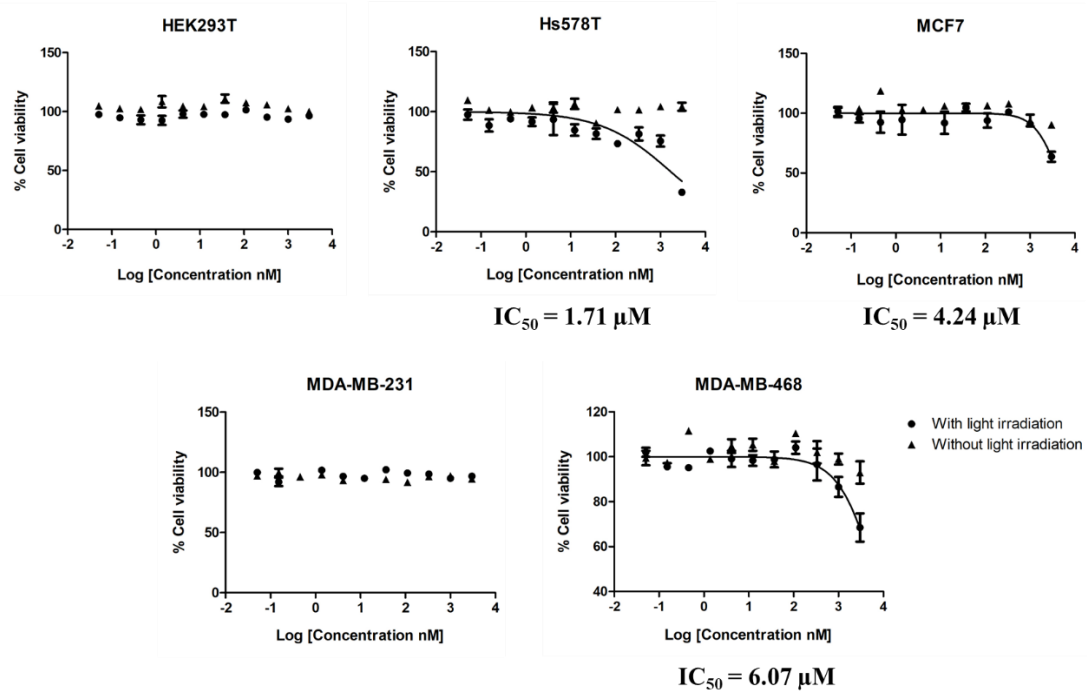

Figure 45: Dose-response curves demonstrating the photocytotoxic activity of αCD44(scFv)-SNAPf-IR700 *in vitro*. The cytotoxic activity was assessed using an XTT-based viability assay after incubation with the drug for 3 hours. Cells were treated with (3-fold serially diluted) increasing concentrations of the drug (in the presence (●) and absence (▲) of NIR light at 690 nm) and the IC_{50} values (relative to the untreated and Zeocin-treated (100 µg/ml) cells) were calculated using GraphPad Prism v5. Data are mean ± standard deviation (SD) of each measurement (presented as a percentage of cell viability), and the measurements were performed in triplicate at least 3 times.

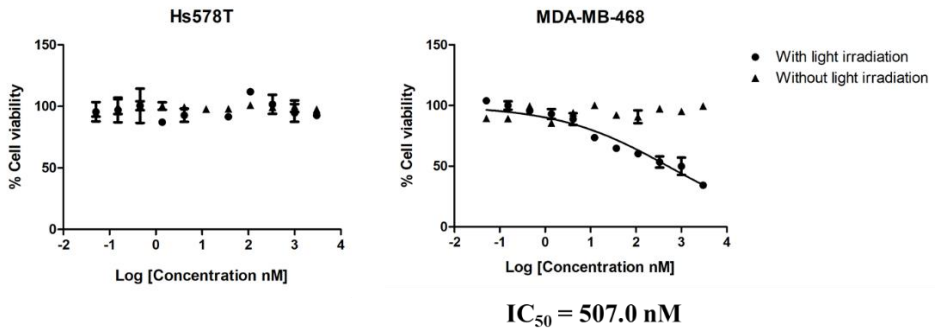

Figure 46: Dose-response curves demonstrating the photocytotoxic activity of αASPH(scFv)-SNAP-IR700 *in vitro*. The cytotoxic activity was assessed using an XTT-based viability assay after incubation with the drug for 3 hours. Cells were treated with (3-fold serially diluted) increasing concentrations of the drug (in the presence (●) and absence (▲) of NIR light at 690 nm) and the IC_{50} values (relative to the untreated and Zeocin-treated (100 µg/ml) cells) were calculated using GraphPad Prism v5. Data are mean

± standard deviation (SD) of each measurement (presented as a percentage of cell viability), and the measurements were performed in triplicate at least 3 times.

Overall, the resulting IC_{50} values generated from the IR700-associated phototoxicity studies in this section, are summarized in Table 11 below.

Table 11: Summary of IC_{50} values for scFv-SNAP-IR700 and unconjugated BG-IR700 in the presence of 690 nm NIR light irradiation

Treatment	Cell lines tested	IC_{50} values (nM)
αCSPG4(scFv)-SNAP-IR700	HEK293T	-
	Hs578T	1320
	MDA-MB-231	-
	MDA-MB-468	817.3
	SK-Mel-28	898.3
αCD44(scFv)-SNAPf-IR700	HEK293T	-
	Hs578T	1710
	MCF-7	4240
	MDA-MB-231	-
	MDA-MB-468	6070
αASPH(scFv)-SNAP-IR700	Hs578T	-
	MDA-MB-468	507
BG-IR700	HEK293T	-
	Hs578T	
	MCF-7	
	MDA-MB-231	
	MDA-MB-468	
	SK-Mel-28	

Chapter 4: Discussion

4.1 Triple-negative breast cancer: An unmet medical need

Breast cancer remains a global public health concern; an estimated 1 million cases of breast cancer are diagnosed annually worldwide, of which approximately 170,000 are described as triple-negative [40]. TNBC, which is characterized by tumors that do not express ER, PR and HER2, represents one of the most aggressive and clinically challenging breast cancer subtypes [444,445]. This unique disease entity often presents with a higher likelihood of brain and lung involvement, poorer prognosis and elevated mortality rates [48,49,446]. Strangely enough, TNBC displays the highest prevalence among premenopausal women of African origin, whereby these women are almost 3 times more likely (than white women) to carry the triple-negative phenotype [43,444]. Given the complexity of this disease, clinicians have thus been challenged with a lack of specific guidelines to address the management of afflicted patients [447]. This situation is further exacerbated by the lack of clinical benefit that can be derived from well-established targeted therapies for breast cancer (such as tamoxifen, trastuzumab and aromatase inhibitors) [447–450]. Currently, there is no clear, proven effective single agent that can target a defining vulnerability in TNBCs [447]. Consequently, there is an increased dependency on traditional treatment modalities, although important limitations need to be addressed in order to achieve significant clinical strides [52,53]. For instance, while chemotherapeutic regimens using anthracyclines and taxanes, remain the mainstay of treatment due to their initial sensitivity, their short disease-free survival does not warrant a relative clinical merit [451,452]. With the identification of 6 TNBC subtypes bearing unique gene expression profiles and ontologies [54], the acute diversity and heterogeneity of this disease is becoming more evident [51]. Based on these premises, there is an urgency to direct multinational research efforts towards the identification of prognostic factors or markers that can reliably stratify high and low risk TNBC patients based on their predicted differential responsiveness to targeted agents. Therefore, at the Medical Biotechnology and Immunotherapy Research Unit, we envisage to develop an array of companion immunodiagnostics, which when combined, should enable the detection of the vast majority of triple-negative breast tumors. In the first instance, such technology will allow the simultaneous detection and quantification of several target proteins (biomarkers) on TNBC biopsies – a fairly recent strategy known as multiplex

immunofluorescence imaging [453,454]. Given the relevance of CSPG4, CD44 and ASPH as promising target antigens in TNBC (as validated by the work of PhD student Natasha Hardcastle on South African TNBC tissue sections), the results generated in this study represent the first step in the engineering of according therapeutics that could be specifically tailored to the needs and disease profiles of each patient, concurrently providing a conducive milieu for the expansion of personalized medicine.

4.2 SNAP-tag based fusion proteins as important tools in passive immunotherapy

Cancer immunotherapy – a major transforming factor in science and oncology [455] – first had its genesis through the idea of stimulating the immune system to produce a potent antitumor immune response [456]. Following this important scientific breakthrough, advanced research into the basis of cancer biology, supported by the claims of a 'magic-bullet' and the initial observations of antigen expression by tumor cells, propelled the expansion of antibody-based therapeutics to unfathomable heights [7,192,195,457]. For instance, full-length (naked) mAbs, specifically targeting cellular markers that are enriched in malignant cells, have demonstrated considerable utility in the management of haematological and solid tumors such as breast (HER2-positive) and pancreatic cancer [450,458,459]. Nonetheless, the majority of FDA-approved mAbs were rarely curative [460], indicating the need to enhance their therapeutic prowess. In addition to early reports of HAMA responses [200], the failure of unconjugated mAbs may be attributed to the manner in which they induce tumor cell killing [461]. In principle, mAbs can exert a therapeutic effect through 3 main pathways: (1) antibody binding to the tumor cell surface receptor prevents downstream signaling, culminating in reduced proliferation and apoptosis, (2) immune-mediated cell killing mechanisms provided by the Fc region of the antibody (including complement-dependent cytotoxicity, ADCC and the activation of cytotoxic T-cells) and (3) inhibition of tumor vasculature and stroma (induced by some antibodies such as bevacizumab) [198,461]. Therefore, an important prerequisite to the clinical efficacy of mAbs is undoubtedly a functional host immune system [462], which may be compromised in patients receiving chemotherapy or radiation therapy. Furthermore, as outlined by Scott *et al*. (2012), many tumors have evolved multiple escape mechanisms to counteract the therapeutic effects of mAbs [461]. While high dosages and repetitive administration could be used to ensure clinical success [463–465], the downside of this approach

entails not only a heightened risk of adverse reactions, but also a selective pressure on tumor cells resulting in the development of resistance, most often arising from the downregulation of the targeted receptor (as exemplified by Trastuzumab resistance in breast cancer) [204,461]. Therefore, concerted efforts (in the field of passive immunotherapy – strategies that do not require an active response from the host immune system to fight disease [466]) have been focalized on the use of antibodies as guiding mechanisms in the specific delivery of toxic agents to tumor cells [467,468], thereby extending the therapeutic efficacies of existing unconjugated mAbs and at the same time alleviating the challenges of non-targeted traditional cancer therapies.

Thus, targeted drug delivery was first achieved through the inception of ADCs – bifunctional molecules exploiting the specificity of mAbs and the differential expression of tumor-associated antigens, to dispatch chemically-conjugated chemotherapeutic compounds that would otherwise be too toxic for systemic application [202,305]. Nonetheless, early work in ADC development revealed that adopting a holistic approach to ADC design was not adequate and that the choice of the mAb carrier, the mode of drug attachment and the toxic payload, should be under more careful scrutiny [243]. As such, unexpected ramifications encountered with ADCs were as follows: (1) only a limited number of drug molecules can be loaded onto antibodies without abrogating their binding activity, (2) poor accumulation of the drug in solid tumors, (3) maintaining serum stability, (4) low expression of tumor cell surface antigens can limit therapeutic levels of drug accumulation in cells and most importantly, (5) difficulty producing homogeneous ADC populations suitable for clinical use [241,242]. Indeed, the mainstream conjugation strategy employed in ADCs is founded on the use of lysine side chains or reduced disulfide residues to arm mAbs with cytotoxic payloads [274,469,470]. However, this method usually results in heterogeneous ADC species (ranging from 0 to 8 DAR), bearing varying pharmacokinetic efficacies and safety profiles [275,460,470]. To this end, understanding the effect of drug loading on the therapeutic potential and stability of mAbs, has been at the forefront of several studies [277,423,471]. In most of these cases, ADC species with a fully drug-loaded hinge region (mainly DAR 6 and DAR 8), have been associated with reduced stability under stress conditions, resulting in the formation of aggregates [471,472]. This propensity for aggregation often arises from protein interactions (example: mAb conjugation to hydrophobic cytotoxic moieties such as MMAE), temperature, agitation and ionic strength

[472–474]. Therefore, this phenomenon represents a major pothole in the ADC development pipeline; aggregation can affect the shelf life of a drug product, as well as its *in vivo* pharmacokinetics [475,476]. As reviewed by Moussa and colleagues (2016), the presence of aggregates in protein drug therapeutics can induce adverse immune reactions in patients, thereby jeopardizing their safety and efficacy [477]. To mitigate these impacts, reduction in the drug loading per antibody (from DAR 8 to DAR 2 or 4) was carried out, culminating in an increase in the therapeutic index (maximum tolerated dose/curative dose) by ≥ 2-fold, albeit at the expense of reduced conjugate yield and increased heterogeneity [277]. In summary, there is a need to devise a strategy that can provide a well-controlled drug stoichiometry, while at the same time conform to the desirable traits of ADCs as targeted therapeutics, including maintaining the structural integrity of the antibody moiety, achieving a high therapeutic index and serum stability, be readily cleavable within target cells to release the active warhead, and realize homogeneity to facilitate drug development [472,478]. Consequently, with the advances in protein engineering, several site-specific conjugation strategies have been developed, capitalizing on the introduction of unnatural amino acids into the antibody to drive the controlled chemical conjugation of cytotoxic compounds [278–280]. However, self-labeling tags (such as SNAP-tag, CLIP-tag and Halo-tag) genetically fused to antibodies or their fragments, are gaining momentum as efficient one-step generation processes in the development of recombinant immunotherapeutics that can bypass chemical conjugation while ensuring product homogeneity [281,282,298,479].

Particularly, SNAP-tag is an engineered mutant of the human O(6)-alkylguanine-DNA alkyltransferase, which can specifically and covalently bind to BG derivatives, in an irreversible manner [283,284,290]. It offers a treasure trove of advantages, ranging from the simplicity of the reaction, the specificity and short duration of conjugation (reacts only with BG-modified substrates), no requirement for activating substrates, as well as a predictable 1:1 stoichiometric reaction with the generation of homogeneous products [285–287,290,292]. In addition to its application in a variety of experimental settings, the versatility of this technology is further validated through the emergence of recombinant SNAP-tag based fusion proteins (scFv-SNAP) bearing specificity towards tumor-associated antigens [285,296]. As such, this class of protein therapeutics displays leading-edge in various aspects: (1) they can be produced in different

expression systems (for example: bacteria and mammalian) with high yields, (2) antibody functionality is maintained (SNAP-tag provides distant conjugation away from the paratope, creating a spacer between the antibody and the effector molecule), (3) their reduced size promotes enhanced tumor penetration and rapid renal clearance and (4) SNAP-tag based fusion proteins have shown to be instrumental in the delivery of diverse effector molecules to target cells, including fluorescent dyes, PSs and antimitotic drugs [296–298,312].

Taken together, the above arguments provide the rationale behind the stipulated aims and objectives of this study (section 1.9). The novelty in this research lies in genetically fusing SNAP-tag to 3 different scFvs (targeting CSPG4, CD44 and ASPH) for the development of diagnostic tools, and at the same time providing an innovative conjugation strategy and targeted approach for the delivery of homogeneous therapeutic agents (AURIF and IR700) to diseased TNBC cells.

4.3 Production of recombinant SNAP-tag based fusion proteins

In this study, pCB-αCD44(scFv)-SNAPf was successfully cloned (as shown by the sequencing results in Figure 14) and all 3 fusion proteins (αCSPG4(scFv)-SNAP, αCD44(scFv)-SNAPf and αASPH(scFv)-SNAP) were effectively expressed in a mammalian expression system (HEK293T cells). However, several unanticipated obstacles were faced during this process. Firstly, in the context of molecular cloning, vector re-ligation was a prominent challenge (Figure 12D), which could be explained by the presence of 5'-phosphate groups from vector molecules or from incomplete restriction digest of the vector to be used for ligation [480]. As an improvement, the digested vector backbone should be treated with a phosphatase prior to the ligation reaction [481]. On the other hand, transformation efficiencies of pCB-αCD44(scFv)-SNAPf were in the range of 10^5 cfu/µg, contradicting the claims of Inoue *et al*. (1990) about DH5α *E. coli* cells being extremely competent organisms for plasmid DNA transformation, with transformation efficiencies of 1-3 x 10^9 cfu/µg [482]. Several factors including the growth conditions, the plasmid size and purity, may have reduced the success of this transformation event [483]. Moreover, monitoring the intracellular expression levels of eGFP (as an indication of successful transfection and potential transient expression of the putative fusion proteins in HEK293T cells) revealed low transfection efficiencies (< 70-80%), that in turn prompted a prolonged Zeocin enrichment step. As an alternative to the

lipid-based method employed in this research, the introduction of exogenous nucleic acids into HEK293T cells could be improved by electroporation (transfection efficiency of 30-80%), calcium phosphate precipitation (transfection efficiency can be close to 100% depending on cell line used) or polycationic non-viral gene delivery vectors such as polyethylenimine (transfection efficiency of 34-56%) [484,485].

Furthermore, the production of genetically engineered recombinant proteins with high purity and yield (up to milligram or gram scale) is indispensable in preclinical and drug discovery studies. To this end, the SNAP-tag based fusion proteins employed in this study, were expressed with a polyhistidine tag (His x 6) fused to the N-terminal peptide sequence (Figure 11) to expedite their purification and detection. The implementation of such fusion tag is fortified by its small size (0.84 kDa for 6 histidine tags) and its ability to enable effective purification without affecting the folding, structure and function of the protein of interest [486,487]. However, SDS-PAGE and western blot analysis of the recovered fusion proteins (Figures 18 and 20), revealed that IMAC purification (as a standard first enrichment step for protein purification) is indeed not sufficient on its own to achieve high purity (> 90%). More explicitly, a significant disadvantage of IMAC purification pertains to the unspecific binding and co-elution of contaminants (endowed with endogenous histidine residues or metal-binding motifs) arising from protein samples harvested from eukaryotic expression systems (as done in the current study) [487]. In consequence, with protein quantification becoming increasingly unreliable due to the presence of contaminating proteins in the concentrated scFv-SNAP fractions (Figure 18), densitometric measurements were carried out (Figure 19), although the exact repercussions of the contaminants on protein binding and activity remains unclear. Nonetheless, it can be speculated that increasing amounts of contaminants (including degradation products potentially containing a functional scFv portion), could compromise toxicity studies by increasing the IC_{50} values of the recombinant immunoconjugates through competitive binding and uptake.

Hence, in an ideal setting (subject to the availability of appropriate devices and expertise), a multistep purification process would be implemented, consisting of IMAC followed by size-exclusion chromatography (as reported previously [71,488,489]). Additionally, while optimization

of the IMAC purification process is encouraged when dealing with poorly expressed proteins, the protein purity can be further increased by the use of dual affinity tags [487]. As illustrated by the work of Manal Amoury (PhD student), inclusion of a streptavidin tag provided an additional purification step (as opposed to his-tag purification alone) which resulted in > 90% purity and a yield of 4 – 5 mg/L for the CSPG4-targeting fusion proteins expressed. Furthermore, while the absolute yield of the fusion proteins (0.02 – 3.65 mg/L) were adequate for *in vitro* binding studies (Table 7), further characterization of their activities will require a cost-effective, fast and scalable procedure that allows the expression of correctly folded proteins. To this end, several strategies have been devised for high-level protein production (50 – 600 mg/L), including the use of alternative expression systems (Chinese hamster ovary cells, yeast or insect cells [490,491]) and protocols (example: periplasmic stress expression in *E. coli* [489]).

In summary, while the generation of αCSPG4(scFv)-SNAP is supported by previous studies [71,295], this research demonstrates for the first time, successful development of SNAP-tag based fusion proteins specifically targeting CD44 and ASPH-expressing triple-negative breast tumors. In the same vein, the results herein presented highlight that despite the absence of industrial production and purification processes in place, single-step enrichment of SNAP-tag based fusion proteins via IMAC, represents an ideal compromise which allows rapid and preliminary analysis to be carried out (sections 3.5 – 3.7). Therefore, with early-stage proof of functionality becoming feasible at university level, the establishment of industrialized production processes (through tight collaboration with biopharmaceutical companies) would need to be addressed. Undoubtedly, to solve this conundrum, the streamlining of process development at universities coupled with mass industrial production, is highly recommended.

4.4 SNAP-tag based recombinant immunodiagnostics for TNBC detection

It is widely known that the key to successful management of breast cancer revolves around early screening and detection [21,492]. Based on the aggressive nature of TNBCs, accurate diagnosis becomes vital for determining prognosis and ensuring delivery of the optimal therapy for patients [493]. Traditionally, TNBC diagnosis is dictated by immunohistochemistry (IHC) (to assess ER, PR and HER2 status), although in clinical practice, it is often a two-step process, combining

morphological imaging and IHC [48]. Intriguingly, despite being extensively studied in oncology and pathology, there are only a few reports describing the imaging features of TNBCs. Unfortunately, despite their large size at diagnosis (as compared to other breast cancer types), up to 18% of TNBCs remain occult on initial mammography [494–496]. As such, TNBCs lack the typical suspicious mammographic characteristics of breast cancer, namely an irregularly shaped mass, spiculated margins and associated calcifications [497,498]. Therefore, mammography alone is a sub-standard strategy in the initial diagnostic assessment of TNBCs. In contrast, while ultrasound demonstrates a higher sensitivity, it fails to produce an enduring diagnostic potential, owing to the presence of benign features encountered in 21-41% of TNBC lesions [496,499]. Additionally, regardless of their ability to reveal smooth borders of some TNBC tumors, ultrasound and mammography fall short of efficiently imaging intratumoral characteristics, such as necrosis and fibrosis, which are common in TNBCs [493,500].

Meanwhile, one may argue that gene-expression profiling has revolutionized our understanding and approach to breast cancer and its molecular subtypes [31,54]. While the above statement may hold true, it can be difficult to establish the practical benefits of this technique in the clinical setting, where such experiments are rarely carried out [32,493]. Therefore, researchers have been questioning whether this approach provides overriding prognostic and predictive information as opposed to conventional IHC [501]. Surprisingly, it was found that ‘good old’ clinical markers provide a similar prognostic power as microarray gene-expression profiling [502]. Thus, the absence of routine high-throughput molecular technologies, has probed the application of molecular breast cancer markers as a surrogate for the classification of TNBC tumor types, based on their prognosis and/or response to specific agents [447]. For instance, a five-marker method (pertaining to the assessment of ER, PR, HER2, cytokeratin 5/6 and EGFR status) has been postulated as a proxy for the identification of basal-like breast cancer [56,503]. In addition to patient selection, molecular biomarkers for TNBC, have the potential to expedite the development of effective therapies for this aggressive disease entity [504]. By virtue of its complex nature, TNBC will undoubtedly necessitate the combination of several different targeted approaches, in order to achieve meaningful progress in the improvement of patient outcomes.

Consequently, through the generation of SNAP-tag based fusion proteins targeting CSPG4, CD44 and ASPH, this study has the potential to contribute (in the long-term) to molecular biomarker-based patient selection. After confirming the self-labeling activity of the fusion proteins through conjugation with BG-Alexa Fluor 488 (Figure 21), the resulting product was used in the screening of TNBC cells. Confocal microscopy (across the various fields of view) indicated that MDA-MB-231 and HEK293T cells were negative for both CSPG4 and CD44, while Hs578T cells were negative for ASPH (Figures 22 – 24). Thereafter, flow cytometry was applied to further confirm the binding capacity of the fusion proteins, in addition to quantifying the relative surface expression of the target receptors within the live cell population. To this end, antibody titrations were first carried out (Figures 25 – 27) to palliate the potential effects of low protein purity (Table 7) on the scFv-SNAP binding potential, while favoring the best separation between the antigen-positive and negative cell populations. Therefore, after selection of the optimal fusion protein concentration that would allow maximal staining of the target receptor (with minimal background interference), MFI values were calculated as a representative of the level of antigen sites expressed per cell. Surprisingly, it was found that less than 50% of TNBC cells expressed the cognate antigen, and those that did (as confirmed by confocal microscopy), displayed an MFI value of 2265 – 6983 (Tables 8 and 9). This result implied that the antigen-negative cells demonstrated on average ~7 times the receptor density as compared to the receptor-expressing TNBC cells (Table 8). Hence, further elucidation of this counter-intuitive phenomenon will necessitate the application of more robust quantification methods, such as the use of commercial calibration beads in flow cytometry (example: BD Quantibrite™ Beads) [505].

However, mirroring the confocal microscopy observations, flow cytometric analysis revealed a corroborating distribution (or frequency) of the antigen-positive cells within the live cell population (Table 9). Therefore, cell lines positive for these receptors were used to assess the cytotoxic activities of the AURIF and IR700-based immunoconjugates. Nonetheless, a closer look at the literature suggests several disparities in the observable binding data and receptor expression status across target cell lines. For example, previous studies showed that CSPG4 expression was detectable on the surface of MDA-MB-231 cells, but not on MDA-MB-468 cells [71,295,369]. Likewise, in contradiction with the current study, Jin and colleagues (2016) demonstrated high

expression of CD44 in MDA-MB-231 (95.1%) and low expression in MCF-7 (1.69%) [334]. On the contrary, the prevailing low expression of ASPH in MDA-MB-468 cells (19.8%) was substantiated by Lin *et al*. (2019) through the expression profiling of ASPH on various human breast cancer cell lines [416]. Consequently, it can be speculated that several environmental and physiological factors play a defining role in the modulation of receptor dynamics within tumor cells. Undoubtedly, while immortal cell lines constitute a cost-effective and effortless method to study biological processes, they also represent very artificial systems (lacking close cell-to-cell contact) which may not adequately mimic primary tumor cells. Additionally, long-term serial passages of cell lines can induce genotypic and phenotypic variations in the cell population [506], which can give rise to further heterogeneity and inconsistencies in the data set. For example, several studies reported the presence of cell subpopulations in MCF-7 that were marked by differential growth rate, DNA synthesis and expression of hormone receptors [507–510]. Following the same trend, it was observed that the mixing of two different cell types (one expressing the tumorigenic target and one negative for the target receptor), can result in one cell type overtaking the entire cell population [511,512]. Such cell culture disparities warrant the need for quality control monitoring of cell lines, as done by the implementation of short tandem repeat (STR) testing [513]. However, Kleensang *et al*. (2016) argue that other methods such as comparative genomic hybridization (CGH) should be used alongside STR profiling, in order to detect cellular and phenotypic heterogeneities that are not detectable by STR markers [514].

Therefore, while the application of cell authentication techniques, goes beyond the mandate of this PhD dissertation, it is hypothesized that a better understanding of receptor dynamics within tumor cells (and the consequences thereof) might be instrumental in future therapeutic predictions. Although the cell lines used in this study offer an excellent platform for initial proof of concept, they are not entirely representative of the tissue of origin, which justifies the need for the establishment of tumor organoids and the acquisition of primary TNBC cells (from biopsies sourced from suitable patient cohorts) for future functionality studies. On this basis, achieving cell culture conditions which can closely mimic the tumor microenvironment, represents the gold standard to deriving patient-relevant data and thus improving treatment outcomes.

4.5 Specific delivery of antimitotic drug AURIF using scFv-SNAP fusion proteins

ADCs are spearheading vectorized chemotherapy against cancer, with 11 FDA-approved ADCs and approximately 80 in clinical trials [246,515,516]. However, in most of these cases, stochastic bioconjugation methods are being implemented, despite the association of site-specific conjugation with improved ADC therapeutic index [517]. As such, several approaches are being promulgated (example: THIOMAB technology, the amber suppressor tRNA/aminoacyl-tRNA synthetase pair and the insertion of a CXPXR consensus sequence [278,518,519]), based on their ability to provide unique conjugation sites through the insertion or substitution of amino acid residues in the native antibody sequence [312]. Nonetheless, as reported by Lucas *et al*. (2018), modifications to the antibody may affect the binding affinity, potency, as well as reduce the rate of clearance [520]. Based on these premises, this study herein reports the site-specific conjugation of a single auristatin derivative onto engineered scFv-SNAP fusion proteins, targeting CSPG4, CD44 and ASPH, thereby generating novel recombinant (next-generation) ADCs. Given their overexpression and multi-dimensional roles in the progression and aggressiveness of cancer, CSPG4, CD44 and ASPH represent clinically relevant targets, especially in the context of TNBCs [368,369,384,413,416]. Most importantly, CSPG4 and CD44 are involved in the functional properties of CSCs [353,384], which are known to promote tumorigenic growth, invasion, metastasis and recurrence [373,374]. Therefore, efficient cancer therapies should not only be able to target tumor cells, but also CSCs which can greatly affect treatment outcomes. Furthermore, the choice of the cytotoxic payload (used in this study) was not random; while MMAE might be the most commonly used in ADC design, AURIF is more hydrophobic and exhibits a lower membrane permeability [305,307,521,522]. Moreover, AURIF is well-suited for the generation of highly potent ADCs [313]. For instance, conjugation of AURIF to a B-cell maturation antigen-specific mAb culminated in an increase in the proportion of late apoptotic/necrotic cells from 24 to 75%, with the application of only ~1 µg/ml of the ADC to target cells [523]. Similarly, as illustrated by Capone and colleagues (2018), EV20-AURIF (an anti-HER3 mAb conjugated to AURIF) was able to kill HER3-positive melanoma cells with an IC_{50} value of 0.002 nM [524]. This potent cell killing activity of AURIF is driven by its ability to inhibit microtubule assembly (typically by forcing cells to build monopolar mitotic spindles instead of normal bipolar spindles [525]) and tubulin-

dependent GTP hydrolysis, resulting in cell cycle arrest and ultimately apoptosis [309,310]. Lastly, while ADCs can mediate the direct killing of antigen-positive tumor cells, they are also endowed with the ability to destroy adjacent antigen-negative cells – a phenomenon known as the 'bystander killing' effect [526]. Fortunately, AURIF is known to possess low bystander activity [527], which can limit the impact on non-target cells.

In the current study, incubation of the target cells with increasing concentrations of αCSPG4(scFv)-SNAP-AURIF, αCD44(scFv)-SNAPf-AURIF and αASPH(scFv)-SNAP-AURIF, caused a reduction in cell viability, with IC_{50} values ranging from 100.4-1660 nM (Table 10). Negligible cytotoxicity was observed on $CSPG4^-/CD44^-$ MDA-MB-231 and HEK293T cells, as well as $ASPH^-$ Hs578T control cells, highlighting the specific intracellular delivery of AURIF to target cells only. As demonstrated by previous studies, scFv-SNAP fusions are unable to induce cell killing on their own (Figures 33 – 35) [313,346], which implies that the observed toxicity is due to the addition of the recombinant immunoconjugate. Moreover, the results obtained, build on existing evidence that conjugation of diverse functional groups (such as fluorophores and toxins) to SNAP-tag, does not compromise the binding specificity of the antibody or prevent its internalization [298,312–314,346]. The mechanism of action of the novel ADCs generated, is as shown in Figure 48; (1) the scFv-SNAP-AURIF binds specifically to the extracellular receptor of the tumor cell (via its scFv) and is internalized into the lysosomal compartment, (2) the enzymatic reactions within the lysosomes promote degradation of the fusion protein, releasing the AURIF toxin into the cytosol, and (3) AURIF induces microtubule disassembly (as visualized by Woitok *et al*. (2017) through automated microscopy), which promotes cell death by apoptosis [313].

Interestingly enough, unconjugated BG-AURIF gave rise to IC_{50} values in the range of 32.3 nM-17.1 µM (Table 10), confirming that modification with BG does not affect its killing potential [312]. In agreement with several findings [312,313,515], these IC_{50} values (treatment with BG-AURIF alone) are higher than that observed with the conjugated fusion protein, validating the fact that targeted drug delivery increases potency and efficacy. As compared to state-of-the-art (BG-AURIF commercialized by Tube Pharmaceuticals (Vienna, Austria) [313]) which relies on the direct attachment of AURIF to BG, a novel aspect of this research pertains to the use of a BG-

PEG_3-NH_2 linker to couple AURIF to SNAP-tag (work of MSc Chemistry student, Allan Huysamen). Such a scheme would allow distancing of the AURIF molecule from the active domain (or binding pocket) of SNAP-tag, while resulting in a more hydrophilic combination product, thereby increasing its water solubility and improving the efficiency of the conjugation reaction (Figure 47).

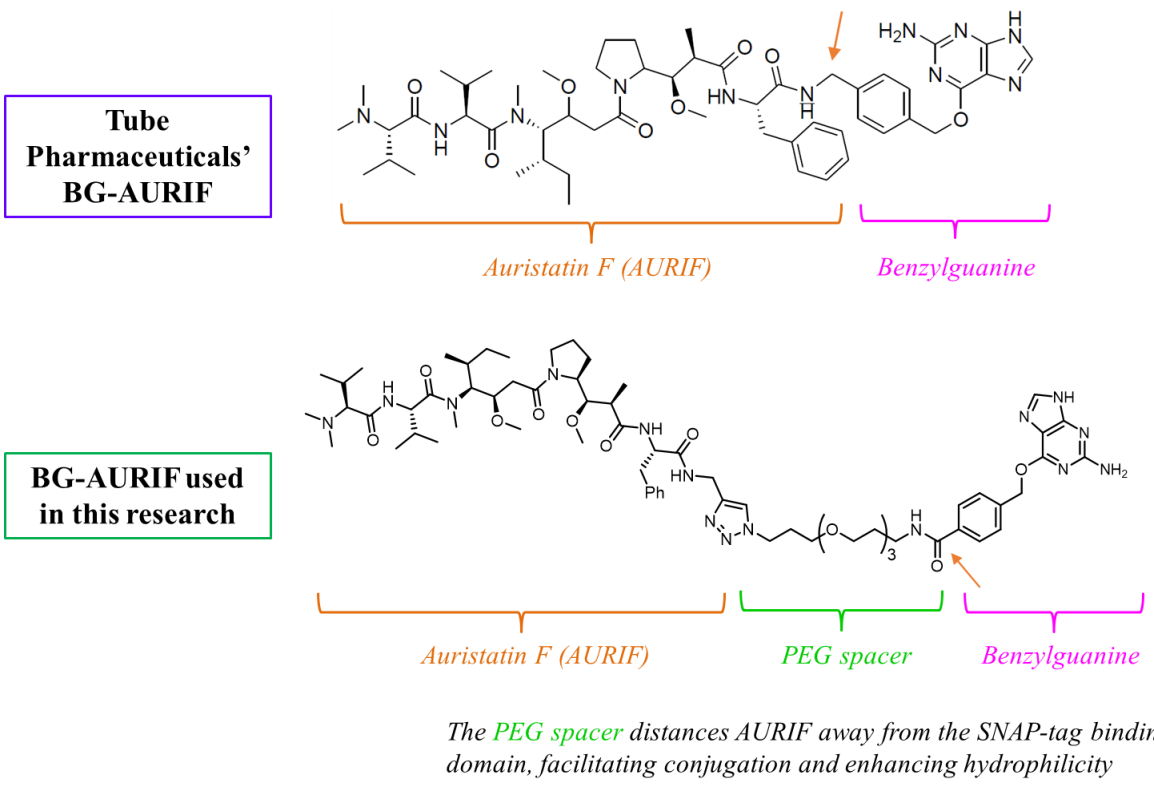

Figure 47: Structural differences between commercially available BG-AURIF (manufactured by Tube Pharmaceuticals, Austria) and BG-AURIF used in this research. While commercial products attach BG directly to AURIF, the BG-AURIF employed in this study, contains a BG-PEG_3-NH_2 (PEG) spacer that links BG to AURIF. Moreover, this linker incorporates a carbonyl group at the benzylic position of the BG group, whereas commercial products have a methylene group (see orange arrows). This was done to increase the efficiency of the SNAP-tag conjugation by promoting the SN2 reaction, while allowing for more versatile design and synthesis options via the carbonyl group (adapted from MSc thesis of Allan Huysamen).

Furthermore, contrary to the IC_{50} values obtained in this study (Table 10), higher cytotoxic activities (0.6-12 nM) were obtained with previous scFv-SNAP-AURIF recombinant ADCs (Table 3) [312,313]. A possible explanation for this discrepancy might be the difference in expression levels of the target receptors (as compared to literature). Likewise, the purity of the fusion proteins

might come into play – the lower the amount of competing degradation product in the recovered protein sample, the lower the expected IC_{50} values. Meanwhile, the flow cytometric analysis conducted in this study, may not be the most accurate reflection of the spatial and temporal receptor dynamics exhibited by tumor cells used in the toxicity studies. For example, a tissue-factor specific mAb conjugated with auristatin derivatives, achieved IC_{50} values of 1.15-100 nM, subject to tissue factor expression on pancreatic tumor cells [315]. Similarly, Sommer and co-workers (2016) demonstrated that high expression levels in cells, correlated with efficient internalization, efficacy and cytotoxic effects *in vitro* (IC_{50} values ranged from 0.097-0.83 nM in cell lines harboring at least 10,000 antibody binding sites) [528]. However, 2 studies found no correlation between cell surface CD22 expression and the activity of the anti-CD22 ADCs [529,530] (as observed in the current study), pointing to the involvement of multiple mechanisms in modulating ADC activity. Indeed, it was found that the intracellular concentration of the released payload was linked with *in vitro* ADC-mediated cytotoxicity, independent of target expression [512]. This also means that patient selection relying solely on antigen expression, may not guarantee ADC anti-tumor efficacy and therefore, additional tumor markers may be required (as being done in this research) to select patients for ADC therapy [520]. In general, it is still unclear what factors contribute to the potency of ADCs; antibody binding affinity, DAR, payload potency, antigen expression level, internalization rate and trafficking, have all been implicated in influencing ADC treatment outcomes *in vitro* [527,531–533]. In addition, several modes of resistance can also affect the potency and pharmacology of ADCs; for instance, downregulation of cell-surface antigen reduces antibody binding, while elevated levels of drug transporters can limit the effectiveness of the payload [534]. Due to these multiple variable parameters, it therefore becomes increasingly difficult to compare the activity of different ADCs across cell lines [512].

ADCs as potential targeted delivery systems (for solid tumors) must be able to overcome all hurdles [535], including travelling through the bloodstream and penetrating the tumor mass. Of note, an unstable linkage can result in premature release of the toxic payload prior to reaching the diseased site [536]. Hence, achieving reasonable chemical stability is instrumental when designing the linkage between the antibody and the effector component [535]. As exemplified by Woitok *et al*. (2016), scFv-SNAP-AURIF maintains its activity even after 48 hours incubation in human

serum [312]. Therefore, in congruity with previous reports [312,313], the results herein presented, showcase the application of SNAP-tag technology as a method to achieve stable and efficient linkage of the small molecule toxin AURIF to scFvs targeting various surface antigens. Additionally, through efficient conjugation with only a 3-fold molar excess of BG-AURIF (Figure 36), SNAP-tag fusion proteins represent an inexpensive and simple strategy for the development of homogeneous ADCs with a defined 1:1 stoichiometry [298,312,314]. This study contributes to a clearer understanding of the potential of SNAP-tag to bypass the integration of unnatural amino acids in the antibody sequence, while allowing the development of recombinant ADCs with an ideal molecular weight of ~50 kDa (to facilitate tumor penetration and reduce retention time in non-target tissues) [313,537,538]. Since the *in vitro* cytotoxic effects of ADCs correlate with the number of effector molecules on the antibody [539], multiple AURIF derivatives could be attached to one BG molecule and conjugated to SNAP-tag, to potentially improve the efficacy of the recombinant ADCs described in this study, without affecting their antigen-binding ability or their homogeneity [312,313]. Alternatively, the introduction of a cleavable linker in-between the scFv and SNAP-tag (such as the cathepsin B cleavable citrulline-valine linker in brentuximab vedotin) could also enhance cytotoxicity by assisting intracellular release of the toxic payload [312]. Overall, this work represents a first important step in the establishment of methodologies geared towards the engineering of more effective ADCs, paving the way for future translation into *in vivo* animal models, in order to evaluate their full potential.

4.6 Theranostic NIR photoimmunotherapy using SNAP-tag based fusion proteins

Conventional PDT – the combination of a photosensitizing agent with the physical energy of non-ionizing light to destroy malignant cells [320] – is dependent on the passive accumulation of the PS in tumor tissues, which makes it difficult to achieve optimal dosage, resulting in damage to healthy tissues and prolonged skin sensitivity [540,541]. In order to palliate these effects, several amalgamations of conventional PSs and mAbs have been devised and tested, but with limited therapeutic success *in vivo* [316–319,542]. Therefore, overcoming these impediments touted a necessary measure, involving PIT, based on the use of tumor-specific mAbs conjugated to the NIR PS phthalocyanine dye IR700, which has demonstrated palpable theranostic activities in several mouse models [320,333,336,543]. Although PIT has been proposed since 1995 [544], its

translation into clinical use, has been fraught mainly by the use of random chemical conjugation methods available to arm mAbs with PS molecules [345]. The vicissitudes of this approach revolve around the limited reproducibility of the conjugate synthesis, which often results in loss of functionality of the mAb (reduced affinity) or the PS (alterations to the photophysical properties affecting PS efficiency) [342,542,545,546]. Based on the pioneering work of von Felbert and associates (2016) [345], this study extends the use of SNAP-tag technology in the generation of homogeneous and pharmaceutically acceptable IR700-based photoimmunoconjugates targeting CSPG4, CD44 and ASPH-positive TNBCs. With this site-specific conjugation method, BG-modified IR700 can be covalently attached to the antibody moiety by the irreversible coupling of an alkyl group to a cysteine residue [283], thereby generating photoimmunotheranostic agents with a defined DAR of 1, while ensuring uniform therapeutic and safety profiles [295,345].

Consistent with previous studies [295,340,345], a dose-dependent decrease in cell viability was observed (on antigen-abundant cell lines only) with increasing concentrations of the IR700-based photoimmunoconjugate (IC_{50} values ranging from 507-6070 nM (Table 11)). Upon binding of scFv-SNAP-IR700 with the target cell surface antigen, activation of IR700 with NIR light at 690 nm, increases water diffusion into the treated cells, resulting in an expansion of the cells to their maximal size, ultimately causing membrane damage and necrosis (Figure 48) [321,325]. Contrary to recombinant AURIF-based ADCs, IR700-mediated phototoxicity does not require intracellular delivery nor involves apoptosis [320,547]. While the generation of αCSPG4(scFv)-SNAP-IR700 has been described before [295], the results herein presented, report for the first time the development of a scFv-SNAP-based system, guiding the targeting of CD44 and ASPH-positive TNBCs with IR700. Intriguingly, Amoury *et al*. (2016) observed lower IC_{50} values (128-131 nM) for αCSPG4(scFv)-SNAP-IR700 on TNBC cells [295]. This difference in phototoxic activity can be ascribed to the variance in receptor status or the number of bound antibody conjugates, as well as the dose of NIR light [548]. For example, cetuximab (an anti-EGFR mAb)-IR700 demonstrated greater cell killing activity with higher EGFR expression *in vitro* [329]. Increased cytotoxic activities can thus be achieved by increasing the dosage of the photoimmunoconjugate (up to the saturating dose) or by increasing the dose of light (up to thermal limits) [548,549]. As such, PIT has the ability to treat larger tumors since a high dose of NuB2 (an anti-CD20 antibody)-IR700

improves the therapeutic effect, without significant toxicity to normal organs [549]. Nonetheless, optimized dosing of the antibody-photoconjugate and NIR light exposure will prove critical in the planning of successful clinical trials, while ensuring therapeutic safety and efficacy [329,548]. To this end, Nagaya and colleagues (2015) demonstrated prolonged survival in TNBC mouse models, upon splitting of the mAb-IR700 dose and using repeated light exposures [329]. Unlike ionizing radiation such as x-rays or gamma-rays, there should theoretically be no limitations on the cumulative irradiation dose of NIR light, implying that repeated PIT may be a possibility for the long-term management of cancer patients [320].

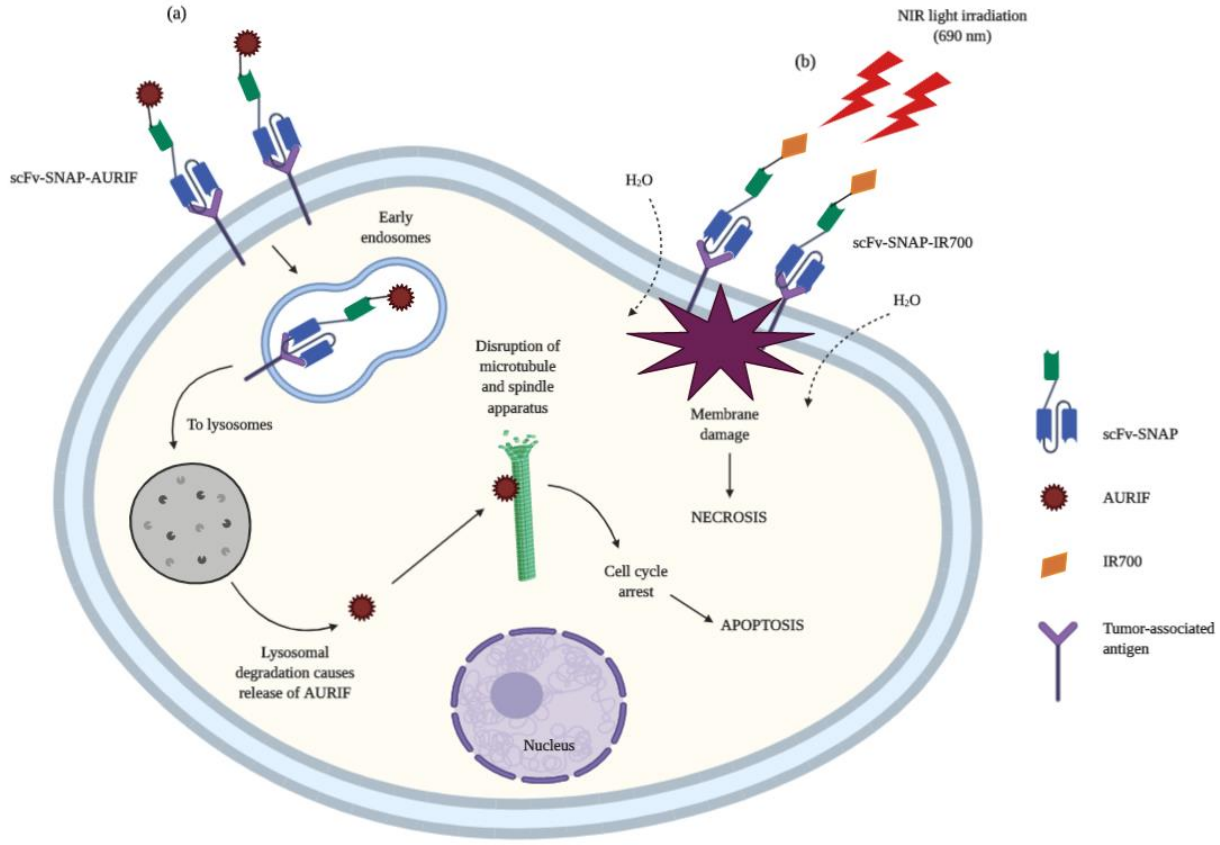

Figure 48: Diagrammatic representation of the cell killing mechanism of AURIF/IR700-containing recombinant SNAP-tag based fusion proteins. (a) After binding to its target antigen, scFv-SNAP-AURIF undergoes internalization and lysosomal degradation. This process induces the intracellular release of AURIF (via degradation of the protein component), which then binds to tubulin and prevents microtubule polymerization, culminating in cell cycle arrest and apoptotic cell death, and (b) Upon NIR light exposure (at 690 nm), conformational changes of the scFv-SNAP-IR700-antigen complex produce physical stress in the cell membrane. The resulting weakening of the latter causes water molecules from outside the cell to enter, leading to cell swelling, bursting and eventually cell death by necrosis.

Most cytotoxic compounds employed in ADCs are highly potent membrane permeable molecules, whose premature release into the bloodstream can be an important safety consideration in ADC design [550,551]. In line with previous reports, IR700, on the other hand, showed minimal or negligible toxicity when presented alone, even after illumination and is only active following receptor-antibody interactions [295,320,336,340,345,543]. Of note, IR700 was modified with a BG linker (BG-PEG_{24}-NH_2) using the NHS ester-amino group reaction (as described previously [552]), with no loss in phototoxic activity [295,340,345]. In principle, IR700 has been described as a theranostic agent of choice as compared to conventional PSs; (1) it lacks passive diffusion properties, (2) it shows great photostability while producing a strong fluorescent signal, (3) it displays a strong absorption peak close to 700 nm, thus allowing improved light penetration into tissues, and (4) it is water-soluble with no biotoxic properties, which ensures safety and easy excretion in urine [320,321,553]. Besides the specificity of the antibody moiety and the overriding advantages of IR700, a major feature of this approach, relates to the use of NIR radiation at 690 nm wavelength, which is non-ionizing and unlikely to be toxic to normal cells (as supported by Figure 40), except at thermal doses [320,321]. Given its ability to penetrate at least several centimeters into tissue [167], fibro-optical diffusers can be used to deliver radiation to otherwise inaccessible tumors [323,324]. Additionally, NIR light exhibits very low autofluorescence, which implies that it is much more likely to show considerable utility in fluorescence imaging [554]. For example, NIR fluorescence imaging using IR700, allowed efficient (*in vitro* and *in vivo*) detection of gastrointestinal stromal tumors in comparison to ultrasound or positron emission tomography (PET) [555]. Apart from detection and elimination, the fluorescence of IR700 can be used to monitor body distribution and tumor accumulation (especially during surgery), thereby providing an immediate assessment of treatment efficacy or guiding the optimum timing for photo-irradiation [334,556].

Another facet of NIR-PIT currently attracting particular attention is the activation of tumor immunity [557]. As exemplified by Sato and co-workers (2016), PIT using an anti-CD25-IR700 conjugate, caused the site-specific killing of regulatory T-cells (or T_{regs}) in the irradiated tumor bed while also inducing regression of distant non-treated tumors [558]. In fact, the rapid nature of the mode of cell death involved, coupled with cell rupture, causes the release of molecules

responsible in the maturation of dendritic cells, thereby activating a patient's innate immune system [321,559]. Interestingly, the induction of the host immune response appears to kill a high percentage of residual tumor cells after NIR-PIT, which means that complete tumor eradication could be achieved after 1-2 treatments [321]. Furthermore, while conventional cancer immunotherapy (such as T-cell activating type 1 cytokines (IL-2 and IL-15) and immune checkpoint inhibitors (anti-CTLA-4 and anti-PD-1/PD-L1 antibodies)) suffer from off-target effects due to their dependence on pre-existing CD8+ T-cells (found in tumor beds and other parts of the body), NIR-PIT locally enhances host immunity, without systemic side effects [321]. Similarly, yet another unique feature of this photoimmunotheranostic approach, concerns its immediate effect on blood drug delivery; most specifically, NIR-PIT has been associated with SUPR effect, which is characterized by increased vascular permeability [321,339,560]. This occurrence allows homogeneous redistribution of the remaining or subsequent antibody-IR700 photoconjugates, concurrently allowing delivery into the deep part of the tumor [339,549]. In order to harness the benefits of super enhanced uptake, several studies have combined NIR-PIT with nanosized anticancer agents (liposome-encapsulated daunorubicin [339] and nanoparticle albumin-bound paclitaxel [561]), the combination of which resulted in improved therapeutic effects as compared to each therapy alone [321]. Following this trend, the recent incorporation of ADCs with photoactivable drug release systems to NIR-PIT, has demonstrated promising activity in the treatment of EGFR-expressing breast tumors [562].

Holistically, the SNAP-tag based photoimmunotheranostics generated in this research, represent the combination of PDT, ADC and optical imaging strategies, all of which have been clinically approved individually [170,265,563]. With the ability to conjugate virtually any antibody to IR700, the application of NIR-PIT using scFv-SNAP, may constitute a highly flexible theranostic platform that could be applied to numerous target molecules across a broad range of tumors. Moreover, while most studies rely on the use of mAbs for NIR-PIT [320,334,336,543], using antibody fragments (as done in the current research) provides several prevailing advantages such as superior tissue penetration, simple introduction of site-specific conjugation sites, facile engineering of fusion proteins and rapid renal clearance [564,565]. However, although scFv-SNAP-IR700 has great potential for extensive application in oncology, it becomes increasingly

important to acknowledge that solid tumors (such as TNBCs) are composed of heterogeneous cell populations (possibly arising from CSCs [566]) that display varying expression levels of cell surface receptors, not only between individuals but also within the same patient [567]. Therefore, as set out in this study, it becomes an acute necessity to develop a compendium of scFv-SNAP-IR700 conjugates bearing specificity towards various tumor-associated antigens. With its ability to bypass the need for ROS, this phototheranostic stratagem simultaneously provides a leeway to selectively destroy CD44-positive CSCs (in primary and metastatic TNBC) that usually exhibit resistance towards ROS-dependent therapies such as PDT [334,568]. Of particular relevance for further research is the phenomenon of 'binding site barrier' (occurs when antibodies with strong binding affinities are used and/or tumor cells express high levels of the antigen) which is characterized by the accumulation of mAbs in the perivascular space instead of infiltration into the tumor bed, thereby posing hurdles to antibody-based therapies [557,569]. To this end, Nakajima and colleagues (2013) were able to solve this problem by applying a cocktail of 2 different mAb-IR700 conjugates that together fostered homogeneous intratumoral distribution, as well as enhanced therapeutic potential compared to each agent alone [570]. Similarly, Amoury *et al*. (2016) reported that using a combination of scFv-SNAP-IR700 conjugates targeting CSPG4, EpCAM and EGFR, resulted in an increase in therapeutic activity against TNBC cells by up to 40% [295]. Alternatively, several studies warrant the implementation of combined treatments consisting of IR700-driven NIR-PIT alongside chemotherapy or radiation therapy, which would increase the probability of tumor cell killing through the engagement of various mechanisms of cell death [333,343,549]. On the other hand, while the use of NIR-PIT with immune checkpoint inhibitors appears to be effective in animal models, data must be interpreted with caution since the risk of unwanted side-effects resulting from the latter is not completely avoided [571]. Furthermore, with the concept of NIR photochemoimmunotherapy gaining momentum (as described by Ito *et al*. (2017) through the generation of a photoactivable bifunctional ADC Trastuzumab-DM1-IR700 [572]), it can be speculated that next-generation scFv-SNAP conjugates will aim to combine NIR-PIT with the intracellular delivery of cytotoxic payloads. In summary, the results generated from this study, provides the basis for future studies aimed at evaluating the efficacy of these agents in preclinical *in vivo* models. This work also provides a blueprint for using SNAP-tag technology to engineer standardized recombinant photoimmunotheranostics, that could

facilitate TNBC patient pre-screening, real-time treatment monitoring, as well as quantifying treatment efficacy [295,346].

Chapter 5: Conclusion and Future Directions

The three major modes of cancer therapy – chemotherapy, surgery and radiation therapy – have remained the cornerstone of modern oncology treatment [320]. However, with the increase in reported side effects, researchers have begun to oppugn their true benefit in the management of cancer. By inducing substantial damage to normal cells, including immune cells, the cumulative effect amounts to an impediment to recovery by contributing to the overall debilitation of the patient [321]. Therefore, to palliate the undesirable effects of traditional therapy, molecular targeted cancer therapies such as armed antibody therapy have been devised, albeit with a limited success rate [320].

A similar phenomenon is observed in the context of TNBC, which represents one of the most lethal subtypes of breast cancer, also well-known for its limited treatment choices [547]. Given its varying morphology, gene expression and signaling pathway activity [54], TNBC often presents with complicated clinicopathological features which negatively impact patient prognosis [573]. The intratumoral and intertumoral heterogeneity of TNBCs, imply that the afflicted patients have a higher risk of disease relapse [44,574]. With endocrine and HER2-targeted therapies being deemed ineffective, cytotoxic chemotherapy is being increasingly advocated, often at the expense of the patient, resulting in collateral damage to healthy tissues, incidences of refractory drug-resistance and earlier metastasis [547,575,576]. Interestingly, further probing into the molecular complexities of this disease, revealed frequent dysregulation of EGFR, with approximately 60-80% of triple-negative breast tumors demonstrating its overexpression [577,578]. This awareness thus led to a randomized phase II clinical trial assessing the efficacy of cetuximab (an anti-EGFR mAb) in combination with carboplatin; nonetheless, responses were observed in fewer than 20% of TNBC patients, suggesting that alternate mechanisms were involved in sustaining survival despite impaired EGFR signaling [579]. In consequence, similar partial responses of targeted molecules encouraged the search for new therapeutic targets or agents aimed at TNBCs [574]. For example, poly (ADP-ribose) polymerase inhibitors [580,581] and angiogenesis inhibitors [93] are being actively investigated in clinical trials, but unfortunately, there continues to be an unmet need for effective precision medicine of this daunting disease [334].

Over the past few decades, progress in cancer genomics research has reinforced the notion that various genetic alterations are at play in promoting tumorigenesis [582]. The complexity, plasticity and resilience of cancer cells is further exacerbated by the presence of tumor subpopulations with stem-like characteristics, which significantly contribute to treatment resistance and disease recurrence [583,584]. Precision medicine takes into account these molecular and biological specificities for each patient (often including environmental and lifestyle factors), in order to classify individuals according to their susceptibility to a particular disease or depending on their response to a specified treatment [574,585,586]. As such, developing personalized therapies for TNBC necessitates a thorough understanding of the molecular basis of its oncogenic pathways and microenvironmental changes, including the effects of the immune system and relevant therapies on these pathways [587]. Therefore, individualized treatment and prognostic analysis for these patients can be a Herculean task, especially when there is a heavy reliance on conventional clinical and pathological features (histological grade, primary tumor size, ER/PR/HER2 expression, lymph node and metastasis status) [573]. In addition, several major scientific and logistical challenges are becoming more apparent; low frequency of targetable molecular alterations, feasibility and affordability of high-throughput technologies in the clinic, costs of companion treatment, as well as the lack of specific drugs to target alterations [588–590].

This study showcases novel human therapeutic fusion proteins with a high translational potential for the targeted diagnosis and elimination of TNBC, including its associated tumor-initiating cells. More explicitly, this research aimed to generate SNAP-tag based fusion proteins endowed with a high affinity towards CSPG4, CD44 and ASPH-expressing TNBC cells. The qualitative and quantitative analysis of the scFv-SNAP binding potential confirms not only differential expression of the cognate antigens on TNBC cell lines, but also demonstrates their relevance towards the establishment of a panel of surface markers to contain the heterogeneity of TNBC through the development of personalized immunotherapies. Undoubtedly, future studies with these fusion proteins should focus on optimization of protein expression and purification, while avoiding the formation of aggregates and degradation products, especially for long-term storage and potential *in vivo* application. By harnessing the favorable properties of SNAP-tag, this research also provides the proof of concept (and working methodologies) for the economical production of

homogeneous recombinant AURIF-based ADCs and IR700 photoimmunotheranostics, each bearing a defined DAR of 1. The functionality of these immunoconjugates was illustrated by their specific cytotoxic activities *in vitro*; IC_{50} values ranged from 100.4-1660 nM for scFv-SNAP-AURIF and from 507-6070 nM for scFv-SNAP-IR700. To better understand the implications of these results, further studies should assess their ability to induce apoptosis/necrosis, usually by setting up cell cycle analysis and apoptosis assays [313]. While the choice of fully human sequences for the scFv and SNAP-tag, reduces the risk of immune rejection, low toxicities (high IC_{50} values) can pose a hurdle *en route* to clinical studies evaluating their inherent safety, tolerability and biodistribution. Therefore, successive constructs should be designed in view of increasing the therapeutic efficacy, either by increasing DARs or by introducing mechanisms that can facilitate intracellular release of toxic payloads [312,313]. Finally, the targeting approach developed here, will be applicable not only to TNBC but can be extended to a wider range of cancers, where CSPG4, CD44 and ASPH represent significant targets.

On a broader scale, this research provides the foundation for the development of a catalogue of companion immunodiagnostic tools and their according therapeutics, thereby providing a much-needed incentive for a shift towards personalized medicine in the management of TNBC patients. For instance, *ex vivo* binding of SNAP-tag based fusion proteins to breast cancer biopsies (work of PhD student Natasha Hardcastle) could enable the identification and quantification of relevant triple-negative breast tumor markers (through multiplex immunofluorescence imaging), in order to recognize and classify patients according to their ability to benefit from a specific treatment plan (Figure 49). Due to the absence of stand-alone drugs in the battle against cancer, this process will simultaneously expedite the implementation of a multi-pronged approach involving the synergistic effect of the best treatment options aimed towards providing a curative benefit.

In conclusion, while much work remains to be done before precision medicine becomes the standard of care for TNBC patients, the results herein presented demonstrate the versatility of SNAP-tag technology in the generation of pharmaceutically acceptable diagnostic and therapeutic agents (bearing various cytotoxic warheads), which when combined together, could enable more effective management of this deadly disease.

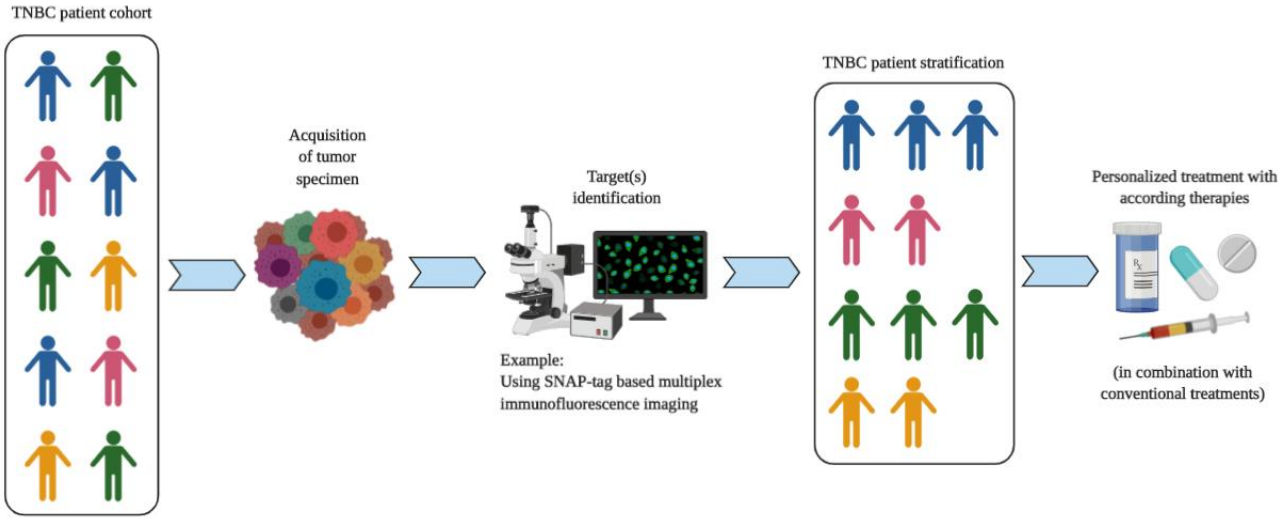

Figure 49: Pictorial representation of a tentative approach to precision medicine of TNBC. Through the establishment of multiplex immunofluorescence imaging based on a diverse collection of SNAP-tag based fusion proteins, the screening of TNBC patients for relevant tumorigenic target(s) will enable the identification and classification of patients, thus streamlining the development of tailored combination treatments for those who are most likely to demonstrate a positive drug response or benefit.

References

1. Sudhakar A. History of Cancer, Ancient and Modern Treatment Methods. J Cancer Sci Ther. 2009; 01: i–iv. doi: 10.4172/1948-5956.100000e2.
2. Siegel RL, Miller KD, Jemal A. Cancer statistics, 2020. CA Cancer J Clin [Internet]. 2020; 0: 1–24. doi: 10.3322/caac.21590.
3. Ginsburg OM. Breast and cervical cancer control in low and middle-income countries: Human rights meet sound health policy. J Cancer Policy [Internet]. Elsevier Ltd.; 2013; 1: e35–41. doi: 10.1016/j.jcpo.2013.07.002.
4. Weigelt B, Reis-Filho JS. Histological and molecular types of breast cancer: Is there a unifying taxonomy? Nat Rev Clin Oncol [Internet]. Nature Publishing Group; 2009; 6: 718–30. doi: 10.1038/nrclinonc.2009.166.
5. Javed A, Lteif A. Development of the human breast. Semin Plast Surg. 2013; 27: 5–12. doi: 10.1055/s-0033-1343989.
6. Li CI, Uribe DJ, Daling JR. Clinical characteristics of different histologic types of breast cancer. Br J Cancer. 2005; 93: 1046–52. doi: 10.1038/sj.bjc.6602787.
7. Klausner RD. The fabric of cancer cell biology—Weaving together the strands. Cancer Cell. 2002; 1: 3–10. doi: 10.1016/S1535-6108(02)00020-X.
8. Trichopoulos D, Li FP, Hunter DJ. What Causes Cancer? Sci Am [Internet]. Scientific American, a division of Nature America, Inc.; 1996; 275: 80–7. Available from http://www.jstor.org.ezproxy.uct.ac.za/stable/24993351
9. Hanahan D, Weinberg RA. The hallmarks of cancer. Cell [Internet]. 2000; 100: 57–70. doi: 10.1007/s00262-010-0968-0.
10. Mcpherson K, Steel CM, Dixon JM. ABC of breast diseases: Breast cancer - epidemiology, risk factors, and genetics. Bmj. 2000; 321: 1198. doi: 10.1136/bmj.321.7261.624.
11. Helmrich S, Shapiro S, Rosenberg L, Kaufman D, Slone D, Bain C. Risk factors for breast cancer. Am J Epidemiol. 1983; 117: 35–45.
12. Pike MC, Henderson BE, Casagrande JT, Rosario I, Gray GE. Oral contraceptive use and early abortion as risk factors for breast cancer in young women. Br J Cancer. 1981; 43: 72–6. doi: 10.1038/bjc.1981.10.
13. Yang X, Lippman ME. BRCA1 and BRCA2 in breast cancer. Breast Cancer Res Treat. 1999; 54: 1–10. doi: 10.1023/A:1006189906896.
14. Lynch H, Albano W, Danes S, Layton M. Genetic predisposition to breast cancer. Cancer. 1984; 53: 612–22. doi: 10.1016/s0960-9776(97)90052-7.
15. Rebbeck TR, Couch FJ, Kant J, Calzone K, Deshano M, Peng Y, Chen K, Garber JE, Weber BL. Genetic heterogeneity in hereditary breast cancer: Role of BRCA1 and BRCA2. Am J Hum Genet. 1996; 59: 547–53.
16. Martin A-M. Genetic and Hormonal Risk Factors in Breast Cancer. J Natl Cancer Inst. 2000;

92: 1126–35. doi: 10.1093/jnci/92.14.1126.

17. Lee W, Boyer TG. BRCA1 and BRCA2 in breast cancer. Lancet. 2001; : 358.

18. Smith SA, Easton DF, Evans DGR, Ponder BAJ. Allele losses in the region 17q12–21 in familial breast and ovarian cancer involve the wild–type chromosome. Nat Genet. 1992; 2: 128–31. doi: 10.1038/ng1092-128.

19. Gowen L, Avrutskaya A, Latour A, Koller B. BRCA1 required for transcription-coupled repair of oxidative DNA damage. Science (80-). 1998; 281: 1–4. doi: 10.7551/mitpress/8876.003.0036.

20. Valentin MD, Da Silva SD, Privat M, Alaoui-Jamali M, Bignon YJ. Molecular insights on basal-like breast cancer. Breast Cancer Res Treat. 2012; 134: 21–30. doi: 10.1007/s10549-011-1934-z.

21. Wu P, Gao Y, Zhang H, Cai C. Aptamer-guided silver-gold bimetallic nanostructures with highly active surface-enhanced Raman scattering for specific detection and near-infrared photothermal therapy of human breast cancer cells. Anal Chem. 2012; 84: 7692–9. doi: 10.1021/ac3015164.

22. Henry L. The diagnosis of breast cancer. A cancer J Clin. 1977; 27: 364. doi: 10.5694/j.1326-5377.1990.tb136967.x.

23. Viale G. The current state of breast cancer classification. Ann Oncol. 2012; 23. doi: 10.1093/annonc/mds326.

24. Nattkemper TW, Arnrich B, Lichte O, Timm W, Degenhard A, Pointon L, Hayes C, Leach MO. Evaluation of radiological features for breast tumour classification in clinical screening with machine learning methods. Artif Intell Med. 2005; 34: 129–39. doi: 10.1016/j.artmed.2004.09.001.

25. Parkin DM, Fernández LMG. Use of statistics to assess the global burden of breast cancer. Breast J. 2006; 12: 70–80. doi: 10.1111/j.1075-122X.2006.00205.x.

26. Ma L, Fishell E, Wright B, Hanna W, Allan S, Boyd NF. Case-control study of factors associated with failure to detect breast cancer by mammography. J Natl Cancer Inst. 1992; 84: 781–5. doi: 10.1093/jnci/84.10.781.

27. Mandelson M, Oestreicher N, Porter P, White D. Breast density as a predictor of Mammographic Detection: Comparison of Interval- and Screen-Detected Cancers. J Nat. 2000; 192: 1081–7. doi: 10.1186/bcr2654.

28. Roubidoux MA, Bailey JE, Wray LA, Helvie MA. Invasive Cancers Detected after Breast Cancer Screening Yielded a Negative Result: Relationship of Mammographic Density to Tumor Prognostic Factors. Radiology. 2004; 230: 42–8. doi: 10.1148/radiol.2301020589.

29. Singletary SE, Greene FL. Revision of breast cancer staging: The 6th edition of the TNM Classification. Semin Surg Oncol. 2003; 21: 53–9. doi: 10.1002/ssu.10021.

30. Wilkinson NW, Shahryarinejad A, Winston JS, Watroba N, Edge SB. Concordance with breast cancer pathology reporting practice guidelines. J Am Coll Surg. 2003; 196: 38–43.

doi: 10.1016/S1072-7515(02)01627-7.

31. Van't Veer LJ, Dai H, Van de Vijver MJ, He YD, Hart AAM, Mao M, Peterse HL, Van Der Kooy K, Marton MJ, Witteveen AT, Schreiber GJ, Kerkhoven RM, Roberts C, et al. Gene expression profiling predicts clinical outcome of breast cancer. Nature. 2002; 415: 530–6. doi: 10.1038/415530a.

32. Eroles P, Bosch A, Alejandro Pérez-Fidalgo J, Lluch A. Molecular biology in breast cancer: Intrinsic subtypes and signaling pathways. Cancer Treat Rev [Internet]. Elsevier Ltd; 2012; 38: 698–707. doi: 10.1016/j.ctrv.2011.11.005.

33. Cheang MCU, Martin M, Nielsen TO, Prat A, Voduc D, Rodriguez-Lescure A, Ruiz A, Chia S, Shepherd L, Ruiz-Borrego M, Calvo L, Alba E, Carrasco E, et al. Defining Breast Cancer Intrinsic Subtypes by Quantitative Receptor Expression. Oncologist. 2015; 20: 474–82. doi: 10.1634/theoncologist.2014-0372.

34. Anderson WF, Rosenberg PS, Katki HA. Tracking and evaluating molecular tumor markers with cancer registry data: HER2 and breast cancer. J Natl Cancer Inst. 2014; 106: 12–4. doi: 10.1093/jnci/dju093.

35. Kennecke H, Yerushalmi R, Woods R, Cheang MCU, Voduc D, Speers CH, Nielsen TO, Gelmon K. Metastatic behavior of breast cancer subtypes. J Clin Oncol. 2010; 28: 3271–7. doi: 10.1200/JCO.2009.25.9820.

36. Engel RH, Kaklamani VG. HER2-positive breast cancer: Current and future treatment strategies. Drugs. 2007; 67: 1329–41. doi: 10.2165/00003495-200767090-00006.

37. Slamon DJ, Clark GM, Wong SG, Levin WJ, Ullrich A, Mcguire WL. Human breast cancer: Correlation of relapse and survival with amplification of the HER-2/neu oncogene. Science (80-). 1987; 235: 177–82.

38. Piccart-Gebhart M, Procter M, Leyland-Jones B, Goldhirsch A. Trastuzumab after Adjuvant Chemotherapy in HER2-Positive Breast Cancer. N Engl J Med [Internet]. 2005; 353: 1659–72. Available from http://heinonlinebackup.com/hol-cgi-bin/get_pdf.cgi?handle=hein.journals/nejccc4&section=6

39. Rakha EA, Reis-Filho JS, Ellis IO. Basal-like breast cancer: A critical review. J Clin Oncol. 2008; 26: 2568–81. doi: 10.1200/JCO.2007.13.1748.

40. Anders CK, Carey LA. Biology, metastatic patterns, and treatment of patients with triple-negative breast cancer. Clin Breast Cancer [Internet]. Elsevier Ltd.; 2009; 9: S73–81. doi: 10.3816/CBC.2009.s.008.

41. Brewster AM, Chavez-MacGregor M, Brown P. Epidemiology, biology, and treatment of triple-negative breast cancer in women of African ancestry. Lancet Oncol. Elsevier Ltd; 2014; 15: e625–34. doi: 10.1016/S1470-2045(14)70364-X.

42. Ovcaricek T, Frkovic SG, Matos E, Mozina B, Borstnar S. Triple negative breast cancer - Prognostic factors and survival. Radiol Oncol. 2011; 45: 46–52. doi: 10.2478/v10019-010-0054-4.

43. Carey LA, Perou CM, Livasy CA, Dressler LG, Cowan D, Conway K, Karaca G, Troester

MA, Chiu KT, Edmiston S, Deming SL, Geradts J, Cheang MCU, et al. Race, breast cancer subtypes, and survival in the Carolina Breast Cancer Study. J Am Med Assoc. 2006; 295: 2492–502. doi: 10.1001/jama.295.21.2492.

44. Bauer KR, Brown M, Cress RD, Parise CA, Caggiano V. Descriptive analysis of estrogen receptor (ER)-negative, progesterone receptor (PR)-negative, and HER2-negative invasive breast cancer, the so-called triple-negative phenotype: A population-based study from the California Cancer Registry. Cancer. 2007; 109: 1721–8. doi: 10.1002/cncr.22618.

45. Morris GJ, Naidu S, Topham AK, Guiles F, Xu Y, McCue P, Schwartz GF, Park PK, Rosenberg AL, Brill K, Mitchell EP. Differences in breast carcinoma characteristics in newly diagnosed African-American and Caucasian patients: A single-institution compilation compared with the national cancer institute's surveillance, epidemiology, and end results database. Cancer. 2007; 110: 876–84. doi: 10.1002/cncr.22836.

46. Cleator S, Heller W, Coombes RC. Triple-negative breast cancer: therapeutic options. Lancet Oncol. 2007; 8: 235–44. doi: 10.1016/S1470-2045(07)70074-8.

47. Millikan RC, Newman B, Tse C, Moorman PG, Smith L V, Labbok MH, Geradts J, Jeannette T, Jackson S, Nyante S, Livasy C, Carey L, Shelton H, et al. Epidemiology of basal-like breast cancer. Breast Cancer Res Treat. 2008; 109: 123–39.

48. Oakman C, Viale G, Di Leo A. Management of triple negative breast cancer. Breast [Internet]. Elsevier Ltd; 2010; 19: 312–21. doi: 10.1016/j.breast.2010.03.026.

49. Podo F, Buydens LMC, Degani H, Hilhorst R, Klipp E, Gribbestad IS, Van Huffel S, W.M. van Laarhoven H, Luts J, Monleon D, Postma GJ, Schneiderhan-Marra N, Santoro F, et al. Triple-negative breast cancer: Present challenges and new perspectives. Mol Oncol. 2010; 4: 209–29. doi: 10.1016/j.molonc.2010.04.006.

50. Wiggans RG, Woolley P V., Smythe T, Hoth D, Macdonald JS, Green L, Schein PS. Phase-II trial of tamoxifen in advanced breast cancer. Cancer Chemother Pharmacol. 1979; 3: 45–8. doi: 10.1007/BF00254419.

51. Carey LA, Dees EC, Sawyer L, Gatti L, Moore DT, Collichio F, Ollila DW, Sartor CI, Graham ML, Perou CM. The triple negative paradox: Primary tumor chemosensitivity of breast cancer subtypes. Clin Cancer Res. 2007; 13: 2329–34. doi: 10.1158/1078-0432.CCR-06-1109.

52. Liedtke C, Mazouni C, Hess KR, André F, Tordai A, Mejia JA, Symmans WF, Gonzalez-Angulo AM, Hennessy B, Green M, Cristofanilli M, Hortobagyi GN, Pusztai L. Response to neoadjuvant therapy and long-term survival in patients with triple-negative breast cancer. J Clin Oncol. 2008; 26: 1275–81. doi: 10.1200/JCO.2007.14.4147.

53. Guarneri V, Broglio K, Kau SW, Cristofanilli M, Buzdar AU, Valero V, Buchholz T, Meric F, Middleton L, Hortobagyi GN, Gonzalez-Angulo AM. Prognostic value of pathologic complete response after primary chemotherapy in relation to hormone receptor status and other factors. J Clin Oncol. 2006; 24: 1037–44. doi: 10.1200/JCO.2005.02.6914.

54. Lehmann B, Bauer J, Chen X, Sanders M. Identification of human triple-negative breast cancer subtypes and preclinical models for selection of targeted therapies. J Clin Invest.

2011; 121: 1–18. doi: 10.1172/JCI45014DS1.

55. Santana-Davila R, Perez EA. Treatment options for patients with triple-negative breast cancer. J Hematol Oncol. 2010; 3: 1–11. doi: 10.1186/1756-8722-3-42.

56. Nielsen TO, Hsu FD, Jensen K, Cheang M, Karaca G, Hu Z, Hernandez-Boussard T, Livasy C, Cowan D, Dressler L, Akslen LA, Ragaz J, Gown AM, et al. Immunohistochemical and clinical characterization of the basal-like subtype of invasive breast carcinoma. Clin Cancer Res. 2004; 10: 5367–74. doi: 10.1158/1078-0432.CCR-04-0220.

57. Bertucci F, Finetti P, Cervera N, Esterni B, Hermitte F, Viens P, Birnbaum D. How basal are triple-negative breast cancers? Int J Cancer. 2008; 123: 236–40. doi: 10.1002/ijc.23518.

58. Kreike B, van Kouwenhove M, Horlings H, Weigelt B, Peterse H, Bartelink H, van de Vijver MJ. Gene expression profiling and histopathological characterization of triple-negative/basal-like breast carcinomas. Breast Cancer Res. 2007; 9: 1–14. doi: 10.1186/bcr1771.

59. Rakha EA, El-Sayed ME, Green AR, Lee AHS, Robertson JF, Ellis IO. Prognostic markers in triple-negative breast cancer. Cancer. 2007; 109: 25–32. doi: 10.1002/cncr.22381.

60. Dawson SJ, Provenzano E, Caldas C. Triple negative breast cancers: Clinical and prognostic implications. Eur J Cancer [Internet]. Elsevier Ltd; 2009; 45: 27–40. doi: 10.1016/S0959-8049(09)70013-9.

61. Chakravarthy AB, Kelley MC, McLaren B, Truica CI, Billheimer D, Mayer IA, Grau AM, Johnson DH, Simpson JF, Beauchamp RD, Jones C, Pietenpol JA. Neoadjuvant concurrent paclitaxel and radiation in stage II/III breast cancer. Clin Cancer Res. 2006; 12: 1570–6. doi: 10.1158/1078-0432.CCR-05-2304.

62. Bauer JA, Chakravarthy AB, Rosenbluth JM, Mi D, Erin H, Granja-ingram NDM, Olivares MG, Kelley MC, Ingrid A, Meszoely IM, Means-powell JA, Johnson KN, Tsai J, et al. Identification of markers of taxane sensitivity using proteomic and genomic analyses of breast tumors from patients receiving neoadjuvant paclitaxel and radiation. Clin Cancer Res. 2011; 16: 681–90. doi: 10.1158/1078-0432.CCR-09-1091.Identification.

63. Dent R, Trudeau M, Pritchard KI, Hanna WM, Kahn HK, Sawka CA, Lickley LA, Rawlinson E, Sun P, Narod SA. Triple-negative breast cancer: Clinical features and patterns of recurrence. Clin Cancer Res. 2007; 13: 4429–34. doi: 10.1158/1078-0432.CCR-06-3045.

64. Collett K, Stefansson I, Eide J, Braaten A, Wang H. A basal epithelial phenotype is more frequent in interval breast cancers compared with screen detected tumors. Breast Dis. 2005; 14: 1108–12. doi: 10.1016/S1043-321X(05)80267-X.

65. Twelves C, Jove M, Gombos A, Awada A. Cytotoxic chemotherapy: Still the mainstay of clinical practice for all subtypes metastatic breast cancer. Crit Rev Oncol Hematol [Internet]. Elsevier Ireland Ltd; 2016; 100: 74–87. doi: 10.1016/j.critrevonc.2016.01.021.

66. Kassam F, Enright K, Dent R, Dranitsaris G, Myers J, Flynn C, Fralick M, Kumar R, Clemons M. Survival outcomes for patients with metastatic triple-negative breast cancer: Implications for clinical practice and trial design. Clin Breast Cancer [Internet]. Elsevier

Inc.; 2009; 9: 29–33. doi: 10.3816/CBC.2009.n.005.

67. Brosnan EM, Anders CK. Understanding patterns of brain metastasis in breast cancer and designing rational therapeutic strategies. Ann Transl Med. 2018; 6: 163–163. doi: 10.21037/atm.2018.04.35.

68. Lin N, Claus E, Sohl J, Razzak A, Arnaout A. Sites of Distant Relapse and Clinical Outcomes in Patients with Metastatic Triple-Negative Breast Cancer: High Incidence of Central Nervous System Metastases. Cancer. 2008; 113: 2638–45. doi: 10.1038/jid.2014.371.

69. Turner N, Moretti E, Siclari O, Migliaccio I, Santarpia L, D'Incalci M, Piccolo S, Veronesi A, Zambelli A, Del Sal G, Di Leo A. Targeting triple negative breast cancer: Is p53 the answer? Cancer Treat Rev [Internet]. Elsevier Ltd; 2013; 39: 541–50. doi: 10.1016/j.ctrv.2012.12.001.

70. Costa R, Shah AN, Santa-Maria CA, Cruz MR, Mahalingam D, Carneiro BA, Chae YK, Cristofanilli M, Gradishar WJ, Giles FJ. Targeting Epidermal Growth Factor Receptor in triple negative breast cancer: New discoveries and practical insights for drug development. Cancer Treat Rev [Internet]. Elsevier Ltd; 2017; 53: 111–9. doi: 10.1016/j.ctrv.2016.12.010.

71. Amoury M, Mladenov R, Nachreiner T, Pham AT, Hristodorov D, Di Fiore S, Helfrich W, Pardo A, Fey G, Schwenkert M, Thepen T, Kiessling F, Hussain AF, et al. A novel approach for targeted elimination of CSPG4-positive triple-negative breast cancer cells using a MAP tau-based fusion protein. Int J Cancer. 2016; 139: 916–27. doi: 10.1002/ijc.30119.

72. Amoury M, Kolberg K, Pham AT, Hristodorov D, Mladenov R, Di Fiore S, Helfrich W, Kiessling F, Fischer R, Pardo A, Thepen T, Hussain AF, Nachreiner T, et al. Granzyme B-based cytolytic fusion protein targeting EpCAM specifically kills triple negative breast cancer cells in vitro and inhibits tumor growth in a subcutaneous mouse tumor model. Cancer Lett. Elsevier Ireland Ltd; 2016; 372: 201–9. doi: 10.1016/j.canlet.2016.01.027.

73. Huang CY, Ju DT, Chang CF, Muralidhar Reddy P, Velmurugan BK. A review on the effects of current chemotherapy drugs and natural agents in treating non-small cell lung cancer. Biomed. 2017; 7: 12–23. doi: 10.1051/bmdcn/2017070423.

74. Waks AG, Winer EP. Breast Cancer Treatment: A Review. JAMA - J Am Med Assoc. 2019; 321: 288–300. doi: 10.1001/jama.2018.19323.

75. Charfare H, Limongelli S, Purushotham AD. Neoadjuvant chemotherapy in breast cancer. Br J Surg. 2005; 92: 14–23. doi: 10.1002/bjs.4840.

76. Von Essen CF, Joseph LBM, Simon GT, Singh SP, Singh AD. Sequential chemotherapy and radiation therapy of buccal mucosa carcinoma in South India: methods and preliminary results. Am J Roentgenol Radium Ther Nucl Med. 1968; 102: 530–40.

77. Banadonna G. Evolving concepts in the systemic adjuvant treatment of breast cancer. Perspect Cancer Res. 1992; 52: 2127–37.

78. Veronesi U, Banfi A, Salvadori B, Luini A, Saccozzi R, Zucali R, Marubini E, Del Vecchio

M, Boracchi P, Marchini S, Merson M, Sacchini V, Riboldi G, et al. Breast conservation is the treatment of choice in small breast cancer: Long-term results of a randomized trial. Eur J Cancer Clin Oncol. 1990; 26: 668–70. doi: 10.1016/0277-5379(90)90113-8.

79. Fisher B, Bauer M, Margolese R, Poisson R. Five-year results of a randomized clinical trial comparing total mastectomy and segmental mastectomy with or without radiation in the treatment of breast cancer. N Engl J Med. 1985; 312: 653–7.

80. Fisher B, Redmond C, Poisson R, Margolese R. Eight-year results of a randomized clinical trial comparing total mastectomy and lumpectomy with or without irradiation in the treatment of breast cancer. N Engl J Med. 1989; 320: 822–8. doi: 10.1056/nejm198811243192103.

81. Bonadonna G, Brusamolino E, Valagussa P, Rossi A. Combination chemotherapy as an adjuvant treatment in operable breast cancer. N Engl J Med. 1976; 294: 405–10.

82. Henderson I, Mouridsen H, Abe O, Abeloff M. Effects of Adjuvant Tamoxifen and of Cytotoxic Therapy on Mortality in Early Breast Cancer. N Engl J Med. 1988; 319: 1681–92. doi: 10.1056/NEJM198812293192601.

83. Hassan MS., Ansari J, Spooner D, Hussain S. Chemotherapy for breast cancer. Oncol Rep. 2010; 24: 1121–31. doi: 10.3892/or.

84. Asselain B, Barlow W, Bartlett J, Bergh J, Bergsten-Nordström E, Bliss J, Boccardo F, Boddington C, Bogaerts J, Bonadonna G, Bradley R, Brain E, Braybrooke J, et al. Long-term outcomes for neoadjuvant versus adjuvant chemotherapy in early breast cancer: meta-analysis of individual patient data from ten randomised trials. Lancet Oncol. 2018; 19: 27–39. doi: 10.1016/S1470-2045(17)30777-5.

85. Valachis A, Mauri D, Polyzos NP, Chlouverakis G, Mavroudis D, Georgoulias V. Trastuzumab combined to neoadjuvant chemotherapy in patients with HER2-positive breast cancer: A systematic review and meta-analysis. Breast [Internet]. Elsevier Ltd; 2011; 20: 485–90. doi: 10.1016/j.breast.2011.06.009.

86. Chen Y, Shi XE, Tian JH, Yang XJ, Wang YF, Yang KH. Survival benefit of neoadjuvant chemotherapy for resectable breast cancer. Med (United States). 2018; 97. doi: 10.1097/MD.0000000000010634.

87. Mauri D, Pavlidis N, Ioannidis JPA. Neoadjuvant versus adjuvant systemic treatment in breast cancer: A meta-analysis. J Natl Cancer Inst. 2005; 97: 188–94. doi: 10.1093/jnci/dji021.

88. Pomponio MK, Burkbauer L, Goldbach M, Nazarian SM, Xie F, Clark AS, Matro JM, Fox KR, Shulman LN, Keele LJ, Tchou J. Refining the indications for neoadjuvant chemotherapy for patients with HER2+ breast cancer: A single institution experience. J Surg Oncol. 2019; 121: 447–55. doi: 10.1002/jso.25814.

89. Carter S. Single and combination nonhormonal chemotherapy in breast cancer. Cancer. 1972; 30: 1543–54.

90. Hortobagyi G. Development in Chemotherapy of Breast Cancer. Cancer. 2000; 88: 3073–

8. doi: 10.1093/annonc/10.suppl_6.S139.

91. Harbeck N, Gnant M. Breast cancer. Lancet [Internet]. Elsevier Ltd; 2017; 389: 1134–50. doi: 10.1016/S0140-6736(16)31891-8.

92. Ando M, Yamauchi H, Aogi K, Shimizu S, Iwata H, Masuda N, Yamamoto N, Inoue K, Ohono S, Kuroi K, Hamano T, Sukigara T, Fujiwara Y. Randomized phase II study of weekly paclitaxel with and without carboplatin followed by cyclophosphamide/epirubicin/5-fluorouracil as neoadjuvant chemotherapy for stage II/IIIA breast cancer without HER2 overexpression. Breast Cancer Res Treat. 2014; 145: 401–9. doi: 10.1007/s10549-014-2947-1.

93. Sikov WM, Berry DA, Perou CM, Singh B, Cirrincione CT, Tolaney SM, Kuzma CS, Pluard TJ, Somlo G, Port ER, Golshan M, Bellon JR, Collyar D, et al. Impact of the addition of carboplatin and/or bevacizumab to neoadjuvant once-per-week paclitaxel followed by dose-dense doxorubicin and cyclophosphamide on pathologic complete response rates in stage II to III triple-negative breast cancer: CALGB 40603 (A. J Clin Oncol. 2015; 33: 13–21. doi: 10.1200/JCO.2014.57.0572.

94. Abe O, Abe R, Enomoto K, Kikuchi K, Koyama H, Masuda H, Nomura Y, Sakai K, Sugimachi K, Tominaga T, Uchino J, Yoshida M, Haybittle JL, et al. Effects of chemotherapy and hormonal therapy for early breast cancer on recurrence and 15-year survival: An overview of the randomised trials. Lancet. 2005; 365: 1687–717. doi: 10.1016/S0140-6736(05)66544-0.

95. Harlan LC, Clegg LX, Abrams J, Stevens JL, Ballard-Barbash R. Community-based use of chemotherapy and hormonal therapy for early-stage breast cancer: 1987-2000. J Clin Oncol. 2006; 24: 872–7. doi: 10.1200/JCO.2005.03.5840.

96. Giordano SH, Lin Y, Kuo YF, Hortobagyi GN, Goodwin JS. Decline in the Use of Anthracyclines for Breast Cancer. J Clin Oncol. 2012; 30: 2232–9. doi: 10.1200/JCO.2011.40.1273.

97. Pinder MC, Duan Z, Goodwin JS, Hortobagyi GN, Giordano SH. Congestive heart failure in older women treated with adjuvant anthracycline chemotherapy for breast cancer. J Clin Oncol. 2007; 25: 3808–15. doi: 10.1200/JCO.2006.10.4976.

98. Piccart-Gebhart MJ, Burzykowski T, Buyse M, Sledge G, Carmichael J, Lück HJ, Mackey JR, Nabholtz JM, Paridaens R, Biganzoli L, Jassem J, Bontenbal M, Bonneterre J, et al. Taxanes alone or in combination with anthracyclines as first-line therapy of patients with metastatic breast cancer. J Clin Oncol. 2008; 26: 1980–6. doi: 10.1200/JCO.2007.10.8399.

99. Holmes FA, Walters RS, Theriault RL, Forman AD, Newton LK, Raber MN, Buzdar AU, Frye DK, Hortobagyi GN. Phase II trial of taxol, an active drug in the treatment of metastatic breast cancer. J Natl Cancer Inst. United States; 1991; 83: 1797–805. doi: 10.1093/jnci/83.24.1797-a.

100. Mechetner E, Kyshtoobayeva A, Zonis S, Kim H, Stroup R, Garcia R, Parker RJ, Fruehauf JP. Levels of multidrug resistance (MDR1) P-glycoprotein expression by human breast cancer correlate with in vitro resistance to taxol and doxorubicin. Clin Cancer Res. United

States; 1998; 4: 389–98.

101. Lakhtakia R. A brief history of breast cancer: Part I: Surgical domination reinvented. Sultan Qaboos Univ Med J. 2014; 14: 166–9.

102. Wyld L, Audisio RA, Poston GJ. The evolution of cancer surgery and future perspectives. Nat Rev Clin Oncol [Internet]. Nature Publishing Group; 2015; 12: 115–24. doi: 10.1038/nrclinonc.2014.191.

103. Karellas A, Vedantham S. Breast cancer imaging: A perspective for the next decade. Med Phys. 2008; 35: 4878–97. doi: 10.1118/1.2986144.

104. Zhang C, Hu G, Biskup E, Qiu X, Zhang H, Zhang H. Depression Induced by Total Mastectomy, Breast Conserving Surgery and Breast Reconstruction: A Systematic Review and Meta-analysis. World J Surg [Internet]. Springer International Publishing; 2018; 42: 2076–85. doi: 10.1007/s00268-018-4477-1.

105. Yiimazer N, Aydincr A, Ozkau S, Aslay I, Blige N. A comparison of body image, self-esteem and social support in total mastectomy and breast-conserving therapy in Turkish women. Support Care Cancer. 1994; 2: 238–41. doi: 10.1007/BF00365728.

106. Devoogdt N, Van Kampen M, Christiaens MR, Troosters T, Piot W, Beets N, Nys S, Gosselink R. Short- and long-term recovery of upper limb function after axillary lymph node dissection. Eur J Cancer Care (Engl). 2011; 20: 77–86. doi: 10.1111/j.1365-2354.2009.01141.x.

107. Hayes SC, Johansson K, Stout NL, Prosnitz R, Armer JM, Gabram S, Schmitz KH. Upper-body morbidity after breast cancer: Incidence and evidence for evaluation, prevention, and management within a prospective surveillance model of care. Cancer. 2012; 118: 2237–49. doi: 10.1002/cncr.27467.

108. Bellavance EC, Kesmodel SB. Decision-making in the surgical treatment of breast cancer: Factors influencing women's choices for mastectomy and breast conserving surgery. Front Oncol. 2016; 6: 1–7. doi: 10.3389/fonc.2016.00074.

109. Tesson S, Richards I, Porter D, Phillips KA, Rankin N, Musiello T, Marven M, Butow P. Women's preferences for contralateral prophylactic mastectomy: An investigation using protection motivation theory. Patient Educ Couns [Internet]. Elsevier Ireland Ltd; 2016; 99: 814–22. doi: 10.1016/j.pec.2015.11.012.

110. Gu J, Groot G, Holtslander L, Engler-Stringer R. Understanding women's choice of mastectomy versus breast conserving therapy in early-stage breast cancer. Clin Med Insights Oncol. 2017; 11. doi: 10.1177/1179554917691266.

111. Chagpar AB, Studts JL, Scoggins CR, Martin RCG, Carlson DJ, Laidley AL, El-Eid SE, McGlothin TQ, Noyes RD, McMasters KM. Factors associated with surgical options for breast carcinoma. Cancer. 2006; 106: 1462–6. doi: 10.1002/cncr.21728.

112. Bride MB Mac, Neal L, Dilaveri CA, Sandhu NP, Hieken TJ, Ghosh K, Wahner-Roedler DL. Factors associated with surgical decision making in women with early-stage breast cancer: A literature review. J Women's Heal. 2013; 22: 236–42. doi:

10.1089/jwh.2012.3969.

113. Pesce CE, Liederbach E, Czechura T, Winchester DJ, Yao K. Changing surgical trends in young patients with early stage breast cancer, 2003 to 2010: A report from the national cancer data base. J Am Coll Surg [Internet]. Elsevier Ltd; 2014; 219: 19–28. doi: 10.1016/j.jamcollsurg.2014.03.043.

114. Seneviratne S, Scott N, Lawrenson R, Campbell I. Ethnic, socio-demographic and socio-economic differences in surgical treatment of breast cancer in New Zealand. ANZ J Surg. 2017; 87: E32–9. doi: 10.1111/ans.13011.

115. Zhou J, Enewold L, Zahm SH, Jatoi I, Shriver C, Anderson WF, Jeffery DD, Andaya A, Potter JF, McGlynn KA, Zhu K. Breast conserving surgery versus mastectomy: The influence of comorbidities on choice of surgical operation in the department of defense health care system. Am J Surg. 2013; 206: 393–9. doi: 10.1016/j.amjsurg.2013.01.034.

116. Ahn SH, Park BW, Noh DY, Nam SJ, Lee ES, Lee MK, Kim SH, Lee KM, Park SM, Yun YH. Health-related quality of life in disease-free survivors of breast cancer with the general population. Ann Oncol [Internet]. Elsevier Masson SAS; 2007; 18: 173–82. doi: 10.1093/annonc/mdl333.

117. Stavrou D, Weissman O, Polyniki A, Papageorgiou N, Haik J, Farber N, Winkler E. Quality of life after breast cancer surgery with or without reconstruction. Eplasty [Internet]. 2009; 9: e18. Available from http://www.ncbi.nlm.nih.gov/pubmed/19572009%0Ahttp://www.pubmedcentral.nih.gov/articlerender.fcgi?artid=PMC2691644

118. Fanakidou I, Zyga S, Alikari V, Tsironi M, Stathoulis J, Theofilou P. Mental health, loneliness, and illness perception outcomes in quality of life among young breast cancer patients after mastectomy: the role of breast reconstruction. Qual Life Res [Internet]. Springer International Publishing; 2018; 27: 539–43. doi: 10.1007/s11136-017-1735-x.

119. Fisher B, Redmond C. Lumpectomy for breast cancer: an update of the NSABP experience. National Surgical Adjuvant Breast and Bowel Project. J Natl Cancer Inst Monogr. United States; 1992; : 7–13.

120. Albain K, Anderson S, Arriagada R, Barlow W. Effect of radiotherapy after breast-conserving surgery on 10-year recurrence and 15-year breast cancer death : meta-analysis of individual patient data for 10 801 women in 17 randomised trials. Lancet [Internet]. Elsevier Ltd; 2011; 378: 1707–16. doi: 10.1016/S0140-6736(11)61629-2.

121. Clough KB, Kaufman GJ, Nos C, Buccimazza I, Sarfati IM. Improving Breast Cancer Surgery: A Classification and Quadrant per Quadrant Atlas for Oncoplastic Surgery. Ann Surg Oncol. 2010; 17: 1375–91. doi: 10.1245/s10434-009-0792-y.

122. Chi C, Du Y, Ye J, Kou D, Qiu J, Wang J, Tian J. Intraoperative Imaging-Guided Cancer Surgery : From Current Fluorescence Molecular Imaging Methods to Future Multi-Modality Imaging Technology. Theranostics. 2014; 4: 1072–84. doi: 10.7150/thno.9899.

123. Rayter Z. History of breast cancer therapy. Med Ther Breast Cancer. 2003; : 1–36. doi: 10.1017/cbo9780511545870.001.

124. Slater J. From X-rays to ion beams: a short history of radiation therapy. Ion Beam Ther Fundam Technol Clin Appl. 2012; 320: 1–6. doi: 10.23880/macij-16000107.

125. Bradley JA, Mendenhall NP. Novel Radiotherapy Techniques for Breast Cancer. Annu Rev Med. 2018; 69: 277–88. doi: 10.1146/annurev-med-042716-103422.

126. Fisher B, Anderson S, Bryant J, Margolese RG, Deutsch M, Fisher ER, Jeong JH, Wolmark N. Twenty-year follow-up of a randomized trial comparing total mastectomy, lumpectomy, and lumpectomy plus irradiation for the treatment of invasive breast cancer. N Engl J Med. 2002; 347: 1233–41. doi: 10.1056/NEJMoa022152.

127. Veronesi U, Cascinelli N, Mariani L, Greco M, Saccozzi R, Luini A, Aguilar M, Marubini E. Twenty-year follow-up of a randomized study comparing breast-conserving surgery with radical mastectomy for early breast cancer. N Engl J Med. 2002; 347: 1227–32. doi: 10.1056/NEJMoa020989.

128. Kaidar-Person O, Meattini I, Poortmans P. Radiation therapy after breast conserving surgery increases long-term breast conservation for DCIS patients. Breast [Internet]. Elsevier Ltd; 2018; 37: 179–80. doi: 10.1016/j.breast.2017.10.013.

129. Hughes K, Schnaper L, Berry D, Cirrincione C. Lumpectomy plus tamoxifen with or without irradiation in women 70 years of age or older with early breast cancer. Breast Dis. 2004; 351: 971–7. doi: 10.1016/S1043-321X(05)80235-8.

130. Guidolin K, Lock M, Richard L, Boldt G, Brackstone M. Predicting which patients actually receive radiation following breast conserving therapy in Canadian populations. Can J Surg. 2016; 59: 358–60. doi: 10.1503/cjs.000516.

131. Pan IW, Smith BD, Shih YCT. Factors contributing to underuse of radiation among younger women with breast cancer. J Natl Cancer Inst. 2014; 106: 1–10. doi: 10.1093/jnci/djt340.

132. Guidolin K, Lock M, Brackstone M. Patient-perceived barriers to radiation therapy for breast cancer. Can J Surg. 2017; 61: 141–3. doi: 10.1503/cjs.015716.

133. Overgaard M, Hansen P, Overgaard J, Rose C. Postoperative radiotherapy in high-risk premenopausal women with breast cancer who receive adjuvant chemotherapy. Danish Breast Cancer Cooperative Group 82b Trial. N Engl J Med. 1997; VOLUME 337: 949–55.

134. Overgaard M, Jensen MB, Overgaard J, Hansen PS, Rose C, Andersson M, Kamby C, Kjær M, Gadeberg CC, Rasmussen BB, Blichert-Toft M, Mouridsen HT. Postoperative radiotherapy in high-risk postmenopausal breast-cancer patients given adjuvant tamoxifen: Danish Breast Cancer Cooperative Group DBCG 82c randomised trial. Lancet. 1999; 353: 1641–8. doi: 10.1016/S0140-6736(98)09201-0.

135. Taylor ME, Haffty BG, Rabinovitch R, Arthur DW, Halberg FE, Strom EA, White JR, Cobleigh MA, Edge SB. ACR Appropriateness Criteria® on Postmastectomy Radiotherapy. Expert Panel on Radiation Oncology-Breast. Int J Radiat Oncol Biol Phys. 2009; 73: 997–1002. doi: 10.1016/j.ijrobp.2008.10.080.

136. De Gonzalez BA, Curtis RE, Gilbert E, Berg CD, Smith SA, Stovall M, Ron E. Second solid cancers after radiotherapy for breast cancer in SEER cancer registries. Br J Cancer

[Internet]. Nature Publishing Group; 2010; 102: 220–6. doi: 10.1038/sj.bjc.6605435.

137. Meric F, Buchholz TA, Mirza NQ, Vlastos G, Ames FC, Ross MI, Pollock RE, Singletary SE, Feig BW, Kuerer HM, Newman LA, Perkins GH, Strom EA, et al. Long-term complications associated with breast-conservation surgery and radiotherapy. Ann Surg Oncol. 2002; 9: 543–9. doi: 10.1007/BF02573889.

138. Darby SC, Ewertz M, McGale P, Bennet AM, Blom-Goldman U, Brnønum D, Correa C, Cutter D, Gagliardi G, Gigante B, Jensen MB, Nisbet A, Peto R, et al. Risk of ischemic heart disease in women after radiotherapy for breast cancer. N Engl J Med. 2013; 368: 987–98. doi: 10.1056/NEJMoa1209825.

139. Lind PARM, Marks LB, Hardenbergh PH, Clough R, Fan M, Hollis D, Hernando ML, Lucas D, Piepgrass A, Prosnitz LR. Technical factors associated with radiation pneumonitis after local ± regional radiation therapy for breast cancer. Int J Radiat Oncol Biol Phys. 2002; 52: 137–43. doi: 10.1016/S0360-3016(01)01715-1.

140. Schaapveld M, Visser O, Louwman MJ, De Vries EGE, Willemse PHB, Otter R, Van Der Graaf WTA, Coebergh JWW, Van Leeuwen FE. Risk of new primary nonbreast cancers after breast cancer treatment: A dutch population-based study. J Clin Oncol. 2008; 26: 1239–46. doi: 10.1200/JCO.2007.11.9081.

141. Tailby E, Boyages J. Conservation surgery and radiation therapy in early breast cancer - An update. Aust Fam Physician. 2017; 46: 214–9.

142. Hickey BE, James ML, Lehman M, Hider PN, Jeffery M, Francis DP, See AM. Fraction size in radiation therapy for breast conservation in early breast cancer. Cochrane Database Syst Rev. 2016; 2016. doi: 10.1002/14651858.CD003860.pub4.

143. Klimberg VS, Rivere A, Peacock L. Alternatives to whole breast irradiation in early breast cancer. Chinese Clin Oncol. 2016; 5: 1–10. doi: 10.21037/cco.2016.03.25.

144. Castaneda SA, Strasser J. Updates in the Treatment of Breast Cancer with Radiotherapy. Surg Oncol Clin N Am [Internet]. Elsevier Inc; 2017; 26: 371–82. doi: 10.1016/j.soc.2017.01.013.

145. Smith BD, Arthur DW, Buchholz TA, Haffty BG, Hahn CA, Hardenbergh PH, Julian TB, Marks LB, Todor DA, Vicini FA, Whelan TJ, White J, Wo JY, et al. Accelerated Partial Breast Irradiation Consensus Statement From the American Society for Radiation Oncology (ASTRO). Int J Radiat Oncol Biol Phys. 2009; 74: 987–1001. doi: 10.1016/j.ijrobp.2009.02.031.

146. Veronesi U, Gatti G, Luini A, Intra M. Intraoperative radiation therapy for breast cancer: Technical Notes. Breast J. 2003; 9: 106–12. doi: 10.1016/S1055-3207(03)00098-X.

147. Veronesi U, Marubini E, Mariani L, Galimberti V, Luini A, Veronesi P, Salvadori B, Zucali R. Radiotherapy after breast-conserving surgery in small breast carcinoma: Long-term results of a randomized trial. Ann Oncol. 2001; 12: 997–1003. doi: 10.1023/A:1011136326943.

148. Benov L. Photodynamic therapy: Current status and future directions. Med Princ Pract.

2015; 24: 14–28. doi: 10.1159/000362416.

149. Agostinis P, Buytaert E, Breyssens H, Hendrickx N. Regulatory pathways in photodynamic therapy induced apoptosis. Photochem Photobiol Sci. 2004; 3: 721–9. doi: 10.1039/b315237e.

150. Casas A, Venosa G, Hasan T, Batlle A. Mechanisms of Resistance to Photodynamic Therapy. Curr Med Chem. 2011; 18: 2486–515. doi: 10.1038/jid.2014.371.

151. Klotz L-O, Kroncke K-D, Sies H. Singlet oxygen-induced signaling effects in mammalian cells. Photochem Photobiol Sci. England; 2003; 2: 88–94. doi: 10.1039/b210750c.

152. Oleinick NL, Morris RL, Nieminen A-L. Photodynamic Therapy-Induced Apoptosis. Apoptosis, Senescence, and Cancer. 2007. p. 557–78. doi: 10.1007/978-1-59745-221-2_27.

153. Ferreira dos Santos, A Queiroz de Almeida, D Fereira Terra, L Baptista M, Labriola L. Photodynamic therapy in cancer treatment - an update review. J Cancer Metastasis Treat. 2019; 5: 1–20. doi: 10.20517/2394-4722.2018.83.

154. Banerjee SM, MacRobert AJ, Mosse CA, Periera B, Bown SG, Keshtgar MRS. Photodynamic therapy: Inception to application in breast cancer. Breast. Elsevier Ltd; 2017; 31: 105–13. doi: 10.1016/j.breast.2016.09.016.

155. Calixto GMF, Bernegossi J, De Freitas LM, Fontana CR, Chorilli M, Grumezescu AM. Nanotechnology-based drug delivery systems for photodynamic therapy of cancer: A review. Molecules. 2016; 21: 1–18. doi: 10.3390/molecules21030342.

156. Agostinis P, Berg K, Cengel K, Foster T. Photodynamic therapy of cancer: an update. CA Cancer J Clin. 2011; 61: 250–81. doi: 10.1038/jid.2014.371.

157. Kwiatkowski S, Knap B, Przystupski D, Saczko J, Kędzierska E, Knap-Czop K, Kotlińska J, Michel O, Kotowski K, Kulbacka J. Photodynamic therapy – mechanisms, photosensitizers and combinations. Biomed Pharmacother. 2018; 106: 1098–107. doi: 10.1016/j.biopha.2018.07.049.

158. Castano A, Demidova T, Hamblin M. Mechanisms in photodynamic therapy: part two-cellular signaling, cell metabolism and modes of cell death. Photodiagnosis Photodyn Ther. 2005; 2: 1–23. doi: 10.1038/jid.2014.371.

159. Plaetzer K, Kiesslich T, Krammer B, Hammerl P. Characterization of the cell death modes and the associated changes in cellular energy supply in response to AlPcS4-PDT. Photochem Photobiol Sci. 2002; 1: 172–7. doi: 10.1039/b108816e.

160. Buytaert E, Dewaele M, Agostinis P. Molecular effectors of multiple cell death pathways initiated by photodynamic therapy. Biochim Biophys Acta - Rev Cancer. 2007; 1776: 86–107. doi: 10.1016/j.bbcan.2007.07.001.

161. Mehraban N, Freeman HS. Developments in PDT sensitizers for increased selectivity and singlet oxygen production. Materials. 2015. 4421–4456 p. doi: 10.3390/ma8074421.

162. Spring BQ, Rizvi I, Xu N, Hasan T, Hospital MG, Medical H, Hospital SE. The role of photodynamic therapy in overcoming cancer drug resistance. Photochem Photobiol Sci.

2015; 14: 1476–91. doi: 10.1039/c4pp00495g.The.

163. van Straten D, Mashayekhi V, de Bruijn HS, Oliveira S, Robinson DJ. Oncologic photodynamic therapy: Basic principles, current clinical status and future directions. Cancers (Basel). 2017; 9: 1–54. doi: 10.3390/cancers9020019.

164. Acedo P, Stockert JC, Cañete M, Villanueva A. Two combined photosensitizers: A goal for more effective photodynamic therapy of cancer. Cell Death Dis. 2014; 5: 1–12. doi: 10.1038/cddis.2014.77.

165. Vrouenraets MB, Visser GWM, Snow GB, van Dongen GAMS. Basic principles, applications in oncology and improved selectivity of photodynamic therapy. Anticancer Res. Greece; 2003; 23: 505–22.

166. Cruz PMR, Mo H, McConathy WJ, Sabnis N, Lacko AG. The role of cholesterol metabolism and cholesterol transport in carcinogenesis: A review of scientific findings, relevant to future cancer therapeutics. Front Pharmacol. 2013; 4: 1–7. doi: 10.3389/fphar.2013.00119.

167. Dougherty TJ, Gomer CJ, Henderson BW, Jori G, Kessel D, Korbelik M, Moan J, Peng Q. Photodynamic Therapy. J Natl Cancer Inst [Internet]. 1998; 90: 889–905. doi: 10.1007/s00726-005-0244-3.

168. Cuenca RE, Allison RR, Sibata C, Downie GH. Breast Cancer With Chest Wall Progression : Treatment With Photodynamic Therapy. 2004; 11: 322–7. doi: 10.1245/ASO.2004.03.025.

169. Schweitzer VG. PHOTOFRIN-mediated photodynamic therapy for treatment of early stage oral cavity and laryngeal malignancies. Lasers Surg Med. 2001; 29: 305–13. doi: 10.1002/lsm.1133.

170. Allison RR, Sibata CH. Oncologic photodynamic therapy photosensitizers: A clinical review. Photodiagnosis Photodyn Ther [Internet]. Elsevier B.V.; 2010; 7: 61–75. doi: 10.1016/j.pdpdt.2010.02.001.

171. Bonnett R, Martinez G. Photobleaching of Sensitisers Used in Photodynamic Therapy. Tetrahedron. 2001; 57: 9513–47. doi: 10.1002/chin.200211234.

172. Macdonald IJ, Dougherty T. Basic principles of photodynamic therapy. J Porphyr Phthalocyanines [Internet]. World Scientific Publishing Co.; 2001; 05: 105–29. doi: 10.1002/jpp.328.

173. Taber SW, Fingar VH, Coots CT, Wieman TJ. Photodynamic therapy using mono-L-aspartyl chlorin e6 (Npe6) for the treatment of cutaneous disease: a Phase I clinical study. Clin Cancer Res. United States; 1998; 4: 2741–6.

174. Khan SA, Dougherty TJ, Mang TS. An evaluation of photodynamic therapy in the management of cutaneous metastases of breast cancer. Eur J Cancer. 1993; 29: 1686–90. doi: 10.1016/0959-8049(93)90105-O.

175. Detty MR, Gibson SL, Wagner SJ. Current clinical and preclinical photosensitizers for use in photodynamic therapy. J Med Chem. 2004; 47: 3897–915. doi: 10.1021/jm040074b.

176. Mfouo-tynga I, Houreld NN, Abrahamse H. Therapy Using a Metallophthalocyanine Photosensitizer in Breast Cancer Cells. Photomed Laser Siurgery. 2014; 32: 205–11. doi: 10.1089/pho.2013.3650.

177. Lou PJ, Jäger HR, Jones L, Theodossy T, Bown SG, Hopper C. Interstitial photodynamic therapy as salvage treatment for recurrent head and neck cancer. Br J Cancer. 2004; 91: 441–6. doi: 10.1038/sj.bjc.6601993.

178. Story W, Sultan AA, Bottini G, Vaz F, Lee G, Hopper C. Strategies of airway management for head and neck photo-dynamic therapy. Lasers Surg Med. 2013; 45: 370–6. doi: 10.1002/lsm.22149.

179. Bown S, Rogowska A, Whitelaw D, Lees W. Photodynamic therapy for cancer of the pancreas. Photonics Lasers Med. 2002; 50: 549–57. doi: 10.1515/plm-2016-0001.

180. Wyss P, Schwarz V, Dobler-Girdziunaite D, Hornung R, Walt H, Degen A, Fehr M. Photodynamic therapy of locoregional breast cancer recurrences using a chlorin-type photosensitizer. Int J Cancer. 2001; 93: 720–4. doi: 10.1002/ijc.1400.

181. Moore CM, Nathan TR, Lees WR, Mosse CA, Freeman A, Emberton M, Bown SG. Photodynamic therapy using meso tetra hydroxy phenyl chlorin (mTHPC) in early prostate cancer. Lasers Surg Med. 2006; 38: 356–63. doi: 10.1002/lsm.20275.

182. Montazerabadi AR, Sazgarnia A, Bahreyni-Toosi MH, Ahmadi A, Aledavood A. The effects of combined treatment with ionizing radiation and indocyanine green-mediated photodynamic therapy on breast cancer cells. J Photochem Photobiol B Biol [Internet]. Elsevier B.V.; 2012; 109: 42–9. doi: 10.1016/j.jphotobiol.2012.01.004.

183. Crescenzi E, Varriale L, Iovino M, Chiaviello A, Veneziani BM, Palumbo G. Photodynamic therapy with indocyanine green complements and enhances low-dose cisplatin cytotoxicity in MCF-7 breast cancer cells. Mol Cancer Ther. 2004; 3: 537–44.

184. Zimmermann A, Walt H, Haller U, Baas P, Klein SD. Effects of chlorin-mediated photodynamic therapy combined with fluoropyrimidines in vitro and in a patient. Cancer Chemother Pharmacol. 2003; 51: 147–54. doi: 10.1007/s00280-002-0549-9.

185. Tong ZS, Miao PT, Liu TT, Jia YS, Liu XD. Enhanced antitumor effects of BPD-MA-mediated photodynamic therapy combined with adriamycin on breast cancer in mice. Acta Pharmacol Sin [Internet]. Nature Publishing Group; 2012; 33: 1319–24. doi: 10.1038/aps.2012.45.

186. Aniogo EC, George BPA, Abrahamse H. In vitro combined effect of Doxorubicin and sulfonated zinc Phthalocyanine–mediated photodynamic therapy on MCF-7 breast cancer cells. Tumor Biol. 2017; 39: 1–9. doi: 10.1177/1010428317727278.

187. D'Cruz AK, Robinson MH, Biel MA. mTHPC-mediated photodynamic therapy in patients with advanced, incurable head and neck cancer: A multicenter study of 128 patients. Head Neck. 2004; 26: 232–40. doi: 10.1002/hed.10372.

188. Hopper C, Niziol C, Sidhu M. The cost-effectiveness of Foscan mediated photodynamic therapy (Foscan-PDT) compared with extensive palliative surgery and palliative

chemotherapy for patients with advanced head and neck cancer in the UK. Oral Oncol. 2004; 40: 372–82. doi: 10.1016/j.oraloncology.2003.09.003.

189. Sitnik TM, Hampton JA, Henderson BW. Reduction of tumour oxygenation during and after photodynamic therapy in vivo: Effects of fluence rate. Br J Cancer. 1998; 77: 1386–94. doi: 10.1038/bjc.1998.231.

190. Dang J, He H, Chen D, Yin L. Manipulating tumor hypoxia toward enhanced photodynamic therapy (PDT). Biomater Sci. 2017; 5: 1500–11. doi: 10.1039/c7bm00392g.

191. Mallidi S, Anbil S, Bulin AL, Obaid G, Ichikawa M, Hasan T. Beyond the barriers of light penetration: Strategies, perspectives and possibilities for photodynamic therapy. Theranostics. 2016; 6: 2458–87. doi: 10.7150/thno.16183.

192. Schwartz RS. Paul Ehrlich ’s Magic Bullets. Blood. 2004; : 1079–80. doi: 10.1056/NEJMp048021.

193. Köhler G, Milstein C. Continuous cultures of fused cells secreting antibody of predefined specificity. Nature. 1975; 256: 495–7. doi: 10.1038/256495a0.

194. Reichert J. Monoclonal Antibodies as Innovative Therapeutics. Curr Pharm Biotechnol [Internet]. 2008; 9: 423–30. doi: 10.2174/138920108786786358.

195. Cai HH. Therapeutic monoclonal antibodies approved by FDA in 2017. 2018; 1: 2017–9. doi: 10.15406/moji.2018.06.00198.

196. Ryman JT, Meibohm B. Pharmacokinetics of monoclonal antibodies. CPT Pharmacometrics Syst Pharmacol. 2017; 6: 576–88. doi: 10.1002/psp4.12224.

197. Von Mehren M, Adams G, Weiner L. Monoclonal antibody therapy for cancer. Annu Rev Med. 2003; 54: 343–69. doi: 10.1146/annurev.med.54.101601.152442.

198. Green MC, Murray JL, Hortobagyi GN. Monoclonal antibody therapy for solid tumors. Cancer Treat Rev. 2000; 26: 269–86. doi: 10.1053/ctr.

199. Miller R, Maloney D, Warnke R, Levy R. Treatment of B-cell lymphoma with monoclonal anti-idiotype antibody. N Engl J Med. 1982; 306: 517–22.

200. Khazaeli M, Conry R, LoBuglio A. Human immune response to monoclonal antibodies. J Immunother. 1994; 15: 42–52.

201. Mungra N, Jordaan S, Hlongwane P, Naran K, Chetty S, Barth S. Targeted human cytolytic fusion proteins at the cutting edge: Harnessing the apoptosis-inducing properties of human enzymes for the selective elimination of tumor cells. Oncotarget. 2019; 10: 897–915. doi: 10.18632/oncotarget.26618.

202. Alley SC, Okeley NM, Senter PD. Antibody-drug conjugates: Targeted drug delivery for cancer. Curr Opin Chem Biol [Internet]. Elsevier Ltd; 2010; 14: 529–37. doi: 10.1016/j.cbpa.2010.06.170.

203. Willems A, Gauger K, Henrichs C, Harbeck N. Antibody therapy for breast cancer. Anticancer Res. 2005; 25: 1483–9.

204. Mohit E, Hashemi A, Allahyari M. Breast cancer immunotherapy: Monoclonal antibodies and peptide-based vaccines. Expert Rev Clin Immunol. Informa UK, Ltd.; 2014; 10: 927–61. doi: 10.1586/1744666X.2014.916211.

205. Yamauchi H, Stearns V, Hayes DF. When is a tumor marker ready for prime time? A case study of c-erbB-2 as a predictive factor in breast cancer. J Clin Oncol. 2001; 19: 2334–56. doi: 10.1200/JCO.2001.19.8.2334.

206. Cobleigh BMA, Vogel CL, Tripathy D, Robert NJ, Scholl S, Fehrenbacher L, Wolter JM, Paton V, Shak S, Lieberman G, Slamon DJ. Multinational Study of the efficacy and safety of humanized anti- HER 2 Monoclonal antibody in woman who have HER2-overexpresing metastatic breast cancer. J Clin Oncol. 1999; 17: 2639–48.

207. Baselga J, Tripathy D, Mendelsohn J, Baughman S, Benz CC, Dantis L, Sklarin NT, Seidman AD, Hudis CA, Moore J, Rosen PP, Twaddell T, Henderson IC, et al. Phase II study of weekly intravenous trastuzumab (Herceptin) in patients with HER2/neu-overexpressing metastatic breast cancer. J Clin Invest. 1996; 14: 737–44.

208. Ahn ER, Vogel CL. Dual HER2-targeted approaches in HER2-positive breast cancer. Breast Cancer Res Treat. 2012; 131: 371–83. doi: 10.1007/s10549-011-1781-y.

209. Yin W, Jiang Y, Shen Z, Shao Z, Lu J. Trastuzumab in the adjuvant treatment of HER2-positive early breast cancer patients: A meta-analysis of published randomized controlled trials. PLoS One. 2011; 6. doi: 10.1371/journal.pone.0021030.

210. Buzdar AU, Ibrahim NK, Francis D, Booser DJ, Thomas ES, Theriault RL, Pusztai L, Green MC, Arun BK, Giordano SH, Cristofanilli M, Frye DK, Smith TL, et al. Significantly higher pathologic complete remission rate after neoadjuvant therapy with trastuzumab, paclitaxel, and epirubicin chemotherapy: Results of a randomized trial in human epidermal growth factor receptor 2-positive operable breast cancer. J Clin Oncol. 2005; 23: 3676–85. doi: 10.1200/JCO.2005.07.032.

211. Slamon D, Leyland-Jones B, Shak S, Fuchs H. Use of chemotherapy plus a monoclonal antibody against HER2 for metastatic breast cancer that overexpresses HER2. N Engl J Med [Internet]. 2001; 344: 783–92. Available from www.nejm.org

212. García-Aranda M, Redondo M. Immunotherapy: A challenge of breast cancer treatment. Cancers (Basel). 2019; 11: 1–18. doi: 10.3390/cancers11121822.

213. Kaufman B, Trudeau M, Awada A, Blackwell K, Bachelot T, Salazar V, DeSilvio M, Westlund R, Zaks T, Spector N, Johnston S. Lapatinib monotherapy in patients with HER2-overexpressing relapsed or refractory inflammatory breast cancer: final results and survival of the expanded HER2+ cohort in EGF103009, a phase II study. Lancet Oncol [Internet]. Elsevier Ltd; 2009; 10: 581–8. doi: 10.1016/S1470-2045(09)70087-7.

214. Tao Z, Li SX, Shen K, Zhao Y, Zeng H, Ma X. Safety and Efficacy Profile of Neratinib: A Systematic Review and Meta-Analysis of 23 Prospective Clinical Trials. Clin Drug Investig [Internet]. Springer International Publishing; 2019; 39: 27–43. doi: 10.1007/s40261-018-0719-0.

215. Baselga J, Albanell J, Ruiz A, Lluch A, Gascón P, Guillém V, González S, Sauleda S,

Marimón I, Tabernero JM, Koehler MT, Rojo F. Phase II and tumor pharmacodynamic study of gefitinib in patients with advanced breast cancer. J Clin Oncol. 2005; 23: 5323–33. doi: 10.1200/JCO.2005.08.326.

216. Lin NU, Winer EP, Wheatley D, Carey LA, Houston S, Mendelson D, Munster P, Frakes L, Kelly S, Garcia AA, Cleator S, Uttenreuther-Fischer M, Jones H, et al. A phase II study of afatinib (BIBW 2992), an irreversible ErbB family blocker, in patients with HER2-positive metastatic breast cancer progressing after trastuzumab. Breast Cancer Res Treat. 2012; 133: 1057–65. doi: 10.1007/s10549-012-2003-y.

217. Arteaga CL, Sliwkowski MX, Osborne CK, Perez EA, Puglisi F, Gianni L. Treatment of HER2-positive breast cancer: Current status and future perspectives. Nat Rev Clin Oncol [Internet]. Nature Publishing Group; 2012; 9: 16–32. doi: 10.1038/nrclinonc.2011.177.

218. Corteś J, Fumoleau P, Bianchi GV, Petrella TM, Gelmon K, Pivot X, Verma S, Albanell J, Conte P, Lluch A, Salvagni S, Servent V, Gianni L, et al. Pertuzumab monotherapy after trastuzumab-based treatment and subsequent reintroduction of trastuzumab: Activity and tolerability in patients with advanced human epidermal growth factor receptor 2-positive breast cancer. J Clin Oncol. 2012; 30: 1594–600. doi: 10.1200/JCO.2011.37.4207.

219. Yu S, Liu Q, Han X, Qin S, Zhao W, Li A, Wu K. Development and clinical application of anti-HER2 monoclonal and bispecific antibodies for cancer treatment. Exp Hematol Oncol [Internet]. BioMed Central; 2017; 6: 1–15. doi: 10.1186/s40164-017-0091-4.

220. Vogel BCL, Cobleigh MA, Tripathy D, Gutheil JC, Harris LN, Fehrenbacher L, Slamon DJ, Murphy M, Novotny WF, Burchmore M, Shak S, Stewart SJ, Press M. Efficacy and Safety of Trastuzumab as a Single Agent in First-Line Treatment of HER2-Overexpressing Metastatic Breast Cancer. J Clin Oncol. 2002; 20: 719–26.

221. Genentech. IMpassion130 Efficacy Results in First-Line PD-L1+ Metastatic Triple-Negative Breast Cancer [Internet]. 2020 [cited 2020 Mar 26]. Available 2020 Mar 26, from https://www.tecentriq-hcp.com/tnbc/clinical-data-efficacy/study-efficacy.html

222. Krop IE, Beeram M, Modi S, Jones SF, Holden SN, Yu W, Girish S, Tibbitts J, Yi JH, Sliwkowski MX, Jacobson F, Lutzker SG, Burris HA. Phase I study of trastuzumab-DM1, an HER2 antibody-drug conjugate, given every 3 weeks to patients with HER2-positive metastatic breast cancer. J Clin Oncol. 2010; 28: 2698–704. doi: 10.1200/JCO.2009.26.2071.

223. Shen K, Ma X, Zhu C, Wu X, Jia H. Safety and Efficacy of Trastuzumab Emtansine in Advanced Human Epidermal Growth Factor Receptor 2-Positive Breast Cancer: A Meta-analysis. Sci Rep [Internet]. Nature Publishing Group; 2016; 6: 1–8. doi: 10.1038/srep23262.

224. Inc. DS. Enhertu (fam-trastuzumab deruxtecan-nxki): US prescribing information. 2019.

225. Bu X, Yao Y, Li X. Immune checkpoint blockade in breast cancer therapy. Adv Exp Med Biol. 2017; 1026: 383–402. doi: 10.1007/978-981-10-6020-5_18.

226. Fontana MF, Vance RE. Two signal models in innate immunity. Immunol Rev. 2011; 243: 26–39. doi: 10.1111/j.1600-065X.2011.01037.x.

227. Pardoll D. The blockade of immune checkpoints in cancer immunotherapy. Nat Rev Cancer. 2012; 12: 252–64. doi: 10.1103/PhysRevB.97.115128.

228. Buchbinder EI, Desai A. CTLA-4 and PD-1 pathways similarities, differences, and implications of their inhibition. Am J Clin Oncol Cancer Clin Trials. 2016; 39: 98–106. doi: 10.1097/COC.0000000000000239.

229. NirschI C, Drake C. Molecular Pathways: Co-Expression of Immune Checkpoint Molecules: Signaling Pathways and Implications for Cancer Immunotherapy. Clin Cancer Res. 2013; 19: 4917–24. doi: 10.1038/jid.2014.371.

230. Hodi FS, O'Day SJ, McDermott DF, Weber RW, Sosman JA, Haanen JB, Gonzalez R, Robert C, Schadendorf D, Hassel JC, Akerley W, Van Den Eertwegh AJM, Lutzky J, et al. Improved survival with ipilimumab in patients with metastatic melanoma. N Engl J Med. 2010; 363: 711–23. doi: 10.1056/NEJMoa1003466.

231. Pre-Operative, Single-Dose Ipilimumab and/or Cryoablation in Early Stage/Resectable Breast Cancer [Internet]. US National Library of Medicine. 2011 [cited 2020 Mar 28]. Available 2020 Mar 28, from https://clinicaltrials.gov/ct2/show/NCT01502592?term=ipilimumab&cond=breast+cancer&draw=2&rank=4

232. Nivolumab plus Ipilimumab in metastatic hypermutated HER2-negative breast cancer [Internet]. US National Library of Medicine. 2018 [cited 2020 Mar 28]. Available 2020 Mar 28, from https://clinicaltrials.gov/ct2/show/NCT03789110?term=ipilimumab&cond=breast+cancer&draw=2&rank=1

233. FDA. Tecentriq (atezolizumab) Approval History [Internet]. Drugs.com. [cited 2020 Mar 28]. Available 2020 Mar 28, from https://www.drugs.com/history/tecentriq.html

234. García-Aranda M, Redondo M. Targeting protein kinases to enhance the response to anti-PD-1/PD-l1 immunotherapy. Int J Mol Sci. 2019; 20: 1–22. doi: 10.3390/ijms20092296.

235. Darvin P, Toor SM, Nair VS, Elkord E. Immune checkpoint inhibitors : recent progress and potential biomarkers. Exp Mol Med. Springer US; 2018; 50: 1–11. doi: 10.1038/s12276-018-0191-1.

236. Mittendorf E, Philips A, Meric-Bernstam F, Qiao N, Wu Y. FDA Approves Atezolizumab for PD-L1 Positive Unresectable Locally Advanced or Metastatic Triple-Negative Breast Cancer [Internet]. Cancer Immunology Research. 2014. p. 361–79. doi: 10.1038/jid.2014.371.

237. FDA. FDA approves atezolizumab for PD-L1 positive unresectable locally advanced or metastatic triple-negative breast cancer [Internet]. 2019 [cited 2020 Mar 28]. doi: 10.31525/cmr-14804dc.

238. Birrer MJ, Moore KN, Betella I, Bates RC. Antibody-Drug Conjugate-Based Therapeutics : State of the Science. J Natl Cancer Inst. 2019; 111: 538–49.

239. Chari RVJ. Targeted cancer therapy: Conferring specificity to cytotoxic drugs. Acc Chem

Res. 2008; 41: 98–107. doi: 10.1021/ar700108g.

240. Lambert JM, Berkenblit A. Antibody–Drug Conjugates for Cancer Treatment. Annu Rev Med. Annual Reviews; 2018; 69: 191–207. doi: 10.1146/annurev-med-061516-121357.

241. Sievers EL, Senter PD. Antibody-Drug Conjugates in Cancer Therapy. Annu Rev Med [Internet]. 2013; 64: 15–29. doi: 10.1146/annurev-med-050311-201823.

242. McCombs JR, Owen SC. Antibody Drug Conjugates: Design and Selection of Linker, Payload and Conjugation Chemistry. AAPS J [Internet]. 2015; 17: 339–51. doi: 10.1208/s12248-014-9710-8.

243. Pietersz GA, Rowland A, Smyth MJ, Mckenzie IFC. Chemoimmunoconjugates for the Treatment of Cancer. In: Dixon FJBT-A in I, editor. Academic Press; 1994. p. 301–87. doi: https://doi.org/10.1016/S0065-2776(08)60455-1.

244. Dan N, Setua S, Kashyap VK, Khan S, Jaggi M, Yallapu MM, Chauhan SC. Antibody-drug conjugates for cancer therapy: Chemistry to clinical implications. Pharmaceuticals. 2018; 11. doi: 10.3390/ph11020032.

245. Mehrling T, Soltis D. Challenges in Optimising the Successful Construction of Antibody Drug Conjugates in Cancer Therapy. Antibodies. 2018; 7: 11. doi: 10.3390/antib7010011.

246. Biochempeg. Anti-Cancer ADC Drugs: 3 Design Elements, 7 Approved ADCs, Multiple Clinical Trials [Internet]. 2020 [cited 2020 Mar 31]. Available 2020 Mar 31, from https://www.biochempeg.com/article/74.html

247. Chalouni C, Doll S. Fate of Antibody-Drug Conjugates in Cancer Cells. J Exp Clin Cancer Res. Journal of Experimental & Clinical Cancer Research; 2018; 37: 1–12. doi: 10.1186/s13046-017-0667-1.

248. Keam SJ. Trastuzumab Deruxtecan: First Approval. Drugs [Internet]. Springer International Publishing; 2020; 80: 501–8. doi: 10.1007/s40265-020-01281-4.

249. Damelin M, Zhong W, Myers J, Sapra P. Evolving Strategies for Target Selection for Antibody-Drug Conjugates. Pharm Res. 2015; 32: 3494–507. doi: 10.1007/s11095-015-1624-3.

250. Diamantis N, Banerji U. Antibody-drug conjugates - An emerging class of cancer treatment. Br J Cancer [Internet]. Nature Publishing Group; 2016; 114: 362–7. doi: 10.1038/bjc.2015.435.

251. Donaghy H. Effects of antibody, drug and linker on the preclinical and clinical toxicities of antibody-drug conjugates. MAbs [Internet]. Taylor & Francis; 2016; 8: 659–71. doi: 10.1080/19420862.2016.1156829.

252. Peters C, Brown S. Antibody-drug conjugates as novel anti-cancer chemotherapeutics. Biosci Rep. 2015; 35. doi: 10.1042/BSR20150089.

253. Hughes B. Antibody-drug conjugates for cancer: Poised to deliver? Nat Rev Drug Discov [Internet]. Nature Publishing Group; 2010; 9: 665–7. doi: 10.1038/nrd3270.

254. Khongorzul P, Ling CJ, Khan FU, Ihsan AU, Zhang J. Antibody-drug conjugates: A

comprehensive review. Mol Cancer Res. 2019; 18: 3–19. doi: 10.1158/1541-7786.MCR-19-0582.

255. Alley SC, Benjamin DR, Jeffrey SC, Okeley NM, Meyer DL, Sanderson RJ, Senter PD. Contribution of linker stability to the activities of anticancer immunoconjugates. Bioconjug Chem. 2008; 19: 759–65. doi: 10.1021/bc7004329.

256. Nagayama A, Ellisen LW, Chabner B, Bardia A. Antibody–Drug Conjugates for the Treatment of Solid Tumors: Clinical Experience and Latest Developments. Target Oncol. Targeted Oncology; 2017; 12: 719–39. doi: 10.1007/s11523-017-0535-0.

257. Chari RVJ, Miller ML, Widdison WC. Antibody-drug conjugates: An emerging concept in cancer therapy. Angew Chemie - Int Ed. 2014; 53: 3796–827. doi: 10.1002/anie.201307628.

258. Tsuchikama K, An Z. Antibody-drug conjugates: recent advances in conjugation and linker chemistries. Protein Cell. Higher Education Press; 2018; 9: 33–46. doi: 10.1007/s13238-016-0323-0.

259. Lewis Phillips GD, Li G, Dugger DL, Crocker LM, Parsons KL, Mai E, Blättler WA, Lambert JM, Chari RVJ, Lutz RJ, Wong WLT, Jacobson FS, Koeppen H, et al. Targeting HER2-positive breast cancer with trastuzumab-DM1, an antibody-cytotoxic drug conjugate. Cancer Res. 2008; 68: 9280–90. doi: 10.1158/0008-5472.CAN-08-1776.

260. Nakada T, Sugihara K, Jikoh T, Abe Y, Agatsuma T. The Latest Research and Development into the Antibody–Drug Conjugate, [fam-] Trastuzumab Deruxtecan (DS-8201a), for HER2 Cancer Therapy. Chem Pharm Bull. 2019; 67: 173–85. doi: 10.1248/cpb.c18-00744.

261. Nasiri H, Valedkarimi Z, Aghebati-Maleki L, Majidi J. Antibody-drug conjugates: Promising and efficient tools for targeted cancer therapy. J Cell Physiol. 2018; 233: 6441–57. doi: 10.1002/jcp.26435.

262. Bouchard H, Viskov C, Garcia-Echeverria C. Antibody-drug conjugates - A new wave of cancer drugs. Bioorganic Med Chem Lett. 2014; 24: 5357–63. doi: 10.1016/j.bmcl.2014.10.021.

263. Li F, Emmerton KK, Jonas M, Zhang X, Miyamoto JB, Setter JR, Nicholas ND, Okeley NM, Lyon RP, Benjamin DR, Law C. Intracellular Released Payload In fl uences Potency and Bystander-Killing Effects of Antibody-Drug Conjugates in Preclinical Models. Ther Targets, Chem Biol. 2016; 76: 2710–20. doi: 10.1158/0008-5472.CAN-15-1795.

264. Oroudjev E, Lopus M, Wilson L, Audette C, Provenzano C, Erickson H, Kovtun Y, Chari R, Jordan MA. Maytansinoid-Antibody Conjugates Induce Mitotic Arrest by Suppressing Microtubule Dynamic Instability. Mol Cancer Ther. 2010; 9: 2700–14. doi: 10.1158/1535-7163.MCT-10-0645.

265. Verma S, Miles D, Gianni L, Krop I, Welslau M. Trastuzumab Emtansine for HER2-Positive Advanced Breast Cancer. New. 2012; 367: 1783–91. doi: 10.1016/j.physbeh.2017.03.040.

266. Krop IE, Kim SB, González-Martín A, LoRusso PM, Ferrero JM, Smitt M, Yu R, Leung ACF, Wildiers H. Trastuzumab emtansine versus treatment of physician's choice for

pretreated HER2-positive advanced breast cancer (TH3RESA): A randomised, open-label, phase 3 trial. Lancet Oncol. 2014; 15: 689–99. doi: 10.1016/S1470-2045(14)70178-0.

267. Junttila TT, Li G, Parsons K. Trastuzumab-DM1 (T-DM1) retains all the mechanisms of action of trastuzumab and efficiently inhibits growth of lapatinib insensitive breast cancer. Breast Cancer Res. 2011; 128: 347–56. doi: 10.1007/s10549-010-1090-x.

268. Hunter FW, Barker HR, Lipert B, Rothé F, Gebhart G, Piccart-Gebhart MJ, Sotiriou C, Jamieson SMF. Mechanisms of resistance to trastuzumab emtansine (T-DM1) in HER2-positive breast cancer. Br J Cancer [Internet]. Springer US; 2019; 122: 603–12. doi: 10.1038/s41416-019-0635-y.

269. Brandão M, Pondé NF, Poggio F, Kotecki N, Salis M, Lambertini M, de Azambuja E. Combination therapies for the treatment of HER2-positive breast cancer: current and future prospects. Expert Rev Anticancer Ther [Internet]. Taylor & Francis; 2018; 18: 629–49. doi: 10.1080/14737140.2018.1477596.

270. Takegawa N, Nonagase Y, Yonesaka K, Sakai K, Maenishi O, Ogitani Y, Tamura T, Nishio K, Nakagawa K, Tsurutani J. DS-8201a, a new HER2-targeting antibody–drug conjugate incorporating a novel DNA topoisomerase I inhibitor, overcomes HER2-positive gastric cancer T-DM1 resistance. Int J Cancer. 2017; 141: 1682–9. doi: 10.1002/ijc.30870.

271. Ogitani Y, Aida T, Hagihara K, Yamaguchi J, Ishii C, Harada N, Soma M, Okamoto H, Oitate M, Arakawa S, Hirai T, Atsumi R, Nakada T, et al. DS-8201a, a novel HER2-targeting ADC with a novel DNA topoisomerase I inhibitor, demonstrates a promising antitumor efficacy with differentiation from T-DM1. Clin Cancer Res. 2016; 22: 5097–108. doi: 10.1158/1078-0432.CCR-15-2822.

272. Loganzo F, Tan X, Sung M, Jin G, Myers JS, Melamud E, Wang F, Diesl V, Follettie MT, Musto S, Lam MH, Hu W, Charati MB, et al. Tumor cells chronically treated with a trastuzumab-maytansinoid antibody-drug conjugate develop varied resistance mechanisms but respond to alternate treatments. Mol Cancer Ther. 2015; 14: 952–63. doi: 10.1158/1535-7163.MCT-14-0862.

273. Ogitani Y, Hagihara K, Oitate M, Naito H, Agatsuma T. Bystander killing effect of DS-8201a, a novel anti-human epidermal growth factor receptor 2 antibody–drug conjugate, in tumors with human epidermal growth factor receptor 2 heterogeneity. Cancer Sci. 2016; 107: 1039–46. doi: 10.1111/cas.12966.

274. Hussain AF, Heppenstall PA, Kampmeier F, Meinhold-Heerlein I, Barth S. One-step site-specific antibody fragment auto-conjugation using SNAP-tag technology. Nat Protoc [Internet]. Springer US; 2019; 14: 3101–25. doi: 10.1038/s41596-019-0214-y.

275. Beck A, Goetsch L, Dumontet C, Corvaïa N. Strategies and challenges for the next generation of antibody-drug conjugates. Nat Rev Drug Discov [Internet]. Nature Publishing Group; 2017; 16: 315–37. doi: 10.1038/nrd.2016.268.

276. Panowski S, Bhakta S, Raab H, Polakis P, Junutula JR. Site-specific antibody drug conjugates for cancer therapy. MAbs. 2014; 6: 34–45. doi: 10.4161/mabs.27022.

277. Hamblett KJ, Senter PD, Chace DF, Hamblett KJ, Senter PD, Chace DF, Sun MMC, Lenox

J, Cerveny CG, Kissler KM, Bernhardt SX, Kopcha AK, Zabinski RF, et al. Effects of Drug Loading on the Antitumor Activity of a Monoclonal Antibody Drug Conjugate Effects of Drug Loading on the Antitumor Activity of a Monoclonal Antibody Drug Conjugate. Clin Cancer Res. 2004; 10: 7063–70. doi: 10.1158/1078-0432.CCR-04-0789.

278. Axup JY, Bajjuri KM, Ritland M, Hutchins BM, Kim CH, Kazane SA, Halder R, Forsyth JS, Santidrian AF, Stafin K, Lu Y, Tran H, Seller AJ, et al. Synthesis of site-specific antibody-drug conjugates using unnatural amino acids. Proc Natl Acad Sci U S A. 2012; 109: 16101–6. doi: 10.1073/pnas.1211023109.

279. Hallam TJ, Wold E, Wahl A, Smider V V. Antibody conjugates with unnatural amino acids. Mol Pharm. 2015; 12: 1848–62. doi: 10.1021/acs.molpharmaceut.5b00082.

280. Kim C, Axup J, Dubrovska A, Kazane S. Synthesis of Bispecific Antibodies with Genetically Encoded Unnatural Amino Acids. J Am Chem Soc. 2012; 134: 9918–21. doi: 10.1161/CIRCULATIONAHA.110.956839.

281. Keppler A, Gendreizig S, Gronemeyer T, Pick H, Vogel H, Johnsson K. A general method for the covalent labeling of fusion proteins with small molecules in vivo. Nat Biotechnol. 2002; 21: 86–9. doi: 10.1038/nbt765.

282. Los G V, Encell LP, Mcdougall MG, Hartzell DD, Karassina N, Zimprich C, Wood MG, Learish R, Ohana RF, Urh M, Simpson D, Mendez J, Zimmerman K, et al. Halo Tag: Protein labeling Technology for cell imaging and protein analysis. ACS Chem Biol. 2008; 3: 373–82.

283. Gautier A, Juillerat A, Heinis C, Corrêa IR, Kindermann M, Beaufils F, Johnsson K. An Engineered Protein Tag for Multiprotein Labeling in Living Cells. Chem Biol. 2008; 15: 128–36. doi: 10.1016/j.chembiol.2008.01.007.

284. Cole NB. Site-Specific Protein Labeling with SNAP-Tags. Curr Protoc Protein Sci. 2014; 73: 1–7. doi: 10.1038/jid.2014.371.

285. Hussain A, Amoury M, Barth S. SNAP-Tag Technology: A Powerful Tool for Site Specific Conjugation of Therapeutic and Imaging Agents. Curr Pharm Des. 2013; 19: 5437–42. doi: 10.2174/1381612811319300014.

286. Juillerat A, Gronemeyer T, Keppler A, Gendreizig S. Directed Evolution of O6-Alkylguanine-DNA Alkyltransferase for Efficient Labeling of Fusion Proteins with Small Molecules In Vivo. Chemistry (Easton) [Internet]. 2003; 10: 313–7. doi: 10.1016/S.

287. Gronemeyer T, Godin G, Johnsson K. Adding value to fusion proteins through covalent labelling. Curr Opin Biotechnol. 2005; 16: 453–8. doi: 10.1016/j.copbio.2005.06.001.

288. Gronemeyer T, Chidley C, Juillerat A, Heinis C, Johnsson K. Directed evolution of O6-alkylguanine-DNA alkyltransferase for applications in protein labeling. Protein Eng Des Sel. 2006; 19: 309–16. doi: 10.1093/protein/gzl014.

289. Srikun D, Albers AE, Nam CI, Iavarone AT, Chang CJ. Organelle-targetable fluorescent probes for imaging hydrogen peroxide in living cells via SNAP-Tag protein labeling. J Am Chem Soc. 2010; 132: 4455–65. doi: 10.1021/ja100117u.

290. Keppler A, Kindermann M, Gendreizig S, Pick H, Vogel H, Johnsson K. Labeling of fusion proteins of O6-alkylguanine-DNA alkyltransferase with small molecules in vivo and in vitro. Methods. 2004; 32: 437–44. doi: 10.1016/j.ymeth.2003.10.007.

291. Padayachee ER, Adeola HA, Van Wyk JC, Nsole Biteghe FA, Chetty S, Khumalo NP, Barth S. Applications of SNAP-tag technology in skin cancer therapy. Heal Sci Reports. 2018; 2: 1–12. doi: 10.1002/hsr2.103.

292. Macias-Contreras M, He H, Zhu L. Beyond O 6 -Benzylguanine: O 6 -(5-Pyridylmethyl)guanine as a Substrate for the Self-Labeling Enzyme SNAP-Tag. Bioconjug Chem. 2018; 29: 4104–9. doi: 10.1021/acs.bioconjchem.8b00703.

293. Amoury M, Blume T, Brehm H, Niesen J, Tenhaef N, Barth S, Gattenlohner S, Helfrich W, Fitting J, Nachreiner T, Pardo A. SNAP-tag based agents for preclinical in vitro imaging in malignant diseases. Curr Pharm Des. Netherlands; 2013; 19: 5429–36.

294. Song X, Bian H, Wang C, Hu M, Li N, Xiao Y. Development and applications of a near-infrared dye-benzylguanine conjugate to specifically label SNAP-tagged proteins. Org Biomol Chem. Royal Society of Chemistry; 2017; 15: 8091–101. doi: 10.1039/c7ob01698k.

295. Amoury M, Bauerschlag D, Zeppernick F, von Felbert V, Berges N, Di Fiore S, Mintert I, Bleilevens A, Maass N, Bräutigam K, Meinhold-Heerlein I, Stickeler E, Barth S, et al. Photoimmunotheranostic agents for triple-negative breast cancer diagnosis and therapy that can be activated on demand. Oncotarget. 2016; 7: 54925–36. doi: 10.18632/oncotarget.10705.

296. Kampmeier F, Ribbert M, Nachreiner T, Dembski S, Beaufils F, Brecht A, Barth S. Site-specific, covalent labeling of recombinant antibody fragments via fusion to an engineeredKampmeier, F., Ribbert, M., Nachreiner, T., Dembski, S., Beaufils, F., Brecht, A., & Barth, S. (2009). Site-specific, covalent labeling of recombinant antibody f. Bioconjug Chem. 2009; 20: 1010–5. doi: 10.1021/bc9000257.

297. Kampmeier F, Niesen J, Koers A, Ribbert M, Brecht A, Fischer R, Kießling F, Barth S, Thepen T. Rapid optical imaging of EGF receptor expression with a single-chain antibody SNAP-tag fusion protein. Eur J Nucl Med Mol Imaging. 2010; 37: 1926–34. doi: 10.1007/s00259-010-1482-5.

298. Hussain AF, Kampmeier F, Von Felbert V, Merk HF, Tur MK, Barth S. SNAP-tag technology mediates site specific conjugation of antibody fragments with a photosensitizer and improves target specific phototoxicity in tumor cells. Bioconjug Chem. 2011; 22: 2487–95. doi: 10.1021/bc200304k.

299. Pettit GR, Kamano Y, Herald CL, Tuinman AA, Boettner FE, Kizu H, Schmidt JM, Baczynskyi L, Tomer KB, Bontems RJ. The Isolation and Structure of a Remarkable Marine Animal Antineoplastic Constituent: Dolastatin 10. J Am Chem Soc. 1987; 109: 6883–5. doi: 10.1021/ja00256a070.

300. Hu ZB, Gignac SM, Quentmeier H, Pettit GR, Drexler HG. Effects of dolastatins on human B-lymphocytic leukemia cell lines. Leuk Res. 1993; 17: 333–9. doi: 10.1016/0145-2126(93)90020-L.

301. Akaiwa M, Dugal-Tessier J, Mendelsohn BA. Drug Discovery : Recent Progress and the Future Antibody – Drug Conjugate Payloads; Study of Auristatin Derivatives. Chem Pharm Bull (Tokyo). 2020; 68: 201–11.

302. Von Mehren M, Balcerzak SP, Kraft AS, Edmonson JH, Okuno SH, Davey M, McLaughlin S, Beard MT, Rogatko A. Phase II trial of dolastatin-10, a novel anti-tubulin agent, in metastatic soft tissue sarcomas. Sarcoma. 2004; 8: 107–11. doi: 10.1080/13577140400009163.

303. Vaishampayan U, Glode M, Du W, Kraft A, Hudes G, Wright J, Hussain M. Phase II study of dolastatin-10 in patients with hormone-refractory metastatic prostate adenocarcinoma. Clin Cancer Res. United States; 2000; 6: 4205–8.

304. Saad ED, Kraut EH, Hoff PM, Moore DF, Jones D, Pazdur R, Abbruzzese JL. Phase II Study of Dolastatin-10 as First-Line Treatment for Advanced Colorectal Cancer. Am J Clin Oncol Cancer Clin Trials. 2002; 25: 451–3.

305. Polakis P. Antibody Drug Conjugates for Cancer Treatment. Pharmacol Rev. 2016; 68: 3–19. doi: 10.1001/jamaoncol.2019.3552.

306. Perez HL, Cardarelli PM, Deshpande S, Gangwar S, Schroeder GM, Vite GD, Borzilleri RM. Antibody-drug conjugates: Current status and future directions. Drug Discov Today [Internet]. Elsevier Ltd; 2014; 19: 869–81. doi: 10.1016/j.drudis.2013.11.004.

307. Morrison K, Challita-Eid PM, Raitano A, An Z, Yang P, Abad JD, Liu W, Lortie DR, Snyder JT, Capo L, Verlinsky A, Avïna H, Dõnate F, et al. Development of ASG-15ME, a novel antibody-drug conjugate targeting SLITRK6, a new urothelial cancer biomarker. Mol Cancer Ther. 2016; 15: 1301–10. doi: 10.1158/1535-7163.MCT-15-0570.

308. Jerjian T V., Glode AE, Thompson LA, O'Bryant CL. Antibody-Drug Conjugates: A Clinical Pharmacy Perspective on an Emerging Cancer Therapy. Pharmacotherapy. 2016; 36: 99–116. doi: 10.1002/phar.1687.

309. Francisco JA, Cerveny CG, Meyer DL, Mixan BJ, Klussman K, Chace DF, Rejniak SX, Gordon KA, DeBlanc R, Toki BE, Law CL, Doronina SO, Siegall CB, et al. cAC10-vcMMAE, an anti-CD30-monomethyl auristatin E conjugate with potent and selective antitumor activity. Blood. 2003; 102: 1458–65. doi: 10.1182/blood-2003-01-0039.

310. Bai R, Petit GR, Hamel E. Dolastatin 10, a powerful cytostatic peptide derived from a marine animal: Inhibition of tubulin polymerization mediated through the vinca alkaloid binding domain. Biochem Pharmacol [Internet]. 1990; 39: 1941–9. doi: https://doi.org/10.1016/0006-2952(90)90613-P.

311. Otani M, Natsume T, Watanabe J, Kobayashi M, Mikami T, Nakayama T. TZT-1027 , an Antimicrotubule Agent , Attacks Tumor Vasculature and Induces Tumor Cell Death. Japanese J Cancer Res. 2000; 91: 837–44.

312. Woitok M, Klose D, Niesen J, Richter W, Abbas M, Stein C, Fendel R, Bialon M, Püttmann C, Fischer R, Barth S, Kolberg K. The efficient elimination of solid tumor cells by EGFR-specific and HER2-specific scFv-SNAP fusion proteins conjugated to benzylguanine-modified auristatin F. Cancer Lett [Internet]. Elsevier Ireland Ltd; 2016; 381: 323–30. doi:

10.1016/j.canlet.2016.08.003.

313. Woitok M, Klose D, Di Fiore S, Richter W, Stein C, Gresch G, Grieger E, Barth S, Fischer R, Kolberg K, Niesen J. Comparison of a mouse and a novel human scFv-SNAP-auristatin F drug conjugate with potent activity against EGFR-overexpressing human solid tumor cells. Onco Targets Ther. 2017; 10: 3313–27. doi: 10.2147/OTT.S140492.

314. Hussain AF, Krüger HR, Kampmeier F, Weissbach T, Licha K, Kratz F, Haag R, Calderón M, Barth S. Targeted delivery of dendritic polyglycerol-doxorubicin conjugates by scFv-SNAP fusion protein suppresses EGFR+ cancer cell growth. Biomacromolecules. 2013; 14: 2510–20. doi: 10.1021/bm400410e.

315. Koga Y, Manabe S, Aihara Y, Sato R, Tsumura R, Iwafuji H, Furuya F, Fuchigami H, Fujiwara Y, Hisada Y, Yamamoto Y, Yasunaga M, Matsumura Y. Antitumor effect of antitissue factor antibody-MMAE conjugate in human pancreatic tumor xenografts. Int J Cancer. 2015; 137: 1457–66. doi: 10.1002/ijc.29492.

316. Mew D, Wat CK, Towers GH, Levy JG. Photoimmunotherapy: treatment of animal tumors with tumor-specific monoclonal antibody-hematoporphyrin conjugates. J Immunol. United States; 1983; 130: 1473–7.

317. Sobolev AS, Jans DA, Rosenkranz AA. Targeted intracellular delivery of photosensitizers. Prog Biophys Mol Biol. 2000; 73: 51–90. doi: 10.1016/S0079-6107(00)00002-X.

318. Carcenac M, Dorvillius M, Garambois V, Glaussel F, Larroque C, Langlois R, Hynes NE, Van Lier JE, Pèlegrin A. Internalisation enhances photo-induced cytotoxicity of monoclonal antibody-phthalocyanine conjugates. Br J Cancer. 2001; 85: 1787–93. doi: 10.1054/bjoc.2001.2170.

319. Vrouenraets MB, Visser GW, Stewart FA, Stigter M, Oppelaar H, Postmus PE, Snow GB, van Dongen GA. Development of meta-tetrahydroxyphenylchlorin-monoclonal antibody conjugates for photoimmunotherapy. Cancer Res. United States; 1999; 59: 1505–13.

320. Mitsunaga M, Ogawa M, Kosaka N, Rosenblum L. Cancer Cell-Selective In Vivo Near Infrared Photoimmunotherapy Targeting Specific Membrane Molecules. Nat Med. 2011; 17: 1685–91. doi: 10.1016/j.physbeh.2017.03.040.

321. Kobayashi H, Choyke PL. Near-Infrared Photoimmunotherapy of Cancer. Acc Chem Res. 2019; 52: 2332–9. doi: 10.1021/acs.accounts.9b00273.

322. Kobayashi H. Chapter 22 Theranostic Near-Infrared Photoimmunotherapy. Make Life Visible. 2019. p. 219–25. doi: 10.1007/978-981-13-7908-6.

323. Nagaya T, Okuyama S, Ogata F, Maruoka Y, Choyke PL, Kobayashi H. Endoscopic near infrared photoimmunotherapy using a fiber optic diffuser for peritoneal dissemination of gastric cancer. Cancer Sci. 2018; 109: 1902–8. doi: 10.1111/cas.13621.

324. Okuyama S, Nagaya T, Sato K, Ogata F, Maruoka Y, Choyke PL, Kobayashi H. Interstitial near-infrared photoimmunotherapy: Effective treatment areas and light doses needed for use with fiber optic diffusers. Oncotarget. 2018; 9: 11159–69. doi: 10.18632/oncotarget.24329.

325. Ogawa M, Yamauchi T, Iwai H, Magata Y, Choyke PL, Kobayashi H. Investigation of dynamic morphological changes of cancer cells during photoimmuno therapy (PIT) by low-coherence quantitative phase microscopy. Prog Biomed Opt Imaging. 2014; : 893110–3. doi: 10.1117/12.2036944.

326. Allison RR, Moghissi K. Photodynamic therapy (PDT): PDT mechanisms. Clin Endosc. 2013; 46: 24–9. doi: 10.5946/ce.2013.46.1.24.

327. Nakamura Y, Ohler ZW, Householder D, Nagaya T, Sato K, Okuyama S, Ogata F, Daar D, Hoa T, Peter L, Kobayashi H, Program I, National F. Near infrared photoimmunotherapy in a transgenic mouse model of spontaneous epidermal growth factor receptor (EGFR)-expressing lung cancer. Mol Cancer Ther. 2016; 16: 408–14. doi: 10.1158/1535-7163.MCT-16-0663.Near.

328. Railkar R, Krane L, Quentin Li Q, Sanford T. Epidermal Growth Factor Receptor (EGFR) Targeted Photoimmunotherapy (PIT) for the Treatment of EGFR expressing Bladder Cancer. Mol Cancer Ther. 2017; 16: 2201–14. doi: 10.1158/1535-7163.MCT-16-0924.Epidermal.

329. Nagaya T, Sato K, Harada T, Nakamura Y, Choyke PL, Kobayashi H. Near infrared photoimmunotherapy targeting EGFR positive triple negative breast cancer: Optimizing the conjugate-light regimen. PLoS One. 2015; 10: 1–14. doi: 10.1371/journal.pone.0136829.

330. Sato K, Watanabe R, Hanaoka H, Harada T, Nakajima T, Kim I, Paik CH, Choyke PL, Kobayashi H. Photoimmunotherapy: Comparative effectiveness of two monoclonal antibodies targeting the epidermal growth factor receptor. Mol Oncol. 2014; 8: 620–32. doi: 10.1016/j.molonc.2014.01.006.

331. Ito K, Mitsunaga M, Arihiro S, Saruta M, Matsuoka M, Kobayashi H, Tajiri H. Molecular targeted photoimmunotherapy for HER2-positive human gastric cancer in combination with chemotherapy results in improved treatment outcomes through different cytotoxic mechanisms. BMC Cancer [Internet]. BMC Cancer; 2016; 16: 1–10. doi: 10.1186/s12885-016-2072-0.

332. Sato K, Nagaya T, Mitsunaga M, Choyke P, Kobayashi H. Near infrared photoimmunotherapy for lung metastases. Cancer Lett. 2015; 365: 112–21. doi: 10.1016/j.physbeh.2017.03.040.

333. Maawy AA, Hiroshima Y, Zhang Y, Heim R, Makings L, Garcia-Guzman M, Luiken GA, Kobayashi H, Hoffman RM, Bouvet M. Near infra-red photoimmunotherapy with anti-CEA-IR700 results in extensive tumor lysis and a significant decrease in tumor burden in orthotopic mouse models of pancreatic cancer. PLoS One. 2015; 10: 1–11. doi: 10.1371/journal.pone.0121989.

334. Jin J, Krishnamachary B, Mironchik Y, Kobayashi H, Bhujwalla ZM. Phototheranostics of CD44-positive cell populations in triple negative breast cancer. Sci Rep. Nature Publishing Group; 2016; 6. doi: 10.1038/srep27871.

335. Jing H, Weidensteiner C, Reichardt W, Gaedicke S, Zhu X, Grosu AL, Kobayashi H, Niedermann G. Imaging and selective elimination of glioblastoma stem cells with

theranostic Near-Infrared-Labeled CD133-Specific antibodies. Theranostics. 2016; 6: 862–74. doi: 10.7150/thno.12890.

336. Mitsunaga M, Nakajima T, Sano K, Choyke P, Kobayashi H. Near Infrared Theranostic Photoimmunotherapy (PIT): Repeated Exposure of Light Enhances the Effect of Immunoconjugate. Bioconjug Chem. 2012; 23: 604–9. doi: 10.1038/jid.2014.371.

337. Harris AL. Hypoxia - A key regulatory factor in tumour growth. Nat Rev Cancer. 2002; 2: 38–47. doi: 10.1038/nrc704.

338. Ogata F, Nagaya T, Nakamura Y, Sato K. Near-infrared photoimmunotherapy : a comparison of light dosing schedules. Oncotarget. 2017; 8: 35069–75.

339. Sano K, Nakajima T, Choyke P, Kobayashi H. Markedly Enhanced Permeability and Retention Effects Induced by Photo-Immunotherapy of Tumors. ACS Nano. 2013; 7: 717–24. doi: 10.1038/jid.2014.371.

340. Bauerschlag D, Meinhold-Heerlein I, Maass N, Bleilevens A, Bräutigam K, Al Rawashdeh W, Di Fiore S, Haugg AM, Gremse F, Steitz J, Fischer R, Stickeler E, Barth S, et al. Detection and Specific Elimination of EGFR+ Ovarian Cancer Cells Using a Near Infrared Photoimmunotheranostic Approach. Pharm Res. Pharmaceutical Research; 2017; 34: 696–703. doi: 10.1007/s11095-017-2096-4.

341. Ito K, Mitsunaga M, Nishimura T, Kobayashi H, Tajiri H. Combination photoimmunotherapy with monoclonal antibodies recognizing different epitopes of human epidermal growth factor receptor 2: an assessment of phototherapeutic effect based on fluorescence molecular imaging. Oncotarget. 2016; 7: 14143–52. doi: 10.18632/oncotarget.7490.

342. Sandland J, Boyle RW. Photosensitizer Antibody-Drug Conjugates: Past, Present, and Future. Bioconjug Chem. American Chemical Society; 2019; 30: 975–93. doi: 10.1021/acs.bioconjchem.9b00055.

343. Serebrovskaya EO, Edelweiss EF, Stremovskiy OA, Lukyanov KA, Chudakov DM, Deyev SM. Targeting cancer cells by using an antireceptor antibody-photosensitizer fusion protein. Proc Natl Acad Sci U S A. 2009; 106: 9221–5. doi: 10.1073/pnas.0904140106.

344. Pye H, Stamati I, Yahioglu G, Butt M, Deonarain M. Antibody-Directed Phototherapy (ADP). Antibodies. 2013; 2: 270–305. doi: 10.3390/antib2020270.

345. von Felbert V, Bauerschlag D, Maass N, Bräutigam K, Meinhold-Heerlein I, Woitok M, Barth S, Hussain AF. A specific photoimmunotheranostics agent to detect and eliminate skin cancer cells expressing EGFR. J Cancer Res Clin Oncol. Springer Berlin Heidelberg; 2016; 142: 1003–11. doi: 10.1007/s00432-016-2122-7.

346. von Felbert V, Bauerschlag D, Maass N, Bräutigam K, Meinhold-Heerlein I, Woitok M, Barth S, Hussain AF. A specific photoimmunotheranostics agent to detect and eliminate skin cancer cells expressing EGFR. J Cancer Res Clin Oncol. Springer Berlin Heidelberg; 2016; 142: 1003–11. doi: 10.1007/s00432-016-2122-7.

347. Yokota T, Milenic DE, Whitlow M, Schlom J. Rapid Tumor Penetration of a Single-Chain

Fv and Comparison with Other Immunoglobulin Forms. Cancer Res. 1992; 52: 3402–8.

348. Choi HS, Liu W, Misra P, Tanaka E, Zimmer JP, Itty Ipe B, Bawendi MG, Frangioni J V. Renal clearance of nanoparticles. Nat Biotechnol [Internet]. 2007; 25: 1165–70. doi: 10.1038/nbt1340.Renal.

349. Batra SK, Jain M, Wittel UA, Chauhan SC, Colcher D. Pharmacokinetics and biodistribution of genetically engineered antibodies. Curr Opin Biotechnol. England; 2002; 13: 603–8. doi: 10.1016/s0958-1669(02)00352-x.

350. Ilieva KM, Cheung A, Mele S, Chiaruttini G, Crescioli S, Griffin M, Nakamura M, Spicer JF, Tsoka S, Lacy KE, Tutt ANJ, Karagiannis SN. Chondroitin sulfate proteoglycan 4 and its potential as an antibody immunotherapy target across different tumor types. Front Immunol. 2018; 8: 1–15. doi: 10.3389/fimmu.2017.01911.

351. Wilson BS, Imai K, Natali PG, Ferrone S. Distribution and molecular characterization of a cell-surface and a cytoplasmic antigen detectable in human melanoma cells with monoclonal antibodies. Int J Cancer. 1981; 28: 293–300. doi: 10.1002/ijc.2910280307.

352. Stallcup WB. The NG2 proteoglycan: Past insights and future prospects. J Neurocytol. 2002; 31: 423–35. doi: 10.1023/A:1025731428581.

353. Wang X, Wang Y, Yu L, Sakakura K, Visus C, Schwab JH, Ferrone CR, Favoino E, Koya Y, Campoli MR, McCarthy JB, DeLeo AB, Ferrone S. CSPG4 in Cancer: Multiple Roles. Curr Mol Med. 2010; 10: 419–29. doi: 10.2174/156652410791316977.

354. Stegmüller J, Schneider S, Hellwig A, Garwood J, Trotter J. AN2, the mouse homologue of NG2, is a surface antigen on glial precursor cells implicated in control of cell migration. J Neurocytol. 2002; 31: 497 ppl= – 505. doi: 10.1023/A:1025743731306.

355. Timpl R, Tisi D, Talts JF, Andac Z, Sasaki T, Hohenester E. Structure and function of laminin LG modules. Matrix Biol. 2000; 19: 309–17. doi: 10.1016/S0945-053X(00)00072-X.

356. Iida J, Wilhelmson KL, Ng J, Lee P, Morrison C, Tam E, Overall CM, McCarthy JB. Cell surface chondroitin sulfate glycosaminoglycan in melanoma: Role in the activation of pro-MMP-2 (pro-gelatinase A). Biochem J. 2007; 403: 553–63. doi: 10.1042/BJ20061176.

357. Iida J, Meijne AML, Oegema TR, Yednock TA, Kovach NL, Furcht LT, McCarthy JB. A role of chondroitin sulfate glycosaminoglycan binding site in α4β1 integrin-mediated melanoma cell adhesion. J Biol Chem. 1998; 273: 5955–62. doi: 10.1074/jbc.273.10.5955.

358. Iida J, Pei D, Kang T, Simpson MA, Herlyn M, Furcht LT, McCarthy JB. Melanoma Chondroitin Sulfate Proteoglycan Regulates Matrix Metalloproteinase-dependent Human Melanoma Invasion into Type I Collagen. J Biol Chem. 2001; 276: 18786–94. doi: 10.1074/jbc.M010053200.

359. Barritt DS, Pearn MT, Zisch AH, Lee SS, Javier RT, Pasquale EB, Stallcup WB. The Multi-PDZ Domain Protein MUPP1 Is a Cytoplasmic Ligand for the Membrane-Spanning Proteoglycan NG2. J Cell Biochem. 2000; 79: 213–24.

360. Nicolosi PA, Dallatomasina A, Perris R. Theranostic impact of NG2/CSPG4 proteoglycan

in cancer. Theranostics. 2015; 5: 530–44. doi: 10.7150/thno.10824.

361. Yang J, Price MA, Neudauer CL, Wilson C, Ferrone S, Xia H, Iida J, Simpson MA, McCarthy JB. Melanoma chondroitin sulfate proteoglycan enhances FAK and ERK activation by distinct mechanisms. J Cell Biol. 2004; 165: 881–91. doi: 10.1083/jcb.200403174.

362. Yang J, Price MA, Gui YL, Bar-Eli M, Salgia R, Jagedeeswaran R, Carlson JH, Ferrone S, Turley EA, McCarthy JB. Melanoma proteoglycan modifies gene expression to stimulate tumor cell motility, growth, and epithelial-to-mesenchymal transition. Cancer Res. 2009; 69: 7538–47. doi: 10.1158/0008-5472.CAN-08-4626.

363. Fukushi J, Makagiansar I, Stallcup W. NG2 Proteoglycan Promotes Endothelial Cell Motility and Angiogenesis via Engagement of Galectin-3 and α3β1 Integrin. Mol Biol Cell. 2004; 15: 3580–90. doi: 10.1091/mbc.E04.

364. Wang J, Svendsen A, Kmiecik J, Immervol H, Skaftnesmo KO, Planagumà J, Reed RK, Bjerkvig R, Miletic H, Enger PØ, Rygh CB, Chekenya M. Targeting the NG2/CSPG4 proteoglycan retards tumour growth and angiogenesis in preclinical models of GBM and melanoma. PLoS One. 2011; 6. doi: 10.1371/journal.pone.0023062.

365. Ampofo E, Schmitt BM, Menger MD, Laschke MW. The regulatory mechanisms of NG2/CSPG4 expression. Cell Mol Biol Lett. Cellular & Molecular Biology Letters; 2017; 22: 4. doi: 10.1186/s11658-017-0035-3.

366. Kucharova K, Stallcup WB. NG2-proteoglycan-dependent contributions of oligodendrocyte progenitors and myeloid cells to myelin damage and repair. J Neuroinflammation [Internet]. Journal of Neuroinflammation; 2015; 12: 1–17. doi: 10.1186/s12974-015-0385-6.

367. Kozanoglu I, Boga C, Ozdogu H, Sozer O, Maytalman E, Yazici AC, Sahin FI. Human bone marrow mesenchymal cells express NG2: Possible increase in discriminative ability of flow cytometry during mesenchymal stromal cell identification. Cytotherapy [Internet]. Elsevier; 2009; 11: 527–33. doi: 10.1080/14653240902923153.

368. Hsu NC, Nien PY, Yokoyama KK, Chu PY, Hou MF. High chondroitin sulfate proteoglycan 4 expression correlates with poor outcome in patients with breast cancer. Biochem Biophys Res Commun [Internet]. Elsevier Inc.; 2013; 441: 514–8. doi: 10.1016/j.bbrc.2013.10.093.

369. Wang X, Osada T, Wang Y, Yu L, Sakakura K, Katayama A, McCarthy JB, Brufsky A, Chivukula M, Khoury T, Hsu DS, Barry WT, Lyerly HK, et al. CSPG4 protein as a new target for the antibody-based immunotherapy of triple-negative breast cancer. J Natl Cancer Inst. 2010; 102: 1496–512. doi: 10.1093/jnci/djq343.

370. Eng MS, Kaur J, Prasmickaite L, Engesæter B, Weyergang A, Skarpen E, Berg K, Rosenblum MG, Mælandsmo GM, Høgset A, Ferrone S, Selbo PK. Enhanced targeting of triple-negative breast carcinoma and malignant melanoma by photochemical internalization of CSPG4-targeting immunotoxins. Photochem Photobiol Sci [Internet]. Royal Society of Chemistry; 2018; 17: 539–51. doi: 10.1039/c7pp00358g.

371. Kasten BB, Oliver PG, Kim H, Fan J, Ferrone S, Zinn KR, Buchsbaum DJ. 212Pb-labeled antibody 225.28 targeted to chondroitin sulfate proteoglycan 4 for triple-negative breast cancer therapy in mouse models. Int J Mol Sci. 2018; 19: 1–16. doi: 10.3390/ijms19040925.

372. Amoury M, Mladenov R, Nachreiner T, Pham AT, Hristodorov D, Di Fiore S, Helfrich W, Pardo A, Fey G, Schwenkert M, Thepen T, Kiessling F, Hussain AF, et al. A novel approach for targeted elimination of CSPG4-positive triple-negative breast cancer cells using a MAP tau-based fusion protein. Int J Cancer. 2016; 139: 916–27. doi: 10.1002/ijc.30119.

373. Reya T, Morrison S, Clarke M, Weissman I. Stem cells, cancer and cancer stem cells. Nature. 2001; 414: 105–11. doi: 10.1007/978-1-4614-0809-3_12.

374. Bai J, Chen W Bin, Zhang XY, Kang XN, Jin LJ, Zhang H, Wang ZY. HIF-2α regulates CD44 to promote cancer stem cell activation in triple-negative breast cancer via PI3K/AKT/mTOR signaling. World J Stem Cells. 2020; 12: 87–99. doi: 10.4252/wjsc.v12.i1.87.

375. Al-Hajj M, Wicha MS, Benito-Hernandez A, Morrison SJ, Clarke MF. Prospective identification of tumorigenic breast cancer cells. Proc Natl Acad Sci U S A. 2003; 100: 3983–8. doi: 10.1073/pnas.0530291100.

376. Pindiprolu SKSS, Krishnamurthy PT, Chintamaneni PK. Pharmacological targets of breast cancer stem cells: a review. Naunyn Schmiedebergs Arch Pharmacol. Naunyn-Schmiedeberg's Archives of Pharmacology; 2018; 391: 463–79. doi: 10.1007/s00210-018-1479-3.

377. Mansoori M, Madjd Z, Janani L, Rasti A. Circulating cancer stem cell markers in breast carcinomas: A systematic review protocol. Syst Rev. Systematic Reviews; 2017; 6: 1–6. doi: 10.1186/s13643-017-0660-y.

378. Chen X, Liu Q, Song E. Mammary stem cells: Angels or demons in mammary gland? Signal Transduct Target Ther. 2017; 2: 1–8. doi: 10.1038/sigtrans.2016.38.

379. Liu M, Liu Y, Deng L, Wang D, He X, Zhou L, Wicha MS, Bai F, Liu S. Transcriptional profiles of different states of cancer stem cells in triple-negative breast cancer. Mol Cancer. Molecular Cancer; 2018; 17: 1–6. doi: 10.1186/s12943-018-0809-x.

380. Ren D, Zhu X, Kong R, Zhao Z, Sheng J, Wang J, Xu X, Liu J, Cui K, Zhang XHF, Zhao H, Wong STC. Targeting brain-adaptive cancer stem cells prohibits brain metastatic colonization of triple-negative breast cancer. Cancer Res. 2018; 78: 2052–64. doi: 10.1158/0008-5472.CAN-17-2994.

381. Lu H, Samanta D, Xiang L, Zhang H, Hu H, Chen I, Bullen JW, Semenza GL. Chemotherapy triggers HIF-1-dependent glutathione synthesis and copper chelation that induces the breast cancer stem cell phenotype. Proc Natl Acad Sci U S A. 2015; 112: E4600–9. doi: 10.1073/pnas.1513433112.

382. Geng SQ, Alexandrou AT, Li JJ. Breast cancer stem cells: Multiple capacities in tumor metastasis. Cancer Lett. 2014; 349: 1–7. doi: 10.1016/j.canlet.2014.03.036.

383. Kagara N, Huynh KT, Kuo C, Okano H, Sim MS, Elashoff D, Chong K, Giuliano AE, Hoon

DSB. Epigenetic regulation of cancer stem cell genes in triple-negative breast cancer. Am J Pathol [Internet]. Elsevier Inc.; 2012; 181: 257–67. doi: 10.1016/j.ajpath.2012.03.019.

384. Idowu MO, Kmieciak M, Dumur C, Burton RS, Grimes MM, Powers CN, Manjili MH. CD44 +/CD24 -/low cancer stem/progenitor cells are more abundant in triple-negative invasive breast carcinoma phenotype and are associated with poor outcome. Hum Pathol [Internet]. Elsevier Inc.; 2012; 43: 364–73. doi: 10.1016/j.humpath.2011.05.005.

385. Chen C, Zhao S, Karnad A, Freeman JW. The biology and role of CD44 in cancer progression: Therapeutic implications. J Hematol Oncol. Journal of Hematology & Oncology; 2018; 11: 1–23. doi: 10.1186/s13045-018-0605-5.

386. Goldstein LA, Zhou DFH, Picker LJ, Minty CN, Bargatze RF, Ding JF, Butcher EC. A human lymphocyte homing receptor, the Hermes antigen, is related to cartilage proteoglycan core and link proteins. Cell. 1989; 56: 1063–72. doi: 10.1016/0092-8674(89)90639-9.

387. Yamano S, Gi M, Tago Y, Doi K, Okada S, Hirayama Y, Tachibana H, Ishii N, Fujioka M, Tatsumi K, Wanibuchi H. Role of deltaNp63posCD44vpos cells in the development of N-nitroso-tris-chloroethylurea-induced peripheral-type mouse lung squamous cell carcinomas. Cancer Sci. 2016; 107: 123–32. doi: 10.1111/cas.12855.

388. Orian-Rousseau V, Chen L, Sleeman JP, Herrlich P, Ponta H. CD44 is required for two consecutive steps in HGF/c-Met signaling. Genes Dev. 2002; 16: 3074–86. doi: 10.1101/gad.242602.

389. Brown R, Reinke L, Damerow M, Perez D. CD44 splice isoform switching in human and mouse epithelium is essential for epithelial-mesenchymal transition and breast cancer progression. J Clin Invest. 2011; 121: 1064–74. doi: 10.1172/JCI44540DS1.

390. Ouhtit A, Abd Elmageed ZY, Abdraboh ME, Lioe TF, Raj MHG. In vivo evidence for the role of CD44s in promoting breast cancer metastasis to the liver. Am J Pathol. 2007; 171: 2033–9. doi: 10.2353/ajpath.2007.070535.

391. Lopez JI, Camenisch TD, Stevens M V., Sands BJ, McDonald J, Schroeder JA. CD44 attenuates metastatic invasion during breast cancer progression. Cancer Res. 2005; 65: 6755–63. doi: 10.1158/0008-5472.CAN-05-0863.

392. Collina F, Di Bonito M, Li Bergolis V, De Laurentiis M, Vitagliano C, Cerrone M, Nuzzo F, Cantile M, Botti G. Prognostic value of cancer stem cells markers in triple-negative breast cancer. Biomed Res Int. 2015; 2015. doi: 10.1155/2015/158682.

393. Miwa T, Nagata T, Kojima H, Sekine S, Okumura T. Isoform switch of CD44 induces different chemotactic and tumorigenic ability in gallbladder cancer. Int J Oncol. 2017; 51: 771–80. doi: 10.3892/ijo.2017.4063.

394. Bajorath J. Molecular organization, structural features, and ligand binding characteristics of CD44, a highly variable cell surface glycoprotein with multiple functions. Proteins. United States; 2000; 39: 103–11.

395. Ponta H, Sherman L, Herrlich PA. CD44: From adhesion molecules to signalling regulators.

Nature Reviews Molecular Cell Biology. 2003. p. 33–45. doi: 10.1038/nrm1004.

396. Lv L, Liu HG, Dong SY, Yang F, Wang QX, Guo GL, Pan YF, Zhang XH. Upregulation of CD44v6 contributes to acquired chemoresistance via the modulation of autophagy in colon cancer SW480 cells. Tumor Biol. 2016; 37: 8811–24. doi: 10.1007/s13277-015-4755-6.

397. Bourguignon LYW, Xia W, Wong G. Hyaluronan-mediated CD44 interaction with p300 and SIRT1 regulates β-catenin signaling and NFκB-specific transcription activity leading to MDR1 and Bcl-xL gene expression and chemoresistance in breast tumor cells. J Biol Chem. 2009; 284: 2657–71. doi: 10.1074/jbc.M806708200.

398. Neame SJ, Isacke CM. The cytoplasmic tail of CD44 is required for basolateral localization in epithelial MDCK cells but does not mediate association with the detergent- insoluble cytoskeleton of fibroblasts. J Cell Biol. 1993; 121: 1299–310. doi: 10.1083/jcb.121.6.1299.

399. Cywes C, Stamenkovic I, Wessels MR. CD44 as a receptor for colonization of the pharynx by group A Streptococcus. J Clin Invest. 2000; 106: 995–1002. doi: 10.1172/JCI10195.

400. Liu D, Sy MS. Phorbol myristate acetate stimulates the dimerization of CD44 involving a cysteine in the transmembrane domain. J Immunol. United States; 1997; 159: 2702–11.

401. Neame SJ, Uff CR, Sheikh H, Wheatley SC, Isacke CM. CD44 exhibits a cell type dependent interaction with triton X-100 insoluble, lipid rich, plasma membrane domains. J Cell Sci. England; 1995; 108 (Pt 9: 3127–35.

402. Gronke RS, VanDusen WJ, Garsky VM, Jacobs JW, Sardana MK, Stern AM, Friedman PA. Aspartyl beta-hydroxylase: in vitro hydroxylation of a synthetic peptide based on the structure of the first growth factor-like domain of human factor IX. Proc Natl Acad Sci U S A. 1989; 86: 3609–13. doi: 10.1073/pnas.86.10.3609.

403. Stenflo J, Holmet E, Lindstedtt S, Chandramoulit N, Huang LHT, Tamt JP, Merrifield RB. Hydroxylation of aspartic acid in domains homologous to the epidermal growth factor precursor is catalyzed by a. Prod Nat Acad Sci. 1989; 86: 444.

404. Huyan T, Li Q, Dong DD, Yang H, Xue XP, Huang QS. Development of a novel anti-human aspartyl-(Asparaginyl) β-hydroxylase monoclonal antibody with diagnostic and therapeutic potential. Oncol Lett. 2017; 13: 1539–46. doi: 10.3892/ol.2017.5642.

405. Dinchuk JE, Focht RJ, Kelley JA, Henderson NL, Zolotarjova NI, Wynn R, Neff NT, Link J, Huber RM, Burn TC, Rupar MJ, Cunningham MR, Selling BH, et al. Absence of post-translational aspartyl β-hydroxylation of epidermal growth factor domains in mice leads to developmental defects and an increased incidence of intestinal neoplasia. J Biol Chem. 2002; 277: 12970–7. doi: 10.1074/jbc.M110389200.

406. Ho SP, Scully MS, Krauthauser CM, Wexler EJ, Stow MD, Dinchuk JE, Kerr JS, Friedman PA. Antisense oligonucleotides selectively regulate aspartyl β-hydroxylase and its truncated protein isoform in vitro but distribute poorly into A549 tumors in vivo. J Pharmacol Exp Ther. 2002; 302: 795–803. doi: 10.1124/jpet.302.2.795.

407. Ince N, de la Monte SM, Wands JR. Overexpression of human aspartyl (asparaginyl) beta-

hydroxylase is associated with malignant transformation. Cancer Res. United States; 2000; 60: 1261–6.

408. Dinchuk JE, Henderson NL, Burn TC, Huber R, Ho SP, Link J, O'Neil KT, Focht RJ, Scully MS, Hollis JM, Hollis GF, Friedman PA. Aspartyl β-hydroxylase (Asph) and an evolutionarily conserved isoform of Asph missing the catalytic domain share exons with junctin. J Biol Chem. 2000; 275: 39543–54. doi: 10.1074/jbc.M006753200.

409. Treves S, Feriotto G, Moccagatta L, Gambari R, Zorzato F. Molecular cloning, expression, functional characterization, chromosomal localization, and gene structure of junctate, a novel integral calcium binding protein of sarco(endo)plasmic reticulum membrane. J Biol Chem. 2000; 275: 39555–68. doi: 10.1074/jbc.M005473200.

410. Lavaissiere L, Jia S, Nishiyama M, De La Monte S, Stern AM, Wands JR, Friedman PA. Overexpression of human aspartyl(asparaginyl)β-hydroxylase in hepatocellular carcinoma and cholangiocarcinoma. J Clin Invest. 1996; 98: 1313–23. doi: 10.1172/JCI118918.

411. Palumbo KS, Wands JR, Safran H, King T, Carlson RI, De la Monte SM. Human aspartyl (Asparaginyl) β-hydroxylase monoclonal antibodies: Potential biomarkers for pancreatic carcinoma. Pancreas. 2002; 25: 39–44. doi: 10.1097/00006676-200207000-00010.

412. Sepe PS, Lahousse SA, Gemelli B, Chang H, Maeda T, Wands JR, De la Monte SM. Role of the aspartyl-asparaginyl-β-hydroxylase gene in neuroblastoma cell motility. Lab Investig. 2002; 82: 881–91. doi: 10.1097/01.LAB.0000020406.91689.7F.

413. Yang H, Song K, Xue T, Xue X, Huyan T. The distribution and expression profiles of human Aspartyl/Asparaginyl beta-hydroxylase in tumor cell lines and human tissues. Oncol Rep. 2010; 24: 1257–64. doi: 10.3892/or.

414. Revskaya E, Jiang Z, Morgenstern A, Bruchertseifer F, Sesay M, Walker S, Fuller S, Lebowitz MS, Gravekamp C, Ghanbari HA, Dadachova E. A Radiolabeled Fully Human Antibody to Human Aspartyl (Asparaginyl) β-Hydroxylase Is a Promising Agent for Imaging and Therapy of Metastatic Breast Cancer. Cancer Biother Radiopharm. 2017; 32: 57–65. doi: 10.1089/cbr.2016.2141.

415. Shimoda M, Hori A, Wands JR, Tsunashima R, Naoi Y, Miyake T, Tanei T, Kagara N, Shimazu K, Kim SJ, Noguchi S. Endocrine sensitivity of estrogen receptor-positive breast cancer is negatively correlated with aspartate-β-hydroxylase expression. Cancer Sci. 2017; 108: 2454–61. doi: 10.1111/cas.13416.

416. Lin Q, Chen X, Meng F, Ogawa K, Li M, Song R, Zhang S, Zhang Z, Kong X, Xu Q, He F, Bai X, Sun B, et al. ASPH-notch Axis guided Exosomal delivery of Prometastatic Secretome renders breast Cancer multi-organ metastasis. Mol Cancer. Molecular Cancer; 2019; 18: 1–17. doi: 10.1186/s12943-019-1077-0.

417. Tang C, Hou Y, Wang H, Wang K, Xiang H, Wan X, Xia Y, Li J, Wei W, Xu S, Lei Z, Pawlik TM, Wang H, et al. Aspartate β-hydroxylase disrupts mitochondrial DNA stability and function in hepatocellular carcinoma. Oncogenesis. 2017; 6: e362–e362. doi: 10.1038/oncsis.2017.64.

418. Hou G, Xu B, Bi Y, Wu C, Ru B, Sun B, Bai X. Recent advances in research on aspartate

β-hydroxylase (ASPH) in pancreatic cancer: A brief update. Bosn J Basic Med Sci. 2018; 18: 297–304. doi: 10.17305/bjbms.2018.3539.

419. Artavanis-Tsakonas S, Rand MD, Lake RJ. Notch signaling: Cell fate control and signal integration in development. Science (80-). 1999; 284: 770–6. doi: 10.1126/science.284.5415.770.

420. Xue T, Xue XP, Huang QS, Wei L, Sun K, Xue T. Monoclonal antibodies against human aspartyl (asparaginyl) beta-hydroxylase developed by DNA immunization. Hybridoma. 2009; 28: 251–7. doi: 10.1089/hyb.2009.0017.

421. Yeung YA, Finney AH, Koyrakh IA, Lebowitz MS, Ghanbari HA, Wands JR, Wittrup KD. Isolation and characterization of human antibodies targeting human aspartyl (asparaginyl) beta-hydroxylase. Hum Antibodies. Netherlands; 2007; 16: 163–76.

422. Ma D, Hopf CE, Malewicz AD, Donovan GP, Senter PD, Goeckeler WF, Maddon PJ, Olson WC. Potent antitumor activity of an auristatin-conjugated, fully human monoclonal antibody to prostate-specific membrane antigen. Clin Cancer Res. 2006; 12: 2591–6. doi: 10.1158/1078-0432.CCR-05-2107.

423. Junutula JR, Raab H, Clark S, Bhakta S, Leipold DD, Weir S, Chen Y, Simpson M, Tsai SP, Dennis MS, Lu Y, Meng YG, Ng C, et al. Site-specific conjugation of a cytotoxic drug to an antibody improves the therapeutic index. Nat Biotechnol. 2008; 26: 925–32. doi: 10.1038/nbt.1480.

424. Hu QY, Berti F, Adamo R. Towards the next generation of biomedicines by site-selective conjugation. Chem Soc Rev [Internet]. Royal Society of Chemistry; 2016; 45: 1691–719. doi: 10.1039/c4cs00388h.

425. Smith RL, Traul DL, Schaack J, Clayton GH, Staley KJ. Characterization of Promoter Function and Cell-Type-Specific Expression from Viral Vectors in the Nervous System. J Virol. 2000; 74: 11254–61.

426. Arafat W, Gómez-Navarro J, Xiang J, Siegal GP, Alvarez RD, Curiel DT. Antineoplastic effect of anti-erbB-2 intrabody is not correlated with scFv affinity for its target. Cancer Gene Ther. 2000; 7: 1250–6. doi: 10.1038/sj.cgt.7700228.

427. Mohanty AK, Wiener MC. Membrane protein expression and production: Effects of polyhistidine tag length and position. Protein Expr Purif. 2004; 33: 311–25. doi: 10.1016/j.pep.2003.10.010.

428. Sun X, Zhang A, Baker B, Sun L, Howard A, Buswell J, Maurel D, Masharina A, Johnsson K, Noren CJ, Xu MQ, Corrêa IR. Development of SNAP-tag fluorogenic probes for wash-free fluorescence imaging. ChemBioChem. 2011; 12: 2217–26. doi: 10.1002/cbic.201100173.

429. Hermening S, Kügler S, Bähr M, Isenmann S. Increased protein expression from adenoviral shuttle plasmids and vectors by insertion of a small chimeric intron sequence. J Virol Methods. 2004; 122: 73–7. doi: 10.1016/j.jviromet.2004.08.005.

430. Czarniecki D, Noel RJ, Reznikoff WS. The -45 region of the Escherichia coli lac promoter:

CAP-dependent and CAP-independent transcription. J Bacteriol. 1997; 179: 423–9. doi: 10.1128/jb.179.2.423-429.1997.

431. Schmit JC, Cogniaux J, Hermans P, Van Vaeck C, Sprecher S, Van Remoortel B, Witvrouw M, Balzarini J, Desmyter J, De Clercq E, Vandamme AM. Multiple drug resistance to nucleoside analogues and nonnucleoside reverse transcriptase inhibitors in an efficiently replicating human immunodeficiency virus type 1 patient strain. J Infect Dis. 1996; 174: 962–8. doi: 10.1093/infdis/174.5.962.

432. Busby S, Ebright RH. Transcription activation by catabolite activator protein (CAP). J Mol Biol. 1999; 293: 199–213. doi: 10.1006/jmbi.1999.3161.

433. Lippert K, Galinski EA. Enzyme stabilization be ectoine-type compatible solutes: protection against heating, freezing and drying. Appl Microbiol Biotechnol. 1992; 37: 61–5. doi: 10.1007/BF00174204.

434. Perfetto SP, Chattopadhyay PK, Lamoreaux L, Nguyen R, Ambrozak D, Koup RA, Roederer M. Amine-reactive dyes for dead cell discrimination in fixed samples. Curr Protoc Cytom. 2010; : 1–20. doi: 10.1002/0471142956.cy0934s53.

435. Hulspas R. Titration of fluorochrome-conjugated antibodies for labeling cell surface markers on live cells. Curr Protoc Cytom. 2010; : 1–9. doi: 10.1002/0471142956.cy0629s54.

436. Roederer M. Spectral compensation for flow cytometry: Visualization artifacts, limitations, and caveats. Cytometry. 2001; 45: 194–205. doi: 10.1002/1097-0320(20011101)45:3<194::AID-CYTO1163>3.0.CO;2-C.

437. Szalóki G, Goda K. Compensation in multicolor flow cytometry. Cytom Part A. 2015; 87: 982–5. doi: 10.1002/cyto.a.22736.

438. Maecker H, Trotter J. Selecting reagents for multicolor BD flow cytometry. BD Biosci. 2012; : 1–8.

439. Brinas L, Zarazaga M, Saenz Y, Ruiz-larrea F, Torres C. Beta-Lactamases in Ampicillin-Resistant Escherichia coli Isolates from Foods, Humans and Healthy Animals. Antimicrob Agents Chemother. 2002; 46: 3156–63. doi: 10.1128/AAC.46.10.3156.

440. Sheerar D. Titrating Antibodies for Flow Cytometry Titrating Antibodies for Flow Cytometry Why Titrate? UWCC Flow Cytom Lab. 2016; : 1–2.

441. Institut für HIV Forschung. Antibody Titrations. 2017; 03: 1–8.

442. Mittag A, Tárnok A. Basics of standardization and calibration in cytometry - A review. J Biophotonics. 2009; 2: 470–81. doi: 10.1002/jbio.200910033.

443. Mizrahi O, Ish Shalom E, Baniyash M, Klieger Y. Quantitative Flow Cytometry: Concerns and Recommendations in Clinic and Research. Cytom Part B - Clin Cytom. 2018; 94: 211–8. doi: 10.1002/cyto.b.21515.

444. Ismail-Khan R, Bui MM. A review of triple-negative breast cancer. Cancer Control. 2010; 17: 173–6. doi: 10.1177/107327481001700305.

445. Mehanna J, Haddad FGH, Eid R, Lambertini M, Kourie HR. Triple-negative breast cancer: Current perspective on the evolving therapeutic landscape. Int J Womens Health. 2019; 11: 431–7. doi: 10.2147/IJWH.S178349.

446. Lin N, Vanderplas A, Hughes M, Theriault R. Clinicopathological Features, Patterns of Recurrence, and Survival Among Women With Triple-Negative Breast Cancer in the National Comprehensive Cancer Network. SpringerReference. 2012; 118: 5463–72. doi: 10.1007/springerreference_178671.

447. Hudis CA, Gianni L. Triple-Negative Breast Cancer: An Unmet Medical Need. Oncologist. 2011; 16: 1–11. doi: 10.1634/theoncologist.2011-s1-01.

448. Cuzick J, Sestak I, Baum M, Buzdar A, Howell A, Dowsett M, Forbes JF. Effect of anastrozole and tamoxifen as adjuvant treatment for early-stage breast cancer: 10-year analysis of the ATAC trial. Lancet Oncol [Internet]. Elsevier Ltd; 2010; 11: 1135–41. doi: 10.1016/S1470-2045(10)70257-6.

449. Chumsri S. Clinical utilities of aromatase inhibitors in breast cancer. Int J Womens Health. 2015; 7: 493–9. doi: 10.2147/IJWH.S69907.

450. Gianni L, Dafni U, Gelber RD, Azambuja E, Muehlbauer S, Goldhirsch A, Untch M, Smith I, Baselga J, Jackisch C, Cameron D, Mano M, Pedrini JL, et al. Treatment with trastuzumab for 1 year after adjuvant chemotherapy in patients with HER2-positive early breast cancer: A 4-year follow-up of a randomised controlled trial. Lancet Oncol [Internet]. Elsevier Ltd; 2011; 12: 236–44. doi: 10.1016/S1470-2045(11)70033-X.

451. Kaplan HG, Malmgren JA, Atwood M. TINO triple negative breast cancer: Risk of recurrence and adjuvant chemotherapy. Breast J. 2009; 15: 454–60. doi: 10.1111/j.1524-4741.2009.00789.x.

452. Verma S, Provencher L, Dent R. Emerging trends in the treatment of triple-negative breast cancer in canada:A survey. Curr Oncol. 2011; 18: 180–90. doi: 10.3747/co.v18i4.913.

453. Yeong J, Tan T, Chow ZL, Cheng Q, Lee B, Seet A, Lim JX, Lim JCT, Ong CCH, Thike AA, Saraf S, Tan BYC, Poh YC, et al. Multiplex immunohistochemistry/immunofluorescence (mIHC/IF) for PD-L1 testing in triple-negative breast cancer: A translational assay compared with conventional IHC. J Clin Pathol. 2020; : 1–6. doi: 10.1136/jclinpath-2019-206252.

454. He TF, Yost SE, Frankel PH, Dagis A, Cao Y, Wang R, Rosario A, Tu TY, Solomon S, Schmolze D, Mortimer J, Lee P, Yuan Y. Multi-panel immunofluorescence analysis of tumor infiltrating lymphocytes in triple negative breast cancer: Evolution of tumor immune profiles and patient prognosis. PLoS One [Internet]. 2020; 15: 1–15. doi: 10.1371/journal.pone.0229955.

455. Couzin-Frankel J. Cancer immunotherapy. Science (80-). 2013; 342: 1432–3. doi: 10.1126/science.342.6165.1432.

456. Hoption Cann SA, van Netten JP, van Netten C. Dr William Coley and tumour regression: a place in history or in the future. Postgrad Med J. 2003; 79: 672–80.

457. Rettig WJ, Old LJ. Immunogenetics of human cell surface differentiation. Annu Rev Immunol. 1989; 7: 481–511. doi: 10.1146/annurev.iy.07.040189.002405.

458. Luedke E, Jaime-Ramirez A, Bhave N, Carson W. Cetuximab : Potential for Immune Modulation. J Immunother. 2012; 35: 367–73. doi: 10.1097/CJI.0b013e3182562d76.

459. Gisselbrecht C, Glass B, Mounier N, Gill DS, Linch DC, Trneny M, Bosly A, Ketterer N, Shpilberg O, Hagberg H, Ma D, Brière J, Moskowitz CH, et al. Salvage regimens with autologous transplantation for relapsed large B-cell lymphoma in the rituximab era. J Clin Oncol. 2010; 28: 4184–90. doi: 10.1200/JCO.2010.28.1618.

460. Senter PD. Potent antibody drug conjugates for cancer therapy. Curr Opin Chem Biol. 2009; 13: 235–44. doi: 10.1016/j.cbpa.2009.03.023.

461. Scott AM, Wolchok JD, Old LJ. Antibody therapy of cancer. Nat Rev Cancer [Internet]. Nature Publishing Group; 2012; 12. doi: 10.1038/nrc3236.

462. Kohrt H, Houot R, Marabelle A, Cho H, Osman K. Combination strategies to enhance antitumor ADCC. Immunotherapy [Internet]. 2012; 4: 511–27. doi: 10.2217/imt.12.38.

463. Boekhout A, Beijnen J, Schellens J. Trastuzumab. Oncologist. 2011; 16: 800–10. doi: 10.1634/theoncologist.2010-0035.

464. Tai Y-T, Anderson KC. Antibody-Based Therapies in Multiple Myeloma. Bone Marrow Res. 2011; 2011: 1–14. doi: 10.1155/2011/924058.

465. Marabondo S, Kaufman HL. High-dose interleukin-2 (IL-2) for the treatment of melanoma: safety considerations and future directions. Expert Opin Drug Saf [Internet]. Taylor & Francis; 2017; 16: 1347–57. doi: 10.1080/14740338.2017.1382472.

466. Galluzzi L, Vacchelli E, Pedro J-MB-S, Buqué A, Senovilla L, Baracco EE, Bloy N, Castoldi F, Abastado J-P, Agostinis P, Apte RN, Aranda F, Ayyoub M, et al. Classification of current anticancer immunotherapies. Oncotarget [Internet]. 2014; 5: 12472–508. Available from www.impactjournals.com/oncotarget/

467. Janthur WD, Cantoni N, Mamot C. Drug conjugates such as antibody drug conjugates (ADCs), immunotoxins and immunoliposomes challenge daily clinical practice. Int J Mol Sci. 2012; 13: 16785–95. doi: 10.3390/ijms131216020.

468. Lambert JM. Drug-conjugated antibodies for the treatment of cancer. Br J Clin Pharmacol. 2012; 76: 248–62. doi: 10.1111/bcp.12044.

469. Shefet-Carasso L, Benhar I. Antibody-targeted drugs and drug resistance—Challenges and solutions. Drug Resist Updat. Elsevier Ltd; 2015; 18: 36–46. doi: 10.1016/j.drup.2014.11.001.

470. Beerli RR, Hell T, Merkel AS, Grawunder U. Sortase enzyme-mediated generation of site-specifically conjugated antibody drug conjugates with high In Vitro and In Vivo potency. PLoS One. 2015; 10: 1–17. doi: 10.1371/journal.pone.0131177.

471. Beckley NS, Lazzareschi KP, Chih HW, Sharma VK, Flores HL. Investigation into temperature-induced aggregation of an antibody drug conjugate. Bioconjug Chem. 2013;

24: 1674–83. doi: 10.1021/bc400182x.

472. Adem YT, Schwarz KA, Duenas E, Patapoff TW, Galush WJ, Esue O. Auristatin antibody drug conjugate physical instability and the role of drug payload. Bioconjug Chem. 2014; 25: 656–64. doi: 10.1021/bc400439x.

473. Mahler HC, Friess W, Grauschopf U, Kiese S. Protein aggregation: Pathways, induction factors and analysis. J Pharm Sci [Internet]. Elsevier Masson SAS; 2009; 98: 2909–34. doi: 10.1002/jps.21566.

474. Cromwell MEM, Hilario E, Jacobson F. Protein aggregation and bioprocessing. AAPS J. 2006; 8. doi: 10.1208/aapsj080366.

475. Hollander I, Kunz A, Hamann PR. Selection of reaction additives used in the preparation of monomeric antibody-calicheamicin conjugates. Bioconjug Chem. United States; 2008; 19: 358–61. doi: 10.1021/bc700321z.

476. Manning MC, Chou DK, Murphy BM, Payne RW, Katayama DS. Stability of protein pharmaceuticals: an update. Pharm Res. United States; 2010; 27: 544–75. doi: 10.1007/s11095-009-0045-6.

477. Moussa EM, Panchal JP, Moorthy BS, Blum JS, Joubert MK, Narhi LO, Topp EM. Immunogenicity of Therapeutic Protein Aggregates. J Pharm Sci. 2016; 105: 417–30. doi: 10.1016/j.xphs.2015.11.002.

478. McDonagh CF, Turcott E, Westendorf L, Webster JB, Alley SC, Kim K, Andreyka J, Stone I, Hamblett KJ, Francisco JA, Carter P. Engineered antibody-drug conjugates with defined sites and stoichiometries of drug attachment. Protein Eng Des Sel. 2006; 19: 299–307. doi: 10.1093/protein/gzl013.

479. Kolberg K, Puettmann C, Pardo A, Fitting J, Barth S. SNAP-Tag Technology : A General Introduction. 2013; : 5406–13.

480. Lucigen. Fast-Link™ DNA Ligation Kits [Internet]. 2012. Available from http://www.biomarket.cc/UpFiles/product/LK11025.pdf

481. Addgene. Molecular Biology Protocol - Restriction Digest of Plasmid DNA [Internet]. 2016 [cited 2020 May 23]. p. 1–2. Available 2020 May 23, from https://www.addgene.org/protocols/restriction-digest/

482. Inoue H, Nojima H, Okayama H. High efficiency transformation of Escherichia coli with plasmids. Gene. Netherlands; 1990; 96: 23–8. doi: 10.1016/0378-1119(90)90336-p.

483. Hanahan D. Studies on transformation of Escherichia coli with plasmids. J Mol Biol. 1983; 166: 557–80. doi: 10.1016/S0022-2836(83)80284-8.

484. Thomas P, Smart TG. HEK293 cell line: A vehicle for the expression of recombinant proteins. J Pharmacol Toxicol Methods. 2005; 51: 187–200. doi: 10.1016/j.vascn.2004.08.014.

485. Nimesh S, Chandra R. Guanidinium-grafted polyethylenimine: An efficient transfecting agent for mammalian cells. Eur J Pharm Biopharm. 2008; 68: 647–55. doi:

10.1016/j.ejpb.2007.09.008.

486. Carson M, Johnson DH, McDonald H, Brouillette C, DeLucas LJ. His-tag impact on structure. Acta Crystallogr Sect D Biol Crystallogr. 2007; 63: 295–301. doi: 10.1107/S0907444906052024.

487. Spriestersbach A, Kubicek J, Schäfer F, Block H, Maertens B. Purification of His-Tagged Proteins. Methods Enzymol. 2015; 559: 1–15. doi: 10.1016/bs.mie.2014.11.003.

488. Hristodorov D, Mladenov R, Pardo A, Pham AT, Huhn M, Fischer R, Thepen T, Barth S. Microtubule-associated protein tau facilitates the targeted killing of proliferating cancer cells in vitro and in a xenograft mouse tumour model in vivo. Br J Cancer [Internet]. Nature Publishing Group; 2013; 109: 1570–8. doi: 10.1038/bjc.2013.457.

489. Barth S, Huhn M, Matthey B, Klimka A, Galinski EA, Engert A. Compatible-solute-supported periplasmic expression of functional recombinant proteins under stress conditions. Appl Environ Microbiol. 2000; 66: 1572–9. doi: 10.1128/AEM.66.4.1572-1579.2000.

490. Liu C, Dalby B, Chen W, Kilzer JM, Chiou HC. Transient transfection factors for high-level recombinant protein production in suspension cultured mammalian cells. Mol Biotechnol. 2008; 39: 141–53. doi: 10.1007/s12033-008-9051-x.

491. Aricescu AR, Lu W, Jones EY. A time- and cost-efficient system for high-level protein production in mammalian cells. Acta Crystallogr Sect D Biol Crystallogr. 2006; 62: 1243–50. doi: 10.1107/S0907444906029799.

492. Nover AB, Jagtap S, Anjum W, Yegingil H, Shih WY, Shih WH. Modern breast cancer detection: A technological review. Int J Biomed Imaging. 2009; 2009: 1–14. doi: 10.1155/2009/902326.

493. Penault-Llorca F, Viale G. Pathological and molecular diagnosis of triple-negative breast cancer: A clinical perspective. Ann Oncol [Internet]. Elsevier Masson SAS; 2012; 23: vi19–22. doi: 10.1093/annonc/mds190.

494. Yang WT, Dryden M, Broglio K, Gilcrease M, Dawood S, Dempsey PJ, Valero V, Hortobagyi G, Atchley D, Arun B. Mammographic features of triple receptor-negative primary breast cancers in young premenopausal women. Breast Cancer Res Treat. 2008; 111: 405–10. doi: 10.1007/s10549-007-9810-6.

495. Wang Y, Ikeda DM, Narasimhan B, Longacre TA, Bleicher RJ, Pal S, Jackman RJ, Jeffrey SS. Estrogen receptor-negative invasive breast cancer: Imaging features of tumors with and without human epidermal growth factor receptor type 2 overexpression. Radiology. 2008; 246: 367–75. doi: 10.1148/radiol.2462070169.

496. Dogan BE, Gonzalez-Angulo AM, Gilcrease M, Dryden MJ, Yang WT. Multimodality imaging of triple receptor-negative tumors with mammography, ultrasound, and MRI. Am J Roentgenol. 2010; 194: 1160–6. doi: 10.2214/AJR.09.2355.

497. Dogan BE, Turnbull LW. Imaging of triple-negative breast cancer. Ann Oncol [Internet]. Elsevier Masson SAS; 2012; 23: vi23–9. doi: 10.1093/annonc/mds191.

498. American College of Radiology. ACR BI-RADS: Mammography, 4th edition. ACR Breast Imaging Reporting and Data System. 2003. doi: 10.1109/ICSEngT.2019.8906494.

499. Kojima Y, Tsunoda H. Mammography and ultrasound features of triple-negative breast cancer. Breast Cancer. 2010; 18: 146–51. doi: 10.1007/s12282-010-0223-8.

500. Uematsu T, Kasami M, Yuen S. Triple-negative breast cancer: Correlation between MR imaging and pathologic findings. Radiology. 2009; 250: 638–47. doi: 10.1148/radiol.2503081054.

501. Weigelt B, Reis-Filho JS. Molecular profiling currently offers no more than tumour morphology and basic immunohistochemistry. Breast Cancer Res. 2010; 12: 15–8. doi: 10.1186/bcr2734.

502. Edén P, Ritz C, Rose C, Fernö M, Peterson C. "Good Old" clinical markers have similar power in breast cancer prognosis as microarray gene expression profilers. Eur J Cancer. 2004; 40: 1837–41. doi: 10.1016/j.ejca.2004.02.025.

503. Cheang MCU, Voduc D, Bajdik C, Leung S, McKinney S, Chia SK, Perou CM, Nielsen TO. Basal-like breast cancer defined by five biomarkers has superior prognostic value than triple-negative phenotype. Clin Cancer Res. 2008; 14: 1368–76. doi: 10.1158/1078-0432.CCR-07-1658.

504. Sharma P. Biology and Management of Patients With Triple-Negative Breast Cancer. Oncologist. 2016; 21: 1050–62. doi: 10.1634/theoncologist.2016-0067.

505. Vasilyev FF, Lopatnikova JA, Sennikov SV. Optimized flow cytometry protocol for analysis of surface expression of interleukin-1 receptor types I and II. Cytotechnology. 2013; 65: 795–802. doi: 10.1007/s10616-013-9546-6.

506. Kaur G, Dufour JM. Cell lines. Spermatogenesis. 2012; 2: 1–5. doi: 10.4161/spmg.19885.

507. Resnicoff M, Medrano EE, Podhajcer OL, Bravo AI, Bover L, Mordoh J. Subpopulations of MCF7 cells separated by Percoll gradient centrifugation: A model to analyze the heterogeneity of human breast cancer. Proc Natl Acad Sci U S A. 1987; 84: 7295–9. doi: 10.1073/pnas.84.20.7295.

508. Hiorns LR, Bradshaw TD, Skelton LA, Yu Q, Kelland LR, Leyland-Jones B. Variation in RNA expression and genomic DNA content acquired during cell culture. Br J Cancer. 2004; 90: 476–82. doi: 10.1038/sj.bjc.6601405.

509. Jones C, Payne J, Wells D, Delhanty JDA, Lakhani SR, Kortenkamp A. Variation Among Different MCF-7 Cell Stocks. Cell Prolif. 2000; 158: 153–8.

510. Nugoli M, Chucana P, Vendrell J, Orsetti B, Ursule L, Nguyen C, Birnbaum D, Douzery EJP, Cohen P, Theillet C. Genetic variability in MCF-7 sublines: Evidence of rapid genomic and RNA expression profile modifications. BMC Cancer. 2003; 3: 1–12. doi: 10.1186/1471-2407-3-13.

511. Kovtun Y V., Audette CA, Ye Y, Xie H, Ruberti MF, Phinney SJ, Leece BA, Chittenden T, Blättler WA, Goldmacher VS. Antibody-drug conjugates designed to eradicate tumors with homogeneous and heterogeneous expression of the target antigen. Cancer Res. 2006;

66: 3214–21. doi: 10.1158/0008-5472.CAN-05-3973.

512. Li F, Emmerton KK, Jonas M, Zhang X, Miyamoto JB, Setter JR, Nicholas ND, Okeley NM, Lyon RP, Benjamin DR, Law CL. Intracellular released payload influences potency and bystander-killing effects of antibody-drug conjugates in preclinical models. Cancer Res. 2016; 76: 2710–9. doi: 10.1158/0008-5472.CAN-15-1795.

513. Roth JS, Lee TD, Cheff DM, Gosztyla ML, Asawa RR, Danchik C, Michael S, Simeonov A, Klumpp-Thomas C, Wilson KM, Hall MD. Keeping It Clean: The Cell Culture Quality Control Experience at the National Center for Advancing Translational Sciences. SLAS Discov. 2020; 25: 491–7. doi: 10.1177/2472555220911451.

514. Kleensang A, Vantangoli MM, Odwin-Dacosta S, Andersen ME, Boekelheide K, Bouhifd M, Fornace AJ, Li HH, Livi CB, Madnick S, Maertens A, Rosenberg M, Yager JD, et al. Genetic variability in a frozen batch of MCF-7 cells invisible in routine authentication affecting cell function. Sci Rep [Internet]. Nature Publishing Group; 2016; 6: 1–10. doi: 10.1038/srep28994.

515. Aubrey N, Allard-Vannier E, Martin C, Bryden F, Letast S, Colas C, Lakhrif Z, Collinet N, Dimier-Poisson I, Chourpa I, Viaud-Massuard MC, Joubert N. Site-Specific Conjugation of Auristatins onto Engineered scFv Using Second Generation Maleimide to Target HER2-positive Breast Cancer in Vitro. Bioconjug Chem. 2018; 29: 3516–21. doi: 10.1021/acs.bioconjchem.8b00668.

516. Coats S, Williams M, Kebble B, Dixit R, Tseng L, Yao NS, Tice DA, Soria JC. Antibody-drug conjugates: Future directions in clinical and translational strategies to improve the therapeutic index. Clin Cancer Res. 2019; 25: 5441–8. doi: 10.1158/1078-0432.CCR-19-0272.

517. Strop P, Delaria K, Foletti D, Witt JM, Hasa-Moreno A, Poulsen K, Casas MG, Dorywalska M, Farias S, Pios A, Lui V, Dushin R, Zhou D, et al. Site-specific conjugation improves therapeutic index of antibody drug conjugates with high drug loading. Nat Biotechnol. 2015; 33: 694–6. doi: 10.1038/nbt.3274.

518. Sukumaran S, Gadkar K, Zhang C, Bhakta S, Liu L, Xu K, Raab H, Yu SF, Mai E, Fourie-O'Donohue A, Kozak KR, Ramanujan S, Junutula JR, et al. Mechanism-based pharmacokinetic/pharmacodynamic model for THIOMAB^{TM} drug conjugates. Pharm Res. 2015; 32: 1884–93. doi: 10.1007/s11095-014-1582-1.

519. Drake PM, Albers AE, Baker J, Banas S, Barfield RM, Bhat AS, De Hart GW, Garofalo AW, Holder P, Jones LC, Kudirka R, McFarland J, Zmolek W, et al. Aldehyde tag coupled with HIPS chemistry enables the production of ADCs conjugated site-specifically to different antibody regions with distinct in vivo efficacy and PK outcomes. Bioconjug Chem. 2014; 25: 1331–41. doi: 10.1021/bc500189z.

520. Lucas A, Price L, Schorzman A, Storrie M, Piscitelli J, Razo J, Zamboni W. Factors Affecting the Pharmacology of Antibody–Drug Conjugates. Antibodies. 2018; 7: 10. doi: 10.3390/antib7010010.

521. Parslow A, Parakh S, Lee F-T, Gan H, Scott A. Antibody–Drug Conjugates for Cancer

Therapy. Biomedicines [Internet]. 2016; 4: 14. doi: 10.3390/biomedicines4030014.

522. Kim EG, Kim KM. Strategies and advancement in antibody-drug conjugate optimization for targeted cancer therapeutics. Biomol Ther. 2015; 23: 493–509. doi: 10.4062/biomolther.2015.116.

523. Tai YT, Mayes PA, Acharya C, Zhong MY, Cea M, Cagnetta A, Craigen J, Yates J, Gliddon L, Fieles W, Hoang B, Tunstead J, Christie AL, et al. Novel anti-B-cell maturation antigen antibody-drug conjugate (GSK2857916) selectively induces killing of multiple myeloma. Blood. 2014; 123: 3128–38. doi: 10.1182/blood-2013-10-535088.

524. Capone E, Lamolinara A, D'Agostino D, Rossi C, De Laurenzi V, Iezzi M, Iacobelli S, Sala G. EV20-mediated delivery of cytotoxic auristatin MMAF exhibits potent therapeutic efficacy in cutaneous melanoma. J Control Release [Internet]. Elsevier; 2018; 277: 48–56. doi: 10.1016/j.jconrel.2018.03.016.

525. Orth J, Tang Y, Shi J, Loy C, Amendt C. Quantitative live imaging of cancer and normal cells treated with Kinesin-5 inhibitors indicates significant differences in phenotypic responses and cell fate. Mol Cancer Ther. 2008; 7: 3480–9. doi: 10.1158/1535-7163.MCT-08-0684.

526. Sahin U, Hartmann F, Senter P, Pohl C, Engert A, Diehl V, Pfreundschuh M. Specific Activation of the Prodrug Mitomycin Phosphate by a Bispecific Anti-CD30/Anti-Alkaline Phosphatase Monoclonal Antibody. Cancer Res. 1990; 50: 6944–8.

527. Doronina SO, Mendelsohn BA, Bovee TD, Cerveny CG, Alley SC, Meyer DL, Oflazoglu E, Toki BE, Sanderson RJ, Zabinski RF, Wahl AF, Senter PD. Enhanced activity of monomethylauristatin F through monoclonal antibody delivery: Effects of linker technology on efficacy and toxicity. Bioconjug Chem. 2006; 17: 114–24. doi: 10.1021/bc0502917.

528. Sommer A, Kopitz C, Schatz CA, Nising CF, Mahlert C, Lerchen HG, Stelte-Ludwig B, Hammer S, Greven S, Schuhmacher J, Braun M, Zierz R, Wittemer-Rump S, et al. Preclinical efficacy of the auristatin-based antibody-drug conjugate BAY 1187982 for the treatment of FGFR2-positive solid tumors. Cancer Res. 2016; 76: 6331–9. doi: 10.1158/0008-5472.CAN-16-0180.

529. Li D, Poon KA, Yu SF, Dere R, Go MA, Lau J, Zheng B, Elkins K, Danilenko D, Kozak KR, Chan P, Chuh J, Shi X, et al. DCDT2980S, an anti-CD22-monomethyl auristatin E antibody-drug conjugate, is a potential treatment for non-hodgkin lymphoma. Mol Cancer Ther. 2013; 12: 1255–65. doi: 10.1158/1535-7163.MCT-12-1173.

530. Polson AG, Williams M, Gray AM, Fuji RN, Poon KA, McBride J, Raab H, Januario T, Go M, Lau J, Yu SF, Du C, Fuh F, et al. Anti-CD22-MCC-DM1: An antibody-drug conjugate with a stable linker for the treatment of non-Hodgkin's lymphoma. Leukemia. 2010; 24: 1566–73. doi: 10.1038/leu.2010.141.

531. Carter PhD PJ, Senter PhD PD. Antibody-Drug Conjugates for Cancer Therapy. Cancer J. 2008; 14: 154–69. doi: 10.3390/biomedicines4030014.

532. Polson AG, Calemine-Fenaux J, Chan P, Chang W, Christensen E, Clark S, De Sauvage FJ,

Eaton D, Elkins K, Michael Elliott J, Frantz G, Fuji RN, Gray A, et al. Antibody-drug conjugates for the treatment of non-Hodgkin's lymphoma: Target and linker-drug selection. Cancer Res. 2009; 69: 2358–64. doi: 10.1158/0008-5472.CAN-08-2250.

533. Sutherland MSK, Walter RB, Jeffrey SC, Burke PJ, Yu C, Kostner H, Stone I, Ryan MC, Sussman D, Lyon RP, Zeng W, Harrington KH, Klussman K, et al. SGN-CD33A: a novel CD33-targeting antibody–drug conjugate using a pyrrolobenzodiazepine dimer is active in models of drug-resistant AML. Blood. 2013; 122: 1455–63. doi: 10.1182/blood-2013-03-491506.

534. Loganzo F, Sung M, Gerber HP. Mechanisms of resistance to antibody-drug conjugates. Mol Cancer Ther. 2016; 15: 2825–34. doi: 10.1158/1535-7163.MCT-16-0408.

535. Nejadmoghaddam M, Minai-tehrani A, Ghahremanzadeh R. Antibody-Drug Conjugates: Possibilities and Challenges. Avicenna J Med Biotech. 2019; 11: 3–23.

536. Khandelwal A, Saber H, Shapiro M, Zhao H. Antibody-drug conjugates and immunotoxins: From pre-clinical development to therapeutic applications. New York Human Press. 2013. p. 23–38. doi: 10.1007/978-1-4614-5456-4.

537. Robinson MK, Doss M, Shaller C, Narayanan D, Marks JD, Adler LP, González Trotter DE, Adams GP. Quantitative immuno-positron emission tomography imaging of HER2-positlve tumor xenografts with an iodine-124 labeled anti-HER2 diabody. Cancer Res. 2005; 65: 1471–8. doi: 10.1158/0008-5472.CAN-04-2008.

538. Sundaresan G, Yazaki PJ, Shively JE, Finn D, Larson SM, Raubitschek AA, Lawrence E. I124-Labeled Engineered Anti-CEA Minibodies and Diabodies Imaging of Xenografts in Athymic Mice. J Nucl Med. 2003; 44: 1962–9.

539. Pillow TH, Tien J, Parsons-Reponte KL, Bhakta S, Li H, Staben LR, Li G, Chuh J, Fourie-Odonohue A, Darwish M, Yip V, Liu L, Leipold DD, et al. Site-specific trastuzumab maytansinoid antibody-drug conjugates with improved therapeutic activity through linker and antibody engineering. J Med Chem. 2014; 57: 7890–9. doi: 10.1021/jm500552c.

540. Huang Z. A review of progress in clinical photodynamic therapy. Technol Cancer Res Treat. 2005; 4: 283–93. doi: 10.1177/153303460500400308.

541. Majumdar P, Nomula R, Zhao J. Activatable triplet photosensitizers: Magic bullets for targeted photodynamic therapy. J Mater Chem C. 2014; 2: 5982–97. doi: 10.1039/c4tc00659c.

542. Vrouenraets MB, Visser GW, Stigter M, Oppelaar H, Snow GB, van Dongen GA. Targeting of aluminum (III) phthalocyanine tetrasulfonate by use of internalizing monoclonal antibodies: improved efficacy in photodynamic therapy. Cancer Res. United States; 2001; 61: 1970–5.

543. Mitsunaga M, Nakajima T, Sano K, Kramer-Marek G, Choyke PL, Kobayashi H. Immediate in vivo target-specific cancer cell death after near infrared photoimmunotherapy. BMC Cancer [Internet]. BMC Cancer; 2012; 12: 1. doi: 10.1186/1471-2407-12-345.

544. Hu LK, Hasan T, Gragoudas ES, Young LH. Photoimmunotherapy of human uveal

melanoma cells. Exp Eye Res. England; 1995; 61: 385–91. doi: 10.1016/s0014-4835(05)80133-2.

545. Staneloudi C, Smith KA, Hudson R, Malatesti N, Savoie H, Boyle RW, Greenman J. Development and characterization of novel photosensitizer:scFv conjugates for use in photodynamic therapy of cancer. Immunology. 2007; 120: 512–7. doi: 10.1111/j.1365-2567.2006.02522.x.

546. Aveline BM, Hasan T, Redmond RW. The effects of aggregation, protein binding and cellular incorporation on the photophysical properties of benzoporphyrin derivative monoacid ring A (BPDMA). J Photochem Photobiol B Biol. 1995; 30: 161–9. doi: 10.1016/1011-1344(95)07174-Z.

547. Jin J, Krishnamachary B, Mironchik Y, Kobayashi H, Bhujwalla ZM. Phototheranostics of CD44-positive cell populations in triple negative breast cancer. Sci Rep. Nature Publishing Group; 2016; 6: 1–12. doi: 10.1038/srep27871.

548. Nakajima T, Sato K, Hanaoka H, Watanabe R, Harada T, Choyke PL, Kobayashi H. The effects of conjugate and light dose on photo-immunotherapy induced cytotoxicity. BMC Cancer. 2014; 14: 1–7. doi: 10.1186/1471-2407-14-389.

549. Heryanto YD, Hanaoka H, Nakajima T, Yamaguchi A, Tsushima Y. Applying near-infrared photoimmunotherapy to B-cell lymphoma: comparative evaluation with radioimmunotherapy in tumor xenografts. Ann Nucl Med. Springer Japan; 2017; 31: 669–77. doi: 10.1007/s12149-017-1197-9.

550. Springa BQ, Abu-Yousif AO, Palanisami A, Rizvi I, Zheng X, Mai Z, Anbil S, Sears RB, Mensah LB, Goldschmidt R, Erdem SS, Oliva E, Hasan T. Selective treatment and monitoring of disseminated cancer micrometastases in vivo using dual-function, activatable immunoconjugates. Proc Natl Acad Sci U S A. 2014; 111. doi: 10.1073/pnas.1319493111.

551. Dosio FD, Brusa P, Cattel L. Immunotoxins and anticancer drug conjugate assemblies: The role of the linkage between components. Toxins (Basel). 2011; 3: 848–83. doi: 10.3390/toxins3070848.

552. Hermanson G. Chapter 20: Antibody modification and conjugation. Bioconjugate Techniques, 3rd Edition Academic Press, Boston. 2013. p. 867–920.

553. Peng X, Draney DR, Volcheck WM, Bashford GR, Lamb DT, Grone DL, Zhang Y, Johnson CM. Phthalocyanine dye as an extremely photostable and highly fluorescent near-infrared labeling reagent. In: Achilefu SI, Bornhop DJ, Raghavachari R, editors. Optical Molecular Probes for Biomedical Applications [Internet]. SPIE; 2006. p. 113–24. doi: 10.1117/12.669173.

554. Kosaka N, Ogawa M, Choyke PL, Kobayashi H. Clinical implications of near-infrared fluorescence imaging in cancer. Futur Oncol. 2009; 5: 1501–11. doi: 10.2217/fon.09.109.

555. Fujimoto S, Muguruma N, Okamoto K, Kurihara T, Sato Y, Miyamoto Y, Kitamura S, Miyamoto H, Taguchi T, Tsuneyama K, Takayama T. A novel theranostic combination of near-infrared fluorescence imaging and laser irradiation targeting c-KIT for gastrointestinal stromal tumors. Theranostics. 2018; 8: 2313–28. doi: 10.7150/thno.22027.

556. Nakajima T, Sano K, Mitsunaga M, Choyke P, Kobayashi H. Real-time monitoring of in vivo acute necrotic cancer cell death induced by near infrared photoimmunotherapy using fluorescence lifetime imaging. Cancer Res. 2013; 72: 4622–8. doi: 10.1038/jid.2014.371.

557. Shirasu N, Shibaguchi H, Yamada H, Kuroki M, Yasunaga S. Highly versatile cancer photoimmunotherapy using photosensitizer-conjugated avidin and biotin-conjugated targeting antibodies. Cancer Cell Int. BioMed Central; 2019; 19: 1–13. doi: 10.1186/s12935-019-1034-4.

558. Sato K, Sato N, Xu B, Nakamura Y, Nagaya T, Choyke PL, Hasegawa Y, Kobayashi H. Spatially selective depletion of tumor-associated regulatory T cells with near-infrared photoimmunotherapy. Sci Transl Med. 2016; 8. doi: 10.1126/scitranslmed.aaf6843.

559. Ogawa M, Tomita Y, Nakamura Y, Lee MJ, Lee S, Tomita S, Nagaya T, Sato K, Yamauchi T, Iwai H, Kumar A, Haystead T, Shroff H, et al. Immunogenic cancer cell death selectively induced by near infrared photoimmunotherapy initiates host tumor immunity. Oncotarget. 2017; 8: 10425–36. doi: 10.18632/oncotarget.14425.

560. Kobayashi H, Choyke P. Super enhanced permeability and retention (SUPR) effects in tumors following near infrared photoimmunotherapy. Nanoscale. 2016; 8: 12504–9. doi: 10.1016/j.physbeh.2017.03.040.

561. Hanaoka H, Nakajima T, Sato K, Watanabe R, Phung Y, Gao W. Photoimmunotherapy of hepatocellular carcinoma-targeting Glypican-3 combined with nanosized albumin-bound paclitaxel. Nanomedicine. 2015; 10: 1139–47. doi: 10.1016/j.physbeh.2017.03.040.

562. Nagaya T, Gorka AP, Nani RR, Okuyama S, Ogata F, Maruoka Y, Choyke PL, Schnermann MJ, Kobayashi H. Molecularly targeted cancer combination therapy with near-infrared photoimmunotherapy and near-infrared photorelease with duocarmycin–antibody conjugate. Mol Cancer Ther. 2018; 17: 661–70. doi: 10.1158/1535-7163.MCT-17-0851.

563. Boni L, David G, Mangano A, Dionigi G, Rausei S, Spampatti S, Cassinotti E, Fingerhut A. Clinical applications of indocyanine green (ICG) enhanced fluorescence in laparoscopic surgery. Surg Endosc [Internet]. Springer US; 2015; 29: 2046–55. doi: 10.1007/s00464-014-3895-x.

564. Carter P, Merchant AM. Engineering antibodies for imaging and therapy. Curr Opin Biotechnol. 1997; 8: 449–54. doi: 10.1016/S0958-1669(97)80067-5.

565. Kim SJ, Park Y, Hong HJ. Antibody engineering for the development of therapeutic antibodies. Mol Cells. Korea (South); 2005; 20: 17–29.

566. Codd AS, Kanaseki T, Torigo T, Tabi Z. Cancer stem cells as targets for immunotherapy. Immunology. 2018; 153: 304–14. doi: 10.1111/imm.12866.

567. Heemskerk B, Kvistborg P, Schumacher TNM. The cancer antigenome. EMBO J [Internet]. Nature Publishing Group; 2013; 32: 194–203. doi: 10.1038/emboj.2012.333.

568. Diehn M, Cho RW, Lobo NA, Kalisky T, Jo M, Kulp AN, Qian D, Lam JS, Ailles LE, Wong M, Joshua B, Kaplan MJ, Wapnir I, et al. Association of Reactive Oxygen Species Levels and Radioresistance in Cancer Stem Cells.pdf. Nature. 2009; 458: 780–3. doi:

10.1038/nature07733.Association.

569. Glassman PM, Abuqayyas L, Balthasar JP. Assessments of antibody biodistribution. J Clin Pharmacol. 2015; 55: S29–38. doi: 10.1002/jcph.365.

570. Nakajima T, Sano K, Choyke PL, Kobayashi H. Improving the efficacy of photoimmunotherapy (PIT) using a cocktail of antibody conjugates in a multiple antigen tumor model. Theranostics. 2013; 3: 357–65. doi: 10.7150/thno.5908.

571. Nagaya T, Friedman J, Maruoka Y, Ogata F, Okuyama S, Clavijo PE, Choyke PL, Allen C, Kobayashi H. Host immunity following near-infrared photoimmunotherapy is enhanced with PD-1 checkpoint blockade to eradicate established antigenic tumors. Cancer Immunol Res. American Association for Cancer Research Inc.; 2019; 7: 401–13. doi: 10.1158/2326-6066.CIR-18-0546.

572. Ito K, Mitsunaga M, Nishimura T, Saruta M, Iwamoto T, Kobayashi H, Tajiri H. Near-Infrared Photochemoimmunotherapy by Photoactivatable Bifunctional Antibody-Drug Conjugates Targeting Human Epidermal Growth Factor Receptor 2 Positive Cancer. Bioconjugate Chemistry. 2017. 1458–1469 p. doi: 10.1021/acs.bioconjchem.7b00144.

573. Wu N, Zhang J, Zhao J, Mu K, Zhang J, Jin Z, Yu J, Liu J. Precision medicine based on tumorigenic signaling pathways for triple-negative breast cancer. Oncol Lett. 2018; 16: 4984–96. doi: 10.3892/ol.2018.9290.

574. Bettaieb A, Paul C, Plenchette S, Shan J, Chouchane L, Ghiringhelli F. Precision medicine in breast cancer: Reality or utopia? J Transl Med. BioMed Central; 2017; 15: 1–13. doi: 10.1186/s12967-017-1239-z.

575. Carey L, Winer E, Viale G, Cameron D, Gianni L. Triple-negative breast cancer: Disease entity or title of convenience? Nat Rev Clin Oncol [Internet]. Nature Publishing Group; 2010; 7: 683–92. doi: 10.1038/nrclinonc.2010.154.

576. Foulkes W, Smith I, Reis-Filho J. Triple-Negative Breast Cancer. N Engl J Med. 2010; 363: 1938–48.

577. Burness M, Grushko T, Olopade O. Epidermal Growth Factor Receptor in Triple-Negative and Basal-Like Breast Cancer. Promising Clinical Target or Only a Marker? Cancer J. 2010; 16: 23–32. doi: 10.3892/ol.2017.6221.

578. Siziopikou KP, Ariga R, Proussaloglou KE, Gattuso P, Cobleigh M. The challenging estrogen receptor-negative/progesterone receptor-negative/HER-2-negative patient: A promising candidate for epidermal growth factor receptor-targeted therapy? Breast J. 2006; 12: 360–2. doi: 10.1111/j.1075-122X.2006.00276.x.

579. Carey LA, Rugo HS, Marcom PK, Mayer EL, Esteva FJ, Ma CX, Liu MC, Storniolo AM, Rimawi MF, Forero-Torres A, Wolff AC, Hobday TJ, Ivanova A, et al. TBCRC 001: Randomized phase II study of cetuximab in combination with carboplatin in stage IV triple-negative breast cancer. J Clin Oncol. 2012; 30: 2615–23. doi: 10.1200/JCO.2010.34.5579.

580. Dent RA, Lindeman GJ, Clemons M, Wildiers H, Chan A, McCarthy NJ, Singer CF, Lowe ES, Watkins CL, Carmichael J. Phase I trial of the oral PARP inhibitor olaparib in

combination with paclitaxel for first- or second-line treatment of patients with metastatic triple-negative breast cancer. Breast Cancer Res. 2013; 15: 1. doi: 10.1186/bcr3484.

581. O'Shaughnessy J, Hellerstedt B, Schwartzberg L, Yardley DA, Danso MA, Robert N, Richards P, Miller KD, Rugo HS, Carlson RW, Finn RS, Neubauer M, Saleh M, et al. Phase III study of iniparib plus gemcitabine and carboplatin versus gemcitabine and carboplatin in patients with metastatic triple-negative breast cancer. J Clin Oncol. 2014; 32: 3840–7. doi: 10.1200/JCO.2014.55.2984.

582. Kandoth C, McLellan MD, Vandin F, Ye K, Niu B, Lu C, Xie M, Zhang Q, McMichael JF, Wyczalkowski MA, Leiserson MDM, Miller CA, Welch JS, et al. Mutational landscape and significance across 12 major cancer types. Nature. Nature Publishing Group; 2013; 502: 333–9. doi: 10.1038/nature12634.

583. Stratford AL, Reipas K, Maxwell C, Dunn SE. Targeting tumour-initiating cells to improve the cure rates for triple-negative breast cancer. Expert Rev Mol Med. 2010; 12. doi: 10.1017/S1462399410001535.

584. Kai K, Arima Y, Kamiya T, Saya H. Breast cancer stem cells. Breast Cancer. 2010; 17: 80–5. doi: 10.1007/s12282-009-0176-y.

585. Ginsburg GS, Phillips KA. Precision medicine: From science to value. Health Aff. 2018; 37: 694–701. doi: 10.1377/hlthaff.2017.1624.

586. Collins F, Varmus H. A new initiative on precision medicine. N Engl J Med. 2015; 372: 793–5. doi: 10.3389/fpsyt.2015.00088.

587. Du F Le, Eckhardt BL, Lim B, Litton JK, Moulder S, Meric-Bernstam F, Gonzalez-Angulo AM, Ueno NT. Is the future of personalized therapy in triple-negative breast cancer based on molecular subtype? Oncotarget. 2015; 6: 12890–908. doi: 10.18632/oncotarget.3849.

588. Sachdev JC, Sandoval AC, Jahanzeb M. Update on Precision Medicine in Breast Cancer. Cancer Treatment and Research. 2019. 45–80 p. doi: 10.1007/978-3-030-16391-4_2.

589. Kasztura M, Richard A, Bempong NE, Loncar D, Flahault A. Cost-effectiveness of precision medicine: a scoping review. Int J Public Health [Internet]. Springer International Publishing; 2019; 64: 1261–71. doi: 10.1007/s00038-019-01298-x.

590. Arnedos M, Vicier C, Loi S, Lefebvre C, Michiels S, Bonnefoi H, Andre F. Precision medicine for metastatic breast cancer-limitations and solutions. Nat Rev Clin Oncol [Internet]. Nature Publishing Group; 2015; 12: 693–704. doi: 10.1038/nrclinonc.2015.123.